

**Stochastic Characterization  
of Strong Ground Motion  
and Applications to Structural Response**

Thesis by  
**Konstantinos Papadimitriou**

In Partial Fulfillment  
of the Requirements for the Degree of  
Doctor of Philosophy

California Institute of Technology  
Pasadena, California

1991

(Submitted October 2, 1990)

© 1990

Konstantinos Papadimitriou

All Rights Reserved

## **Acknowledgments**

I am deeply grateful to my advisor, Professor J.L. Beck, for his guidance and encouragement throughout the course of my research. His continuous availability and enthusiastic guidance are greatly appreciated.

I am sincerely grateful for the generous financial support provided to me by the California Institute of Technology, which made my studies here possible.

I would like to thank all my professors for the excellent education they offered me during my graduate studies. I also thank the people in Thomas who created a friendly environment, making my stay here a very pleasant experience.

My deepest thanks to Lambros Katafygiotis, Petros Koumoutsakos, and Roberto Camassa for the many memorable experiences we shared. The assistance of Suzette Martinez and Sharon Beckenbach with the typing of this thesis is greatly appreciated.

Finally, I am deeply grateful to my parents, to whom this thesis is dedicated, for their unsurpassed love and their continuous support in the pursuit of my educational goals.

## Abstract

This study addresses the problem of characterizing strong ground motion for the purpose of computing the dynamic response of structures to earthquakes. A new probabilistic ground motion model is proposed which can act as an interface between ground motion prediction studies and structural response studies. The model is capable of capturing, with at most nine parameters, all those features of the ground acceleration history which have an important influence on the dynamic response of linear and nonlinear structures, including the amplitude and frequency content nonstationarities of the shaking. Using a Bayesian probabilistic framework, a simple and effective statistical method is developed for extracting the “optimal” model from an actual accelerogram. The proposed ground motion model can be efficiently applied in simulations as well as analytical response and reliability studies of linear and inelastic structures.

The random response of linear and nonlinear oscillators subjected to the proposed stochastic excitation is considered. The nonlinearity of the oscillator is accounted for by equivalent linearization. A formulation is developed which approximates the original lengthy expressions for the second-moment statistics of the transient response by much simpler expressions. The results provide insight into the characteristics of the nonstationary response and the effect of the ground motion nonstationarities. It is found that the temporal nonstationarity in the frequency content of the ground motion significantly influences the response of both linear and nonlinear structural models. Simulations are also used to study the sensitivity of inelastic structural response parameters to the details of the ground motion which are left “random” by the model. The results can also be used to provide a quantitative assessment of the expected structural damage associated with the ground motion described by the model.

## Table of Contents

<b>Acknowledgments</b>	iii
<b>Abstract</b>	iv
<b>Table of Contents</b>	v
<b>List of Tables and Figures</b>	x
<b>Chapter 1: Introduction</b>	1
1.1 Motivation and Objectives	1
1.2 Summary of this Study	3
<b>Chapter 2: Modeling of Strong Ground Motion by Stochastic Differential and Difference Equations</b>	6
2.1 Introduction	6
2.2 General Class of Strong Ground Motion Models	11
2.2.1 Continuous Model	12
2.2.2 Discrete Model	12
2.3 Subclasses of Strong Ground Motion Model	14
2.3.1 Stationary Stochastic Model	14
2.3.2 Piecewise Time-Invariant Model	17
2.3.3 Envelope-Modulated White Noise Model	18
2.3.4 Piecewise Time-Invariant Frequency Content Model	19
2.4 Bayesian Methodology for Parameter Estimation	19
2.4.1 General AR(p) Model with Time-Varying Coefficients	20
2.4.2 Piecewise Time-Invariant Model	22
2.4.3 Envelope-Modulated White-Noise Model	23
2.4.4 Piecewise Time-Invariant Frequency Content Model	24
2.5 Structural Response and Ground Motion Model Adequacy	25
2.5.1 Nonlinear Hysteretic Model	25
2.5.2 Equation of Motion	26
2.5.3 Probabilistic Linear Elastic and Inelastic Response Spectra	28
2.6 Analysis of Earthquake Accelerograms Using Autoregressive Models	30

2.6.1 Moving Time-Window Approach . . . . .	30
2.6.2 Physical Interpretation of Time Variation of the Model Coefficients . . . . .	31
2.7 Modeling and Simulation of Earthquake Accelerograms . . . . .	33
2.7.1 Modeling of the Intensity Using Various Models . . . . .	34
2.7.2 Modeling of the Frequency Content Using PTIFC Models . . . . .	35
2.7.3 Modeling of the Very Low Frequency Content . . . . .	38
2.8 Conclusions . . . . .	40
<b>Chapter 3: Parsimonious Probabilistic Modeling of Strong Ground Motion . . . . .</b>	<b>64</b>
3.1 Introduction . . . . .	64
3.2 Stochastic Second-Order Differential Equations with Variable Coefficients . . . . .	65
3.2.1 Autocovariance Function . . . . .	65
3.2.2 Evolutionary Power Spectral Density Function . . . . .	68
3.2.3 Relation Between ACF and EPSD Function . . . . .	69
3.3 Discrete Equation and Its Relation to the Continuous One . . . . .	69
3.4 Parsimonious Ground Motion Model . . . . .	71
3.4.1 Analysis and Simulation of Earthquake Accelerograms . . . . .	74
3.4.2 Structural Response and Model Adequacy . . . . .	75
3.5 Concluding Remarks . . . . .	76
<b>Chapter 4: Transient Response Characteristics of Stochastically Excited Linear and Nonlinear Systems . . . . .</b>	<b>89</b>
4.1 Introduction . . . . .	89
4.2 Mathematical Formulation of the Response . . . . .	91
4.2.1 Mean-Square Response . . . . .	92
4.2.2 Covariance Response . . . . .	93
4.2.3 Special Case: Modulated White-Noise Excitation . . . . .	93
4.3 Formulation for the Mean-Square Response of Linear Time Invariant SDOF Oscillators . . . . .	95
4.3.1 Mean-Square Displacement . . . . .	95

4.3.2 Mean-Square Velocity . . . . .	96
4.3.3 Mean-Square Absolute Acceleration . . . . .	97
4.3.4 Displacement-Velocity Correlation . . . . .	97
4.3.5 Similarities Between Transient and Stationary Mean-Square Response . . . . .	97
4.3.6 Exact Solution for the Mean-Square Response . . . . .	98
4.3.7 Exact Solution for the Covariance of the Response: Modu- lated White-Noise Excitation . . . . .	99
4.4 Approximation for the Mean-Square Response of a Linear Time- Invariant SDOF Oscillator . . . . .	99
4.4.1 Approximate First-Order Differential Equation for the Mean- Square Displacement . . . . .	100
4.4.2 Accuracy of the Approximations using Modulated White- Noise Excitation . . . . .	101
4.5 Formulation for the Mean-Square Response of Nonlinear SDOF Os- cillators . . . . .	105
4.5.1 Mean-Square Displacement . . . . .	106
4.5.2 Mean-Square Velocity . . . . .	107
4.5.3 Mean-Square Absolute Acceleration . . . . .	107
4.5.4 Displacement-Velocity Correlation . . . . .	108
4.5.5 Similarities Between Transient and Stationary Mean-Square Response . . . . .	108
4.6 Approximation of the Liapunov Matrix Equation for a Nonlinear SDOF Oscillator . . . . .	109
4.6.1 Covariance of the Response: Modulated White-Noise Excita- tion . . . . .	110
4.7 Approximation of the Forcing Integral Term of the Liapunov Matrix Equation . . . . .	111
4.7.1 Broadband Excitation and Slowly-Varying Structural Param- eters . . . . .	111
4.7.2 Lightly-Damped Oscillators . . . . .	113
4.8 Application to Some Special Cases of Nonstationary Excitation . . . . .	114

4.8.1	Modulated Filtered White-Noise Excitation . . . . .	114
4.8.2	Filtered Modulated White-Noise Excitation . . . . .	116
4.8.3	Stochastic Ground Motion Models . . . . .	116
4.8.4	Accuracy of the Approximations Using the Proposed Stochastic Ground Motion Model . . . . .	120
4.8.5	Computational Aspects . . . . .	121
4.9	Extension of the Approximations to Classically-Damped MDOF Linear Systems . . . . .	122
4.10	Conclusions . . . . .	126
<b>Chapter 5: Importance of Temporal Nonstationarity In the Frequency Content of Ground Motion for Linear and Non-linear Structural Models . . . . .</b>		
5.1	Introduction . . . . .	147
5.2	Description of Earthquake Ground Motions . . . . .	148
5.3	Linear SDOF Structural Model . . . . .	149
5.4	Nonlinear SDOF Structural Model . . . . .	152
5.4.1	Force-Deflection Relation . . . . .	152
5.4.2	Equation of Motion Using the Equivalent Linearization Method . . . . .	153
5.4.3	Characteristics of the Mean-Square Response; Moving Resonance Effect . . . . .	154
<b>Chapter 6: Conclusions . . . . .</b>		
<b>References . . . . .</b>		
<b>Appendix A.1 Solutions of Homogenous Second-Order Differential Equation with Slowly-Varying Coefficients . . . . .</b>		
<b>Appendix A.2 Principal Matrix Solution . . . . .</b>		
<b>Appendix A.3 Evolutionary Spectral Representation of a Stochastic Process . . . . .</b>		
<b>Appendix B Relationships Between the Coefficients of Second-Order Discrete and Continuous Equations . . . . .</b>		
<b>Appendix C Second-Order Discrete Equation . . . . .</b>		

<b>Appendix D</b>	Solution of the Second-Order Differential Equation Using the Two-Timing Method . . . . .	188
<b>Appendix E</b>	Covariance Response of A Linear Oscillator Subjected to Modulated White-Noise Excitation . . . . .	191
<b>Appendix F</b>	Complete Set of Equations for the Mean-Square Displacement of the Nonlinear Response . . . . .	192

## List of Tables and Figures

- Figure 2.1. (a) Model I, (b) Model II, for ground acceleration.
- Figure 2.2. Effect of  $n$  on the force-displacement curve [from Jayakumar, (1987)].
- Figure 2.3. Hysteresis loop for periodic response of the structural model [from Jayakumar, (1987)].
- Figure 2.4. Force-displacement curves for arbitrary loading of the structural model [from Jayakumar, (1987)].
- Figure 2.5. Schematic diagram of a SDOF structure.
- Figure 2.6. Acceleration time histories for the six accelerograms in Table 2.1.
- Figure 2.7. Time variation of the frequency content of the accelerograms in Table 2.1, plotted in terms of the undamped frequency  $\omega_1$  (solid), bandwidth  $\omega_1\zeta_1$  (dashed-dotted) and damping ratio  $\zeta_1$ .
- Figure 2.8. Comparison of the standard deviation computed for the accelerograms in Table 2.1 by the moving time-window approach (solid) and by the envelope-modulated white-noise model for the functions (2.1) (dashed-dotted), (2.2) (dashed) and (2.58) (dotted).
- Figure 2.9. The transformed series of stationary intensity for the N00W component of the C048 record.
- Figure 2.10. The N00W component and one simulation for each optimal model of different subclasses. (a) "Target" accelerogram. (b) and (c) TIFC models with  $p=2$  and  $p=4$ , respectively. (d) and (e) PTIFC models with  $p=2$  and  $p=4$ , respectively.
- Figure 2.11. The computed "white-noise" sample that generates the N00W compo-

ment for each optimal model in Figure 2.10.

Figure 2.12. Comparison between the 5% damped response spectra of the "target" accelerogram (solid line), the mean response spectra (dashed-dotted line) and the probabilistic response spectra (dashed lines which from top to bottom correspond to  $p = 0.99, 0.90, 0.50, 0.10, 0.01$ ) computed for each optimal model in Figure 2.10. (a) and (b) correspond to time-invariant frequency content models with  $p=2$  and  $p=4$ , respectively. (c) and (d) correspond to piecewise time-invariant models with  $p=2$  and  $p=4$ , respectively.

Figure 2.13. Comparison between the 5% damped response spectra of the "target" accelerogram (solid line), the mean response spectra (dashed-dotted line) and the probabilistic response spectra (dashed lines which from top to bottom correspond to  $p = 0.99, 0.90, 0.50, 0.10, 0.01$ ) computed for the optimal PTIFC AR(2) model given in Table 2.2.

Figure 2.14. The Fourier transform of the "white-noise" samples in Figure 2.11.

Figure 2.15. Schematic diagram of the earthquake model, including Brune's source model.

Figure 2.16. Power spectral density of the AR( $p$ ) model (dashed-dotted curved) and the combined AR( $p$ ) and Brune's model (solid curve).

Figure 2.17. Comparison between the 5% damped acceleration response spectra of the "target" accelerogram (solid line), the mean response spectra (dashed-dotted line) and the probabilistic response spectra (dashed lines which from top to bottom correspond to  $p = 0.99, 0.90, 0.50, 0.10, 0.01$ ) computed for optimal PTIFC AR(2) model in Figure 2.10, including Brune's source model. (a) 0.04–20s period, (b) 0.1–2s period.

Figure 2.18. Comparison between the 5% damped response spectra of the "target"

accelerogram (solid line), the mean response spectra (dashed-dotted line) and the probabilistic response spectra (dashed lines which from top to bottom correspond to  $p = 0.99, 0.90, 0.50, 0.10, 0.01$ ) computed for optimal PTIFC AR(2) model in Figure 2.10, including Brune's source model. (a) Velocity, (b) Displacement.

Figure 2.19. Comparison between the inelastic response spectra of the "target" accelerogram (solid line), the mean response spectra (dashed-dotted line) and the probabilistic response spectra (dashed lines which from top to bottom correspond to  $p = 0.99, 0.90, 0.50, 0.10, 0.01$ ) computed for optimal PTIFC AR(2) model in Figure 2.10, including Brune's source model. Structural parameters  $n = 3$ ,  $\eta = 0.3$  and  $\zeta = 0.05$ . (a) Acceleration, (b) Velocity.

Figure 2.20. Comparison between the inelastic response spectra of the "target" accelerogram (solid line), the mean response spectra (dashed-dotted line) and the probabilistic response spectra (dashed lines which from top to bottom correspond to  $p = 0.99, 0.90, 0.50, 0.10, 0.01$ ) computed for optimal PTIFC AR(2) model in Figure 2.10, including Brune's source model. Structural parameters  $n = 3$ ,  $\eta = 0.3$  and  $\zeta = 0.05$ . (a) Ductility, (b) Residual Ductility.

Table 2.1. List of some representative accelerograms for assessing stochastic ground motion model.

Table 2.2. Various technical information about the accelerograms in Table 2.1 for PTIFC modelling.

Figure 3.1. (a) Nondimensional time variation of the ground motion intensity for different values of  $\beta$ . (b) Relation between the nondimensional duration and  $\beta$  for  $\lambda = 10$  and  $\lambda = 20$ .

Figure 3.2. Time variation of (a) undamped frequency  $\omega_g$  (solid curves), band-

width  $\omega_g \zeta_g$  (dashed-dotted curves), damping ratio  $\zeta_g$ , and (b) intensity  $I_g$  obtained by the nine-parameter model (smooth curves) and the moving time-window approach (other curves) for the C048.1 record in Table 2.1.

Figure 3.3. Comparison of (a) the C048.1 accelerogram and (b), (c) two artificial accelerograms.

Figure 3.4. Time variation of (a) undamped frequency  $\omega_g$  (solid curves), bandwidth  $\omega_g \zeta_g$  (dashed-dotted curves), damping ratio  $\zeta_g$ , and (b) intensity  $I_g$  obtained by the nine-parameter model (smooth curves) and the moving time-window approach (other curves) for the El Centro Array, Stn 12 record in Table 2.1.

Figure 3.5. Comparison of (a) the El Centro Array, Stn 12 accelerogram and (b), (c) two artificial accelerograms.

Figure 3.6. Comparison of the exact (solid curve) and approximate (dashed-dotted curve) autocorrelation function  $R_{yy}(t, s)$  of the stochastic process modeling the C048.1 accelerogram.

Figure 3.7. The EPSD function plotted at different times (a) C048.1, (b) El Centro Array, Stn 12.

Figure 3.8. Comparison between the 5% response spectra of the C048.1 accelerogram (solid line), the mean response spectra (dashed-dotted line) and the probabilistic response spectra (dashed lines which from top to bottom correspond to  $p = 0.99, 0.90, 0.50, 0.10, 0.01$ ) computed for the nine-parameter optimal model.

Figure 3.9. Comparison between the inelastic response spectra of the C048.1 accelerogram (solid line), the mean response spectra (dashed-dotted line) and the probabilistic response spectra (dashed lines which from top to

bottom correspond to  $p = 0.99, 0.90, 0.50, 0.10, 0.01$ ) computed for the nine-parameter optimal model. Structural parameters  $n = 3$ ,  $\eta = 0.3$ , and  $\zeta = 0.05$ .

Figure 4.1. Number of cycles of oscillations needed for the oscillatory term to decay to  $n\%$  of its maximum value.  $n=1$  (solid curve),  $n=5$  (dashed-dotted curve),  $n=10$  (dotted curve).

Figure 4.2. (a) Comparison between the nondimensional exact (dashed curve) and approximate (solid curve) mean-square displacement response of a linear SDOF oscillator subjected to a modulated (dashed-dotted curve) white-noise excitation.  $\eta = \frac{t_m}{T_0} = 5.0$ .

Figure 4.2. (b) Comparison between the nondimensional exact (dashed curve) and approximate (solid curve) mean-square displacement response of a linear SDOF oscillator subjected to a modulated (dashed-dotted curve) white-noise excitation.  $\eta = \frac{t_m}{T_0} = 2.0$ .

Figure 4.2. (c) Comparison between the nondimensional exact (dashed curve) and approximate (solid curve) mean-square displacement response of a linear SDOF oscillator subjected to a modulated (dashed-dotted curve) white-noise excitation.  $\eta = \frac{t_m}{T_0} = 1.0$ .

Figure 4.2. (d) Comparison between the nondimensional exact (dashed curve) and approximate (solid curve) mean-square displacement response of a linear SDOF oscillator subjected to a modulated (dashed-dotted curve) white-noise excitation.  $\eta = \frac{t_m}{T_0} = 0.5$ .

Figure 4.3. (a) Time variation of normalized mean-square displacement,  $\epsilon_{12}$ ,  $\epsilon_{22}$ , and  $\epsilon_a$  for different damping ratios.  $\beta = 0.5$ ,  $\eta = 5$ . Dotted curve corresponds to the time variation of the input modulation.

Figure 4.3. (b) Time variation of normalized mean-square displacement,  $\epsilon_{12}$ ,  $\epsilon_{22}$ ,

and  $\epsilon_a$  for different damping ratios.  $\beta = 0.5$ ,  $\eta = 1$ . Dotted curve corresponds to the time variation of the input modulation.

Figure 4.3. (c) Time variation of normalized mean-square displacement,  $\epsilon_{12}$ ,  $\epsilon_{22}$ , and  $\epsilon_a$  for different damping ratios.  $\beta = 4$ ,  $\eta = 5$ . Dotted curve corresponds to the time variation of the input modulation.

Figure 4.3. (d) Time variation of normalized mean-square displacement,  $\epsilon_{12}$ ,  $\epsilon_{22}$ , and  $\epsilon_a$  for different damping ratios.  $\beta = 4$ ,  $\eta = 1$ . Dotted curve corresponds to the time variation of the input modulation.

Figure 4.4. Approximate nondimensional mean-square displacement (solid curves) of the response of a linear SDOF oscillator subjected to a modulated (dashed-dotted curve) white-noise excitation.

Figure 4.5. Contour plots of the fractional error  $\epsilon_L$  as defined in (4.112). The excitation is modeled by MODEL 1.

Figure 4.6. Contour plots of  $\lambda(\omega_0)$  as defined in (4.94). The excitation is modeled by MODEL 1.

Figure 4.7. Time variation of (a) the standard deviation and (b) the damped-frequency of the nine-parameter earthquake model fitted to the Orion Blvd. recording.

Figure 4.8. Comparison between the exact (solid curve) and approximate (dashed curve) mean-square displacement response of a linear SDOF oscillator with 5% damping and  $\omega_0 = 7, 5, 3, 1$ Hz. The excitation is the nine-parameter model shown in Figure 4.7.

Figure 4.9. Artificially designed time variation of the standard deviation and the damped-frequency of the nine-parameter excitation model.

Figure 4.10. Comparison between the exact (solid curve) and approximate (dashed

curve) mean-square displacement response of a linear SDOF oscillator with 5% damping and  $\omega_0 = 7, 5, 3, 1$ Hz. The excitation is the nine-parameter model shown in Figure 4.9.

Figure 4.11. Comparison between the exact (solid curve) and approximate (dashed-curve) response of an equivalent linear SDOF oscillator. (a) STD of the response (b) structural frequency  $\omega(t)$ .  $\omega_0 = 5$ Hz,  $\zeta_0 = 0.05$ . The excitation is the nine-parameter model shown in Figure 4.7 whose damped frequency variation is repeated again in (b).

Figure 4.12. Comparison between the exact (solid curve) and approximate (dashed-curve) response of an equivalent linear SDOF oscillator. (a) STD of the response (b) structural frequency  $\omega(t)$ .  $\omega_0 = 1$ Hz,  $\zeta_0 = 0.05$ . The excitation is the nine-parameter model shown in Figure 4.7 whose damped frequency variation is repeated again in (b).

Figure 4.13. Comparisons between the exact (solid curve), the proposed approximate (dashed curve), and Bucher's approximate (dashed-dotted curve) solution for the covariance response of two modes  $i$  and  $j$ .  $\beta = 0.5$ ,  $\zeta = 0.02$ .

Figure 4.14. Comparisons between the exact (solid curve), the proposed approximate (dashed curve), and Bucher's approximate (dashed-dotted curve) solution for the covariance response of two modes  $i$  and  $j$ .  $\beta = 0.5$ ,  $\zeta = 0.05$ ,  $\omega = 1$ Hz.

Figure 5.1. Time variation of (a) the standard deviation  $\sqrt{q_g(t)}$  and (b) the dominant frequency  $\omega'_g(t)$  for the (TV) and the (TI) excitation models fitted to the Orion Blvd. record shown in Figure 2.1(a).

Figure 5.2. Nonstationary linear response characteristics computed for the (TV) (solid curves) and for the (TI) excitation (dashed-dotted curves) for varying structural frequencies  $\omega_0$ . Damping  $\zeta = 0.05$ .

Figure 5.3. Comparison of (a) the r.m.s. displacement responses and (b) the equivalent linear structural frequencies, for the (TV) (solid curve) and (TI) (dashed-dotted curve) excitation.  $\omega_0 = 1.5\text{Hz}$ ,  $\zeta = 0.05$ . Dashed curves correspond to the damped frequencies  $\omega'_g$  of (TV) and (TI) excitations.

Figure 5.4. Comparison of (a) the r.m.s. displacement responses and (b) the equivalent linear structural frequencies, for the (TV) (solid curve) and (TI) (dashed-dotted curve) excitation.  $\omega_0 = 3.2\text{Hz}$ ,  $\zeta = 0.05$ . Dashed curves correspond to the damped frequencies  $\omega'_g$  of (TV) and (TI) excitations.

Figure 5.5. Comparison of (a) the r.m.s. displacement responses and (b) the equivalent linear structural frequencies, for the (TV) (solid curve) and (TI) (dashed-dotted curve) excitation.  $\omega_0 = 6\text{Hz}$ ,  $\zeta = 0.05$ . Dashed curves correspond to the damped frequencies  $\omega'_g$  of (TV) and (TI) excitations.

Figure 5.6. Softening elastic restoring force.

Figure 5.7. Comparison between the normalized EPSD functions computed by the (TV) (dashed curves) model at times 1, 4, 7, 10, 16, 22 seconds and the (TI) (solid curve) model for the Orion Blvd. recording.

Figure 5.8. Nonstationary nonlinear response characteristics computed for the (TV) excitation (solid curves) and the (TI) (dashed-dotted curves) excitations for varying initial structural frequencies.  $\zeta_0 = 0.05$ ,  $x_y = 1/3$ .

Figure 5.9. Comparison between the response characteristics computed for the (TV) (solid curves) and the (TI) (dashed-dotted curves) excitation. (a) r.m.s. displacement of the response (b) equivalent linear structural frequency.  $\omega_0 = 6\text{Hz}$ ,  $\zeta_0 = 0.05$ ,  $x_y = 1/3$ . Dashed curves correspond to the damped frequencies  $\omega'_g$  of (TV) and (TI) excitations.

Figure 5.10. Comparison between the response characteristics computed for the (TV) (solid curves) and the (TI) (dashed-dotted curves) excitation. (a) r.m.s. displacement of the response (b) equivalent linear structural frequency.  $\omega_0 = 6\text{Hz}$ ,  $\zeta_0 = 0.05$ ,  $x_y = 1/5$ . Dashed curves correspond to the damped frequencies  $\omega'_g$  of (TV) and (TI) excitations.

Figure 5.11. Comparison between the response characteristics computed for the (TV) (solid curves) and the (TI) (dashed-dotted curves) excitation. (a) r.m.s. displacement of the response (b) equivalent linear structural frequency.  $\omega_0 = 4\text{Hz}$ ,  $\zeta_0 = 0.05$ ,  $x_y = 1/3$ . Dashed curves correspond to the damped frequencies  $\omega'_g$  of (TV) and (TI) excitations.

Figure 5.12. Comparison between the response characteristics computed for the (TV) (solid curves) and the (TI) (dashed-dotted curves) excitation. (a) r.m.s. displacement of the response (b) equivalent linear structural frequency.  $\omega_0 = 3\text{Hz}$ ,  $\zeta_0 = 0.05$ ,  $x_y = 1/3$ . Dashed curves correspond to the damped frequencies  $\omega'_g$  of (TV) and (TI) excitations.

## Chapter 1

### Introduction

#### 1.1 Motivation and Objectives

In earthquake-resistant design of major civil engineering projects, there are two major problems to be considered. One is predicting structural response to earthquake shaking so that the proposed structure can be designed to respond satisfactorily. This problem is in the domain of the earthquake engineer. The other problem is predicting the ground shaking that a structure may experience during its lifetime. This problem may be considered the domain of the geologist and strong-motion seismologist, although earthquake engineers and geotechnical engineers may also get involved.

The earthquake engineer would like a description of the ground motion which is complete enough to reliably predict the corresponding dynamic response of a structure. Peak ground acceleration alone is clearly too crude for this purpose. A response spectrum provides a better description but it leads to difficulties, for example, in predicting nonlinear response and in-structure equipment response (the so-called “response of secondary systems”). Ideally, the earthquake engineer would like the geologist and seismologist together to provide full time histories of possible ground shaking and their probability of occurrence during the proposed lifetime of the structure.

On the other hand, these scientists are limited by current theory and lack of knowledge of subsurface properties, fault rupture recurrence intervals, and so on, so that only a relatively simple description of the ground motion is possible. For example, the source model of Brune (1970) appears adequate for deterministic

predictions at very low frequencies, given two source parameters such as seismic moment and corner frequency, but the “high”-frequency content (say over 1 Hz) observed in accelerograms is generated at the source by local stress concentrations at “asperities,” a mechanism not well understood. Also, the propagation of these frequencies is affected by variations in material properties which are uncertain on the scale of the wave lengths involved. Thus, deterministic prediction of high-frequency ground motion requires detailed knowledge of the state of the Earth and the physical processes involved which is not usually available. One way to account for the uncertainty in such knowledge is to employ a stochastic process which gives a probabilistic description of the ground shaking.

One goal of this study is to develop a model to characterize ground shaking which is complete enough for structural response studies and yet is simple enough for ground motion prediction. Ideally, we would like a description of strong ground motion which is independent of source and propagation models on the one hand and of structural dynamics models on the other hand. The description would then form a “fixed” interface through which ground motion prediction and structural response prediction can be coupled, while still allowing independent developments in theory and methodology in these two areas. Thus, we want to avoid expressing the ground motion in such a way that it is dependent on a particular structural dynamics model. If response spectra are used, for example, the earthquake engineer faces difficulties in predicting the inelastic response of a structure, since what is given is the peak response of a simple linear system. At the same time, if theoretical source models and propagation models are used to describe the ground motion, these are likely to be inadequate at “high” frequencies. A more complete description is preferable even if it does require complementing the theoretical models with an empirical approach.

The first objective of this thesis is to characterize strong ground motion in terms of a model in such a way that:

- 1) It captures with a small number of parameters the essential features of the ground motion for the purpose of computing dynamic response, including the amplitude and frequency content nonstationarity of the ground motion, and since

a small number of parameters cannot give a complete description of the ground motion time history, a stochastic model is employed.

2) It is simple to use in processing existing accelerograms and estimating the most probable model that gives the “best” fit, in a statistical sense, to the acceleration data;

3) It is efficient to use in simplified analytical random vibration and reliability studies;

4) It is computationally efficient in generating artificial accelerograms for computing structural response using simulations;

5) The model parameters are physically meaningful so that they can be related to variables accounting for the earthquake source mechanism and propagation and local site effects in a seismic risk analysis.

The second objective of this thesis is to approximate the existing lengthy expressions for the covariance of the nonstationary response of linear and equivalent linear systems (derived by applying the equivalent linearization method to nonlinear systems) in such a way that a) the approximations preserve the essential features of the response without significant loss of accuracy, and b) direct insight into the effect of the ground motion nonstationarities on the nonstationary structural response can be gained.

## 1.2 Summary of this Study

A selective review of existing stochastic models is first presented in Chapter 2, and then a general class of parametric models is proposed to stochastically characterize the nonstationarity of both the amplitude and frequency content observed in strong-motion accelerograms. The model is formulated in both continuous and discrete time by differential and difference equations, respectively. The discrete-time formulation leads to a nonstationary autoregressive model of order  $p$  (AR( $p$ )). Using a Bayesian probabilistic framework, a new simple and effective statistical method is developed in the discrete time-domain for extracting the “optimal” nonstationary AR( $p$ ) model from an accelerogram. Representative accelerograms from

different earthquake events are studied by special subclasses of the general class of models in order to assess the extent to which the class needs to be parameterized. The adequacy of each subclass is judged by analyzing the residuals generated by each optimal model, by comparing the target accelerogram and a sample of simulated accelerograms, as well as by comparing the corresponding elastic and inelastic response spectra. Brune’s earthquake source model is incorporated in the model to increase the accuracy of the spectral amplitudes at very low frequencies. The correlation between the time variation of the model parameters and the different wave groups present in strong motion accelerograms is also investigated.

In Chapter 3, a parsimonious probabilistic ground motion model is proposed based on the findings reported in Chapter 2. The model is capable of capturing, with at most nine parameters, all those features of the ground acceleration history which have an important influence on the dynamic response of linear and nonlinear structures, including the amplitude and frequency content nonstationarities of the shaking. The model, which is a special case of the general class of models presented in Chapter 2, is formulated in both continuous and discrete time by stochastic second-order differential and difference equations, respectively. The coefficients of both equations are treated as slowly-varying functions of time. Statistical properties of the stochastic processes generated by these equations are studied in detail, and appropriate conversion relationships are developed to link the two formulations. The proposed ground motion model can be efficiently applied in simulations as well as analytical response and reliability studies of linear and nonlinear structures. The Bayesian statistical method for estimating the model parameters is illustrated by using representative recorded “target” accelerograms. The applicability of the model is checked by comparing the statistics of various linear elastic and inelastic response parameters of a single-degree-of-freedom structure computed for the ground motion model with the deterministic values of the same response parameters computed for the “target” accelerogram.

In Chapter 4, random vibration analysis of both linear and nonlinear (softening) single-degree-of-freedom oscillators subjected to a stochastic excitation is considered. The nonlinearity of the softening structure is accounted for by the equiva-

lent linearization method. A formulation is developed to approximate the original computationally lengthy expressions for the covariance of the transient response of the equivalent second-order linear oscillator by much simpler expressions. The proposed approximation holds for a broad range of oscillator and excitation parameters. In particular, it treats time-varying equivalent linear oscillators with any value of the damping ratio, as well as excitations with time-varying amplitude and frequency content. Classically-damped multi-degree-of-freedom linear systems are also considered and the original equation for the covariance response of two modes is approximated by a much simpler equation. The approximations reduce the computational time involved in computing the response by more than an order of magnitude and they preserve the essential features of the response without significant loss of accuracy. The results provide physically meaningful insight into the characteristics of the nonstationary response to “earthquake-like” excitations.

Chapter 5 uses the ground motion model proposed in Chapter 3 and the approximate simplified expressions for the covariance response developed in Chapter 4 to provide insight into the effect of the ground motion nonstationarities on the response of linear and nonlinear elastic structural models. A simple mathematical analysis demonstrates the effects of softening of nonlinear structural models on their response. It is found that the temporal nonstationarity in the frequency content of the ground motion significantly influences the response of both linear and nonlinear structures, and therefore it should not be neglected in the modeling of strong ground motion.

Conclusions and directions for future work are presented in Chapter 6.

## Chapter 2

# Modeling of Strong Ground Motion by Stochastic Differential and Difference Equations

### 2.1 Introduction

Earthquake accelerograms are obviously nonstationary time series. The non-stationarity is manifested primarily in two different ways. First, the intensity of the ground acceleration varies with time; after arrival of the first seismic waves, it builds up to a maximum value over several seconds and then decreases gradually until it vanishes into the background noise. Second, the frequency content varies with time with a tendency to shift to lower frequencies as time increases. These non-stationarities can be attributed partly to the different intensity, frequency content and arrival times of the P-wave, S-wave and surface-wave groups, and partly due to the finite rupture-time and finite fault area.

The time-domain stochastic models that have been employed in the past to represent one or both of the above non-stationary features have generally had one of the following two types of structure. In Model I, shown in Figure 2.1(a), a stationary white-noise process is passed through a linear system in order to obtain the desired correlation structure (or power spectral density) and the result is multiplied by a deterministic envelope function so that the stationary filtered white noise gets the desired time-dependent variance. In Model II, shown in Figure 2.1(b), the action of the linear system and the envelope function is reversed, so that stationary white noise is multiplied by an envelope function to give non-stationary white noise, which is then fed through a linear system, and the output represents an accelerogram. Models I and II are also referred to as a “modulated stationary process” and a “filtered modulated white-noise process,” respectively. The structure of the linear

system and the envelope function is chosen so that the output stochastic process resembles certain prominent features observed in real accelerograms. The linear system is usually assumed to be described in continuous or discrete time by a linear differential or difference equation, respectively. These equations might have either constant or time-varying coefficients.

Housner and Jennings (1964) have computed and analyzed the response spectra of artificial accelerograms generated by Model I. In their work, the output of the linear system corresponds to the absolute acceleration response of a single-degree-of-freedom oscillator subjected to white-noise base excitation. The power spectral density of the acceleration then has the form proposed by Kanai (1957) and Tajimi (1960). This model was motivated by a simple representation of the dynamics of a surface layer between the ground surface and the basement rock. In order to remove the unrealistic nonzero components at the very low frequency, Clough and Penzien (1975) included a high-pass filter into the low-pass Kanai-Tajimi filter.

The envelope function proposed by Housner and Jennings is composed of a quadratic build-up phase, a constant phase, and an exponentially-decaying tail. Based on a theoretical result, Saragoni and Hart (1974) proposed the envelope function:

$$f(t) = \alpha t^\beta \exp(-\gamma t) \quad 0 \leq t \leq T_0, \quad (2.1)$$

whereas Shinozuka and Sato (1967) suggested the parametric form:

$$f(t) = \alpha (\exp(-\beta t) - \exp(-\gamma t)) \quad 0 \leq t \leq T_0. \quad (2.2)$$

In these expressions,  $T_0$  is the duration of the strong-motion record. The above functions have simple parametric forms and were assumed to be representative of the time variation of the amplitude, or intensity, of ground shaking, thereby modelling the rate of build-up, rate of decay, maximum intensity and strong-motion duration of the accelerograms. These authors employed continuous-time formulations of the models and, with the exception of Saragoni and Hart, the models had a stationary frequency content. The work of Saragoni and Hart (1974) divides each accelerogram into three segments and models the frequency content of each segment by stationary processes. However, the arbitrary division into segments and

the abrupt change in the frequency content from segment to segment is not very satisfactory for simulating strong ground motion.

Recently seismologists have also become interested in the stochastic representation of ground motion with stationary frequency content using simple versions of models I or II but relating the parameters of the model to theoretical models for source mechanisms and wave propagation (for example, Boore, 1983 and Safak, 1988).

Most recently, Yeh and Wen (1989) modeled the time variation of the frequency content by continuously changing the time scale of a stationary stochastic process to obtain a frequency modulated stochastic process. A frequency modulation function was used to relate the time-varying power spectrum to the original stationary process. Methods based on least-squares fit were proposed to separately estimate the frequency and the amplitude modulation of the model. The energy function and the cumulative zero-crossings corresponding to the amplitude and the frequency modulation of the model were fitted to the expected energy function and cumulative zero-crossings of real accelerograms.

The availability of recorded earthquake accelerograms in terms of discrete time series, as well as engineering interest in generating artificial accelerograms for numerical linear and non-linear response predictions, suggest the formulation of a stochastic ground motion model in discrete time. A general class of discrete stochastic models are the autoregressive moving-average (ARMA) models, which are commonly used to give a parsimonious parametric representation of time series which exhibit significant complexity (Box and Jenkins, 1976, Pandit and Wu, 1983).

Recently, several studies have examined the suitability of ARMA models in characterizing ground accelerations. These models can be viewed as belonging to the class of models I and II (Figures 2.1(a) and 2.1(b)), with the linear system represented by a discrete difference equation. In the work by Chang *et al.* (1982), several ARMA models of different orders were identified, parameters were estimated and statistical measures were evaluated to test the goodness of fit between the models and the actual data. In the cases studied, it was found that ARMA(2,1) or ARMA(4,1) models provided good fits to time segments of the earthquake accel-

eration time histories. Polhemus and Cakmak (1981) also used ARMA(2,1) and ARMA(4,1) models for the linear system in Figure 2.1(a) and a polynomial expression for the envelope function. A non-linear least squares procedure was applied to estimate the number of the polynomial terms needed as well as the values of the polynomial coefficients. Using the estimated time-dependent variance of the earthquake accelerogram, a “normalized” series was constructed and a stationary ARMA model was fitted to that series. The estimation of the ARMA parameters was done according to procedures discussed by Box and Jenkins (1976). Comparisons between the response spectra of the original and simulated accelerograms showed good agreement for periods less than five seconds.

In contrast to the work mentioned so far using ARMA models, which did not model the nonstationary frequency content observed in accelerograms, Jurkevics and Ulrych (1978) modeled the time-varying character of both the intensity and the frequency content using nonstationary AR(p) processes. The AR parameters were determined either by segmenting the record or by continuously updating the parameters in a time adaptive manner. To smooth out short-period variations, third degree polynomials were fitted to each of the parameters of a second-order model while Saragoni and Hart’s envelope function was fitted to the white-noise variance. The procedure was successfully demonstrated for the Orion Boulevard recording of the 1971 San Fernando earthquake. In a later study (1979), the same authors used their model to analyze 40 “rock-site” accelerograms obtained during intermediate-sized earthquakes in Southern California. The results of the analysis were used to estimate empirical relationships for the duration and attenuation of shaking amplitude with epicentral distance.

Nau *et al.* (1980, 1982) used a Kalman filtering technique to estimate sequentially the coefficients of the ARMA model. Also, a numerical technique was developed for “nonparametric” estimation of the variance (envelope function) of the earthquake accelerogram. A “nonparametric” scheme for time variation of the parameters of an autoregressive (AR) model was also suggested by Gersch and Kitagawa (1985). They expressed the evolution of the AR parameters by a difference equation with white-noise forcing terms of unknown variance. The initial

conditions of the difference equations and the white-noise variances were the only unknown parameters to be estimated.

In summary, the existing ground motion models formulated in continuous time, with the exception of that developed by Yeh and Wen (1989), fail to incorporate the time variation of the frequency content of the ground motion in a manner that is physically justified and is also efficient to use in both structural response simulations and random vibration analyses. The time variation of both the amplitude and the frequency content of the ground motion can be efficiently modeled in detail by employing nonparametric discrete models. However, these models can only be used to match existing accelerograms and generate artificial accelerograms having similar statistical properties with the “target” one. The lack of a small number of physically meaningful parameters in the model restrict their applicability and make them inappropriate to use in seismic risk studies and in predicting possible future ground motions from a given seismic environment. Although nonparametric discrete models generate artificial accelerograms in a computationally efficient way for use in structural response simulations, they cannot be used for simplified analytical random vibration studies unless a simple continuous version of the model is available.

In this chapter, a general class of parametric stochastic models is proposed to investigate in detail and subsequently model the nonstationarities in both amplitude and frequency content observed in strong-motion accelerograms. A small number of SDOF (single-degree-of-freedom) oscillators acting in series and possibly time-varying replace the linear system in Figure 2.1(a) or (b). Each oscillator is described either in continuous time by a second-order differential equation or in discrete time by an AR(2) difference equation. The discrete-time formulation leads to a time-varying AR(p) model and provides a convenient algorithm for analyzing and simulating accelerograms. For special subclasses of the general class of models, the discrete and the continuous model are linked by developing appropriate conversion relationships.

Certain “target” accelerograms are studied to determine the adequacy of special subclasses of the general class of models in order to assess the extent to which the

class needs to be parameterized. The new contributions in this chapter are as follows:

a) The development of a new simple and effective statistical method, based on a Bayesian probabilistic approach, to determine the “optimal” model, which is the most probable stochastic model, for a given subclass and a given “target” accelerogram. Each optimal model is then used to judge the adequacy of the subclass of ground motion models by analyzing the residuals generated by each optimal model, by comparing the target accelerogram and a sample of simulated accelerograms generated by the optimal model, as well as by comparing various linear elastic and inelastic response parameters of a SDOF structure.

b) The incorporation of Brune’s model (1970) in the stochastic formulation to improve the accuracy of the spectral amplitudes at very low frequencies;

c) The correlation of the time variation of the nonstationary features of the accelerograms with the time variation of the model parameters and the physical interpretation of such variations. Certain average trends concerning the time variation of the model coefficients will be identified;

d) The study of the sensitivity of various response parameters to the details of the ground motion which are left “random” by the stochastic model.

The findings in this chapter will provide background for developing and justifying the use of more parsimonious models in Chapter 3. The ultimate goal of these studies is to develop a simple and more efficient probabilistic representation of ground motion time histories.

## **2.2 General Class of Strong Ground Motion Models**

The ground acceleration time history at a site during an earthquake is treated as a specific realization of an appropriate stochastic process. We focus our study on stochastic processes  $y(t)$  generated by the multiple cascading action of  $M$  second-order linear systems. In order to make the ground motion model efficient to use in analytical random vibration studies and structural response simulations, as well as in estimation of its parameters, both continuous and discrete time formulations are

developed. The equivalence between the continuous and the discrete formulation for specific subclasses of the general class of models is also derived by developing appropriate conversion relationships.

### 2.2.1 Continuous Model

The mathematical form of the model has the continuous-time representation:

$$\begin{aligned} L_j(t, \underline{\theta}) y_j(t) &= y_{j-1}(t), \quad j = 1, \dots, M, \\ y_0(t) &= f(t, \underline{\theta}) e(t), \end{aligned} \tag{2.3}$$

with the time-varying operator  $L_j(t, \underline{\theta})$  being defined by:

$$L_j(t, \underline{\theta}) = \frac{d^2}{dt^2} + 2\zeta_j(t, \underline{\theta})\omega_j(t, \underline{\theta})\frac{d}{dt} + \omega_j^2(t, \underline{\theta}), \tag{2.4}$$

where  $y(t) \equiv y_M(t)$ , and  $e(t)$  is a continuous Gaussian stochastic time series with properties

$$E[e(t)] = 0 \quad \text{and} \quad E[e(t)e(\tau)] = \delta(t - \tau), \tag{2.5}$$

usually referred to as a continuous stationary white-noise process. The symbol  $E[ \ ]$  denotes mathematical expectation. The coefficients  $\omega_j(t, \underline{\theta})$ ,  $\zeta_j(t, \underline{\theta})$  and the modulation function  $f(t, \underline{\theta})$  are deterministic. Their time-varying structure is postulated depending on the application and, in general, it depends on a parameter set  $\underline{\theta}$ . These time-varying coefficients control the time-variation of the amplitude and the frequency content of the stochastic process  $y(t)$ . Note that the set of equations (2.3) is equivalent to a continuous differential equation of order  $2M$ , driven by a modulated continuous white-noise process. Because of the linearity of equation (2.3), the process  $y(t)$  is a zero-mean Gaussian stochastic process. Therefore, the autocovariance function (ACF)  $R_{yy}(t_1, t_2)$  defined as

$$R_{yy}(t_1, t_2) = E[y(t_1)y(t_2)], \tag{2.6}$$

completely describes the probability structure of  $y(t)$ .

### 2.2.2 Discrete Model

Consider values of the continuous stochastic process in Section 2.2.1 at regular time intervals  $\Delta t$ , then a stochastic sequence  $y(k\Delta t)$  is obtained which can be approximately described by difference equations. Digitized earthquake accelerograms are modeled as specific realizations of this discrete stochastic process. To introduce a discrete model which approximates the sampled sequence, we first approximate the dynamics of the second-order continuous equation by the second-order difference equation:

$$y_k^{(j)} - b_{1,k}^{(j)}(\underline{\theta})y_{k-1}^{(j)} - b_{2,k}^{(j)}(\underline{\theta})y_{k-2}^{(j)} = c_{1,k}^{(j)}(\underline{\theta})y_{k-1}^{(j-1)}, \quad j = 1, \dots, M \quad (2.7)$$

where  $y_k^{(j)}$  approximates the value of the process  $y_j(t)$  at time  $t = k\Delta t$ . The forcing function  $y_k^{(0)}$  of the discrete version of model (2.3) is  $y_k^{(0)} = \sigma_k^{(0)}e_k$ , where  $e_k$  is a zero-mean, unit-variance Gaussian white-noise sequence with properties

$$E[e_k] = 0 \quad \text{and} \quad E[e_k e_l] = \delta_{kl}. \quad (2.8)$$

It is easy to show that the output stochastic sequence  $\{y_k\} \equiv \{y_k^{(M)}\}$  satisfies an AR model of order  $p = 2M$ , given by the difference equation:

$$y_k = \sum_{i=1}^p a_{i,k}(\underline{\theta}) y_{k-i} + \sigma_k(\underline{\theta}) e_k, \quad k = 1, \dots, N \quad (2.9)$$

where  $a_{i,k}(\underline{\theta})$ ,  $i = 1, \dots, p$  and  $\sigma_k(\underline{\theta})$  are in general time-varying coefficients which depend on the parameter set  $\underline{\theta}$ . From the linearity of equations (2.9), the output discrete process is also a zero-mean Gaussian process, completely defined by its autocovariance function  $R_{kl} = E[y_k y_l]$ .

In the next section, simplified subclasses of the general class of the model are studied. The autocovariance functions will be used in the next section to study the equivalence between continuous and discrete stochastic processes generated by specific subclasses of the general class of ground motion models (2.3) and (2.7). The coefficients of the discrete model are chosen such that the discrete and the continuous stochastic processes have the same statistical properties, that is, the same autocovariance functions. The resulting conversion relationships allow interpretation of the coefficients of the discrete model in terms of the coefficients of the continuous model, and vice versa. In Section 2.4, a general methodology is presented

to estimate the model parameters. The methodology is illustrated for specific subclasses. Section 2.5 deals with the structural response to ground motions generated by the ground motion model. Numerical results for the analysis and the modeling of real earthquake accelerograms are presented in Sections 2.6 and 2.7.

## 2.3 Subclasses of Strong Ground Motion Model

Although a stationary model fails to describe the nonstationarities observed in accelerograms, its structure constitutes a basis for understanding the more complicated structure of the nonstationary model. Therefore, a mathematical description of the time-invariant linear system is first introduced, and it is then extended to include the time-variation of both the amplitude and frequency content which is observed in real accelerograms.

### 2.3.1 Stationary Stochastic Model

The stationary model is a special case of model (2.3) where both the operators  $L_j(t, \underline{\theta})$  and the modulation function  $f(t, \underline{\theta})$  are time-invariant. The mathematical form of the stationary model has the continuous-time representation:

$$\begin{aligned} L_j y_j(t) &= y_{j-1}(t), \quad j = 1, \dots, M, \\ y_0(t) &= f e(t), \end{aligned} \tag{2.10}$$

with the time-invariant operator  $L_j$  being defined by:

$$L_j = \frac{d^2}{dt^2} + 2\zeta_j \omega_j \frac{d}{dt} + \omega_j^2, \tag{2.11}$$

where  $y(t) \equiv y_M(t)$  is a stationary stochastic process. In this case, the parameter set  $\underline{\theta}$  includes the natural frequencies  $\omega_j$ , the damping ratios  $\zeta_j$ , of each linear equation in (2.10) and the constant forcing term coefficient  $f$ . Because of the stationarity of  $y(t)$ , its autocovariance function depends only on the time difference  $\tau = t_1 - t_2$ , that is,  $R_{yy}(t_1, t_2) = R_{yy}(\tau)$ .

For the case  $M = 1$ , the ACF (autocovariance function)  $R_{yy}$  of the output stationary process  $y(t)$  has the simple closed form (Chang *et al.*, 1982):

$$R_{yy}(t) = \frac{f^2}{4\omega_1^3 \zeta_1 \cos(-\phi_1)} e^{-\zeta_1 \omega_1 t} \cos(\omega_1' t - \phi_1) \tag{2.12a}$$

where

$$\tan\phi_1 = \frac{\omega_1 \zeta_1}{\omega'_1}, \quad \omega'_1 = \omega_1 \sqrt{1 - \zeta_1^2} \quad (2.12b)$$

Note that the ACF is a damped cosine wave, defined completely by the natural frequency and damping coefficient of the model, together with the power  $f^2$  of the input white-noise process.

The sampled stationary stochastic sequence  $y(k\Delta t)$  can be approximated as in (2.7) by the set of the time-invariant second-order difference equations

$$y_k^{(j)} - b_1^{(j)} y_{k-1}^{(j)} - b_2^{(j)} y_{k-2}^{(j)} = c_1^{(j)} y_{k-1}^{(j)}, \quad j = 1, \dots, M \quad (2.13)$$

where  $y_k^{(j)}$  approximates the value of the process  $y_j(t)$  at time  $t = k\Delta t$ . Beck and Park (1984) show how to choose each second-order difference equation so that it constitutes the minimal-parameter discrete model that best fits the dynamics of the oscillator described by the second-order differential equation. The coefficients  $b_1^{(j)}$ ,  $b_2^{(j)}$  and  $c_1^{(j)}$  are selected by imposing two conditions. The first condition enforces the free vibration solutions of the discrete and continuous second-order equation to be equal at each time  $t_k = k\Delta t$ , which results in the relationships:

$$b_1^{(j)} = 2\exp(-\omega_j \zeta_j \Delta t) \cos(\omega_j \sqrt{1 - \zeta_j^2} \Delta t); \text{ if } \zeta_j \leq 1 \quad (2.14a)$$

$$b_1^{(j)} = 2\exp(-\omega_j \zeta_j \Delta t) \cosh(\omega_j \sqrt{\zeta_j^2 - 1} \Delta t); \text{ if } \zeta_j \geq 1 \quad (2.14b)$$

$$b_2^{(j)} = -\exp(-2\omega_j \zeta_j \Delta t) \quad (2.14c)$$

For the second condition, the transfer function of the discrete equation is forced to optimally match the transfer function of the continuous one, in a least-squares sense, over the frequency band from DC to the Nyquist frequency  $1/(2\Delta t)$ . This determines the optimum value of the coefficient  $c_j^{(1)}$ . The accuracy of the approximation deteriorates as the oscillator frequency approaches the Nyquist frequency, that is, as the number of time-steps per period decreases. For 10 time-steps per period, a very accurate discrete model is obtained for the oscillator.

Model (2.13) with forcing function  $y_k^{(0)} = \sigma^{(0)} e_k$  is the discrete version of model (2.10) for the stationary case. The value of  $\sigma^{(0)}$  is determined by enforcing the variances of the discrete and the continuous output processes to be equal. The

output stochastic sequence  $\{y_k\} \equiv \{y_k^{(M)}\}$  satisfies a time-invariant AR model of order  $p = 2M$  of the type

$$y_k = \sum_{i=1}^p a_i y_{k-i} + \sigma e_k, \quad k = 1, \dots, N \quad (2.15)$$

In the case  $M = 1$ , the discrete ACF of the stationary output sequence  $\{y_k\}$  takes the simple closed form (Chang *et al.*, 1982):

$$E[y_k y_{k-i}] = \sigma_y^2 (\sqrt{-a_2})^i \frac{\cos(\lambda_d i - \mu_d)}{\cos(-\mu_d)} \quad (2.16a)$$

where

$$a_1 = b_1^{(1)}, \quad a_2 = b_2^{(1)}, \quad \lambda_d = \cos^{-1} \left( \frac{a_1}{2\sqrt{-a_2}} \right), \quad \mu_d = \tan^{-1} \frac{a_1(1+a_2)}{(1-a_2)\sqrt{-a_1^2 - 4a_2}}, \quad (2.16b)$$

and the variance  $\sigma_y^2$  has the form:

$$\sigma_y^2 = E[y_k^2] = \frac{1-a_2}{1+a_2} \frac{\sigma^2}{(1-a_2)^2 - a_1^2} \quad (2.16c)$$

The discrete autocovariance function is also a damped cosine wave, defined completely by the natural frequency and damping coefficient of the model and the variance of the discrete white-noise input process. Enforcing equality of the respective variances in (2.16c) and in (2.12a) ( $t = 0$ ) for the discrete and the continuous output processes, the relationship between  $\sigma$  and  $f$  is obtained in the form:

$$\frac{1-a_2}{1+a_2} \frac{\sigma^2}{(1-a_2)^2 - a_1^2} = \frac{f^2}{4\omega_1^3 \zeta_1} \quad (2.17)$$

The relationships (2.14a-c) are equivalent to equating separately the frequencies and damping factors of the continuous and discrete ACFs. Thus, these relationships also imply that the ACF of the discrete process approximates the ACF of the continuous process at the time intervals where the first is defined. The order of the approximation is controlled by the differences in the phases of the two ACFs. The accuracy of the approximation deteriorates as the oscillator frequency approaches the Nyquist frequency. For 10 time-steps per oscillator period, the match between

the two ACFs is very good. Note that in the case of  $M = 1$  and for a white-noise forcing function, Nau *et al.* (1980) have shown that choosing an ARMA(2,1) model, rather than an AR(2) model, gives an exact match between the discrete and the continuous ACF at the points where the first is defined. The transfer function of the ARMA(2,1) model gives a slightly better fit to the typical strong-motion spectral amplitudes at the very low frequencies where the AR(2) model has a theoretically incorrect behavior. However, the frequency content of real accelerograms in this range is contaminated by noise and so can lead to unreliable estimation. As it will be seen later, Brune’s source model (1970, 1971), which is based on physical considerations, is employed to correct the very low frequency spectrum in this work.

### 2.3.2 Piecewise Time-Invariant Model

The discrete version of the stationary stochastic model is modified herein to account in a piecewise manner for the time-variation of both the amplitude and the frequency content observed in accelerograms. Mathematically, the piecewise time-invariant (PTI) model is described by the difference equation:

$$y_k = \sum_{i=1}^p a_{i,k} y_{k-i} + \sigma_k e_k \quad (2.18)$$

where the coefficients of this equation and the variance of the white-noise input sequence have the piecewise-constant representation:

$$a_{i,k} = \sum_{l=1}^L a_i^{(l)} R_k^{(l)}, \quad \sigma_k = \sum_{l=1}^L \sigma^{(l)} R_k^{(l)}, \quad (2.19)$$

The superscript  $(l)$  specifies a time segment of initial and final time  $t_{l-1} = N_{l-1}\Delta t$  and  $t_l = N_l\Delta t$  respectively, and  $R_k^{(l)}$  is a rectangular window given by

$$\begin{aligned} R_k^{(l)} &= 1 \quad ; \quad N_{l-1} \leq k \leq N_l \\ &= 0 \quad ; \quad \text{elsewhere.} \end{aligned} \quad (2.20)$$

The coefficients  $a_i^{(l)}$ ,  $\sigma^{(l)}$  are the unknown parameters of the model and together they control both the time variation of the frequency content and the intensity

of the ground acceleration. However, the piecewise-constant representation of the coefficients  $a_{i,k}$  accounts primarily for the time variation of the frequency content. On the other hand, the  $\sigma^{(l)}$ 's account primarily for the time variation of the intensity of the accelerogram. The piecewise time-invariant model will be utilized in Section 2.5 to explore in detail the nonstationarity of strong-motion accelerograms.

In the PTI model, the sequence  $\{y_k\}$  within each segment and sufficiently far from the segment boundaries approaches stationarity. The correlation structure of the sequence during each segment is described by the expressions developed in the previous section for the discrete case or the equivalent continuous stationary process. The parameters in those expressions are replaced by the parameters  $a_i^{(l)}$  and  $\sigma^{(l)}$  corresponding to each segment  $l$ . Close to the boundaries of each segment, the process  $\{y_k\}$  is not stationary since its correlation structure is influenced by the transient effect arising from the sudden change of the coefficients according to (2.19). The more the oscillators are damped, the smaller the nonstationary zone close to the boundaries that is influenced by the transient effect. In applications considered herein, the oscillators are heavily damped and also, for purposes concerning stable parameter estimation, the length of each segment is chosen to be much longer than the time-length of the transient zone. The stationary model is a special case of the PTI model for  $L = 1$ .

### 2.3.3 Envelope-Modulated White Noise Model

The envelope-modulated white-noise (EMWN) model has the discrete form

$$y_k = f_k(\underline{\theta}) e_k, \quad k = 1, \dots, N. \quad (2.21)$$

where  $f_k(\underline{\theta})$  measure the intensity of the accelerogram at time  $t = k\Delta t$ . Examples of parametric functions previously used in modeling the intensity are the envelope functions (2.1) and (2.2) and the one proposed by Jennings and Housner (1964). The EMWN model will prove useful for modeling the intensity of earthquake accelerograms and estimating the envelope parameters independently of the frequency content.

### 2.3.4 Piecewise Time-Invariant Frequency Content Model

The Piecewise Time-Invariant Frequency Content (PTIFC) model has the discrete time representation

$$y_k = f_k(\underline{\theta}) y'_k \quad (2.22)$$

where  $y'_k$ ,  $k = 1, \dots, N$  is the PTI discrete process given in equation (2.18). The piecewise constant representation of the coefficients accounts for the time variation of the frequency content. The slowly-varying envelope function  $f_k(\underline{\theta})$ , which may assume the form (2.1), (2.2), or others, models in a continuous manner the variation of the intensity with time and it does not alter significantly the relative contribution of each spectral component to the output for each segment.

## 2.4 Bayesian Methodology for Parameter Estimation

In this section, a probabilistic methodology for estimating the model parameters is presented. We use probability in the Bayesian sense of a multi-valued logic, so  $p(a/c)$  denotes a measure of the plausibility of the proposition  $a$  given the information in proposition  $c$ . Bayes' theorem is a consequence of the axioms of probability logic:

$$p(a/b, c) = \frac{p(b/a, c) p(a/c)}{p(b/c)}. \quad (2.23)$$

Bayes' theorem can be applied to data to extract information about the values of a parameter set of a model (Box and Tiao, 1973). To illustrate this, let  $M$  denote a given class of stochastic models characterized by a parameter set  $\underline{\theta}$  and let  $\underline{y}$  denote a data sample to be characterized by the model. As we are uncertain what value of  $\underline{\theta}$  is appropriate before the data is examined, we treat the parameters as uncertain variables and use probabilities to quantify our uncertainties about their values. Applying Bayes' theorem for the parameter set  $\underline{\theta}$  and the data  $\underline{y}$ , expression (2.23) takes the form:

$$p(\underline{\theta}/\underline{y}, M) = \frac{p(\underline{y}/\underline{\theta}, M) p(\underline{\theta}/M)}{p(\underline{y}/M)} \quad (2.24)$$

where  $p(\underline{\theta}/M)$  is the probability distribution of  $\underline{\theta}$  prior to the collection of the data, and it is a personal judgement of the plausibility of various values of the parameters.

Relation (2.24) can be rewritten

$$p(\underline{\theta}/\underline{y}, M) = \kappa p(\underline{y}/\underline{\theta}, M) p(\underline{\theta}/M) \quad (2.25)$$

where the form of the  $p(\underline{y}/\underline{\theta}, M)$  can be deduced from the structure of the assumed model, as will be seen later in some specific applications. The constant  $\kappa$  is chosen so that it normalizes  $p(\underline{\theta}/\underline{y}, M)$  according to:

$$\int_{\Omega} p(\underline{\theta}/\underline{y}, M) d\underline{\theta} = 1 \quad , \quad (2.26)$$

where  $\Omega$  is the range of interest of the parameter set  $\underline{\theta}$ . Relation (2.25), which gives the posterior probability distribution of the parameter set  $\underline{\theta}$ , indicates how the prior distribution of  $\underline{\theta}$  is modified by the information from the sample  $\underline{y}$ . The most probable values  $\hat{\underline{\theta}}$  given the data  $\underline{y}$  are those which maximize  $p(\underline{\theta}/\underline{y}, M)$  over  $\Omega$ . These are used to give the most probable model in  $M$ , which is taken to represent the observed process. This choice is clearly the most rational one if a single model in  $M$  is to be chosen, but it is also the correct choice asymptotically for large sample sizes in the sense that representing the whole class  $M$  by the most probable model entails no loss of information when the class  $M$  is identifiable (Beck, 1990).

#### 2.4.1 General AR(p) Model with Time-Varying Coefficients

Let  $M_p$  denote the nonstationary AR(p) model

$$y_k = \sum_{i=1}^p a_{i,k}(\underline{\theta}) y_{k-i} + b_k(\underline{\theta}) e_k, \quad (2.27)$$

where  $e_k$  is a zero-mean, unit-variance Gaussian white-noise sequence and  $a_{i,k}(\underline{\theta})$ ,  $b_k(\underline{\theta})$ ,  $i = 1, \dots, p$  are in general time-varying coefficients which depend on the parameter set  $\underline{\theta}$ . Let also  $\underline{y}_N \equiv [y_1, y_2, \dots, y_n]$  be an observed sequence of the process of interest, then using Bayes' theorem for the sets of variables  $\underline{y}_N$  and  $\underline{\theta}$ , the posterior probability distribution of the model parameters is:

$$p(\underline{\theta}/\underline{y}_N, M_p) = \kappa p(\underline{y}_N/\underline{\theta}, M_p) p(\underline{\theta}/M_p). \quad (2.28)$$

From the structure of the AR(p) model, the value  $y_k$  at the time  $t = k\Delta t$  depends only on the  $p$  previous values  $y_{k-1}, \dots, y_{k-p}$  of the linear process. Therefore, the

probability distribution of the sequence  $y_k$  given the parameter values takes the form:

$$p(\underline{y}_N/\underline{\theta}, M_p) = p(y_N, \dots, y_1/\underline{\theta}, M_p) = \prod_{k=1}^N p(y_k/y_{k-1}, \dots, y_{k-p}, \underline{\theta}, M_p). \quad (2.29)$$

Since each  $e_k$  is a unit Gaussian random variable, the  $p(y_k/y_{k-1}, \dots, y_{k-p}, \underline{\theta}, M_p)$  is also Gaussian, given by:

$$p(y_k/y_{k-1}, \dots, y_{k-p}, \underline{\theta}, M_p) = \frac{1}{\sqrt{2\pi}b_k(\underline{\theta})} \exp \left[ -\frac{1}{2b_k^2(\underline{\theta})} \left( y_k - \sum_{i=1}^p a_{i,k}(\underline{\theta}) y_{k-i} \right)^2 \right] \quad (2.30)$$

It is assumed that the  $p(\underline{\theta}/M_p)$  is a locally non-informative prior distribution for the parameter set  $\underline{\theta}$ , which means that all values of the parameters over a large range are considered equally plausible a priori (Box and Tiao, 1973). Mathematically, it is assumed that  $p(\underline{\theta}/M_p)$  is constant over a large but finite range of interest  $\Omega$ . Using this assumption and (2.28), (2.29), and (2.30), the posterior probability distribution of the parameters given the data  $\underline{y}_N$  and the model  $M_p$ , takes the form:

$$p(\underline{\theta}/\underline{y}_N, M_p) = \frac{1}{c} \frac{1}{\prod_{k=1}^N b_k(\underline{\theta})} \exp \left[ -\frac{1}{2} \sum_{k=1}^N \frac{(y_k - \sum_{i=1}^p a_{i,k}(\underline{\theta}) y_{k-i})^2}{b_k^2(\underline{\theta})} \right] \quad (2.31)$$

Expression (2.31) gives the updated joint probability distribution of the parameter set  $\underline{\theta}$ , given the data sequence  $\underline{y}_N$  and the class of models  $M_p$ . The most probable value  $\hat{\underline{\theta}}$  of the model  $M_p$  is obtained by maximizing relation (2.31) and it defines the ‘‘optimal’’ AR(p) model to represent the given sample accelerogram  $\underline{y}_N$ . Defining a more convenient function  $F(\underline{\theta})$ , such that

$$\begin{aligned} F(\underline{\theta}) &= -\ln p(\underline{\theta}/\underline{y}_N, M_p) \\ &= \ln c + \sum_{k=1}^N \ln b_k(\underline{\theta}) + \frac{1}{2} \sum_{k=1}^N \frac{(y_k - \sum_{i=1}^p a_{i,k}(\underline{\theta}) y_{k-i})^2}{b_k^2(\underline{\theta})}, \end{aligned} \quad (2.32)$$

the optimization problem is converted to a nonlinear minimization of the objective function  $F(\underline{\theta})$ .

Expression (2.32) is the general formula for obtaining the most probable non-stationary AR(p) model and is independent of the choice of the parametric form for

the coefficients  $a_{i,k}$  and  $b_k$ . The above method is simple and it is developed fully in the time domain utilizing the acceleration data directly in its digitized form. Unlike frequency-domain methods which are applicable only to stationary cases, the present time-domain method a) is applicable to the estimation of the nonstationary features of accelerograms, b) it can directly incorporate smooth parametric variations of the model parameters and c) it simultaneously treats the amplitude and the frequency content nonstationarities. Next, we specialize expression (2.32) for specific subclasses of the general class of models.

### 2.4.2 Piecewise Time-Invariant Model

Recall that the coefficients of the piecewise time-invariant model have the representation (2.19), so after algebraic manipulations, the posterior probability distribution of the parameter set  $\underline{\theta}$  takes the form:

$$p\left(\underline{\theta}/\underline{y}_N, M_p\right) = \prod_{l=1}^L p^{(l)}\left(\underline{\theta}^{(l)}/\underline{y}_N, M_p\right) \quad (2.33)$$

where

$$\begin{aligned} \underline{\theta}^{(l)} &= \left(a_1^{(l)}, \dots, a_p^{(l)}, \sigma^{(l)}\right), \\ p^{(l)}\left(\underline{\theta}^{(l)}/\underline{y}_N, M_p\right) &= \frac{1}{c^{(l)} \sigma^{(N_l - N_{l-1})}} \exp \left[ \frac{-1}{2 [\sigma^{(l)}]^2} \sum_{k=N_{l-1}+1}^{N_l} \left( y_k - \sum_{i=1}^p a_i^{(l)} y_{k-i} \right)^2 \right] \end{aligned} \quad (2.34)$$

Expression (2.33) implies that the parameter subsets  $\underline{\theta}^{(l)}$  corresponding to different segments are statistically independent. Thus, the most probable values are obtained by maximizing each  $p(\underline{\theta}^{(l)}/\underline{y}, M_p)$  independently.

For simplicity, introduce for each  $l$  the set  $\{\hat{y}_i^{(l)}, i = 1, \dots, N^{(l)}\}$  such that for all  $l$ :

$$y_{N_{l-1}-p+i} = \hat{y}_i^{(l)}, \quad i = 1, \dots, N^{(l)} \quad (2.35)$$

where  $N^{(l)} = N_l - N_{l-1}$ . Then using (2.34), the corresponding objective function  $F^{(l)}(\underline{\theta}^{(l)})$  can be rewritten more conveniently as:

$$\begin{aligned} F^{(l)}(\underline{\theta}^{(l)}) &= \ln c + N \ln \sigma + \frac{1}{2\sigma^2} (\underline{\hat{y}} - \underline{\hat{z}})^T (\underline{\hat{y}} - \underline{\hat{z}}) \\ &\quad + \frac{1}{2\sigma^2} (\underline{a}_p - \underline{\hat{a}}_p)^T (\hat{Y}^T \hat{Y}) (\underline{a}_p - \underline{\hat{a}}_p) \end{aligned} \quad (2.36)$$

where

$$\hat{\underline{a}}_p = \left( \hat{Y}^T \hat{Y} \right)^{-1} \hat{Y}^T \hat{\underline{y}} \quad (2.37a)$$

$$\hat{\underline{z}} = \hat{Y} \hat{\underline{a}}_p, \quad \hat{Y}^T = \begin{pmatrix} \hat{y}_p & \hat{y}_{p+1} & \cdots & \hat{y}_{N-1+p} \\ \hat{y}_{p-1} & \hat{y}_p & \cdots & \hat{y}_{N-2+p} \\ \vdots & \vdots & \ddots & \vdots \\ \hat{y}_1 & \hat{y}_2 & \cdots & \hat{y}_N \end{pmatrix}, \quad (2.37b)$$

$$\hat{\underline{y}} = \begin{pmatrix} \hat{y}_{p+1} \\ \hat{y}_{p+2} \\ \vdots \\ \hat{y}_{N+p} \end{pmatrix}, \quad \underline{a}_p = \begin{pmatrix} a_1 \\ a_2 \\ \vdots \\ a_p \end{pmatrix} \quad (2.37c)$$

We have dropped the superscript  $l$  in equations (2.36) and (2.37) for clarity. For this case, the minimization of (2.36) results in a closed form expression for the most probable values of the model parameters in the form  $\hat{\underline{\theta}}^{(l)} = (\hat{\underline{a}}_p^{(l)}, \hat{\sigma}^{(l)})$ , where  $\hat{\underline{a}}_p^{(l)}$  is given by (2.37a) and  $\hat{\sigma}^{(l)}$  is given by:

$$\left[ \hat{\sigma}^{(l)} \right]^2 = \frac{1}{N^{(l)}} \left( \hat{\underline{y}}^{(l)} - \hat{\underline{z}}^{(l)} \right)^T \left( \hat{\underline{y}}^{(l)} - \hat{\underline{z}}^{(l)} \right) \quad (2.38)$$

### 2.4.3 Envelope-Modulated White-Noise Model

For the envelope-modulated white-noise model defined by (2.21), the objective function  $F(\underline{\theta})$  takes the form:

$$F(\underline{\theta}) = \ln c + \sum_{k=1}^N \ln f_k(\underline{\theta}) + \frac{1}{2} \sum_{k=1}^N \frac{y_k^2}{f_k^2(\underline{\theta})}. \quad (2.39)$$

The condition that is satisfied at the minimum of  $F(\underline{\theta})$ , is:

$$\frac{\partial F(\hat{\underline{\theta}})}{\partial \theta_i} = \sum_{\kappa=1}^N \left[ 1 - \frac{y_k^2}{f_k^2(\hat{\underline{\theta}})} \right] \frac{\partial \left[ \ln f_k(\hat{\underline{\theta}}) \right]}{\partial \theta_i} = 0 \quad (2.40)$$

where  $\hat{\underline{\theta}}$  is the value at which the minimum is attained and  $\theta_i$  is the  $i$ -th parameter of the envelope function  $f_k(\underline{\theta})$ . For  $\theta_i = \alpha$ , the scaling parameter for the envelopes (2.1) or (2.2), condition (2.40) gives

$$\frac{1}{N} \sum_{\kappa=1}^N \left( \frac{y_k}{f_k(\hat{\underline{\theta}})} \right)^2 = 1. \quad (2.41)$$

Therefore using the proposed methodology, the most probable envelope function  $\hat{f}_k = f_k(\hat{\theta})$  is chosen so that the process  $\{y_k/\hat{f}_k, k = 1, \dots, N\}$  has unit sample variance. In general, the optimum value  $\hat{\theta}$  cannot be determined analytically but must be calculated numerically using a minimization algorithm.

#### 2.4.4 Piecewise Time-Invariant Frequency Content Model

The procedure which estimates the parameters of a piecewise time-invariant frequency content (PTIFC) model given an accelerogram is divided into three steps.

*Step 1.* The envelope-modulated white-noise model is utilized to model the intensity of an accelerogram in a prescribed interval  $[t_0, t_1]$ , and the most probable envelope  $\hat{f}(t)$  is estimated by minimizing (2.39). In this case,  $\hat{f}(t)$  is a prescribed continuous-time measure of the standard deviation of the process (equations (2.1) or (2.2), for example) with the optimal estimates of the parameters.

*Step 2.* A time series with constant intensity is obtained by dividing the original accelerogram by the estimate of its time-varying standard deviation  $\hat{f}_k$ , according to

$$\hat{y}_k = \frac{y_k}{\hat{f}_k} \quad k = 1, \dots, N. \quad (2.42)$$

*Step 3.* The “optimal” model with frequency content which is either time-invariant or piecewise time-invariant is obtained using the transformed constant-variance series  $\{\hat{y}_k, k = 1, \dots, N\}$  as described in Section 2.4.2. For parameter estimation purposes, the length of each segment in the piecewise time-invariant case must be chosen:

- a. short enough so that the predominant frequency of the modeled segment remains almost constant over its length and
- b. long enough so that the estimation procedure is capable of reliably determining the information about the frequency content of the segment.

The estimation procedure was divided into three steps to avoid interaction during the optimization between the parameters accounting for the time variation of the amplitude and the frequency content. This interaction, when it was consid-

ered with an inadequate model (for example, the number of segments  $L$  was not sufficient to model an accelerogram with significant time-varying frequency content), led to erroneous results for the most probable envelope function. In addition, the three-step procedure is computationally efficient for the piecewise time-invariant model. In this case, the most probable model is obtained explicitly by the formulas (2.37a) and (2.38) and by an additional numerical minimization of the nonlinear three-parameter function (2.39). However, in the case where the parameters are optimized simultaneously, a numerical minimization of the nonlinear  $(pL+3)$ -parameter function (2.32) is involved.

## 2.5 Structural Response and Ground Motion Model Adequacy

The purpose of this section is to study the adequacy of ground motion models from the structural response point of view. In past studies, the adequacy of a ground motion model was judged by how well it models certain features of the target accelerogram. A few studies have compared linear structural response parameters computed from the simulated and the original accelerograms. However, a few simulations do not provide enough information about the statistics of the structural response, nor do they determine whether the structural response corresponding to the original accelerogram falls within the statistics computed for the ground motion model.

This section deals with the linear elastic and nonlinear inelastic structural response to ground motion defined by the ground motion models. A simple hysteretic model is first defined and then it is used to formulate the equation of motion of a SDOF structure in terms of the ductility of the response. Linear elastic models can be treated as a special case. Finally, the problem of assessing the adequacy of a ground motion model using the statistics of various response parameters is addressed. Applications of this study will be given in Section 2.7, where the modeling of several accelerograms is discussed.

### 2.5.1 Nonlinear Hysteretic Model

References and discussion about various nonlinear hysteretic models may be found in Thyagarajan (1989). For the purpose of this study, it is desirable to use a simple, practical and yet general enough force-deflection relation which is useful to model the dynamic behavior of a wide range of softening materials and structures. The force-deflection relation for the virgin loading of the hysteretic model used in the present study is given by the differential equation

$$\frac{dR}{dx} = K \left[ 1 - \left| \frac{R}{R_u} \right|^n \right] \quad (2.43)$$

The three model parameters  $K$ ,  $R_u$  and  $n$  are sufficient to capture the essential features of the hysteretic behavior being modeled.  $K$  is the initial stiffness,  $R_u$  is the ultimate strength and  $n$  controls the smoothness of the transition from elastic to plastic response of the force-deflection curve. The effect of  $n$  on the force-deflection relation is shown in Figure 2.2 taken from Jayakumar (1987). The force-deflection relation for any loading other than the virgin loading is given by the differential equation

$$\frac{dR}{dx} = K \left[ 1 - \left| \frac{R - R_0}{2R_u} \right|^n \right] \quad (2.44)$$

where  $R_0$  is the restoring force at the point of load reversal chosen appropriately to satisfy the rules for transient loading presented by Jayakumar (1987). The inconsistencies and difficulties associated with the way other models (Wen, 1976 and 1980, and Ozdemir, 1976) handle initial loading, unloading and reloading are eliminated because of a better modeling of the steady-state and transient-loading response behavior. A more complete discussion and comparison of this model with other hysteretic models as well as its application in system identification of hysteretic structures may be found in Jayakumar (1987).

The hysteretic loops for the model (2.44) are closed and exhibit no drift as shown in Figures 2.3 and 2.4. An important feature of the model is that the initial stiffness  $K$  and the ultimate strength  $R_u$  may be selected in a manner that is physically meaningful. For example, they can be determined during design from material properties and the structural drawings of a building. Next, the model is incorporated into the equation of motion of a SDOF structure.

### 2.5.2 Equation of Motion

The SDOF structure under consideration is schematically shown in Figure 2.5. The governing equation of motion of the structure subjected to a horizontal earthquake ground excitation  $y(t)$  is

$$M\ddot{x}(t) + C\dot{x}(t) + R(t) = -My(t) \quad (2.45)$$

where  $M$  is the mass of the system and  $C$  is the viscous damping coefficient. The displacement of the mass  $M$  relative to the ground is denoted by  $x(t)$ . The restoring force  $R(t)$  is nonlinear hysteretic and it is given by (2.43) and (2.44). Define the displacement ductility of the response by

$$\mu(t) = \frac{x(t)}{x_y} \quad (2.46)$$

where

$$x_y = \frac{R_u}{K} \quad (2.47)$$

is the nominal yield displacement of the structure, then the equation of motion (2.45) is given in terms of the ductility of the response as follows

$$\ddot{\mu}(t) + 2\zeta\omega_0\dot{\mu}(t) + \omega_0^2\rho(t) = -\frac{\omega_0^2}{\eta} \frac{y(t)}{g} \quad (2.48)$$

where

$$\omega_0 = \sqrt{\frac{K}{M}} \quad \text{and} \quad \zeta = \frac{C}{2M\omega_0} \quad (2.49)$$

is the initial natural frequency and viscous damping ratio of the structure respectively,

$$\rho(t) = \frac{R(t)}{R_u} \quad (2.50)$$

is the normalized restoring force,  $R_u$  is the ultimate structural strength and

$$\eta = \frac{R_u}{Mg} \quad (2.51)$$

is the nondimensional parameter expressing the structure's strength relative to its weight. The normalized restoring force  $\rho(t)$  is governed by

$$\frac{d\rho}{d\mu} = 1 - |\rho|^n, \quad (2.52)$$

which is the nondimensional version of (2.43). The structural parameters which influence the response are the initial angular frequency  $\omega_0$ , the damping ratio  $\zeta$ , the strength coefficient  $\eta$ , and the parameter  $n$  controlling the transition from the elastic to the plastic response.

Since a stochastic ground motion model is used to probabilistically handle the details of the ground acceleration time history, the structural response to the ground motion is also going to be probabilistic. Simulations can be used to obtain the statistical distribution of various structural response parameters. The remainder of this section deals with the definitions of the probabilistic linear elastic and inelastic response spectra associated with various structural response parameters, and their use in judging the adequacy of a ground motion model.

### 2.5.3 Probabilistic Linear Elastic and Inelastic Response Spectra

The response spectrum can be used in structural engineering to characterize the response of a single-degree-of-freedom linear oscillator with undamped natural frequency  $\omega_0$  and damping ratio  $\zeta$  to a ground motion input. The spectra plotted as a function of frequency  $\omega_0$  is one means of assessing the frequency content of the strong ground motion. For a deterministic input, the response spectrum is defined as a function of  $\omega_0$  and  $\zeta$  as

$$RS(\omega_0, \zeta) = \max_{0 \leq t < \infty} |q(t)| \quad (2.53)$$

where  $q(t)$  might stand for either displacement or velocity or acceleration of the oscillator.

When a stochastic model is used to characterize an earthquake, an extension to the deterministic response spectrum is necessary. If the input of the oscillator is a stochastic process, then the oscillator response  $q(t)$  will be a stochastic process as well. In this case, the quantity that replaces (2.53) could be the mean response spectrum defined as

$$E[RS(\omega_0, \zeta)] = E \left[ \max_{0 \leq t < \infty} |q(t)| \right] \quad (2.54)$$

The mean response spectrum is a measure of the maximum response  $q(t)$  attained by the oscillator, on the average. A more important quantity for design is the level

which has some probability of not being exceeded. This leads to the definition of the probabilistic response spectrum for a level of confidence  $p$  as the value  $PRS(\omega_0, \zeta, p)$  for which the probability relation

$$Prob\{RS(\omega_0, \zeta) \leq PRS(\omega_0, \zeta, p)\} = p \quad (2.55)$$

holds.

The utility of the probabilistic response spectrum is due to the fact that it answers in probabilistic terms the question of whether a structure will “safely” sustain a given class of stochastic ground motion. Thus, when stochastic models are utilized to quantify our uncertainty of the ground motion, probabilistic response spectra are useful tools to assess the threat posed to structures, despite the simple theoretical basis of the spectra. For a fixed  $\zeta$ , the level curves with confidence  $p$  not to be exceeded, where  $p$  ranges between 0 to 1, give a good picture of the statistical distribution of the response quantity under consideration for different  $\omega_0$ .

For an inelastic structure, the use of PRS can be extended to provide the statistical distribution of various response parameters indicative of damage. In general, let  $q(\underline{\theta}_s)$  be a response parameter and  $\underline{\theta}_s$  be the set of the structural parameters influencing the response. For example,  $\underline{\theta}_s = (\omega_0, \zeta, \eta, n)$  for the hysteretic structure (2.48). The mean response defined by

$$q_m(\underline{\theta}_s) = E[q(\underline{\theta}_s)] \quad (2.56)$$

is a measure of the response attained by the oscillator, on the average. The level curves  $q(\underline{\theta}_s, p)$  for a level of confidence  $p$ , are defined such that the probability relation

$$Prob\{q(\underline{\theta}_s) \leq q(\underline{\theta}_s, p)\} = p \quad (2.57)$$

holds. The level curves provide information about the statistical distribution of the response parameter  $q(\underline{\theta}_s)$ . A probabilistic inelastic response spectrum is defined as the set of level curves  $q(\underline{\theta}_s, p)$  plotted versus one structural parameter while holding the other structural parameters fixed. Each curve corresponds to different values of  $p$  ranging between 0 to 1. The inelastic probabilistic response spectra provide an insight into the statistics of various inelastic response parameters and

their sensitivity with respect to structural parameters, and with respect to the details of the ground motion.

These response spectra will be used in Section 2.7 to study the sensitivity of various structural response parameters to the details of the ground motion which are left random by the ground motion model, as well as to evaluate the adequacy of the ground motion models to represent all the important features present in the accelerograms. For this, the mean response and the level curves of confidence  $p = 0.01, 0.1, 0.5, 0.9$  and  $0.99$  are computed for 500 simulations using the optimal model for a given “target” accelerogram. To enable comparisons between different models, the same 500 white-noise samples are used for each probabilistic inelastic response spectrum. The response parameter corresponding to the target accelerogram is also plotted. Since a target accelerogram is considered to be a sample of the underlying stochastic process, its response in most of the ranges of structural parameters should lie between the 1% and 99% level curves. In addition, the variation of the mean response corresponding to the stochastic process should approximately follow the average variation of the deterministic response. The ranges of structural parameters for which the target accelerogram response lies below the 1% and above the 99% level curves can be taken as the ranges for which the ground motion model does not perform well. Also, a measure of the sensitivity of the response to the details of the ground motion which are left random by the ground motion model is provided by the difference of the logarithm values corresponding to the 1% and 99% level curves. Therefore, plotting of the probabilistic response spectra on a logarithmic scale gives a direct measure of the sensitivity by the separation of the 1% and 99% level curves.

## 2.6 Analysis of Earthquake Accelerograms Using Autoregressive Models

### 2.6.1 Moving Time-Window Approach

A moving time-window approach is first used to analyze in detail the non-

stationarity of the accelerograms. Stationary AR(p) models are fitted to successive segments of the accelerogram. Each segment is centered at a time  $t_m$  and has length  $w$ . Using (2.37) and (2.38), the most probable AR model is estimated for each segment. By moving  $t_m$  from the beginning to the end of the record using time steps  $\Delta t_s$ , the nonstationarity of the accelerogram is obtained in terms of the time variation of the model parameters. For the second-order model, the natural frequency  $\omega_1$ , damping ratio  $\zeta_1$  and standard deviation  $\sigma_{y_k}$  can be computed according to the expressions (2.14) and (2.16c) respectively.

### 2.6.2 Physical Interpretation of Time Variation of the Model Coefficients

The earthquake accelerograms, listed in Table 2.1 under their Caltech record name, are analyzed using the second-order model. The records are representative of different types of earthquake events. The acceleration time histories are shown in Figure 2.6. The objective of this analysis is to investigate in detail the time-variation of the correlation structure of the accelerograms in terms of the model parameters and then link it to the corresponding physical processes involved. The undamped frequency  $\omega_1$ , the bandwidth  $\omega_1\zeta_1$  and the damping ratio  $\zeta_1$ , computed by the moving-window approach, are plotted in Figure 2.7, while the standard deviation  $\sigma_{y_k}$  is plotted in Figure 2.8. In the computations,  $\Delta t_s = 0.2$  seconds and the value of  $w$  is shown in Table 2.1.

Although the plots in Figures 2.7 and 2.8 are complicated, certain similarities are observed regarding their time variation for the different earthquake events analyzed. In general, there is a high and a low-frequency variation of the model parameters. The high-frequency variation is a feature of the modeling procedure and it can be smoothed out by increasing the time length of the segment used in the analysis. Primary attention is therefore given to the low-frequency variation. The accelerograms from the San Fernando and the Imperial Valley earthquakes show a significant time variation of the parameters  $\omega_1$  and  $\zeta_1$ . However, the accelerograms from the Helena and Parkfield earthquakes, which are much shorter in duration, could be considered to have constant frequency content throughout the strong shaking, that is, the first four and five seconds of the accelerograms,

respectively. In general, the undamped frequency  $\omega_1$  is decreasing with time while the damping ratio  $\zeta_1$  is increasing with time. In order to interpret the results, we consider the physics of the earthquake process and the resulting wave propagation through the Earth's structure.

Several different kinds of waves are propagated from a disturbance in the Earth. The complexity of the Earth structure results in dispersive body waves (P and S) as well as surface waves. P-waves, which are propagated with the highest velocity, reach the recording site first. S-waves, which have lower velocity of propagation and lower frequency content than P-waves, arrive at a later time. Surface waves, which have even lower velocities of propagation and lower frequency content, reach the recording site after the initial body waves have arrived. The arrival time and the intensity of each wave type depend on the source mechanism, the distance between the source and the site and the complexity of the Earth's structure, resulting in a complex recording with its frequency content in general moving towards lower frequencies with time. The undamped frequency  $\omega_1$ , which is an approximate measure of the predominant frequency present in the accelerogram, is expected to decrease with time. The damping ratio  $\zeta_1$ , which is a measure of the width of the frequency range around  $\omega_1$  which contributes strongly to the accelerogram, is expected to increase with time. The large increase in damping observed in Figure 2.7 at later times is due to the presence of both the lower-frequency surface waves and the higher-frequency body waves, resulting in a more broadband process. An observation common for several accelerograms is that the damping ratio of the second-order model is of the order of 20 to 30% for P and S-waves and only when surface waves are arriving does the damping ratio increase to values as high as 60% or more. These observations are important in structural response and should be taken into account in the ground motion modeling.

The curves in Figures 2.7 and 2.8 can be utilized for identifying the presence, and quantifying the duration, intensity and frequency content, of the different wave groups present in strong-motion accelerograms. Such information is difficult to obtain by direct examination of the acceleration time histories because of the overlapping of the different wave groups. For illustration purposes, the three com-

ponents of the C048 record are analyzed. This record was obtained at 8244 Orion Boulevard in the San Fernando Valley, with the epicenter of the 1971 earthquake approximately due North of the site. Recall that each wave group has a different frequency content, and therefore its arrival time corresponds to the time at which a substantial change of the parameters  $\omega_1$  and  $\zeta_1$  of the stochastic model occurs. In the two horizontal components, such changes occur in Figure 2.7(a,b) at approximately 2, 10 (see  $\omega_1$ -curves) and 15 (see  $\zeta_1$ -curves) seconds. Also, the time variation of the wave group intensity consists of an initial build-up phase followed by a peak and then a decaying tail. The peaks show up in Figure 2.8(a,b) at approximately 7, 12 and 19 seconds. These peaks correspond to different wave groups since the value of the model parameter  $\omega_1$  is different for each peak, ranging from 3 to 4 Hz for the first, 1.5 to 2.5 Hz for the second and 0.5 to 1.0 Hz for the third. Considering wave propagation phenomenon, the first peak corresponds to an S-wave group while the second and the third might correspond to surface wave groups (Love and Rayleigh waves). Weak P-waves show up in the first 2 seconds in the horizontal components with the value of  $\omega_1$  ranging from 4 to 5 Hz. These P-waves clearly show up as the dominant waves in the first 10 seconds in the vertical component in Figures 2.7(c) and 2.8(c). The third peak observed in the two horizontal component, is also recorded in the vertical component, suggesting it is possibly due to Rayleigh waves reflected back from the Santa Monica Mountains to the south of the site. The problem of reliably identifying the presence of each wave group in accelerograms can be resolved better by correlating the results obtained from the analysis of several spatially-distributed accelerograms. This analysis, as well as the consistency observed between the time variation of the model parameters and the different wave groups present in strong-motion accelerograms will be used in future work to develop appropriate relations between the model parameters and the variables accounting for the regional seismicity and the local site effects.

## 2.7 Modeling and Simulation of Earthquake Accelerograms

The objectives of this section are as follows:

- 1) to introduce different subclasses of the general class of models and to verify

the extent to which each subclass characterizes the important features observed in real accelerograms by comparing a) the “target” accelerograms with samples of simulated accelerograms generated by each optimal model, b) the corresponding response spectra and c) the residuals and their Fourier transforms generated for each optimal model. In particular, the effects of higher-order models are studied;

2) to demonstrate how well the statistical time-domain method performs when it is used to estimate the model parameters;

3) to use the probabilistic response spectra to study the sensitivity of various linear elastic and inelastic response parameters to the details of the ground motion which are left random by each ground motion model.

### 2.7.1 Modeling of the Intensity Using Various Models

The envelope functions (2.1) and (2.2) proposed by previous authors to model the intensity of the accelerograms are computed by fitting the envelope-modulated white-noise model. To enable comparisons with the piecewise time-invariant results in Figure 2.8, the most probable envelopes are also plotted in the same Figure for different estimation intervals  $[t_0, t_1]$ . In general, the fit for the envelope (2.1) is better for the cases where the “energy” in the interval of estimation is mostly contributed by the shear-wave groups. This suggests that the shape of the envelope models the time-variation of the intensity of the shear waves quite well. This observation supports the theory developed by Saragoni and Hart (1974) that the time variation of the expected intensity of a wave type propagating through the Earth follows a distribution given by the envelope (2.1). For the time intervals  $[t_0, t_1]$  which include significant energy also from the P-wave and surface-wave groups, the envelope function gives an overall fit to the data, usually underestimating the high intensity of the shear-wave groups and overestimating the lower intensity P-wave (in the case of horizontal components) and surface-wave groups. For these intervals, using the family of curves (2.2), the fit is generally improved.

The envelope functions (2.1) and (2.2) fail to provide a good fit to the initial nonzero intensity always present in the digitized accelerograms coming from analog

accelerographs, and also to the time of the maximum intensity. As can be seen in Figure 2.8, a significant improvement is obtained by considering the four-parameter envelope function:

$$f(t) = \alpha (t + t_0)^\beta \exp(-\gamma(t + t_0)) \quad 0 \leq t \leq T_0, \quad (2.58)$$

which is the Saragoni and Hart’s envelope function shifted in time by  $t_0$ . Therefore, since this envelope function is more flexible to fit the data, it is used to model the intensity of the accelerographs in what follows.

### 2.7.2 Modeling of the Frequency Content Using PTIFC Models

In order to explore the time variation of the frequency content, we consider different numbers  $L$  of segments and we vary the order  $p$  of the AR model from 2 to 8. Although not all of the results are presented, conclusions listed herein are based on detailed analysis of the accelerographs contained in Table I using different subclasses of the model. These accelerographs cover a wide range of ground motion characteristics in both intensity and frequency content. The N00W horizontal component of the C048 record which has a significant time variation of the frequency content is chosen as an example to demonstrate the three steps involved in the modeling procedure. Figure 2.9 shows the transformed series of stationary intensity, constructed according to step 2 in Section 2.4.4 for the most probable envelope function with the form of equation (2.58).

The time-invariant frequency content models are first used to model and simulate this component. The “target” accelerogram and one simulation for each of the second and fourth-order time-invariant frequency content model are shown in Figure 2.10(a,b,c). The plots correspond to the same white-noise sample to aid in comparison of different models. Figure 2.11(a,b) shows the corresponding “white-noise” sample  $\{\hat{e}_k\}$  that generates the “target” accelerogram for each model corresponding to Figure 2.10 (b, c). Such a sample is obtained from equation (2.18) after replacing its parameters with the computed most probable ones and using the real acceleration data sequence. It is obvious from the plots (a), (b) and (c) in Figure 2.10 and the plots (a) and (b) of the residuals in Figure 2.11 that a time variation

of the frequency content is exhibited which is not modeled by the time-invariant frequency-content models. From the probabilistic linear response spectra curves shown in Figure 2.12(a,b) for  $p = 2$  and 4, it is concluded that higher-order models do not significantly improve the match between the probabilistic response spectra and the response spectra of the “target” accelerogram. Although only the acceleration response spectra are shown, similar response characteristics are observed for the displacement and the velocity response spectra.

Since the time variation of the frequency content is expected to be of substantial importance for strongly excited nonlinear (softening) structures, its incorporation into the ground motion model must be considered. The piecewise time-invariant frequency content models are thus used to examine the time variation of the frequency content. Simulations for the N00W component are shown in Figure 2.10(d,e) for each of the most probable second and fourth-order piecewise time-invariant model. For the detail modeling, we arbitrarily chose the number of segments  $L = 9$  and the lengths of each segment according to the last column in Table 2.2. To enable comparison of the different models, the corresponding residuals are plotted in Figure 2.11(c,d). As can be seen from Figures 2.10 and 2.11, the piecewise time-invariant model successfully captures the time-variation of the frequency content of real accelerograms. The improvement obtained by higher-order time-invariant frequency-content models is small compared to that obtained by second-order models with time-varying correlation structure. Plots of the probabilistic response spectra curves are shown in Figure 2.12(c,d). Higher-order piecewise time-invariant models do not alter the probabilistic response spectra significantly.

Figure 2.13 compares the response spectra of the rest of the accelerograms shown in Table 2.1 with the probabilistic response spectra computed for the most probable second-order piecewise time-invariant model. Table 2.2 indicates the number of segments and their corresponding time-lengths used in the computations. The probabilistic response spectra in Figures 2.12 and 2.13 provide a good fit to the response spectra of the “target” accelerograms for periods less than approximately 5 seconds. The overestimation of the response spectra for long periods of the linear oscillator (approximately over 5 seconds) is due to the fact that an AR(p) model

cannot represent the intensity of the low-frequency content of the recorded accelerograms. Complete accelerograms have a zero DC component while AR(p) models always have a non-zero DC component. The low-frequency content is expected to strongly influence the response of inelastic structures (Iwan and Paparizos, 1988). A method that improves the low-frequency content of these models is discussed in Section 2.7.3.

Based on the statistics of the maximum acceleration of the response in Figures 2.12 and 2.13 and on similar statistics for the maximum displacement and velocity of the response, it is concluded that the lower the structural frequency, the more sensitive the response is to the details of the ground motion left random by each ground motion model. Comparing Figure 2.12(a) and Figure 2.12(c), the sensitivity of the maximum acceleration of the response to the details of the ground motion corresponding to the TIFC model is less than the sensitivity corresponding to the PTIFC model, especially in the range of structural frequencies from 1 to 3Hz.

The Fourier transform of the residuals  $\{\hat{e}_k\}$  for the cases considered in Figure 2.11 are shown in Figure 2.14(a,b,c,d). For a suitable member of the given class of models, the average variation with frequency of the input spectrum is expected to be approximately constant like a sample of white noise. Higher order models match better the observed “exponential-like” decay (Anderson and Hough, 1984) of the spectral components in the high-frequency content of the accelerograms. The intensity of this frequency range, which is small compared to the low-frequency spectral components, is overestimated by the second-order model. This overestimation shows up in Figure 2.14 as a deviation of the spectral intensity of the residuals at high frequencies below its expected constant value.

Summarizing, in most cases examined, second and fourth-order models provided a good statistical fit to the data contained within successive sufficiently small portions of accelerograms. This is in agreement with the results obtained by Chang *et al.* (1982) and Nau *et al.* (1980) for the ARMA models. For engineering design purposes, a piecewise time-invariant second-order AR model provides an acceptable description of the ground motion, particularly in the range that corresponds to the larger amplitude spectral components.

### 2.7.3 Modeling of the Very Low Frequency Content

An improvement of the incorrect spectral amplitudes present at low frequencies for the AR(p) model can be obtained by including in the previous analysis Brune’s source model (1970). According to Brune, the source power spectral acceleration for shear waves has the normalized shape:

$$S(\omega, \omega_c) = \frac{(\omega/\omega_c)^2}{1 + (\omega/\omega_c)^2}, \quad (2.59a)$$

where  $\omega_c$  is the corner frequency. Using certain assumptions, Brune related  $\omega_c$  to the source radius  $r$  and the shear-wave velocity  $\beta$  by:

$$\omega_c = 2\pi f_c = \frac{2.34\beta}{r}. \quad (2.59b)$$

Several authors, including Boore (1983) and most recently Safak (1988), have used Brune’s source model for the modeling of ground motion using seismological models.

The proposed modified method which gives the correct low frequency behavior is schematically shown in Figure 2.15. The critically damped oscillator, which corresponds to Brune’s model (2.59a), accounts for the form of the spectral amplitude near the source. The linear second-order system, which corresponds to model (2.7), accounts for the intensity of the source as well as propagation and local site effects. The power spectral density of the combined model is shown in Figure 2.16 for time-invariant AR(2) model. It is clear that the modification introduced by Brune’s model gives an  $\omega$ -square behavior of the very low-frequency spectral amplitudes of the accelerogram without substantially affecting the spectral amplitudes of the model (2.7) at frequencies greater than about  $2\omega_c$ .

The equation for the critically damped oscillator has the form:

$$x = \ddot{z}, \quad \ddot{z} + 2\omega_c \dot{z} + \omega_c^2 z = y, \quad (2.60)$$

Using relationships (2.14) and approximating  $\ddot{z}$  by:

$$\ddot{z}(t_k) = \frac{z_{k+1} - 2z_k + z_{k-1}}{\Delta t^2}, \quad t_k = k\Delta t, \quad \Delta t = \text{sampling period}, \quad (2.61)$$

the discrete system that corresponds to equation (2.60) is given by the difference equation

$$x_k - 2ax_{k-1} + a^2x_{k-2} = (y_k - 2y_{k-1} + y_{k-2}), \quad (2.62)$$

where  $a = e^{-\omega_c \Delta t}$ . The modified model is computationally efficient and generates artificial accelerograms with the correct low-frequency content. To determine the parameter of model (2.62), we do not use the estimation method developed previously because it would be ill-conditioned in view of the low intensity spectral amplitudes, and hence poor signal-to-noise ratio, in the very low frequencies of real accelerograms. The corner frequency  $\omega_c$  can be computed from source mechanism studies of the earthquake generating the ground motion; for example, by using (2.59b). The other parameters of the model are estimated as if Brune’s filter was absent since they control the higher frequency content of the model spectrum not affected by the presence of Brune’s model.

From source mechanism studies of the San Fernando earthquake (McGuire and Hanks, 1980), the value of the corner frequency is  $f_c = 0.2\text{Hz}$ . The probabilistic acceleration response spectra computed for the PTIFC model that includes Brune’s correction are shown in Figure 2.17 for the C048.1 record in Table 2.2. Comparison with Figure 2.13 shows no obvious visual difference for oscillator periods less than about 5 seconds. For oscillator periods over 5 seconds, which correspond to frequencies less than  $f_c = 0.2\text{Hz}$ , there is an improvement in the match of the probabilistic linear response spectra and the response spectra of the target accelerogram. Probabilistic linear elastic response spectra for the velocity and the displacement are shown in Figures 2.18(a) and (b), respectively. A very good “match” between the deterministic and the probabilistic linear elastic response spectra is observed for most of the range of structural frequencies.

Figure 2.19 shows the probabilistic inelastic response spectra for the acceleration and velocity described in Section 2.5.3. The inelastic spectra for the maximum ductility and the residual ductility are shown in Figure 2.20. The PTIFC model corresponding to the C048.1 component in Table 2.2 is used. The structural parameters are  $n = 3$ ,  $\eta = 0.3$  and  $\zeta = 0.05$ . The statistics of the maximum ductility in Figure 2.20(a) indicate that the response of the structure becomes inelastic with high probability for initial structural frequencies with values ranging from about 2 to 10Hz. From Figures 2.19(a), 2.19(b) and 2.20(a), and from comparisons with Figures 2.17(b) and 2.18(a), it is concluded that the more inelastic the response

is, the less sensitive the acceleration and the velocity of the response and the more sensitive the displacement ductility of the response are to the details of the ground motion. However, the residual displacement ductility, shown in Figure 2.20(b), is much more sensitive to the details of the ground motion than the maximum displacement ductility, velocity and acceleration.

From Figures 2.17, 2.18, 2.19 and 2.20, the probabilistic linear elastic and inelastic response spectra match well the response spectra of the target accelerogram, justifying the adequacy of the PTIFC model for capturing the essential features of the ground motion as far as dynamic response is concerned.

## 2.8 Conclusions

A general class of parametric stochastic models, formulated in both continuous and discrete times by stochastic differential and difference equations respectively, has been examined for its adequacy to characterize strong motion accelerograms for use in structural response studies. The ground motion model captures parametrically both the amplitude and the frequency content nonstationarity of the ground motion and it probabilistically treats the uncertainty associated with the details of the ground acceleration time history.

Applying Bayesian statistical inference on the discrete formulation, a methodology was developed to extract from the given class of models the optimal model that best fits, in a probabilistic sense, the characteristics of a “target” accelerogram. In contrast to most other methods for estimating the nonstationary characteristics of an accelerogram, the proposed methodology is simple to implement, and it can simultaneously treat the amplitude and the frequency content nonstationarities. The methodology is successfully demonstrated for specific subclasses of the general class of models by using several “target” accelerograms.

The temporal nonstationarities observed in real accelerograms can be modeled by varying the coefficients of the stochastic equations in a piecewise-constant manner. Using a moving time-window approach and second-order models, the time-variation of the frequency content of the accelerograms is adequately described in

detail in terms of the variation of the undamped frequency and damping ratio (or bandwidth) of the second-order continuous model. The undamped frequency which is an approximate measure of the predominant frequency of the ground motion shifts to lower values as time advances. The damping ratio, which is an approximate measure of the frequency range that strongly contributes to the ground motion increases with time. These variations were linked to seismic wave propagation phenomenon. For most of the accelerograms investigated, the portions controlled by  $P$  and  $S$ -waves correspond to values of the damping ratio in the range of 20 to 30%. The portions controlled by surface waves, however, correspond to damping ratios as high as 60% or more. These average trends are useful when structural response to simulated ground motions is to be considered.

From analysis of several representative accelerograms, it is concluded that the second-order model captures most of the information contained in successive segments of an accelerogram over the range of structural frequencies. Higher-order models do not significantly improve the results. The properties of simulated motions show general characteristics similar to the characteristics observed in real accelerograms. The incorrect low-frequency content present in the AR models is improved by introducing Brune's source model. The probabilistic linear elastic (displacement, velocity, and absolute acceleration) and inelastic (maximum displacement ductility ratio, residual displacement ductility ratio, velocity, and absolute acceleration) response spectra "match" well the corresponding response spectra of the "target" accelerogram over the range of structural frequencies. Linear structures with lower natural frequencies are more sensitive to the details of the ground acceleration time history. In addition, the more inelastic the response is, the less sensitive the velocity and the acceleration of the response is to the details of a the ground acceleration time history which has its overall features fixed. However, the ductility, and especially the residual ductility, of the response are much more sensitive to these details.

The specific subclass of piecewise time-invariant second-order models therefore appears adequate for representing the ground motion for the purpose of computing structural response. However, there are too many parameters in such a model to

contemplate making it a part of seismic risk analyses where the model parameters must be related to the seismic environment of a site. In Chapter 3, a more parsimonious ground motion model is proposed which draws on the results of this chapter and which appears to be promising for seismic risk studies which involve ground motion time histories rather than simplified representations such as peak ground quantities.

Record No.	Earthquake Event	Component	$w$ (sec)
C048.1	San Fernando, 1971	N00W	3
C048.2	San Fernando, 1971	S90W	3
C048.3	San Fernando, 1971	DOWN	2
B025	Helena, Montana, 1935	S90W	3
B034	Parkfield, Ca, 1966	N85E	3
El Centro Array, Stn 12	Imperial Valley, 1979	S50W	2

Table 2.1. List of some representative accelerograms for assessing stochastic ground motion model.

Record No.	$t_i$ (sec)	$t_f$ (sec)	Number of Segments	Time-Length of Each Segment (sec)
C048.1	0	30	9	2,3,3,3,3,3,4,4,5
C048.2	0	30	9	2,3,3,3,3,3,4,4,5
B025	0	5	3	2,2,1
B034	0	10	5	2,2,2,2,2
El Centro Array, Stn 12	0	30	9	1,3,3,3,3,4,4,4,5

Table 2.2. Various technical information about the accelerograms in Table 2.1 for PTIFC modelling.

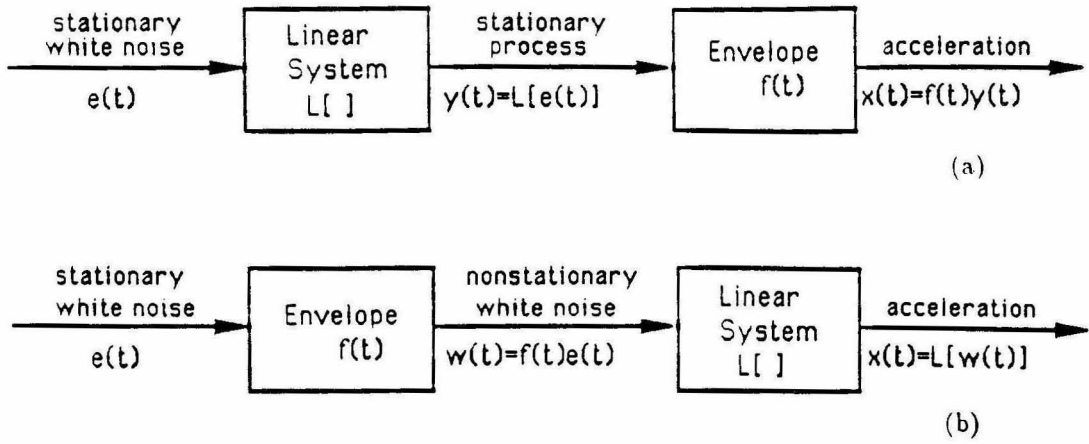


Figure 2.1. (a) Model I, (b) Model II, for ground acceleration.

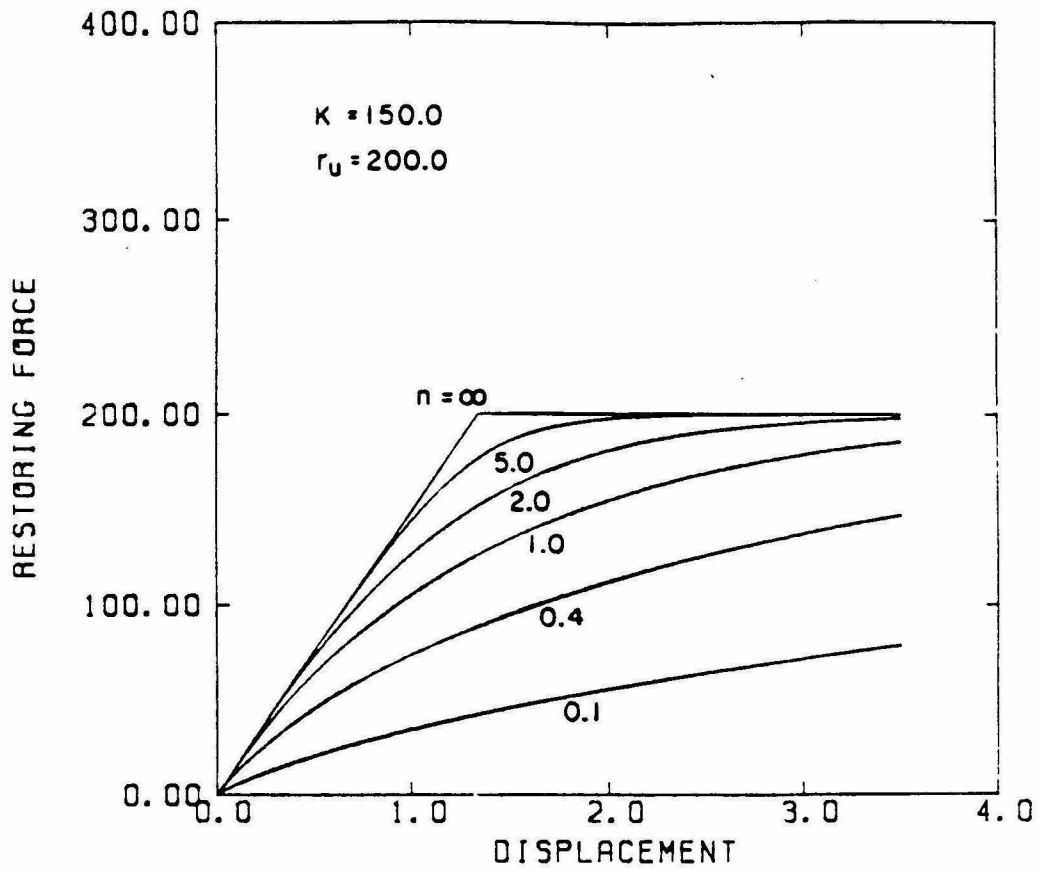


Figure 2.2. Effect of  $n$  on the force-displacement curve [from Jayakumar, (1987)].

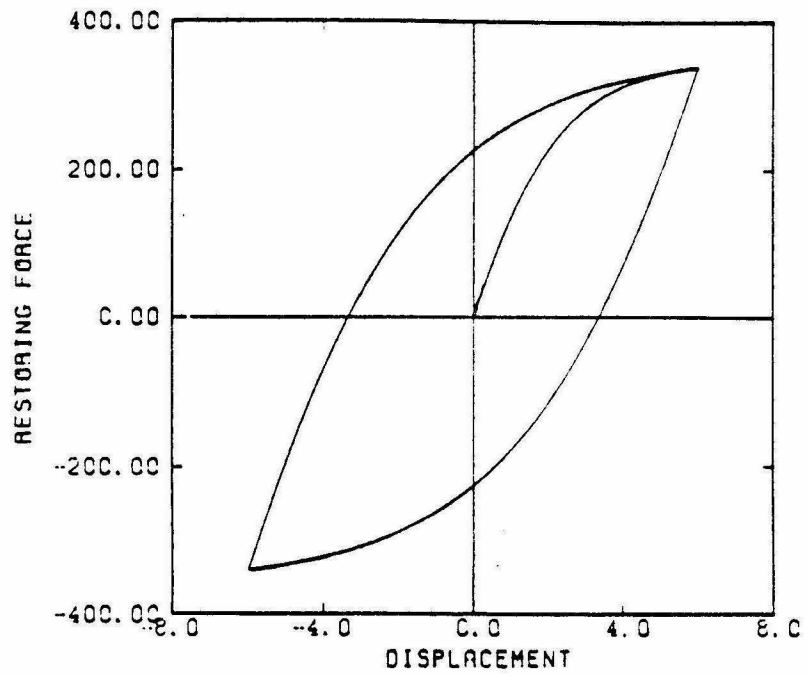


Figure 2.3. Hysteresis loop for periodic response of the structural model [from Jayakumar, (1987)].

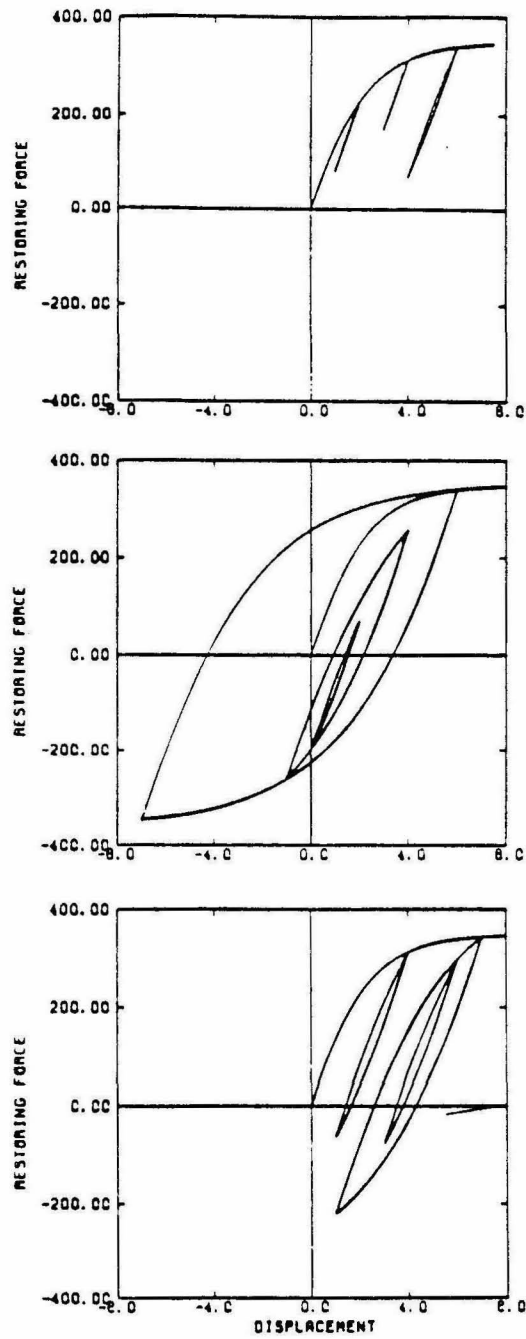


Figure 2.4. Force-displacement curves for arbitrary loading of the structural model [from Jayakumar, (1987)].

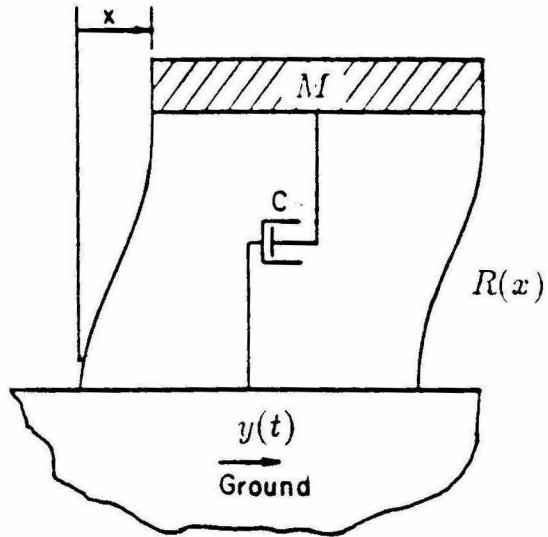


Figure 2.5. Schematic diagram of a SDOF structure.

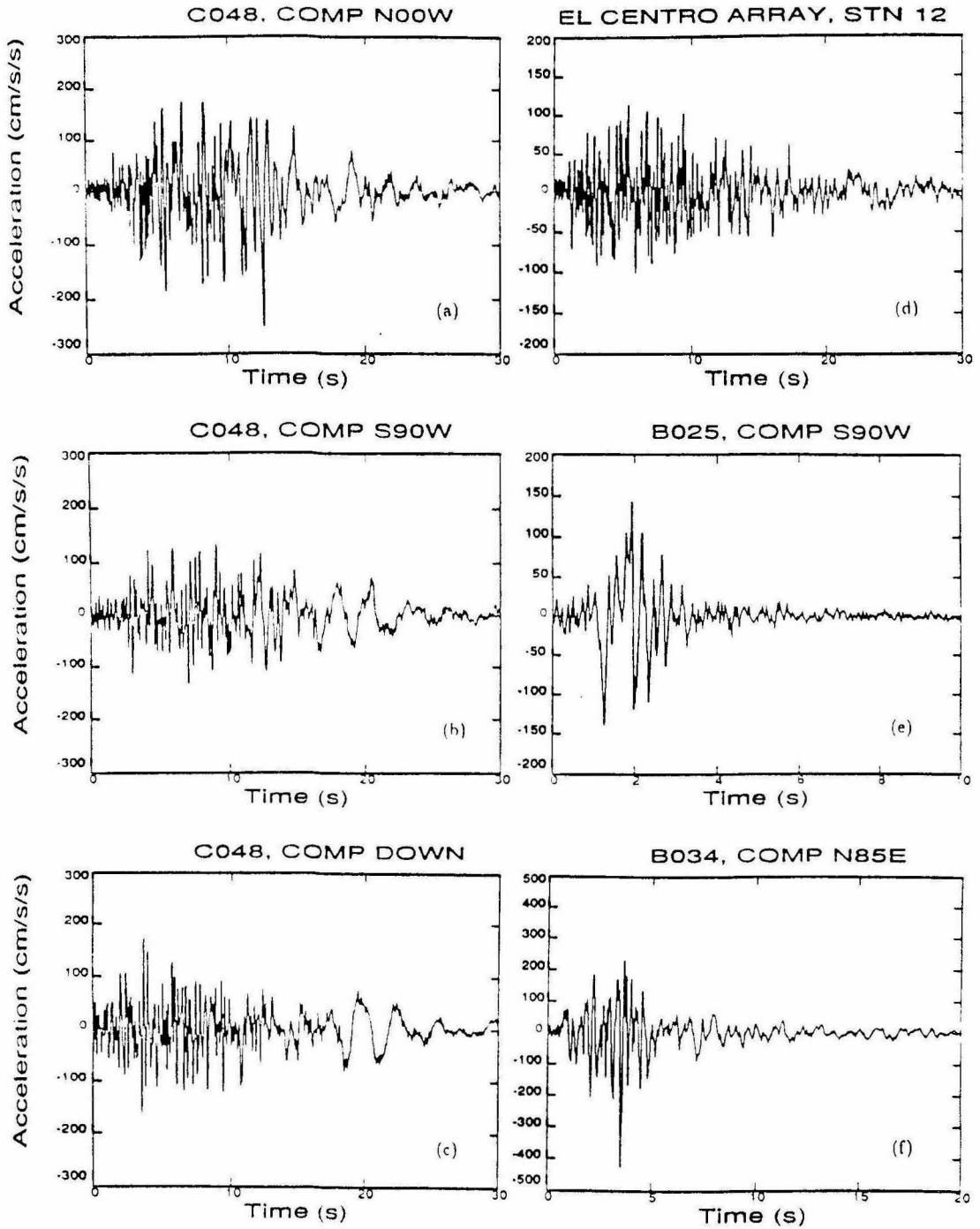


Figure 2.6. Acceleration time histories for the six accelerograms in Table 2.1.

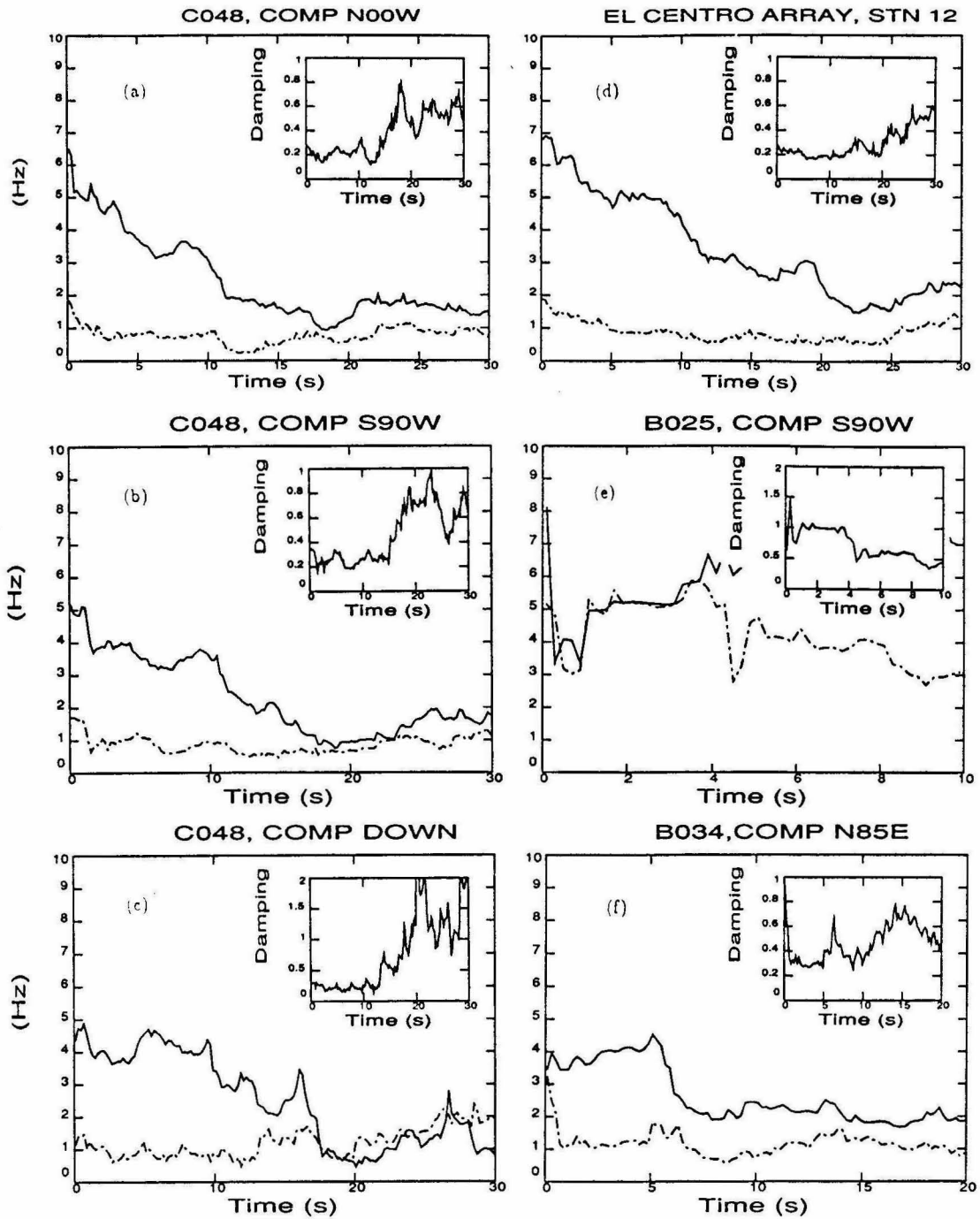


Figure 2.7. Time variation of the frequency content of the accelerograms in Table 2.1, plotted in terms of the undamped frequency  $\omega_1$  (solid), bandwidth  $\omega_1\zeta_1$  (dashed-dotted) and damping ratio  $\zeta_1$ .

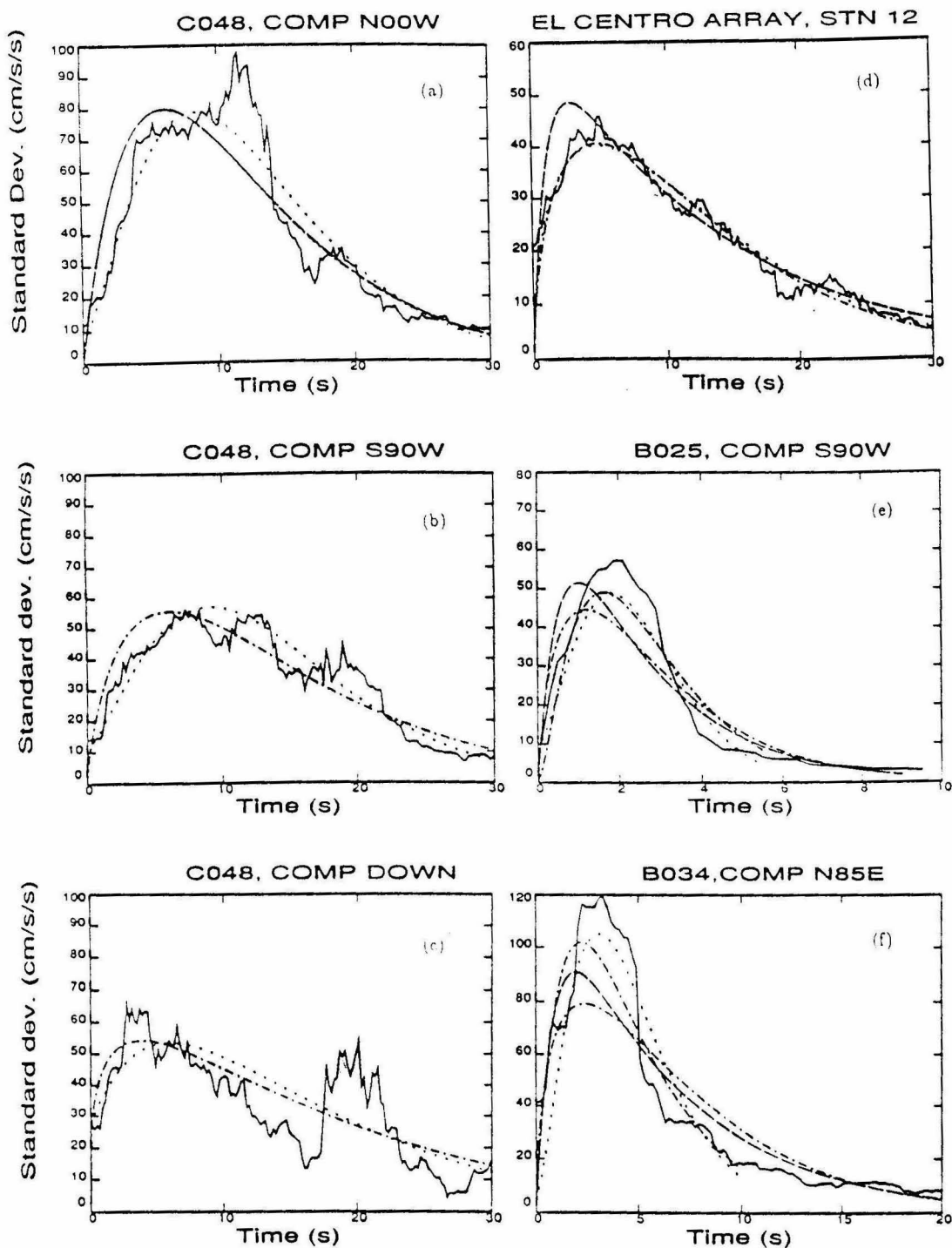


Figure 2.8. Comparison of the standard deviation computed for the accelerograms in Table 2.1 by the moving time-window approach (solid) and by the envelope-modulated white-noise model for the functions (2.1) (dashed-dotted), (2.2) (dashed) and (2.58) (dotted).

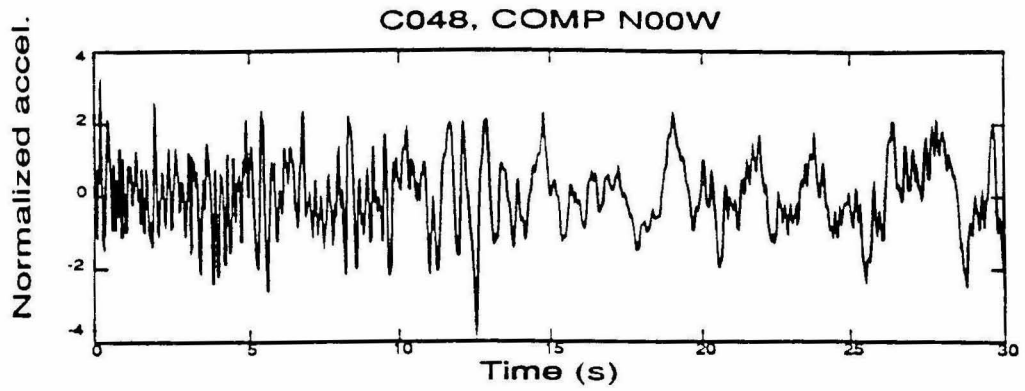


Figure 2.9. The transformed series of stationary intensity for the N00W component of the C048 record.

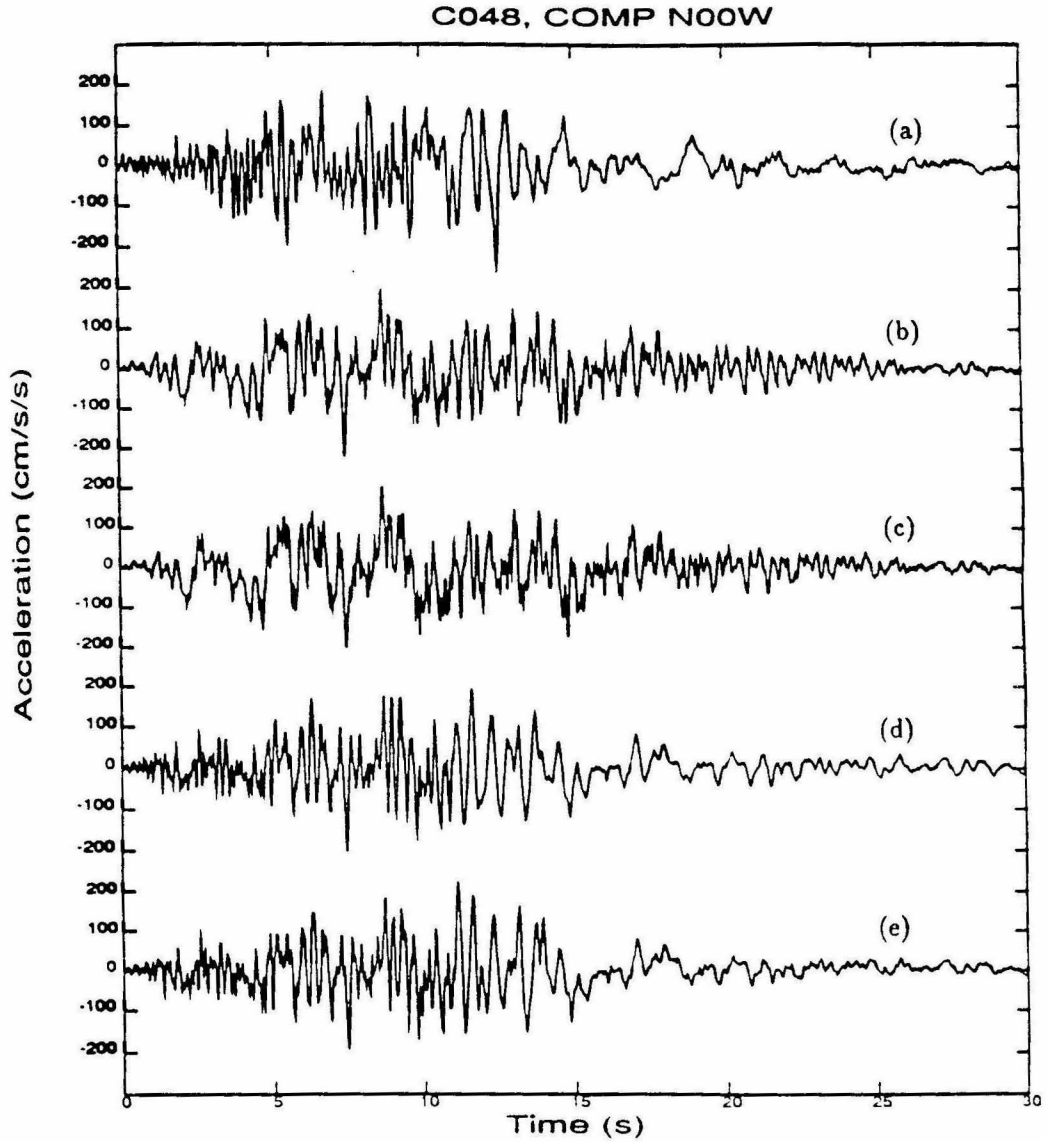


Figure 2.10. The N00W component and one simulation for each optimal model of different subclasses. (a) "Target" accelerogram. (b) and (c) TIFC models with  $p=2$  and  $p=4$ , respectively. (d) and (e) PTIFC models with  $p=2$  and  $p=4$ , respectively.

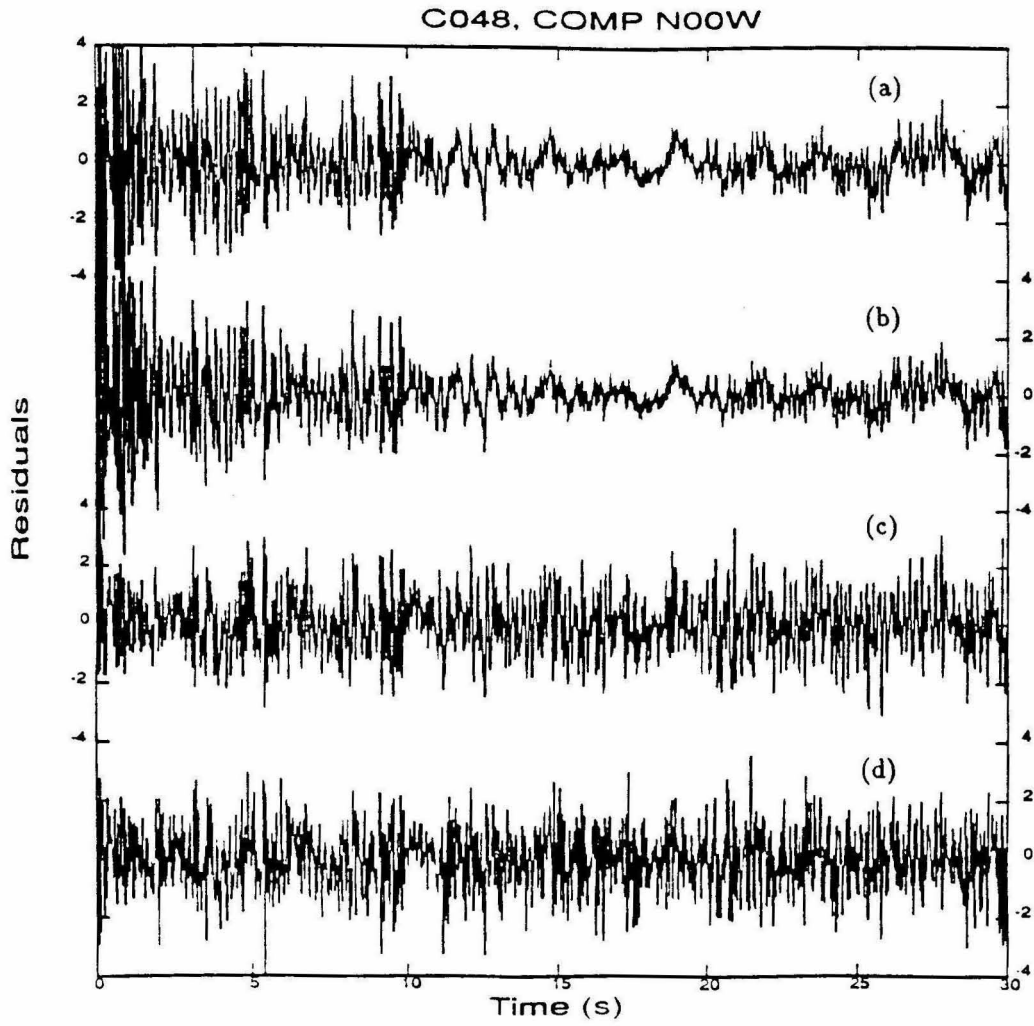


Figure 2.11. The computed "white-noise" sample that generates the N00W component for each optimal model in Figure 2.10.

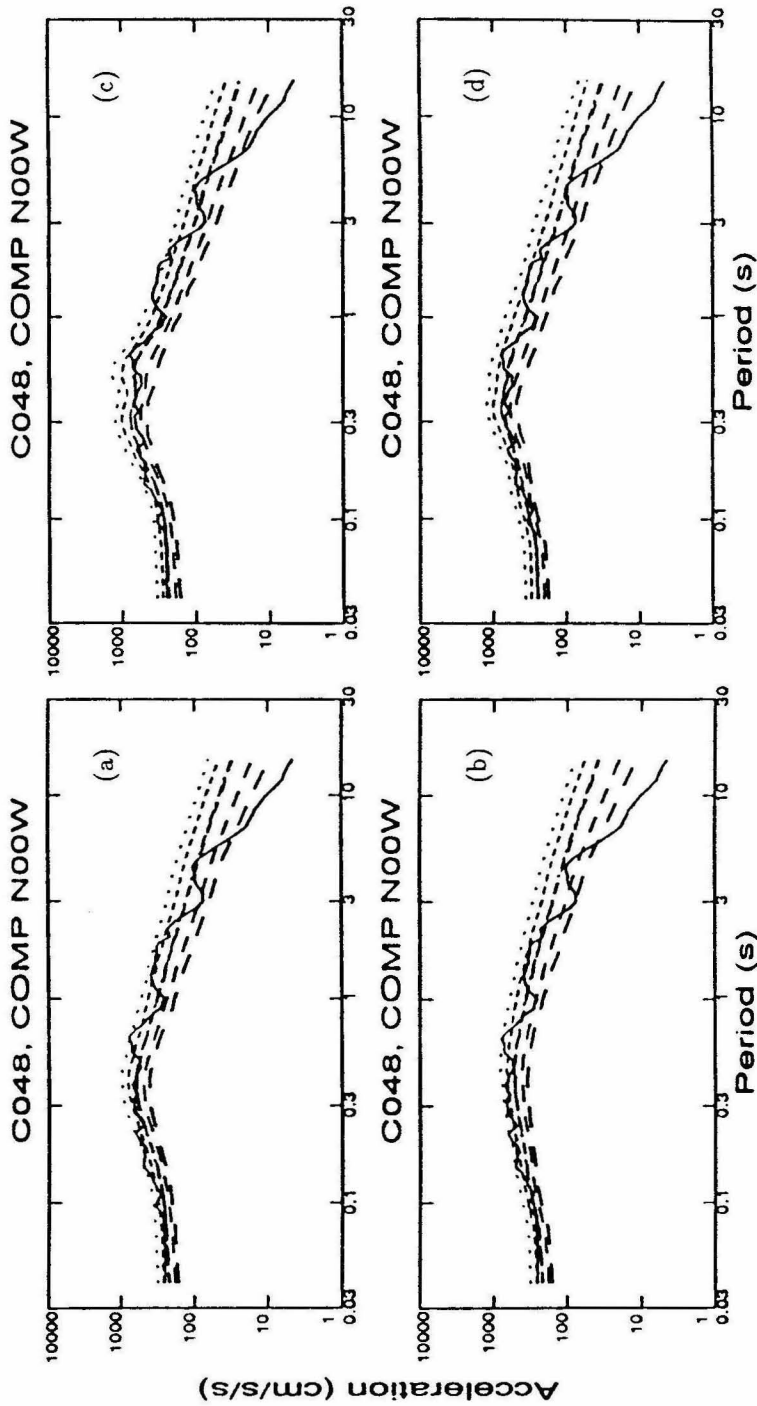


Figure 2.12. Comparison between the 5% damped response spectra of the "target" accelerogram (solid line), the mean response spectra (dashed-dotted line) and the probabilistic response spectra (dashed lines which from top to bottom correspond to  $p=0.99, 0.90, 0.50, 0.10, 0.01$ ) computed for each optimal model in Figure 2.10. (a) and (b) correspond to time-invariant frequency content models with  $p=2$  and  $p=4$ , respectively. (c) and (d) correspond to piecewise time-invariant models with  $p=2$  and  $p=4$ , respectively.

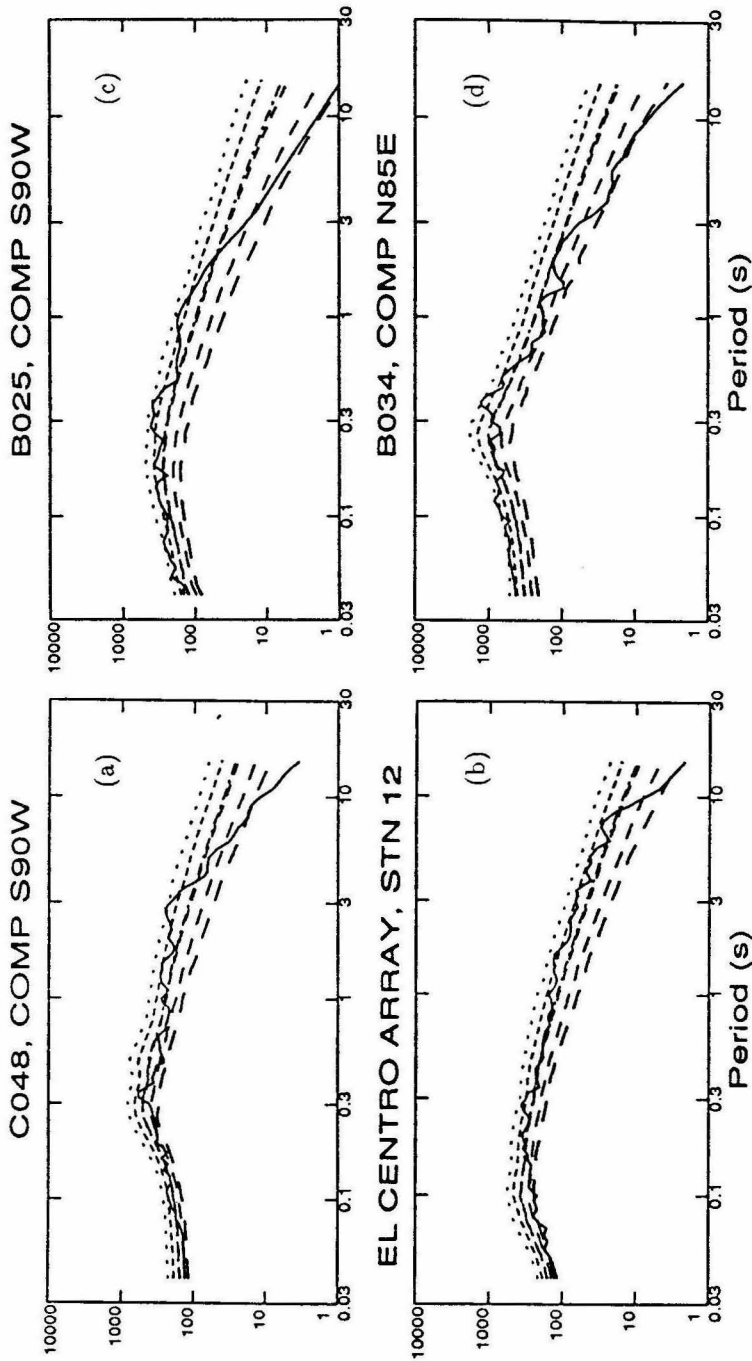


Figure 2.13. Comparison between the 5% damped response spectra of the "target" accelerogram (solid line), the mean response spectra (dashed-dotted line) and the probabilistic response spectra (dashed lines which from top to bottom correspond to  $p = 0.99, 0.90, 0.50, 0.10, 0.01$ ) computed for the optimal PTIFC AR(2) model given in Table 2.2.

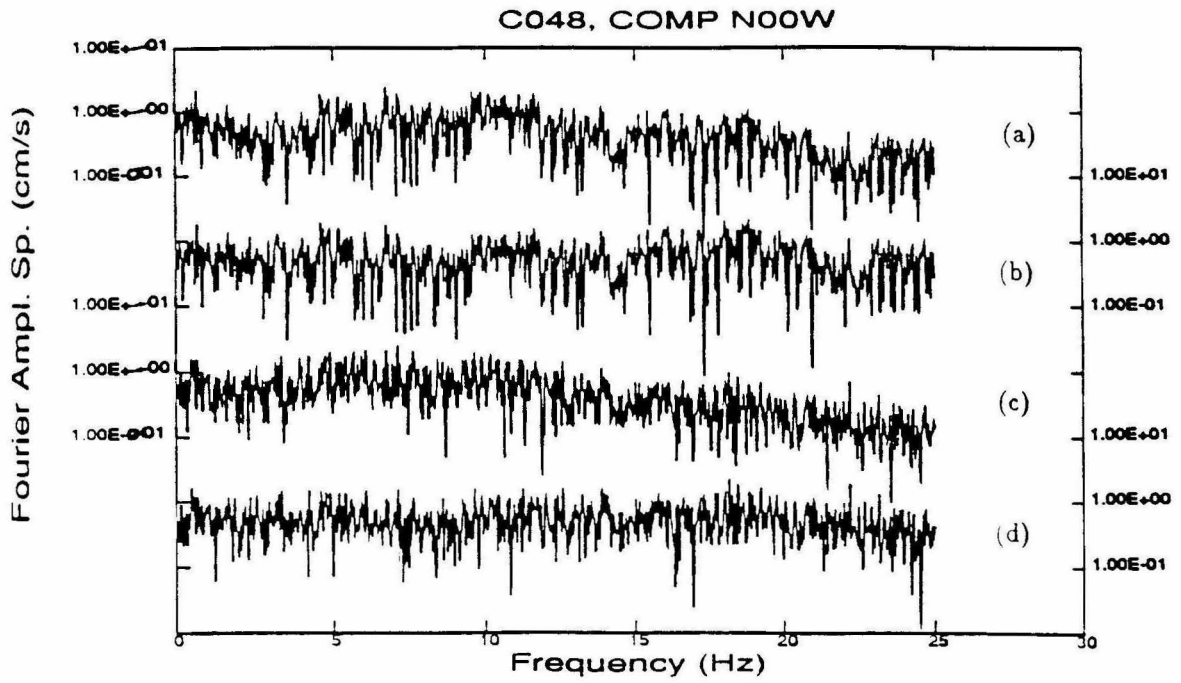


Figure 2.14. The Fourier transform of the "white-noise" samples in Figure 2.11.

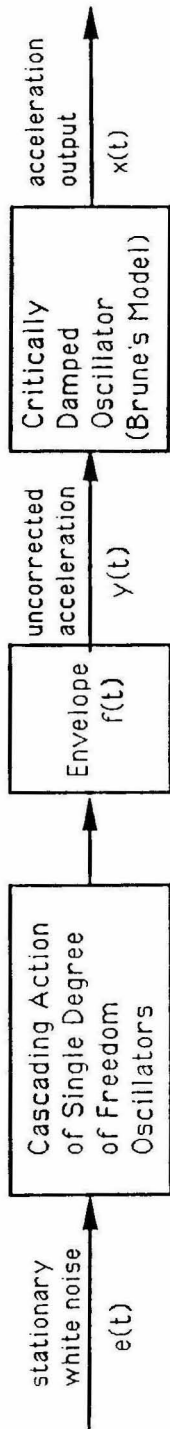


Figure 2.15. Schematic diagram of the earthquake model, including Brune's source model.

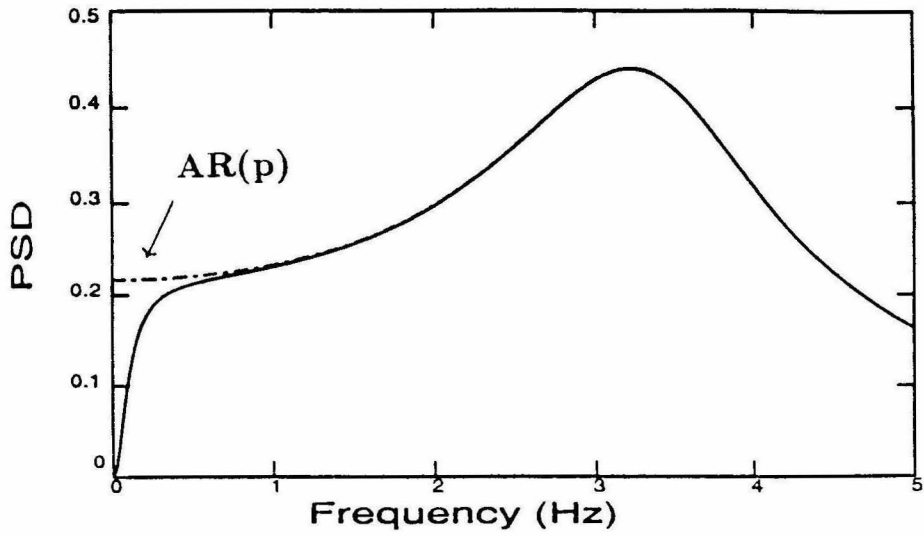


Figure 2.16. Power spectral density of the AR(p) model (dashed-dotted curved) and the combined AR(p) and Brune's model (solid curve).

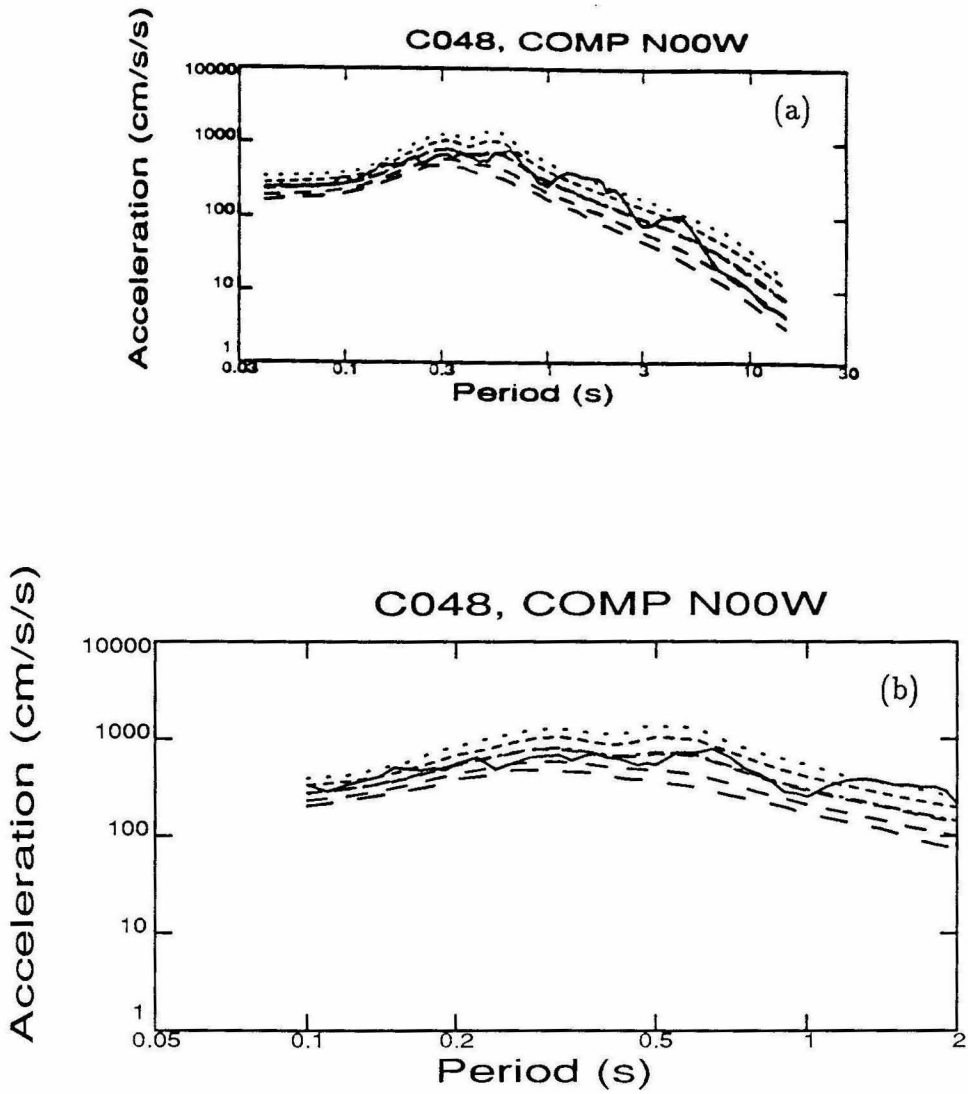


Figure 2.17. Comparison between the 5% damped acceleration response spectra of the "target" accelerogram (solid line), the mean response spectra (dashed-dotted line) and the probabilistic response spectra (dashed lines which from top to bottom correspond to  $p = 0.99, 0.90, 0.50, 0.10, 0.01$ ) computed for optimal PTIFC AR(2) model in Figure 2.10, including Brune's source model. (a) 0.04-20s period, (b) 0.1-2s period.

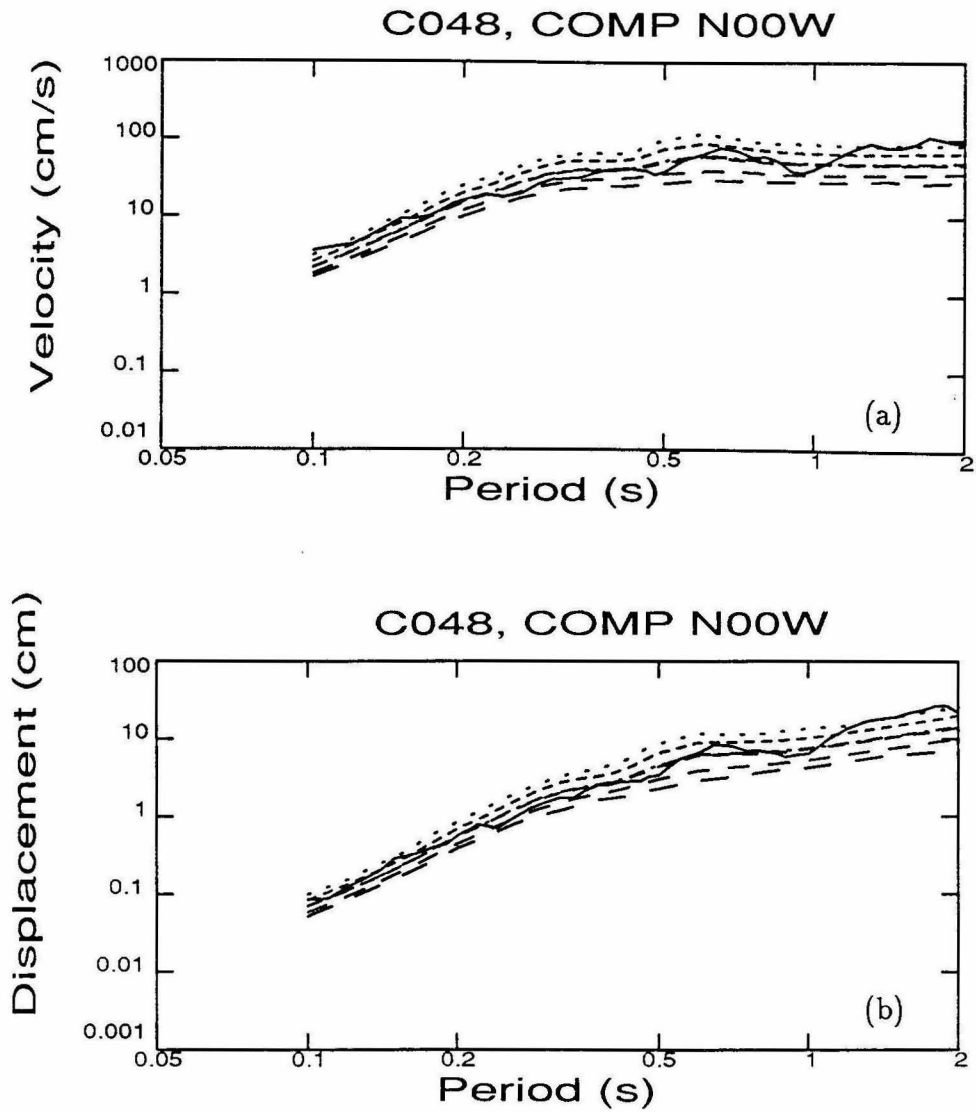


Figure 2.18. Comparison between the 5% damped response spectra of the "target" accelerogram (solid line), the mean response spectra (dashed-dotted line) and the probabilistic response spectra (dashed lines which from top to bottom correspond to  $p = 0.99, 0.90, 0.50, 0.10, 0.01$ ) computed for optimal PTIFC AR(2) model in Figure 2.10, including Brune's source model. (a) Velocity, (b) Displacement.

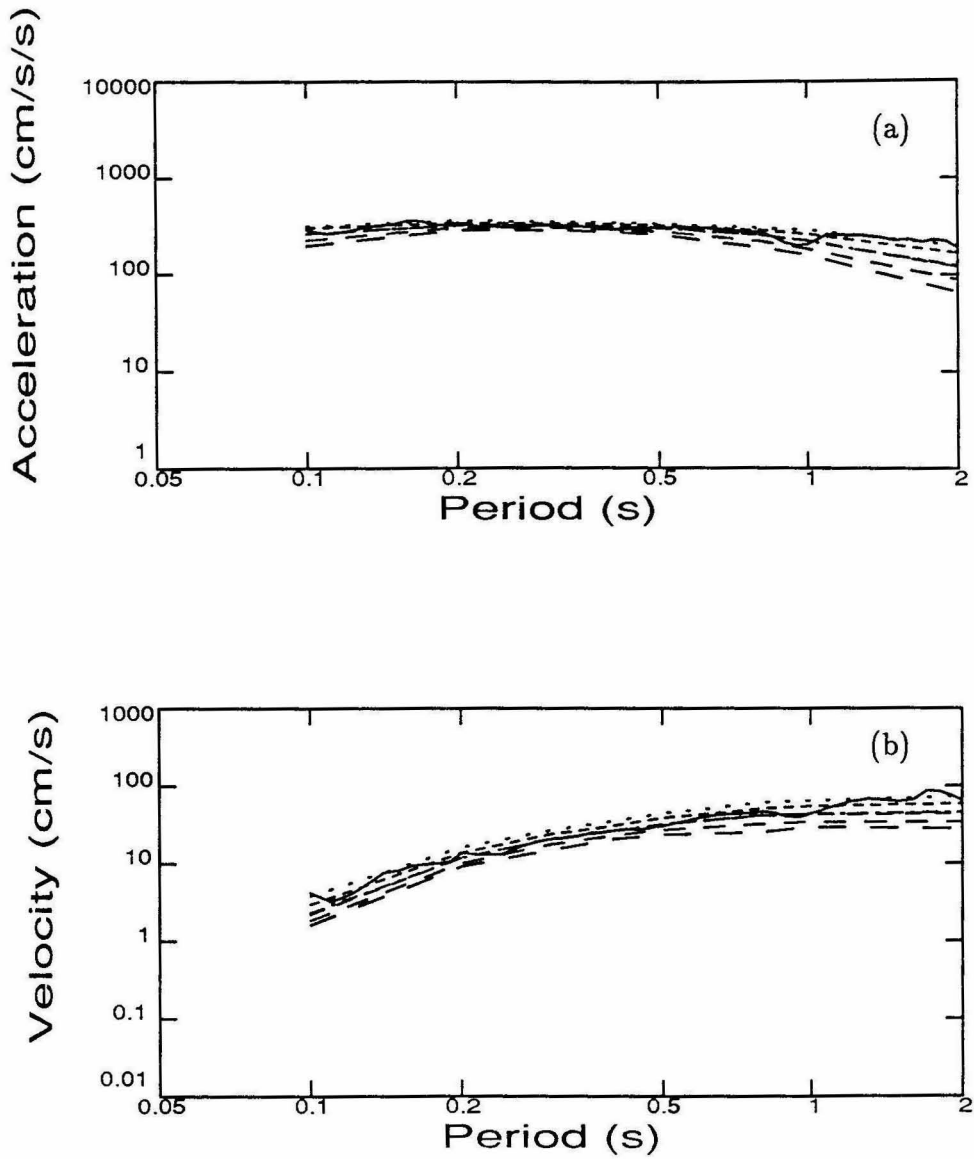


Figure 2.19. Comparison between the inelastic response spectra of the "target" accelerogram (solid line), the mean response spectra (dashed-dotted line) and the probabilistic response spectra (dashed lines which from top to bottom correspond to  $p = 0.99, 0.90, 0.50, 0.10, 0.01$ ) computed for optimal PTIFC AR(2) model in Figure 2.10, including Brune's source model. Structural parameters  $n = 3$ ,  $\eta = 0.3$  and  $\zeta = 0.05$ . (a) Acceleration, (b) Velocity.

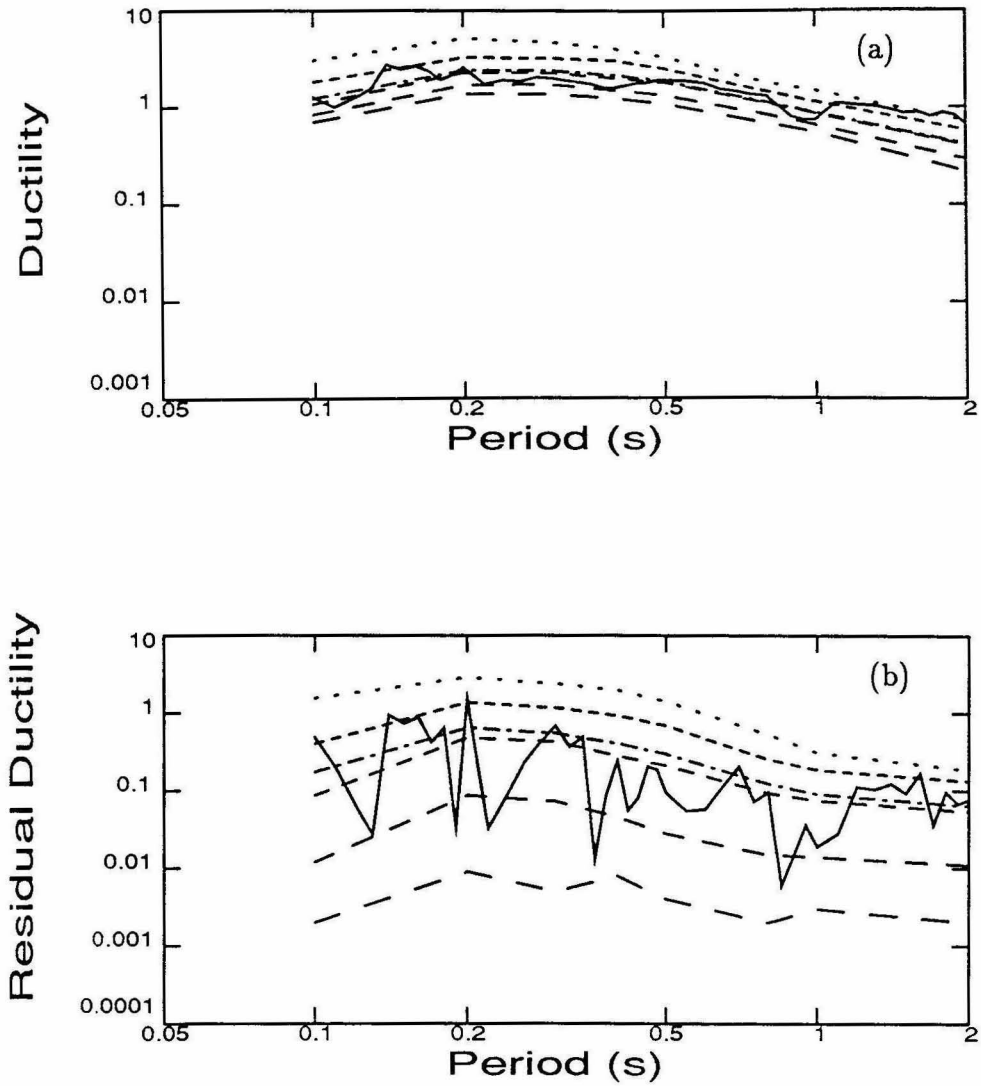


Figure 2.20. Comparison between the inelastic response spectra of the "target" accelerogram (solid line), the mean response spectra (dashed-dotted line) and the probabilistic response spectra (dashed lines which from top to bottom correspond to  $p = 0.99, 0.90, 0.50, 0.10, 0.01$ ) computed for optimal PTIFC AR(2) model in Figure 2.10, including Brune's source model. Structural parameters  $n = 3, \eta = 0.3$  and  $\zeta = 0.05$ . (a) Ductility, (b) Residual Ductility.

## Chapter 3

# Parsimonious Probabilistic Modeling of Strong Ground Motion

### 3.1 Introduction

In Chapter 2, stochastic second-order differential and difference equations were found to be adequate in modeling the details within a segment of the ground acceleration time history. However, the large number of parameters involved in representing the temporal nonstationarity in both the amplitude and the frequency content of ground motion, make the model inappropriate to incorporate in seismic risk studies and to use in constructing future acceleration time histories at a site consistent with a given seismic environment. The purpose of this chapter is to incorporate a small number of physically meaningful parameters in the second-order model in such a way that the model captures the essential features of the motion for the purpose of computing dynamic response. The findings in Chapter 2 will provide the background for proposing more parsimonious models. For this, the coefficients of the stochastic second-order differential and difference equations are treated as slowly-varying. Important statistical quantities such as the autocovariance function and evolutionary power spectral density function are first developed and simplifications are further introduced for broadband processes in Section 3.2. In Section 3.3, appropriate conversion relationships are developed to link the continuous and the discrete formulations. A nine-parameter ground motion model is proposed in Section 3.4. Numerical results for verifying the adequacy of the model are also presented. Several remarks on the practical application of the model are given in Section 3.5.

### 3.2 Stochastic Second-Order Differential Equations with Variable Coefficients

The earthquake ground acceleration  $y(t)$  at a site is treated as a stochastic process described by the second-order linear differential equation

$$\ddot{y} + 2\zeta_g(t)\omega_g(t)\dot{y} + \omega_g^2(t)y = f(t)e(t), \quad (3.1)$$

where a dot denotes derivative with respect to  $t$ ,  $\zeta_g(t)$ ,  $\omega_g(t)$  are in general time-varying coefficients,  $f(t)$  is a deterministic function and  $e(t)$  is a zero-mean Gaussian white-noise process. Equation (3.1) is a special case of the set of equations (2.3). The statistical properties of the process generated by (3.1) are next studied and simplified for slowly-varying coefficients and broadband processes.

#### 3.2.1 Autocovariance Function

Using the generalized Duhamel's integral, the value of the process  $y(t)$  at time  $t$  is

$$y(t) = \int_0^t h(t, s) f(s) e(s) ds, \quad (3.2)$$

where  $h(t, s)$  is the impulse response function of the system. Making use of (3.2) and the property (2.5) of the white-noise process, the autocovariance function of the stochastic process  $y(t)$  has the integral form

$$R_{yy}(t, s) = \int_0^{\min(t, s)} h(t, \tau) h(s, \tau) f^2(\tau) d\tau. \quad (3.3)$$

Letting  $s = t$  in the expression for the autocovariance function, the instantaneous variance  $R_y(t)$  of the process  $y(t)$  takes the form

$$R_y(t) = E [y^2(t)] = R_{yy}(t, t) = \int_0^t h^2(t, \tau) f^2(\tau) d\tau. \quad (3.4)$$

Under the assumption of slowly-varying coefficients, stated in mathematical terms as:

$$\lambda_1(t) \equiv \frac{|\dot{\alpha}_g(t)|}{2\omega_d(t)\omega_g(t)} \ll 1 \quad \text{and} \quad \lambda_2(t) \equiv \frac{|\dot{\omega}_d(t)|}{2\omega_d(t)\omega_g(t)} \ll 1, \quad (3.5)$$

where  $\alpha_g(t) = \zeta_g(t)\omega_g(t)$  and  $\omega_d(t) = \omega_g(t)\sqrt{1 - \zeta_g^2(t)}$ , an approximate closed-form solution for the impulse response function  $h(t, s)$  is derived (Appendix A.1) in the form:

$$h(t, s) = \frac{\exp\left[-\int_s^t \alpha_g(\tau) d\tau\right]}{\sqrt{\omega_d(t)\omega_d(s)}} \sin\left[\int_s^t \omega_d(\tau) d\tau\right] \quad ; \quad t \geq s \quad (3.6)$$

$$= 0 \quad ; \quad t < s$$

The impulse response is an exponentially-decaying oscillatory function with instantaneous rate of decay governed by the bandwidth  $\alpha_g(t)$  and instantaneous frequency of oscillations  $\omega_d(t)$ . In the special case of constant  $\omega_g$  and  $\zeta_g$ , expression (3.6) simplifies to the well-known exact expression for the impulse response function of a differential equation with constant coefficients. For the linear differential equation (3.1), the instantaneous relaxation time is  $\tau_{rel}(t) = 1/\alpha_g(t)$ . This time gives a direct measure of the correlation time  $\tau_{cor}$  of the output stochastic process  $y(t)$ . An approximate measure of the time  $\tau_n(s)$  required for  $h(t, s)$  to decay below  $n$  percent of its maximum value is

$$\tau_n(s) \geq -\ln(0.01n) \max_{s \leq t \leq s + \tau_n} \{\tau_{cor}(t)\} \quad (3.7)$$

This value which depends only on the instant bandwidth  $\alpha_g(t)$  of equation (3.1) decreases as the bandwidth increases.

Using the approximate form (3.6) for the impulse response function, the general expression for the autocovariance function of the process  $y(t)$  becomes

$$R_{yy}(t, s) = \frac{1}{\sqrt{\omega_d(t)\omega_d(s)}} \int_0^{\min(t,s)} \frac{f^2(\tau)}{\omega_d(\tau)} \exp\left[-\int_\tau^t \alpha_g(\xi) d\xi - \int_\tau^s \alpha_g(\xi) d\xi\right] \sin\left[\int_\tau^t \omega_d(\xi) d\xi\right] \sin\left[\int_\tau^s \omega_d(\xi) d\xi\right] d\tau. \quad (3.8)$$

Next, the special case of wide-banded processes is considered. The statistical properties of  $y(t)$  are examined for white-noise excitation and then the results are extended to the case of slowly-modulated white-noise excitation.

Consider the case where  $\alpha_g(t)$  is “sufficiently” large or, equivalently, the correlation time  $\tau_{cor}$  is “sufficiently” small so that the slowly-varying coefficients  $\alpha_g(t)$

and  $\omega_g(t)$  can be assumed to remain constant over the time interval  $[t - \tau_n, t]$ . For small enough  $n$ , the contribution to the value of the integrals in (3.8) comes mostly from the integration in the interval  $[s - \tau_n, s]$ , while the remaining contribution is negligible. Neglecting the contribution of the integration outside the interval  $[s - \tau_n, s]$  in (3.8), the autocovariance function is further approximated by

$$R_{yy}(t, s) \approx \frac{(\exp[-\alpha_g(s)(t-s)])}{\omega_d^2(s)} \int_0^s f^2(\tau) \exp[-2\alpha_g(s)(s-\tau)] \sin[\omega_d(s)(s-\tau)] \sin[\omega_d(t)(t-\tau)] d\tau ; \quad t \geq s \quad (3.9)$$

In the special case of a white-noise input, that is,  $f(t) = f_0$ , the integration in (3.9) is performed analytically, leading to

$$R_{yy}^{(w)}(t, s) = r_{yy}^{(w)}(\tau, s) + A(t, s) \quad (3.10)$$

where

$$r_{yy}^{(w)}(\tau, s) = \frac{f_0 \exp[-\alpha_g(s)|\tau|]}{4\omega_g(s)\omega_d(s)\alpha_g(s)} \cos(\omega_d(s)|\tau| - \phi_g(s)), \quad \tau = t - s, \quad (3.11)$$

$$A(t, s) = \frac{f_0 \exp[-\alpha_g(s)(t+s)]}{4\omega_d^2(s)\omega_g(s)} \left[ \zeta_g(s) \cos\omega_d(s)(t+s) - \sqrt{1 - \zeta_g^2(s)} \sin\omega_d(s)(t+s) \right] + \frac{\exp[-\alpha_g(s)(t+s)]}{4\omega_d^2(s)\omega_g(s)} \left[ -\frac{1}{\zeta_g(s)} \cos\omega_d(s)(t-s) \right], \quad t > s \quad (3.12)$$

and  $\tan\phi_g(s) = \alpha_g(s)/\omega_d(s)$ . The variance of the process  $y(t)$  takes the form

$$R_y^{(w)}(t) = R_{yy}^{(w)}(t, t) = r_y^{(w)}(t) + B(t) \quad (3.13)$$

where

$$r_y^{(w)}(t) = \frac{f_0}{4\omega_g^2(t)\alpha_g(t)} \quad (3.14)$$

$$B(t) = f_0 \frac{e^{-2\alpha_g(t)t}}{4\omega_d^2(t)\omega_g(t)} \left[ -\frac{1}{\zeta_g(t)} + \zeta_g(t) \cos(2\omega_d(t)t) - \sqrt{1 - \zeta_g^2(t)} \sin(2\omega_d(t)t) \right] \quad (3.15)$$

For “sufficiently” large  $t$  and  $s$ , depending on the value of  $\alpha_g(t)$ , the contribution of the terms  $A(t, s)$  and  $B(t)$  containing the exponential factor  $\exp[-\alpha_g(s)(t + s)]$  becomes negligible.

For large time difference  $\tau$ , the presence of the exponential factor in (3.11) leads to negligibly small values for  $r_{yy}^{(w)}(\tau, s)$ . For smaller  $\tau$ , which yields significant values for  $r_{yy}^{(w)}(\tau, s)$ , the coefficients  $\alpha_g(s)$  and  $\omega_g(s)$  are assumed to remain almost constant throughout the interval  $[s, t]$ , and therefore the autocovariance function in the neighborhood of the time  $s$  depends approximately on the properties of the system at the time  $s$  only.

For a slowly-varying function  $f(t)$  whose value can be assumed to remain essentially constant over the time interval  $[s - \tau_n, s]$ , expression (3.9) can be approximated by

$$R_{yy}(t, s) \approx r_{yy}(\tau, s) = r_{yy}^{(w)}(\tau, s) f^2(s) \quad (3.16)$$

Also, for this case, the variance is given by

$$R_y(t) = R_y^{(w)}(t) f^2(t) \quad (3.17)$$

The exact autocovariance function can be obtained numerically by treating equation (3.1) as a two-dimensional vector differential equation. The covariance matrix of the output vector process then satisfies the Liapunov matrix differential equation. Its numerical solution is used as a reference later in the applications to check the accuracy of the analytical approximations (3.16) and (3.17).

### 3.2.2 Evolutionary Power Spectral Density Function

A discussion on the evolutionary spectral representation of a stochastic process is given in Appendix A.3. Using Priestley’s definition, the EPSD function of the stochastic process  $y(t)$  is derived in Appendix A.3 in the form

$$S_{yy}(\omega, t) = \left| \int_0^t h(t, s) f(s) e^{-i\omega(t-s)} ds \right|^2 \quad (3.18)$$

If we assume as before that the bandwidth  $\alpha_g(t)$  is “sufficiently” large so that  $\alpha_g(t)$  and  $\omega_g(t)$  can be assumed to remain essentially constant over the time-interval

$[s - \tau_n, s]$ , then (3.18) takes the approximate form:

$$S_{yy}(\omega, t) \approx \frac{1}{\omega_d^2(t)} \left| \int_{-\infty}^t f(s) \exp[-\alpha_g(t)(t-s)] \sin[\omega_d(t)(t-s)] e^{-i\omega(t-s)} ds \right|^2 \quad (3.19)$$

In the case of white-noise excitation, that is,  $f(t) = f_0 = \text{constant}$ , the integration in (3.19) can be performed to obtain:

$$S_{yy}(\omega, t) = |H(\omega, t)|^2 f_0^2, \quad (3.20)$$

where  $H(\omega, t)$  has the form:

$$H(\omega, t) = \frac{1}{-\omega^2 + \omega_g^2(t) + 2\alpha_g(t)\omega i} \quad (3.21)$$

The quantity  $H(\omega, t)$  can be viewed, in an approximate sense, as the Fourier transform with respect to  $\tau$  of the impulse response function  $h(t + \tau, t)$  referred to time  $t$ , that is,

$$H(\omega, t) = \int_{-\infty}^{\infty} h(t + \tau, t) e^{-i\omega\tau} d\tau \quad (3.22)$$

For a slowly-varying envelope function  $f(t)$ , the expression for the EPSD is approximated by:

$$S_{yy}(\omega, t) = |H(\omega, t)|^2 f^2(t) \quad (3.23)$$

### 3.2.3 Relation Between ACF and EPSD Function

It can be seen that in the case of sufficiently large value of  $\alpha_g(t)$  in addition to  $\alpha_g(t)$ ,  $\omega_g(t)$  and  $f(t)$  being slowly-varying, the covariance function and the EPSD are related by:

$$R_{yy}(t + \tau, t) \approx \int_{-\infty}^{\infty} S_{yy}(\omega, t) e^{i\omega\tau} d\omega, \quad (3.24)$$

i.e.,  $R_{yy}(t + \tau, t)$  is the Fourier transform of the EPSD as it is in the case of constant coefficients. Therefore, the EPSD is also, in an approximate sense, a complete description of the stochastic process  $y(t)$ , since the crucial quantity  $R_{yy}(t + \tau, t)$  is completely determined. The EPSD can be viewed as the frequency decomposition of the total energy at time  $t$ .

### 3.3 Discrete Equation and Its Relation to the Continuous One

The values of the continuous stochastic process  $y(t)$  at regular time intervals  $\Delta t$  form the discrete stochastic sequence  $\{y(k\Delta t)\}$ . Let  $y_k$  be an approximation to the value of  $y(t)$  at the time  $t = k\Delta t$ , then the sequence  $\{y_k\}$  is assumed to satisfy the second-order difference equation:

$$y_k - a_1(k)y_{k-1} - a_2(k)y_{k-2} = \sigma(k)e_k \quad (3.25)$$

where  $a_1(k)$ ,  $a_2(k)$  are slowly-varying coefficients,  $\sigma(k)$  is a deterministic envelope function and  $e_k$ ,  $k = 1, \dots, N$  is a discrete zero-mean, Gaussian white-noise process satisfying (2.8). As in the stationary case, conversion relationships between the parameters of the continuous and the discrete equation are obtained by imposing two conditions. The first condition enforces the free vibration solutions of the discrete and the continuous equation to be equal at time  $t_k = k\Delta t$ ,  $k = 1, \dots, N$ . Therefore, the two linearly independent solutions  $x_h^{(1)}$  and  $x_h^{(2)}$  of the homogeneous part of the continuous equation must satisfy:

$$x_h^{(i)}(t_k) - a_1(k)x_h^{(i)}(t_{k-1}) - a_2(k)x_h^{(i)}(t_{k-2}) = 0, \quad i = 1, 2, \quad k = 1, \dots, N. \quad (3.26)$$

It is shown in Appendix B that the above condition results in the approximate relationships:

$$a_1(k) = 2\exp(-\omega_g(t_k)\zeta_g(t_k)\Delta t) \cos(\omega_g(t_k)\sqrt{1-\zeta_g^2(t_k)}\Delta t) \quad (3.27a)$$

$$a_2(k) = -\exp(-2\omega_g(t_k)\zeta_g(t_k)\Delta t) \quad (3.27b)$$

For time-invariant coefficients, relationships (3.27) are exact and independent of the index  $k$ .

The second condition, which relates the forcing parts of equations (3.1) and (3.25), enforces the autocorrelation functions of the discrete and the continuous process to be equal at the points of definition of the discrete process, that is,

$$E[y(t_k)y(t_j)] = E[y_k y_j]. \quad (3.28)$$

The covariance function of the discrete process is derived in Appendix C and using equation (3.28) it leads to the relationship

$$\sigma(k) = \frac{f(t_k)\sqrt{\Delta t}}{\omega_d(t_k)} \exp[-\alpha_g(t_k)\Delta t] \sin[\omega_d(t_k)\Delta t]. \quad (3.29)$$

The assumption of slowly-varying coefficients  $\alpha_g(t)$  and  $\omega_g(t)$  is involved in the approximations (3.27) and (3.29). According to the relationships developed herein, the coefficients of the discrete model are interpreted in terms of the coefficients of the continuous model, and vice versa.

### 3.4 Parsimonious Ground Motion Model

From the previous analysis, it is concluded that the well-known expressions for the autocovariance function and PSD function of stationary processes generated by stochastically-excited second-order differential equation with constants coefficients  $\omega_g$ ,  $\zeta_g$  and  $f$ , can be extended in an approximate sense to the case of slowly-varying coefficients and heavily-damped equations by just replacing the constants in the stationary expressions with the corresponding time-varying ones. Therefore, the statistical structure of the stochastic process at time  $t$  is approximately equivalent to the statistical structure of the stationary process generated by equation (3.1) holding its parameters  $\omega_g(t)$ ,  $\alpha_g(t)$ , and  $f(t)$  constant at their values at  $t$ .

Guided by the properties of the stationary process, the EPSD function provides all pertinent information regarding the frequency and amplitude content of the stochastic process  $y(t)$  at time  $t$ . The model coefficients  $\omega_g(t)$ ,  $\alpha_g(t)$  and  $f(t)$  have the following interpretations. The instantaneous frequency  $\omega_g(t)$  is an approximate measure of the predominant frequency present in the process at time  $t$ . The damping ratio  $\zeta_g(t)$  is an approximate measure of the frequency range around  $\omega_g(t)$  which contributes strongly to the output at time  $t$ . Using (3.17) to account for the effects of the time variation of  $\omega_g(t)$  and  $\zeta_g(t)$ , the form of the modulation  $f(t)$  determines the output variance  $R_y(t)$  of the stochastic process at time  $t$ . The time variation of  $R_y(t)$  specifies the way the variance of the stochastic process  $y(t)$  changes with time independently of its frequency content. Such interpretations are not true if the assumptions requiring the process to be broadband and coefficients to be slowly varying are removed. For lightly-damped processes and substantial changes of the model coefficients, the frequency decomposition of the process at time  $t$  is given by the integral form (3.18).

The previous concepts are next applied in the modeling of ground motion. The

time variation of  $\omega_g(t)$ ,  $\zeta_g(t)$ , and  $R_y(t)$  is chosen such that the stochastic process  $y(t)$  resembles certain features observed in real accelerograms. In order to make the model efficient to use in seismic risk analyses and in future predictions of acceleration time histories from a given seismic environment at a site, parametric functions need to be constructed for the time variation of the model coefficients in terms of a few physically meaningful parameters. The parametric forms accounting for the time variation of  $\omega_g(t)$ ,  $\alpha_g(t)$ , and  $R_g(t)$  should be consistent with physical considerations and, in addition, they should be general enough to realistically account for the nonstationarities observed in real accelerograms.

Based on detailed analyses of earthquake accelerograms in Chapter 2, an exponentially decaying function for  $\omega_g(t)$  and a linearly varying function for the bandwidth  $\alpha_g(t)$ , that is,

$$\omega_g(t, \underline{\theta}) = \phi_1 + \phi_2 e^{-\phi_3 t} \quad (3.30)$$

$$\alpha_g(t, \underline{\theta}) = \phi_4 + \phi_5 t \quad (3.31)$$

provide an overall adequate fit to the observed average time-variation of these quantities. Here,  $\underline{\theta}$  are the model parameters and those defining the envelope.

The parameters  $\phi_1$ ,  $\phi_2$ , and  $\phi_3$  in the expression for  $\omega_g(t, \underline{\theta})$  can be related to physical parameters accounting approximately for the dominant frequencies  $\omega_p$ ,  $\omega_s$ , and  $\omega_r$  of the  $P$ ,  $S$ , and surface waves present in the ground motion, respectively. Since  $P$ -wave groups dominate the motion in the beginning,  $S$ -waves dominate at the maximum, and surface waves dominate towards the end of the earthquake acceleration time history, the relationship between the parameters  $\phi_1$ ,  $\phi_2$ , and  $\phi_3$  and the parameters  $\omega_p$ ,  $\omega_s$ , and  $\omega_r$  can be obtained by assuming that

$$\omega_p \equiv \omega_g(0, \underline{\theta}) = \phi_1 + \phi_2 \quad (3.32a)$$

$$\omega_s \equiv \omega_g(t_{max}, \underline{\theta}) = \phi_1 + \phi_2 e^{-\phi_3 t_{max}} \quad (3.32b)$$

$$\omega_r \equiv \omega_g(\infty, \underline{\theta}) = \phi_1 \quad (3.32c)$$

where  $t_{max}$  is the time that the intensity of the ground motion attains its maximum. Solving for  $\phi_1$ ,  $\phi_2$ , and  $\phi_3$ , and substituting into (3.30), the expression for  $\omega_g(t, \underline{\theta})$

in terms of the parameters  $\omega_p$ ,  $\omega_s$ , and  $\omega_r$  is

$$\omega_g(t, \underline{\theta}) = \omega_r + (\omega_p - \omega_r) \left( \frac{\omega_s - \omega_r}{\omega_p - \omega_r} \right)^{t/t_{max}} \quad (3.33)$$

The two parameter  $\phi_4$  and  $\phi_5$  in the expression for  $\alpha_g(t, \underline{\theta})$  can be related to the damping ratio of the second-order model at two different times. For example, if  $\zeta_p$  and  $\zeta_r$  are the damping ratios corresponding approximately to  $P$  and surface wave groups, respectively, and assuming that  $\omega(t, \underline{\theta}) \approx \omega_r$  after sufficient time  $t_r$ , then

$$\alpha(0, \underline{\theta}) = \phi_4 = \zeta_p \omega_p, \quad (3.34a)$$

and

$$\alpha_g(t_r, \underline{\theta}) = \phi_4 + \phi_5 t_r = \zeta_r \omega_r \quad (3.34b)$$

In this case, the expression for  $\alpha_g(t, \underline{\theta})$  in terms of  $\zeta_p$  and  $\zeta_r$  is

$$\alpha_g(t, \underline{\theta}) = \omega_p \zeta_p + (\omega_r \zeta_r - \omega_p \zeta_p) \frac{t}{t_r} \quad (3.35)$$

The standard deviation  $I_g(t) = \sqrt{R_y(t)}$  of the output process  $y(t)$ , which accounts for the time-variation of the intensity of the accelerograms, is adequately modeled by the envelope function

$$I_g(t) = I_{max} \tau^\beta \exp[\beta(1 - \tau)], \quad \tau = \frac{t + t_0}{t_{max} + t_0} \quad (3.36)$$

For  $t_0 = 0$ , envelope function (3.36) is the same as the one proposed by Saragoni and Hart [1974] defined by Equation (2.1). In their work, the explicit parameters  $\alpha$  and  $\gamma$  are related to the parameters  $I_{max}$  and  $t_{max}$  as follows:

$$\gamma = \frac{\beta}{t_{max} + t_0}, \quad \alpha = I_{max} \left( \frac{e}{t_{max} + t_0} \right)^\beta. \quad (3.37)$$

The parameters  $I_{max}$  and  $t_{max}$  are the maximum intensity and the time of the maximum intensity of the ground acceleration, respectively. The variable  $t_0$  is the time of the first non-zero acceleration before the triggering time, introduced to provide flexibility in fitting the data, and it is not a real parameter in the model. The parameter  $\beta$  is a nondimensional measure of the duration of the accelerogram.

If the duration of strong ground shaking is defined by the time interval over which the intensity is higher than, say,  $\lambda$  percent of the maximum intensity  $I_{max}$ , then the duration  $t_{dur}$  is related to  $\beta$  by:

$$\frac{t_{dur}}{t_{max} + t_0} = s_2 - s_1 \equiv \tau_{dur} \quad (3.38a)$$

where  $s_1, s_2$  are the roots of the equation

$$\ln(0.01\lambda) = \beta(\ln s_i + 1 - s_i), \quad i = 1, 2 \quad (3.38b)$$

A nondimensional plot of the envelope (3.36) is shown in Figure 3.1(a) for different values of  $\beta$ . The nondimensional duration  $\tau_{dur}$  is plotted in Figure 3.1(b) versus  $\beta$  for  $\lambda = 10$  and 20.

Incorporating these average trends into the second-order time-varying model and including Brune’s source model (Section 2.7.3), an earthquake accelerogram can be completely characterized by at most nine parameters  $\phi_1, \phi_2, \phi_3, \phi_4, \phi_5, I_{max}, t_{max}, \beta$  and  $f_c$ , forming a set  $\underline{\theta}$ . Utilizing the discrete version (3.25) of the model, the Bayesian methodology in Section 2.4.1 can be used efficiently to estimate the optimal model, i.e., the most probable parameter set  $\hat{\underline{\theta}}$  that provides, in a statistical sense, the best fit to a “target” accelerogram. For this, the conversion relationships (3.27a), (3.27b), and (3.29) between the discrete and the continuous formulation are used, and the objective function (2.32) is minimized in terms of the parameter set  $\underline{\theta}$ . The estimation procedure will be illustrated for specific accelerograms in the next section.

### 3.4.1 Analysis and Simulation of Earthquake Accelerograms

The C048.1 and the El Centro Array, Stn 12 accelerograms given in Tables 2.1 and 2.2 are used as examples to demonstrate results and check the model adequacy. Both records are chosen because they show a significant time-variation of their correlation structure. The optimal models were computed for both accelerograms and the corresponding smooth variations of  $\omega_g(t)$ ,  $\alpha_g(t)$  and  $I_g(t)$  are plotted in Figures 3.2 and 3.4. For comparison purposes, the results from the more detailed modeling computed by the moving time-window approach in Chapter 2, are also

shown in the same figures. The discrete model (3.25) is used to synthesize artificial accelerograms. The original accelerogram and two simulations are shown in Figures 3.3 and 3.5 for each target accelerogram. From these figures, it is clear that the nine-parameter model captures very well the average time variation of the amplitude and the frequency content. Also, simulations show characteristics similar to those observed in real accelerograms.

The optimal model for the C048.1 record is next used to test the basic model assumptions and check the accuracy of the approximations developed for the autocovariance function. Comparison of the approximate autocorrelation function (3.16) with the exact one computed numerically is shown in Figure 3.6 for different times  $s$ . The dotted lines in Figure 3.6 correspond to the exact autocovariance function of the equivalent discrete process computed by using the conversion relationships (3.27) and (3.29). A very good accuracy is observed which justifies the use of the simple approximate expressions in modeling broadband ground acceleration time histories.

The EPSD function of the optimal models corresponding to the two recordings are shown in Figures 3.7(a) and (b). These figures demonstrate that the instantaneous frequency components that strongly contribute to the acceleration time history shift to the lower frequencies as time advances. The effect of this shift on the response of linear and nonlinear structures will be studied in Chapter 5.

### 3.4.2 Structural Response and Model Adequacy

The C048.1 record in Table 2.1 is used to study the structural response of linear elastic and inelastic structures. The probabilistic 5% damped linear elastic response spectra computed from the optimal model are shown in Figure 3.8 and they are compared to the response spectra corresponding to the “target” accelerogram. Brune’s model with  $f_c = 0.2\text{Hz}$  has been included to correct the very low frequency components. The probabilistic inelastic response spectra for the acceleration, velocity, displacement ductility, and permanent residual displacement ductility are shown in Figure 3.9 and they are also compared to the inelastic response spectra corresponding to the “target” accelerogram. The values of the structural param-

eters (see Section 2.5) are  $n = 3$ ,  $\eta = 0.3$ , and  $\zeta = 0.05$ . The level curves with probability of 99, 90, 50, 10 and 1 percent to be exceeded are shown. The mean value of each response parameter is also shown. It is expected that the 99 and 1 percent level curves on the spectral will provide a lower and an upper bound for the response spectra of the "target" accelerogram. The response parameters computed from the "target" accelerogram lie between the 1% and 99% level curves for almost every range of initial structural frequencies. This is an indication that the ground motion model performs well in modeling the features of ground acceleration for the purpose of computing structural response.

The separation between the 1% and 99% level curves is directly proportional to the sensitivity of the response to the details of the ground motion left random by the ground motion model. It is observed that the lower the structural frequency, the more sensitive the maximum displacement, velocity, and acceleration are to the random characteristics of the ground motion model. From the maximum ductility response statistics in Figure 3.9(c), the structure becomes inelastic with high probability for initial structural frequencies ranging from 2 to 10Hz. From comparisons between the linear elastic and inelastic response statistics in Figures 3.8 and 3.9, the maximum velocity and acceleration are less sensitive to the random characteristics of the ground motion model than the corresponding elastic quantities in the frequency range from 2 to 10Hz of strong inelastic response. Moreover, in this range, the maximum ductility of the response is more sensitive to the random details of the ground motion than the maximum displacement of the elastic system. Finally, the residual ductility shown in Figure 9(d) is very sensitive to the random details of the ground motion model.

### 3.5 Concluding Remarks

A new ground motion model was proposed to treat probabilistically the uncertainty associated with the ground acceleration time history, and to model with at most nine parameters the features of the acceleration time history which are important for computing dynamic response. Using relationships (3.32), (3.35), and (3.38), the parameters in the set  $\underline{\theta}$  of the model can be explicitly expressed in terms

of the more physical parameter  $I_{max}$ ,  $t_{max}$ ,  $t_{dur}$ ,  $f_c$ ,  $\omega_p$ ,  $\omega_s$ ,  $\omega_r$ ,  $\zeta_p$  and  $\zeta_r$ . These parameters account for the maximum acceleration, the time that the maximum occurs, the duration of shaking, the corner frequency and the average dominant frequencies of the different wave groups present in the accelerogram. One could benefit from the simple interpretation of the model parameters to construct full acceleration time histories with certain desired characteristics.

The probabilistic methodology developed in Chapter 2 to extract the “optimal” nonstationary discrete model from an actual accelerogram was successfully demonstrated by using specific accelerograms that show significant time variation in both amplitude and frequency content. The methodology, which treats simultaneously the amplitude and frequency content nonstationarities, is much simpler to implement than other methods. The discrete model provides an efficient algorithm for the systematic processing of a database of accelerograms, and therefore associates each accelerogram with at most nine parameters. An important application of such a database would be to employ appropriate seismic risk analyses to probabilistically relate the model parameters with variables accounting for the seismic environment at a site. This will provide the means of predicting the full acceleration time histories at a site by probabilistically specifying the nine parameters of the model.

Extracting a stochastic model from an accelerogram also allows the sensitivity of the structural response to the details of the ground motion to be examined, while the overall features of the excitation are fixed. The discrete model provides a simple and computationally efficient algorithm for the generation of an ensemble of artificial digitized accelerograms with similar characteristics to a given earthquake accelerogram, and it treats probabilistically the uncertainty associated with the acceleration time history. These simulated accelerograms could be further used in response studies of linear elastic and inelastic structures. The results of such studies indicate that the lower the structural frequency of linear structures, the more the displacement, velocity and acceleration are sensitive to the details of the ground motion. Also, the more inelastic the response of a structure is, the less sensitive the maximum velocity and absolute acceleration is to ground motion details. However,

the maximum ductility and especially the residual ductility of the inelastic response are very sensitive to the details of an acceleration time history which has its overall features fixed.

The simplified statistical structure of the continuous model is promising for incorporating the model in analytical random vibration studies and for mathematically studying the importance of the temporal nonstationarity in both the amplitude and frequency content of ground motion on the response of both linear and nonlinear structures. These studies are presented in the next two chapters.

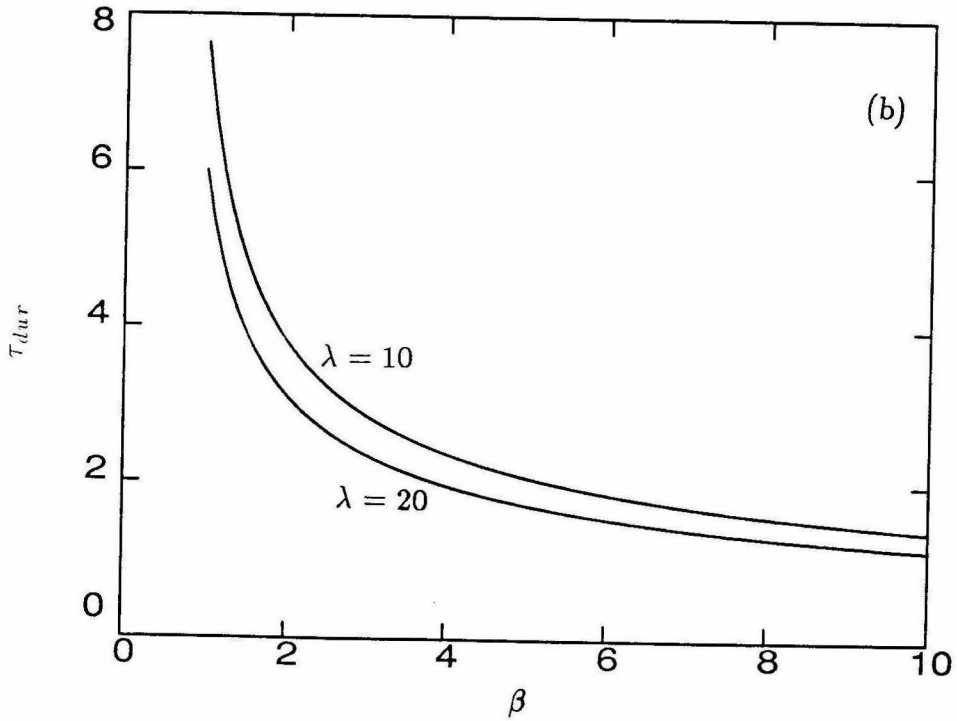
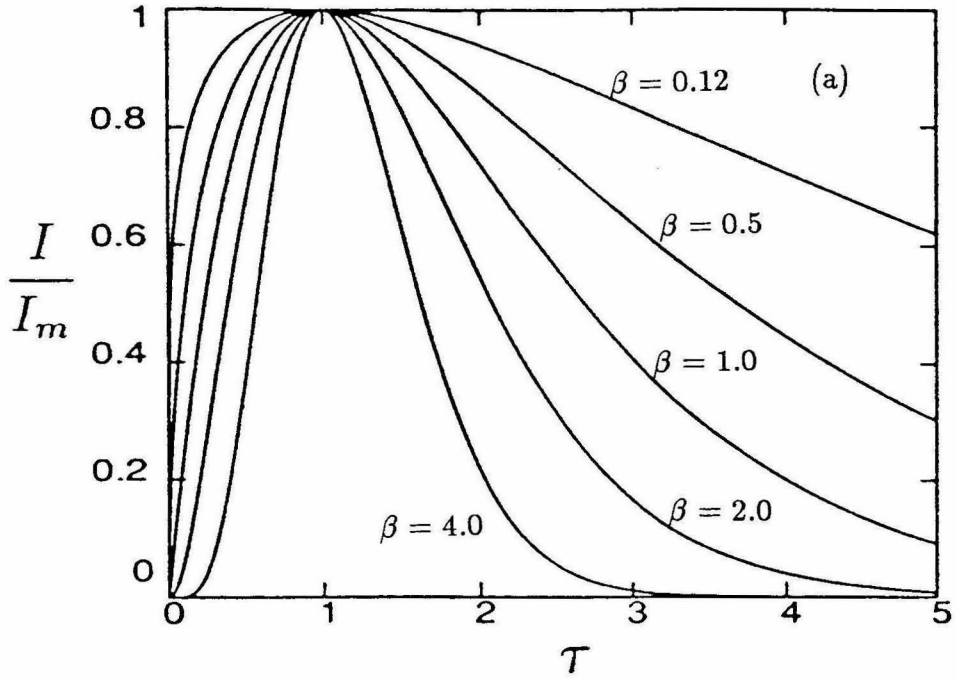


Figure 3.1. (a) Nondimensional time variation of the ground motion intensity for different values of  $\beta$ . (b) Relation between the nondimensional duration and  $\beta$  for  $\lambda = 10$  and  $\lambda = 20$ .

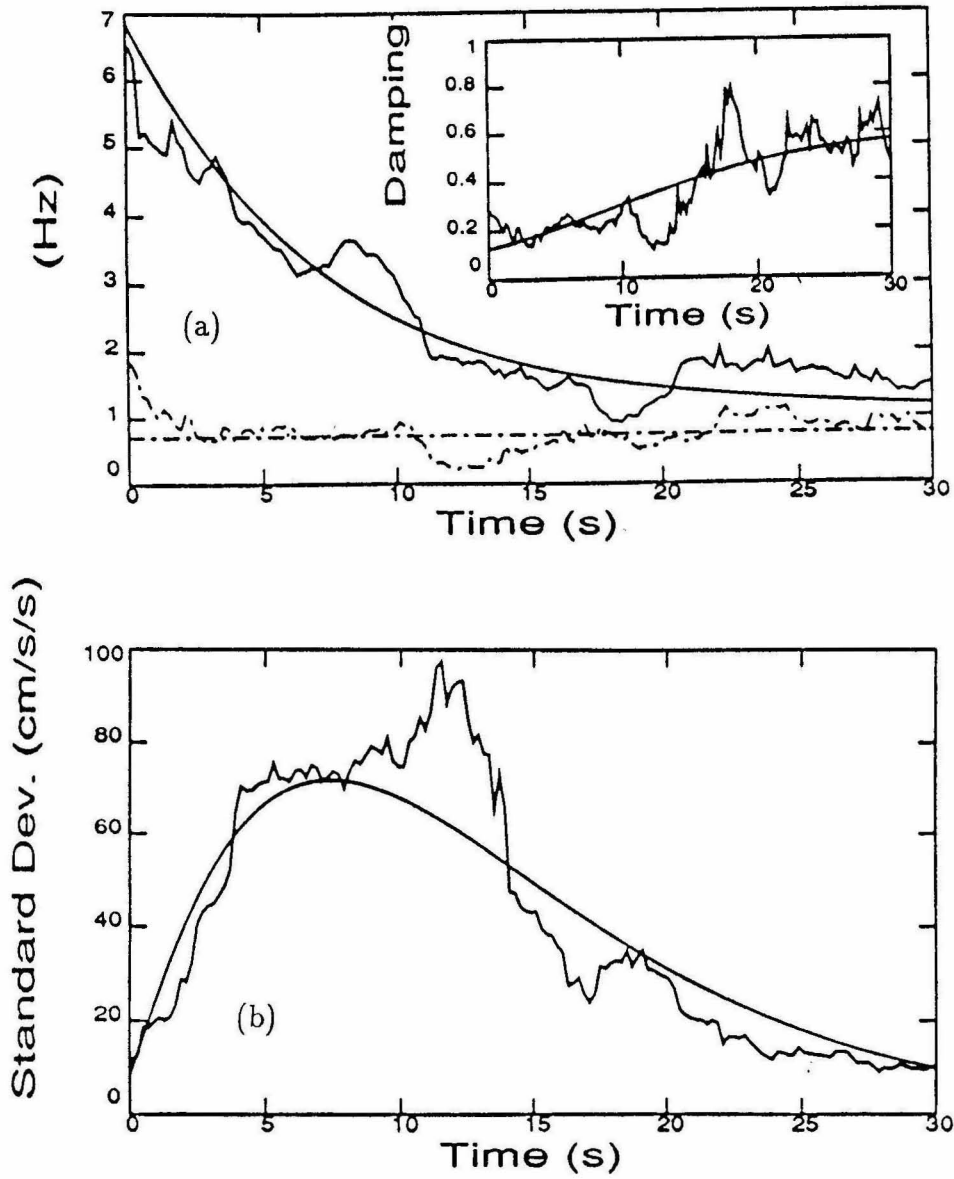


Figure 3.2. Time variation of (a) undamped frequency  $\omega_g$  (solid curves), bandwidth  $\omega_g \zeta_g$  (dashed-dotted curves), damping ratio  $\zeta_g$ , and (b) intensity  $I_g$  obtained by the nine-parameter model (smooth curves) and the moving time-window approach (other curves) for the C048.1 record in Table 2.1.

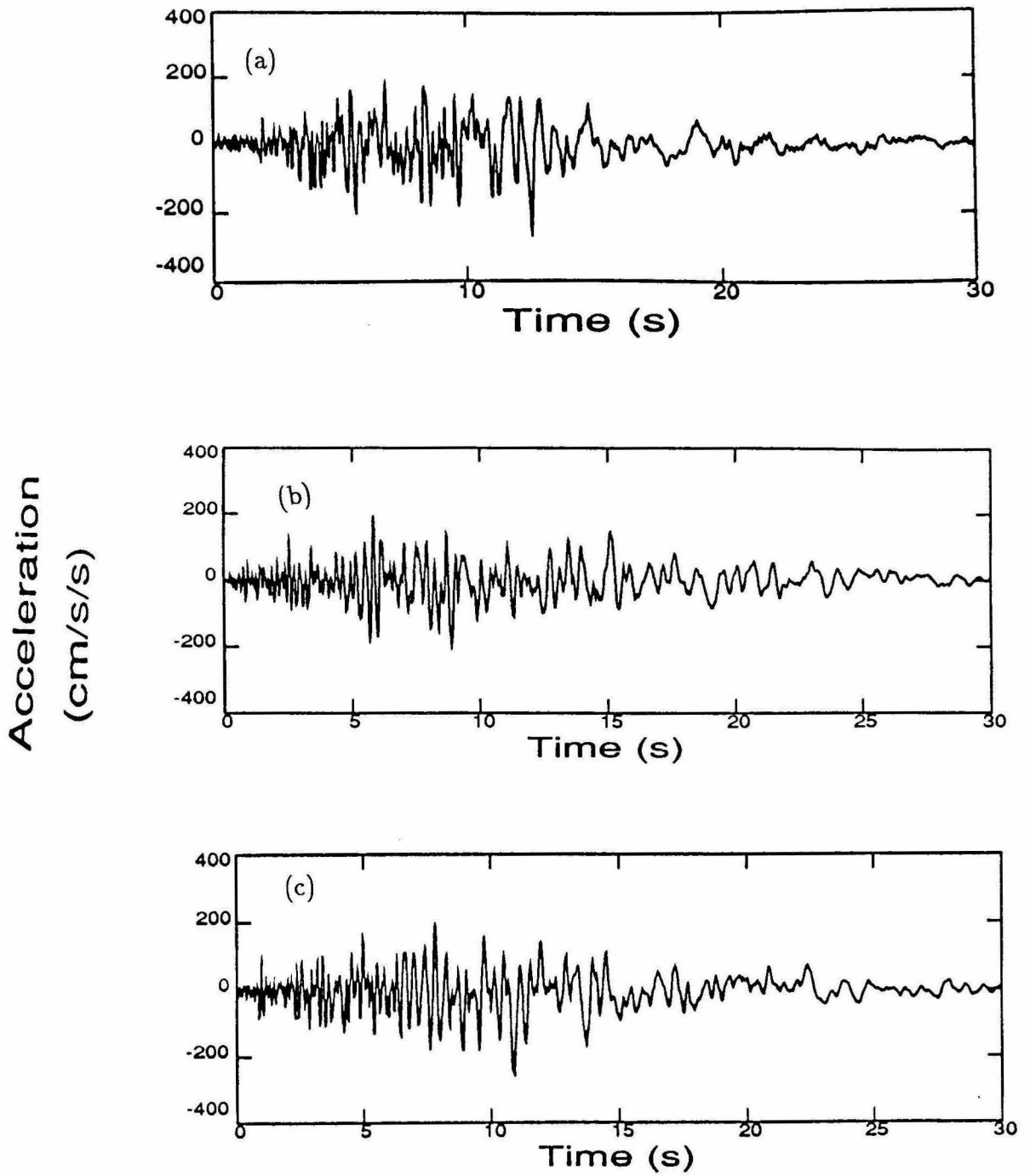


Figure 3.3. Comparison of (a) the C048.1 accelerogram and (b), (c) two artificial accelerograms.

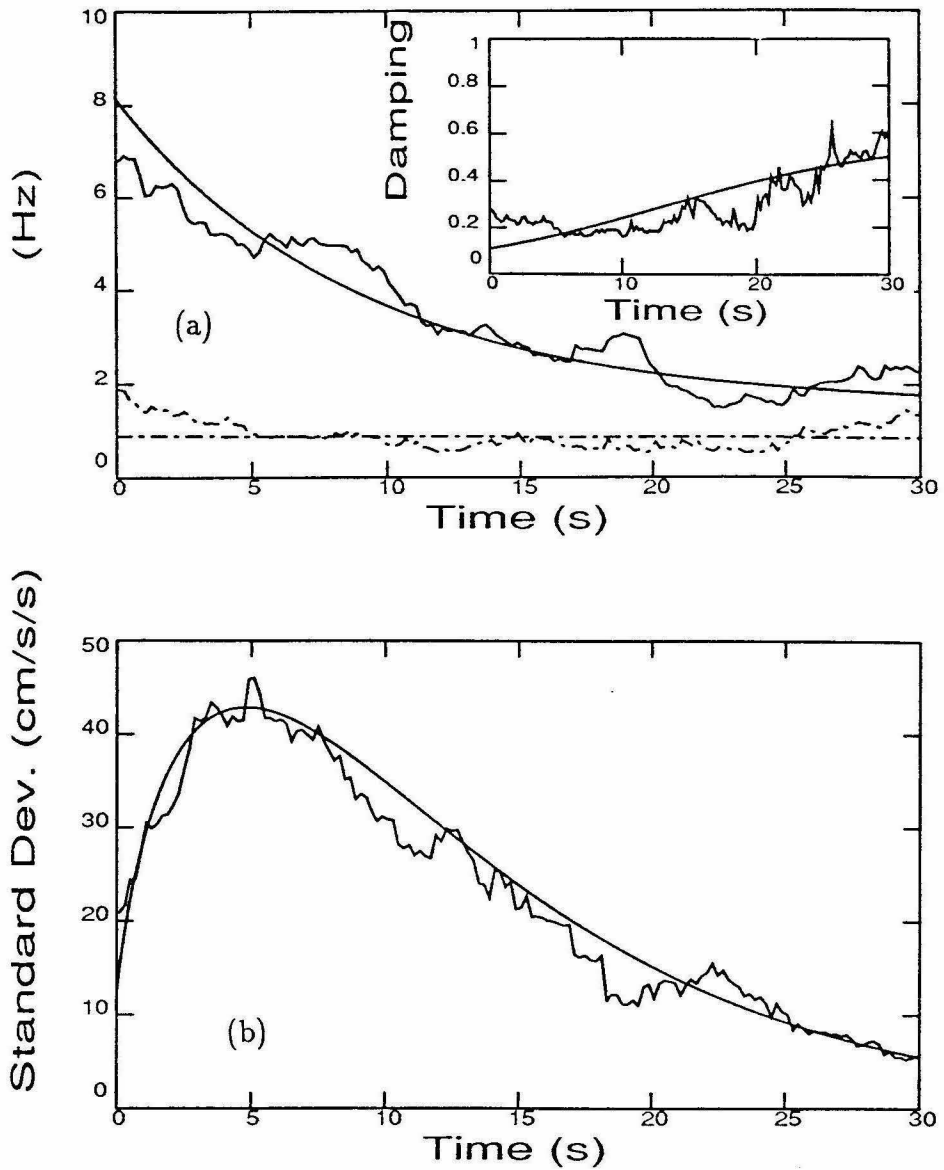


Figure 3.4. Time variation of (a) undamped frequency  $\omega_g$  (solid curves), bandwidth  $\omega_g \zeta_g$  (dashed-dotted curves), damping ratio  $\zeta_g$ , and (b) intensity  $I_g$  obtained by the nine-parameter model (smooth curves) and the moving time-window approach (other curves) for the El Centro Array, Stn 12 record in Table 2.1.

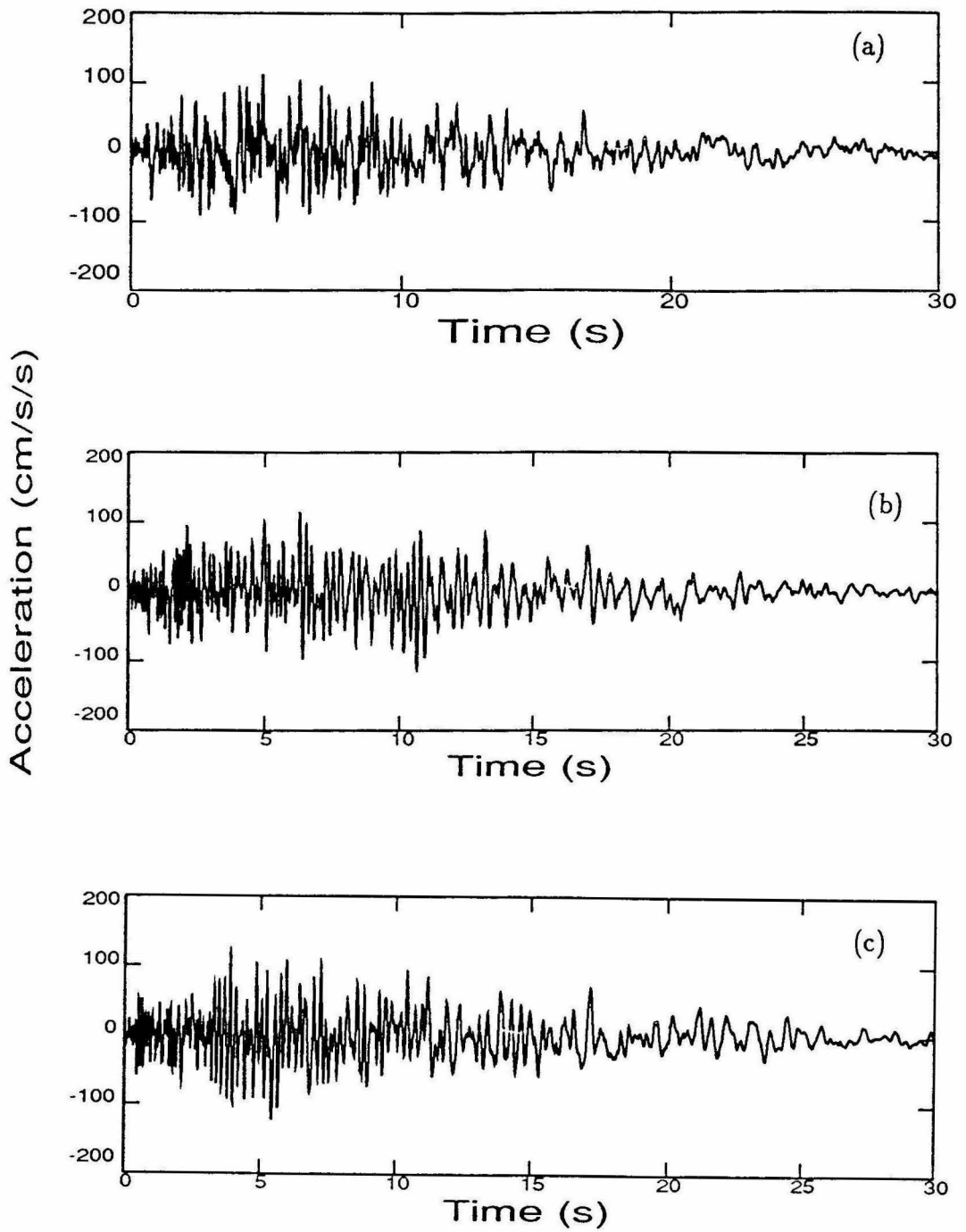


Figure 3.5. Comparison of (a) the El Centro Array, Stn 12 accelerogram and (b), (c) two artificial accelerograms.

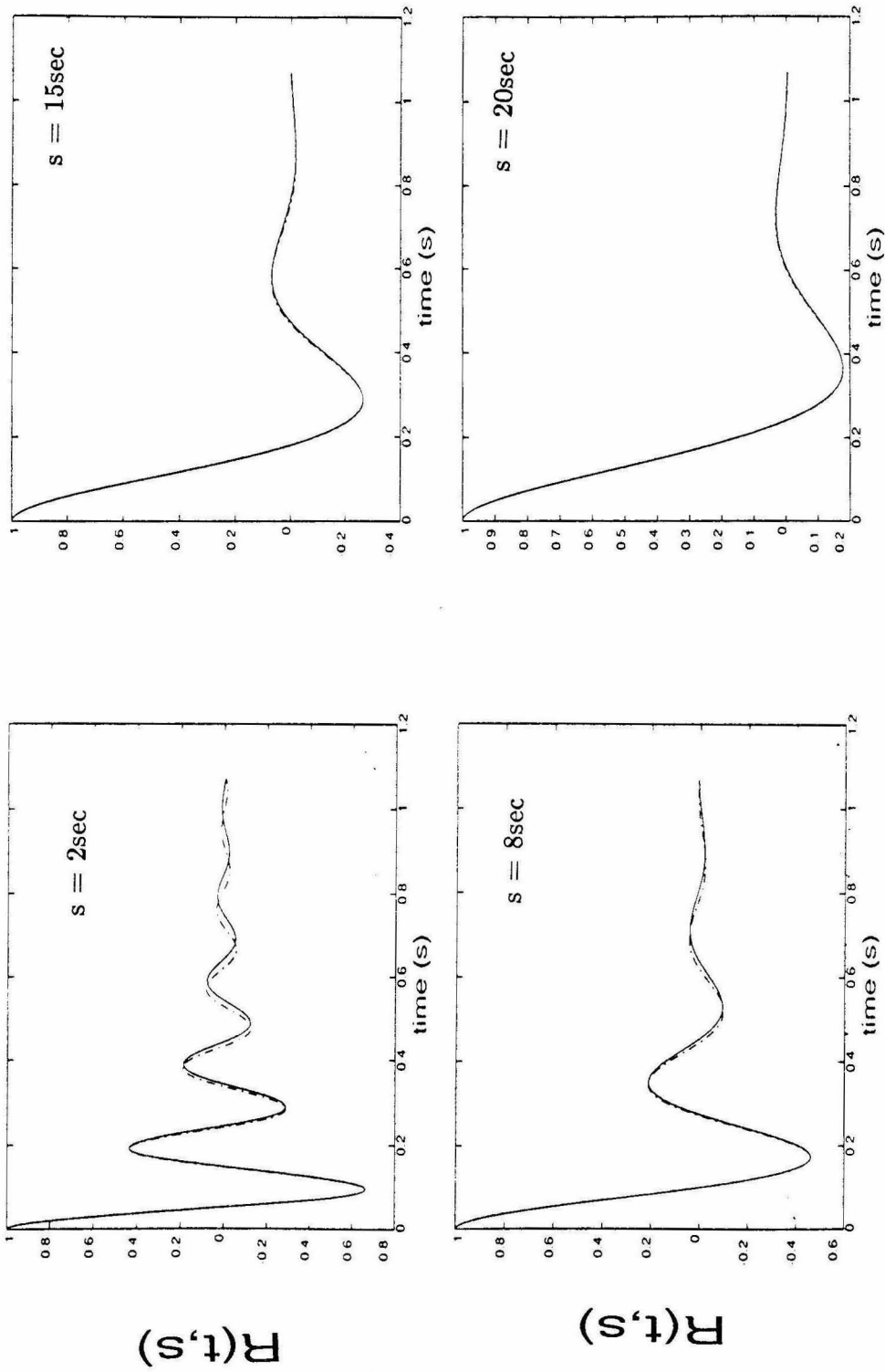


Figure 3.6. Comparison of the exact (solid curve) and approximate (dashed-dotted curve) autocorrelation function  $R_{yy}(t, s)$  of the stochastic process modeling the C048.1 accelerometer.

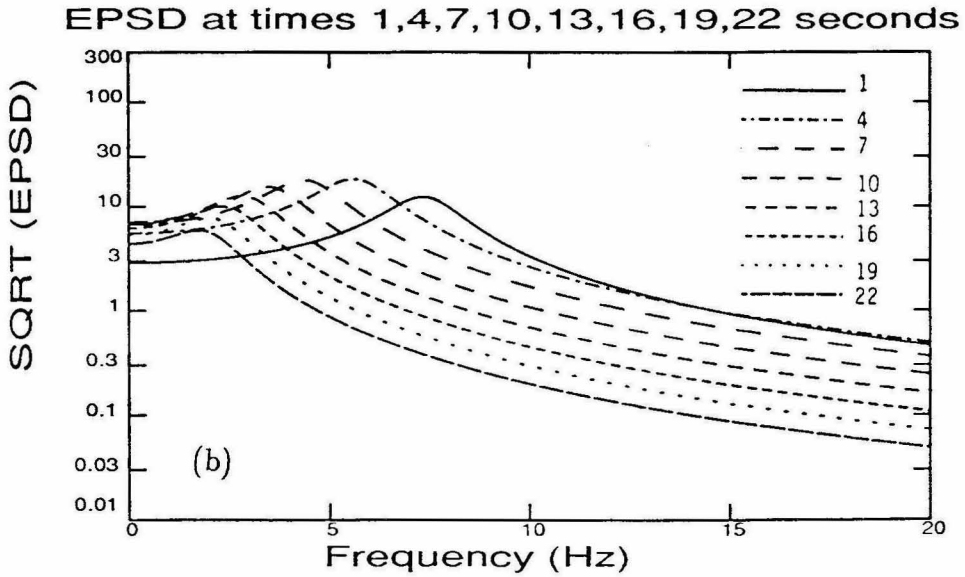
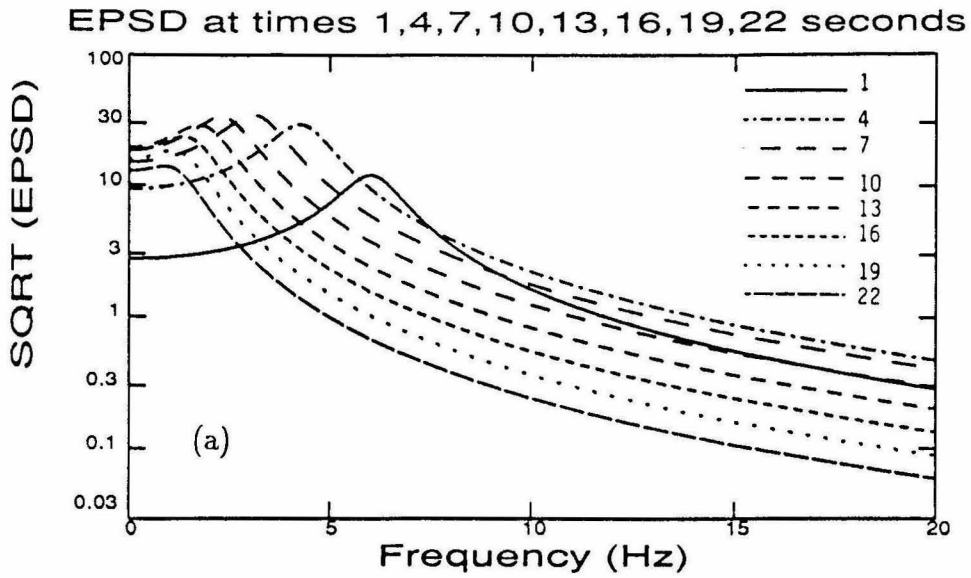


Figure 3.7. The EPSD function plotted at different times (a) C048.1, (b) El Centro Array, Stn 12.

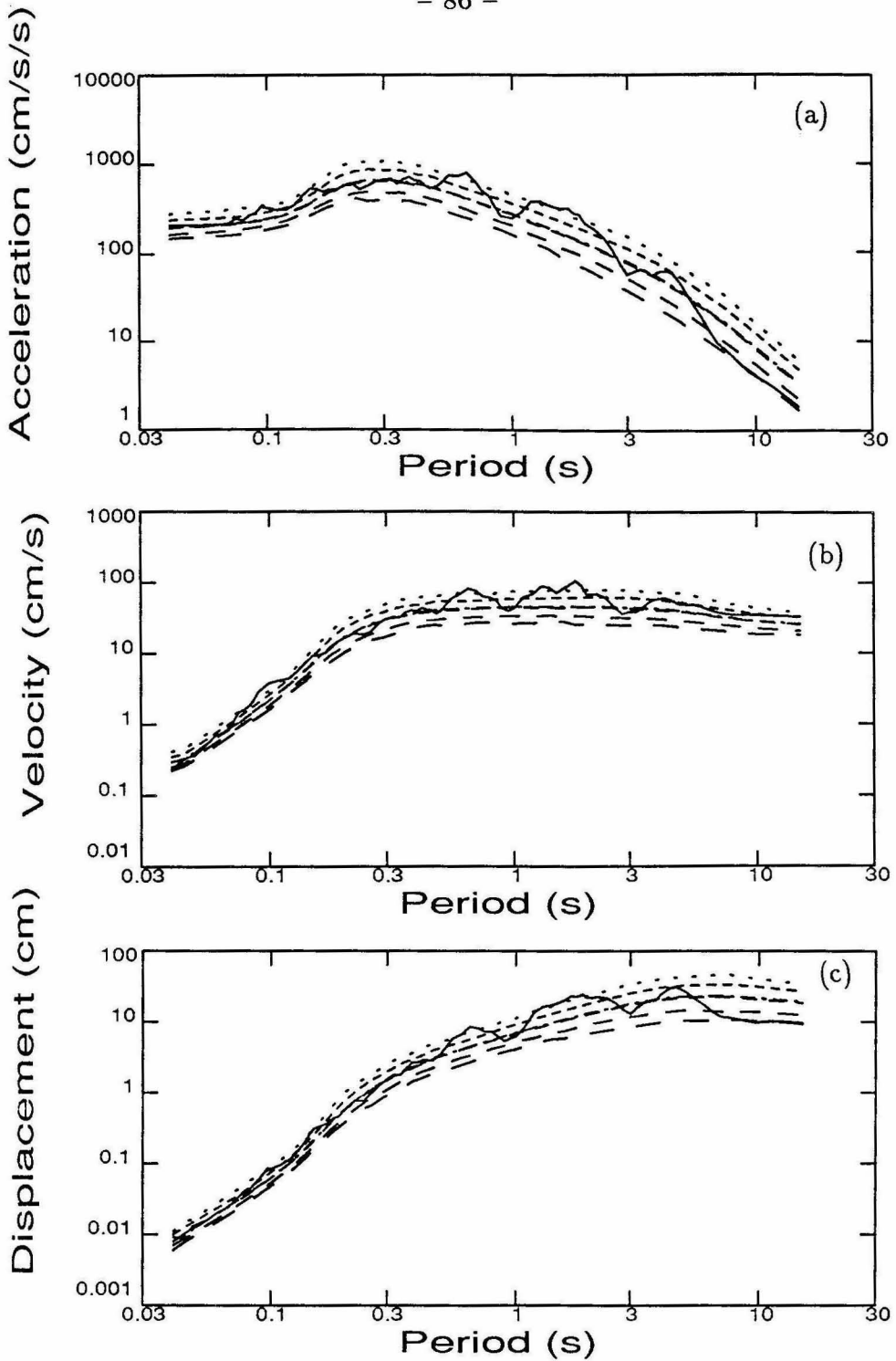


Figure 3.8. Comparison between the 5% response spectra of the C048.1 accelerogram (solid line), the mean response spectra (dashed-dotted line) and the probabilistic response spectra (dashed lines which from top to bottom correspond to  $p = 0.99, 0.90, 0.50, 0.10, 0.01$ ) computed for the nine-parameter optimal model.

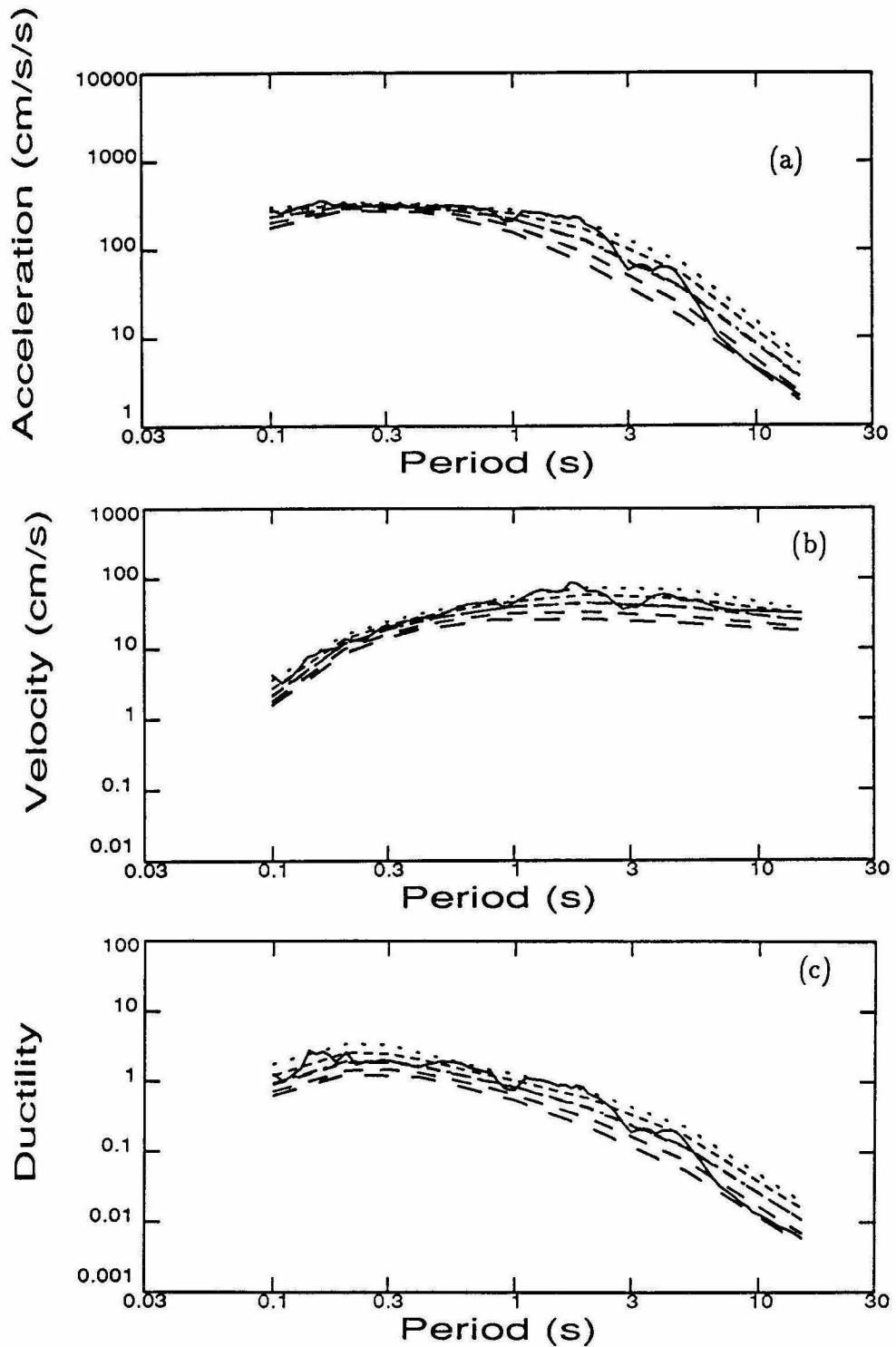


Figure 3.9. Comparison between the inelastic response spectra of the C048.1 accelerogram (solid line), the mean response spectra (dashed-dotted line) and the probabilistic response spectra (dashed lines which from top to bottom correspond to  $p = 0.99, 0.90, 0.50, 0.10, 0.01$ ) computed for the nine-parameter optimal model. Structural parameters  $n = 3$ ,  $\eta = 0.3$ , and  $\zeta = 0.05$ .

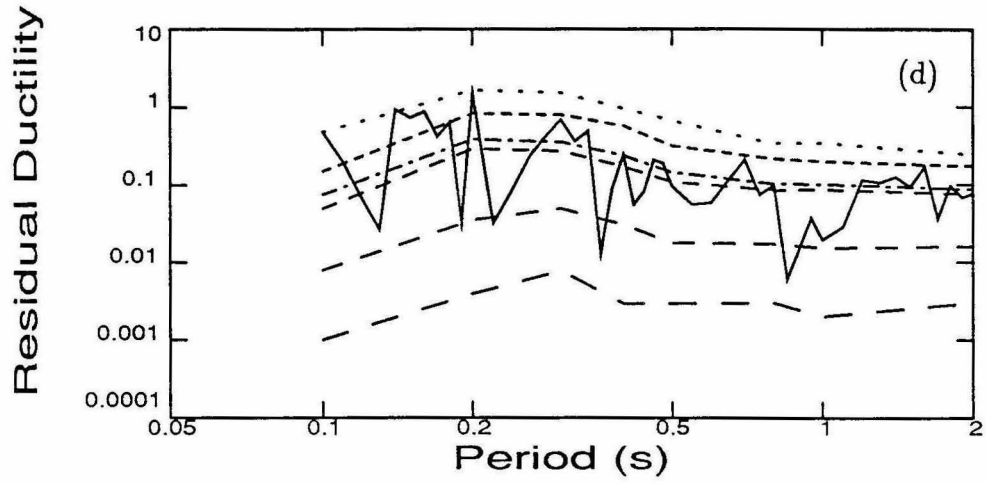


Figure 3.9. (Continued)

## Chapter 4

# Transient Response Characteristics of Stochastically Excited Linear and Nonlinear Systems

### 4.1 Introduction

The stochastic properties of the response of a structure subjected to a stochastic excitation are completely defined by the joint probability density functions of the response. For linear structures and for Gaussian excitation, the response is also Gaussian. Therefore, only the mean and the covariance response is needed to completely determine the joint probability density function of the response. The problem of determining the covariance response of a linear structure subjected to nonstationary excitation has been well-formulated. A selective review of the existing methods may be found in Hou (1990). Among the different methods, the Liapunov direct method is often used to obtain numerical solutions for the covariance response. In the case of lightly-damped structures and wide-banded excitations, approximate methods (Caughey and Stumpf, 1961, Spanos, 1983 and Igusa 1988) have been introduced to considerably simplify the problem. For wide-banded excitations, such as earthquake ground motion, with nonstationarities in both the amplitude and the frequency content, the existing approximate methods often result in significant errors. The reason is that in the range of system and excitation parameters of practical interest, the assumptions for the validity of the approximations are violated.

In this chapter, an approximate method is developed to considerably simplify the original equations for the covariance of the nonstationary response of linear systems for a broader range of system and excitation parameters. The method treats wide-banded excitations often encountered in earthquake applications. The basic

idea is to approximate the Liapunov differential matrix equation for the mean-square response of a structure by a much simpler lower-order differential equation. For the case of single-degree-of-freedom (SDOF) oscillators, the approximations cover any range of oscillator parameters and they are not restricted to the case of lightly-damped oscillators as in Spanos(1983) and Igusa (1988). In addition, conditions for the approximations to be correct as well as higher-order terms that improve the approximations are derived. Multi-degree-of-freedom (MDOF) linear systems are also treated to considerably improve the existing approximations (Bucher, 1988), and to extend their range of applicability to nonstationary non-white excitations.

The response of nonlinear SDOF structures is also considered. Extensive reviews regarding the nonlinear random vibration problem may be found in Graendall and Zhu (1983), and Spanos and Lutes (1986). For the purpose of this study, transient equivalent linearization is used to replace the equation of motion of a nonlinear SDOF oscillator by an equivalent second-order linear differential equation with variable coefficients. For a Gaussian excitation, this approximate solution technique assumes that the response is also Gaussian and, therefore, its statistical properties are completely determined by the mean and the covariance of the response. Considering the equivalent linear system, the Liapunov differential matrix equation for the covariance of the response becomes nonlinear. Assuming that the equivalent linear coefficients are slowly-varying functions of time, a similar formulation to that of the linear oscillator is developed to considerably simplify the equations for the mean-square and the covariance of the response of the equivalent linear oscillator. The approximate analysis developed for the linear SDOF oscillator is used as a guide for treating the case of the nonlinear SDOF oscillator.

Besides the considerable simplifications attained by the approximate formulation, they also provide insight into the nonstationary response characteristics of a linear and nonlinear SDOF oscillator under the following assumptions, i) the excitation process is *broadband* with *slowly-varying* correlation structure (e.g., earthquake loads), and ii) the coefficients of the equivalent linear oscillator are *slowly varying* functions of time. Similarities and differences with the stationary response characteristics are also explored. Simplified example excitations as well as the realistic

earthquake excitation described in Chapters 2 and 3 of this thesis are used to verify the accuracy of the approximations. The results indicate that the essential behaviour of the response is preserved without significant loss of accuracy, which is often of the order of 1% for cases of practical interest.

## 4.2 Mathematical Formulation of the Response

Let the response of a stochastically excited linear or nonlinear SDOF oscillator be governed or approximated by the differential equation

$$\ddot{x}(t) + 2\alpha(t)\dot{x}(t) + \omega^2(t)x(t) = G(t) \quad (4.1)$$

where  $\alpha(t) = \zeta(t)\omega(t)$  and  $\omega(t)$  are deterministic time-varying coefficients and the excitation  $G(t)$  is assumed to be a zero-mean Gaussian stochastic process. In summary, the equation of motion (4.1) arises in the following situations:

1. Modal analysis of linear MDOF structures subjected to random loads. Equation (4.1) corresponds to the modal equation with constant modal frequency  $\omega(t) = \omega_0$  and constant damping ratio  $\zeta(t) = \zeta$ . Usually  $\zeta \ll 1$  with typical range from 0.01 to 0.1.
2. Transient equivalent linearization applied to a stochastically excited nonlinear SDOF oscillator. Equation (4.1) corresponds to the equivalent linear systems with equivalent frequency  $\omega(t) = \omega_{eq}(Q(t))$  and equivalent damping ratio  $\zeta(t) = \zeta_{eq}(Q(t))$ , where  $Q(t)$  is the mean-square matrix of the state vector  $(x(t), \dot{x}(t))^T$ . For strongly excited nonlinear structures, the assumption  $\zeta_{eq}(Q(t)) \ll 1$  need no longer be valid.
3. Modeling of stochastic loads to use as inputs for structural response studies with  $\omega(t)$  and  $\zeta(t)$  being prescribed functions of time. Specific examples are the general class of models proposed in Chapters 3 with evolutionary power spectral density function, and the well-known Kanai (1957) and Tajimi (1961) model. In ground motion modeling, the process  $x(t)$  is usually broadband with typical values of  $\zeta(t)$  ranging from 0.2 to 0.6.

For mathematical convenience, equation (4.1) is rewritten in state-space form

as

$$\dot{\underline{x}}(t) = A(t)\underline{x}(t) + \underline{g}(t) \quad (4.2)$$

where

$$\underline{x}(t) = \begin{pmatrix} x(t) \\ \dot{x}(t) \end{pmatrix}, \quad A(t) = \begin{pmatrix} 0 & 1 \\ -\omega^2(t) & -2\alpha(t) \end{pmatrix}, \quad \underline{g}(t) = \begin{pmatrix} 0 \\ G(t) \end{pmatrix} \quad (4.3)$$

From the linearity of equation (4.1) and the Gaussian assumption of the excitation, the response vector  $(x, \dot{x})^T$  is also a zero-mean Gaussian stochastic process.

The solution of equation (4.2) in terms of the principal matrix  $\Phi(t, \tau)$  is

$$\underline{x}(t) = \Phi(t, 0)\underline{x}(0) + \int_0^t \Phi(t, \tau)\underline{g}(\tau)d\tau \quad (4.4)$$

The principal matrix  $\Phi(t, \tau)$  is obtained from the solution of the system

$$\begin{aligned} \dot{\Phi}(t, \tau) &= A(t)\Phi(t, \tau) \\ \Phi(\tau, \tau) &= I \end{aligned} \quad (4.5)$$

where  $\langle . \rangle$  denotes differentiation with respect to the independent variable  $t$ . For a time-invariant matrix  $A(t) = A$ , a closed-form solution can be obtained for the principal matrix  $\Phi(t, \tau)$  which depends on the time difference  $t - \tau$ . For a time-variant matrix  $A(t)$  a closed-form solution does not exist, in general, and numerical integration is necessary. For slowly varying  $A(t)$ , however, an approximate closed-form solution can be obtained. Such an approximation, together with the appropriate conditions for its validity, are derived in Appendix A, and it will be used later in this analysis.

#### 4.2.1 Mean-Square Response

Let  $Q(t) = E[\underline{x}(t)\underline{x}^T(t)]$  denote the mean-square matrix of the response. Assuming zero initial conditions for  $\underline{x}(t)$ ,  $Q(t)$  is obtained by the solution of the Liapunov differential matrix equation

$$\begin{aligned} \dot{Q}(t) &= A(t)Q(t) + Q(t)A^T(t) + L(t) + L^T(t) \\ Q(0) &= 0 \end{aligned} \quad (4.6)$$

where

$$L(t) = \int_0^t \Phi(t, \tau) E[\underline{g}(\tau) \underline{g}^T(t)] d\tau \quad (4.7)$$

The Liapunov differential matrix equation is nonlinear for a stochastically equivalent linear system since the matrix  $A(t)$ , and the principal solution  $\Phi(t, \tau)$  appearing in the “forcing” integral term  $L(t)$ , depend on the solution matrix  $Q(t)$  in this case.

Let  $q_{ij}(t)$ ,  $i = 1, 2$ ,  $j = 1, 2$  denote the entries of the covariance matrix  $Q(t)$  and  $L_{ij}(t)$ ,  $i = 1, 2$ ,  $j = 1, 2$  denote the entries of the matrix  $L(t)$ . From the symmetry of  $Q(t)$ , equation (4.6) can be cast in the component form

$$\dot{q}_{11}(t) = 2q_{12}(t) \quad (4.8a)$$

$$\dot{q}_{12}(t) = q_{22}(t) - \omega^2(t)q_{11}(t) - 2\alpha(t)q_{12}(t) + L_{12}(t) \quad (4.8b)$$

$$\dot{q}_{22}(t) = -2\omega^2(t)q_{12}(t) - 4\alpha(t)q_{22}(t) + 2L_{22}(t) \quad (4.8c)$$

#### 4.2.2 Covariance Response

Let  $S(t, s) = E[\underline{x}(t)\underline{x}^t(s)]$  denote the covariance of the response vector  $\underline{x}(t)$  between the times  $t$  and  $s$ , then the differential matrix equation for obtaining  $S(t, s)$  is

$$\dot{S}(t, s) = A(t)S(t, s) + U^T(t, s), \quad t \geq s \quad (4.9)$$

$$S(s, s) = Q(s)$$

where

$$U(t, s) = \int_0^s \Phi(s, \tau) E[\underline{g}(\tau) \underline{g}^T(t)] d\tau \quad t \geq s \quad (4.10)$$

with  $U(t, t) = L(t)$ .

For the special case (4.3) of the vector equation (4.2), the quantity  $U(t, s)$  is simplified to

$$U(t, s) = \begin{pmatrix} 0 & \int_0^s \Phi_{12}(s, \tau) E[G(t)G^T(\tau)] d\tau \\ 0 & \int_0^s \Phi_{22}(s, \tau) E[G(t)G^T(\tau)] d\tau \end{pmatrix} \quad (4.11)$$

### 4.2.3 Special Case: Modulated White-Noise Excitation

The case of second-order linear systems with modulated white-noise excitation is of special interest for the following reasons. It simplifies the formulation for the covariance response, it provides the essential characteristics for the mean-square response of wide-banded modulated nonwhite excitations, and it is often used to model stochastic structural loads. Let

$$G(t) = f(t)e(t) \quad (4.12)$$

be a modulated white-noise process, where  $f(t)$  is a deterministic envelope function and  $e(t)$  is a stationary white-noise process with properties

$$E[e(t)] = 0 \quad \text{and} \quad E[e(t)e(s)] = \delta(t - s) \quad (4.13)$$

Under such an excitation, the forcing integral terms  $L(t)$  and  $U(t, s)$  which appear in the formulation of the covariance matrix equation simplify to

$$\begin{aligned} L_{12}(t) &= f^2(t)\Phi_{12}(t, t) = 0 \\ L_{22}(t) &= f^2(t)\Phi_{22}(t, t) = f^2(t) \\ U(t, s) &= 0, \quad t > s \end{aligned} \quad (4.14)$$

and, therefore, they are independent of the principal matrix solution  $\Phi(t, \tau)$ . Solving equation (4.9), the covariance of the response at two different times  $t$  and  $s$  can be expressed in terms of the covariance response for  $t = s$  as

$$S(t, s) = \Phi(t, s)Q(s) \quad (4.15)$$

Once the mean-square matrix of the response has been found, the covariance of the response can easily be obtained by using (4.15).

For the general non-white excitation, the numerical integration for computing the mean-square matrix or the covariance matrix of the response is usually time-consuming because of the additional numerical integration required for each time step to evaluate the convolution integral (4.7) or the integral (4.10), respectively. One of the purposes of this study is to approximate these integrals by simple algebraic expressions, and therefore to reduce considerably the computational time.

Most of the results are presented for the mean-square response and they can be easily extended to evaluating the covariance response since the integral (4.10) is similar to the convolution integral (4.7). In the analysis that follows, it is assumed that the oscillator is underdamped ( $\zeta < 1$ ). The case of linear SDOF oscillators is first treated and then the approximate formulation is extended to the case of nonlinear SDOF oscillators.

### 4.3 Formulation for the Mean-Square Response of Linear Time-Invariant SDOF Oscillators

For a linear SDOF oscillator with angular frequency  $\omega_0$  and damping ratio  $\zeta$ , the Liapunov differential equation (4.8) for the transient mean-square response is linear with time-invariant coefficients  $\omega(t) = \omega_0$  and  $\zeta(t) = \zeta$ .

#### 4.3.1 Mean-Square Displacement

Eliminating  $q_{12}(t)$  and  $q_{22}(t)$  from the set of equations (4.8), the following third-order differential equation in terms of  $q_{11}(t)$  is obtained

$$q_{11}^{(3)}(t) + 6\alpha q_{11}^{(2)}(t) + [4\omega_0^2 + 8\alpha^2] q_{11}^{(1)}(t) + 8\alpha\omega_0^2 q_{11}(t) = 4L_{22}(t) + 8\alpha L_{12}(t) + 2\dot{L}_{12}(t) \quad (4.16)$$

The characteristic equation has one real negative root  $\rho_1 = -2\zeta\omega_0$  and two complex roots  $\rho_2 = -2\zeta\omega_0 + i2\omega_0\sqrt{1-\zeta^2}$  and  $\rho_3 = -2\zeta\omega_0 - i2\omega_0\sqrt{1-\zeta^2}$ . Therefore, the third-order linear differential equation for  $q_{11}(t)$  can be split into the first-order linear differential equation

$$\begin{aligned} \dot{q}_{11}(t) + 2\alpha q_{11}(t) &= 2r(t) \\ q_{11}(0) &= 0 \end{aligned} \quad (4.17)$$

associated with the real negative root, and the second-order linear differential equation

$$\begin{aligned} \ddot{r}(t) + 4\alpha\dot{r}(t) + 4\omega_0^2 r(t) &= g(t) \\ r(0) = 0, \quad \dot{r}(0) &= 0 \end{aligned} \quad (4.18)$$

for the term  $r(t)$ , which is associated with the two complex roots. The forcing term of the second-order linear differential equation is

$$g(t) = 2L_{22}(t) + 4\alpha L_{12}(t) + \dot{L}_{12}(t) \quad (4.19)$$

and it simplifies to  $g(t) = f^2(t)$  for the modulated white-noise excitation (4.12).

The mean-square displacement response satisfies a first-order differential equation which is less complicated and more workable than the third-order differential equation (4.16). The forcing term  $r(t)$  is still complicated and it is obtained by independently solving the second-order differential equation (4.18). As it will be seen later, the dynamics of the first-order differential equation provides all the essential characteristics of the response while the dynamics of the second-order differential equation has secondary effects on the mean-square response.

Spanos (1980, 1983) used an entirely different approach to obtain a first-order differential equation similar to the equation (4.17) obtained herein. In his formulation, Spanos used the stochastic averaging method where he introduced in the beginning of his analysis the following approximations:

- a. The SDOF oscillator is lightly-damped;
- b. The excitation is broadband and its EPSD is slowly varying; and
- c.  $\{excitation\ strength\} = \mathcal{O}(\zeta) \times \{response\ strength\}$ .

The present analysis is general and it does not incorporate any approximations. It results in a first-order differential equation for the mean-square displacement, similar to that obtained by Spanos, with the only difference being in the forcing terms. Our forcing term is a generalized function  $r(t)$  given by (4.18) and does not incorporate any approximations. It turns out that under the approximations used by Spanos, the two formulations yield identical results.

### 4.3.2 Mean-Square Velocity

Using the first-order differential equation (4.17) for the mean-square displacement and (4.8b), the mean-square velocity  $q_{22}(t)$  is related to the mean-square displacement  $q_{11}(t)$  by the simple algebraic expression

$$q_{22}(t) = \omega_0^2 q_{11}(t) \{1 + \epsilon_{22}(t)\} - L_{12}(t) \quad (4.20)$$

where

$$\epsilon_{22}(t) = \frac{\dot{r}(t)}{\omega_0^2 q_{11}(t)} \quad (4.21)$$

### 4.3.3 Mean-Square Absolute Acceleration

If  $-G(t)$  represents the base acceleration of the oscillator, then the absolute acceleration  $a(t)$  of the response is given by

$$a(t) = \ddot{x}(t) - G(t) = -2\alpha\dot{x}(t) - \omega_0^2 x(t) \quad (4.22)$$

Using (4.8a), (4.17), and (4.20), the mean-square absolute acceleration  $q_a(t) = E[a^2(t)]$  is related to the mean-square displacement  $q_{11}(t)$  of the response by the simple algebraic expression

$$q_a(t) = \omega_0^4 (1 + 4\zeta^2) q_{11}(t) \{1 + \epsilon_a(t)\} - 4\zeta^2 \omega_0^2 L_{12}(t) \quad (4.23)$$

where

$$\epsilon_a(t) = \frac{4\zeta^2}{1 + 4\zeta^2} \epsilon_{22}(t) + \frac{4\zeta}{1 + 4\zeta^2} \epsilon_{12}(t) \quad (4.24a)$$

and

$$\epsilon_{12}(t) = \frac{\dot{q}_{11}(t)}{2\omega_0 q_{11}(t)} \quad (4.24b)$$

### 4.3.4 Displacement-Velocity Correlation

Using (4.17) and (4.8a), the quantity  $q_{12}(t)$  is related to the mean-square displacement  $q_{11}(t)$  of the response by the simple algebraic expression

$$q_{12}(t) = -\alpha q_{11}(t) + r(t) \quad (4.25)$$

### 4.3.5 Similarities Between Transient and Stationary Mean-Square Response

The expressions for the transient mean-square response are a generalization of the expressions

$$q_{11} = \frac{2L_{22} + 4\alpha L_{12}}{4\alpha\omega_0^2} \quad (4.26)$$

$$q_{22} = \omega_0^2 q_{11} - L_{12} \quad (4.27)$$

$$q_a = \omega_0^4 (1 + 4\zeta^2) q_{11} - 4\zeta^2 \omega_0^2 L_{12} \quad (4.28)$$

$$q_{12} = 0 \quad (4.29)$$

governing the stationary response of a SDOF oscillator excited by a stationary stochastic process. Relations (4.26) to (4.29) can easily be derived by setting  $\dot{Q} = 0$  in the Liapunov matrix equation (4.6). The mean-square velocity and the mean-square absolute acceleration of the nonstationary response are related to the nonstationary mean-square displacement by simple algebraic expressions which could be viewed as a generalization of the stationary relations (4.27) and (4.28), respectively. The additional terms  $\epsilon_{22}(t)$ ,  $\epsilon_{12}(t)$  and  $\epsilon_a(t)$  appearing in the expressions (4.20) and (4.23) account for the nonstationarity of the response. As it will be seen in the numerical results in Section 4.4.2,  $\epsilon_{22}(t)$ ,  $\epsilon_{12}(t)$  and  $\epsilon_a(t)$  are in general small compared to unity and they can be neglected. Therefore, the mean-square velocity and absolute acceleration can be obtained in terms of the mean-square displacement by the stationary relations, after replacing the time-invariant quantities with the time-varying ones corresponding to time  $t$ .

#### 4.3.6 Exact Solution for the Mean-Square Response

The solution of equation (4.17) can be derived in terms of the convolution integral

$$q_{11}(t) = 2 \int_0^t e^{-2\zeta\omega_0(t-\tau)} r(\tau) d\tau \quad (4.30)$$

where  $r(t)$  is obtained by the solution of (4.18) in terms of the convolution integral

$$r(t) = \frac{1}{2\omega_d} \int_0^t e^{-2\zeta\omega_0(t-\tau)} \sin 2\omega_d(t-\tau) g(\tau) d\tau \quad (4.31)$$

Substituting the integral form (4.31) for  $r(t)$  into (4.30), interchanging the order of integrations and after algebraic manipulations, an exact solution for  $q_{11}(t)$  is derived in the form

$$q_{11}(t) = \frac{1}{2\omega_d^2} \int_0^t e^{-2\zeta\omega_0(t-\tau)} g(\tau) d\tau - \frac{1}{2\omega_d^2} \int_0^t e^{-2\zeta\omega_0(t-\tau)} \cos 2\omega_d(t-\tau) g(\tau) d\tau \quad (4.32)$$

For certain  $g(t)$ , it is possible to evaluate these expressions analytically and so obtain an exact closed-form solution for the mean-square response. If the integrations cannot be performed analytically, it is more efficient to numerically integrate equations (4.8), rather than the integrals in (4.32).

### 4.3.7 Exact Solution for the Covariance of the Response: Modulated White-Noise Excitation

For *modulated white-noise excitation*, the covariance of either the displacement or the velocity or the absolute acceleration of the response has been derived in Appendix E in the form

$$S(t, s) = q(s) \exp(-\alpha(t-s)) \frac{\cos[\omega_d(t-s) + \phi(s)]}{\cos[\phi(s)]} \quad (4.33)$$

where  $q(s)$  is the mean-square of the displacement, or the velocity or the absolute acceleration of the response, respectively. The expressions for  $\phi(s)$  corresponding to a particular response quantity are given in Appendix E in terms of the system parameters and the mean-square matrix of the response. The above expression for  $S(t, s)$  is exact, simple, gives more insight than the original expression (4.15), and it holds for any range of oscillator parameters. Additional simplifications for  $S(t, s)$  depend on simplifying the expressions for the mean-square response.

### 4.4 Approximation for the Mean-Square Response of a Linear Time-Invariant SDOF Oscillator

The objective of the following sections is to approximate the mean-square displacement of the response in such a way that the essential features of the response are preserved without significant loss of accuracy. An efficient way to do this is to use the two-timing method to solve the second-order differential equation (4.18) for an arbitrary forcing term  $g(t)$ . The slow time is governed by  $t$  and the fast time  $\tau = \omega_0 t$  is governed by the reciprocal of the “high” angular frequency  $\omega_0$ . Doing so, a series expansion for  $r(t)$  is derived (Appendix D) in the form:

$$\begin{aligned} r(t) = \frac{g(t)}{(2\omega_0)^2} & \left\{ 1 - \frac{g(0)}{g(t)} \varphi \left( \frac{1}{\sqrt{1-\zeta^2}}, \zeta \right) \right. \\ & - 2\zeta \frac{\dot{g}(t)}{2\omega_0 g(t)} + \frac{\dot{g}(0)}{2\omega_0 g(t)} \varphi \left( \frac{1}{\sqrt{1-\zeta^2}}, -(1-2\zeta^2) \right) \\ & - (1-4\zeta^2) \frac{\ddot{g}(t)}{(2\omega_0)^2 g(t)} + \frac{\ddot{g}(0)}{(2\omega_0)^2 g(t)} \varphi \left( \frac{1}{\sqrt{1-\zeta^2}}, -\zeta(3-4\zeta^2) \right) \\ & \left. + \sum_{i=3}^{\infty} \circ \left( \frac{g^{(i)}(t)}{(2\omega_0)^i g(t)} \right) + \sum_{i=3}^{\infty} \circ \left( \frac{g^{(i)}(0)}{(2\omega_0)^i g(t)} \varphi(\rho, \sin \phi) \right) \right\} \quad (4.34a) \end{aligned}$$

where the function  $\varphi(\rho, \sin \phi)$  has the exponentially decaying oscillatory form

$$\varphi(\rho, \sin \phi) = \rho \exp(-2\zeta\omega_0 t) \cos(2\omega_d t + \phi) \quad (4.34b)$$

The first three terms in the series expansion are derived and only the order of magnitude of the higher-order terms is shown. The solution for  $r(t)$  consists of a non-oscillatory term plus an exponentially decaying oscillatory term with period of oscillations  $\pi/\omega_d$ . In general, the solution of (4.17) to each non-oscillatory term in the expansion for  $r(t)$ , cannot be obtained analytically. However, for the  $i$ -th oscillatory term denoted in general by

$$r_i^{(O)}(t) = \rho_i \frac{g^{(i)}(0)}{(2\omega_0)^i} \exp(-2\zeta\omega_0 t) \cos(2\omega_d t + \phi_i), \quad (4.35)$$

an exact analytical solution exists in the form

$$q_i^{(O)}(t) = \frac{\rho_i}{2\omega_d} \frac{g^{(i)}(0)}{(2\omega_0)^i} \exp(-2\zeta\omega_0 t) [\sin(2\omega_d t + \phi_i) - \sin(\phi_i)] \quad (4.36)$$

and gives the contribution to the value of  $q_{11}(t)$  due to the  $i$ -th oscillatory term in  $r(t)$ . It is interesting to note that the magnitude of the oscillatory terms in  $r(t)$  is divided by the damped angular frequency  $\omega_d$  in the corresponding solution for  $q_{11}(t)$ , and its magnitude depends on  $g^{(i)}(0)/(2\omega_0)^i$ ,  $i = 1, 2, \dots$

For *heavily-damped* oscillators, that is for large  $\zeta$ , the oscillatory terms decay quickly to zero. A feel for the time interval over which the oscillatory terms contribute significantly to the value of the quantity  $r(t)$  can be gained by considering that for a fixed  $\zeta$  each oscillatory term decays to  $n\%$  of its maximum value after

$$p_T = \frac{\ln(100) - \ln(n)}{2\pi\zeta} \sqrt{1 - \zeta^2} \quad (4.37)$$

cycles of oscillations with period  $\pi/\omega_d$ . The value of  $p_T$  versus  $\zeta$  is graphed in Figure 4.1 for different values of  $n$ . For *lightly-damped* oscillators, that is  $\zeta \ll 1$ , the oscillatory terms persist for several cycles of oscillations.

#### 4.4.1 Approximate First-Order Differential Equation for the Mean-Square Displacement

The proposed approximations are a) to neglect the small oscillatory terms in the series expansion, an assumption that preserves the essential features of the response, and b) to treat  $g(t)$  as a slowly-varying function and, assuming that  $g(0) = 0$ , to retain only the dominant term

$$r_0(t) = \frac{g(t)}{4\omega_0^2} \quad (4.38)$$

Substituting (4.38) into (4.17), the mean-square displacement of the response can be obtained by solving the much simpler first-order differential equation

$$\dot{q}_{11}(t) + 2\zeta\omega_0 q_{11}(t) = \frac{g(t)}{2\omega_0^2} \quad (4.39)$$

The solution of (4.39) is

$$q_{11}(t) = \frac{1}{2\omega_0^2} \int_0^t e^{-2\zeta\omega_0(t-\tau)} g(\tau) d\tau \quad (4.40)$$

and involves the evaluation of a convolution integral. Depending on the complexity of  $g(t)$ , the approximate mean-square displacement of the response can either be obtained numerically by integrating equation (4.39), or alternatively, it can be obtained analytically by simplifying the convolution integral in (4.40).

The conditions for neglecting the higher-order terms are directly determined by the series expansion, and they are mathematically stated as

$$\frac{g^{(i)}(t)}{(2\omega_0)^i g(t)} \ll 1, \quad i = 1, 2, \dots \quad (4.41)$$

These conditions specify how slow the forcing term  $g(t)$  should vary with time so that the dominant solution  $r_0(t)$  is an adequate approximation, and they will be referred to as the “slowly-varying” conditions for  $g(t)$ . For example, the condition for  $i = 1$  is roughly that the fractional change of  $g(t)$  over a cycle of oscillation is much less than  $4\pi$ . An advantage of the series expansion is that even if the slowly-varying conditions are violated, the dominant term can be corrected to any degree of accuracy by including the next higher-order terms in the expansion.

#### 4.4.2 Accuracy of the Approximations using Modulated White-Noise Excitation

Numerical studies are performed which are intended to verify the accuracy of the proposed approximations for the transient mean-square response. For the case of modulated white-noise excitation, the forcing term, equation (4.19), admits the simple and exact representation

$$g(t) = f^2(t) \quad (4.42)$$

where  $f(t)$  is the slowly-varying modulation.

Two kinds of modulation function which are widely used in earthquake engineering are the following. (a) The exponential-type modulation (Shinozuka and Sato) given by

$$f(t) = a(e^{-\alpha t} - e^{-\beta t}) \quad (4.43)$$

for which both the exact and the approximate equations for the the mean-square response can be solved analytically. (b) The Gamma modulation (Saragoni and Hart) given by

$$f(t) = f_m \tau^\beta e^{\beta(1-\tau)}, \quad \tau = \frac{t}{t_m} \quad (4.44)$$

for which an analytical solution for the exact or the approximate mean-square response exists only in the case  $2\beta = \text{integer}$ . All other values of  $\beta$  require numerical integration of the exact or the approximate equation. An exact analytical solution in terms of a series may be found in Hou (1990) and Iwan and Hou (1986) for any value of  $\beta$ . However, for  $2\beta$  not an integer, the solution requires the summation of an infinite series.

The Gamma modulation is used as an example to test the accuracy of the first-order differential equation (4.39), and to illustrate the difference between the exact and the approximate mean-square response. The most informative way to present the results is to rewrite the governing equations in a dimensionless form. Define the dimensionless time  $\tau = t/t_m$  where  $t_m$  is the time at which the maximum of the Gamma modulation occurs, the number of cycles of oscillations  $\eta = t_m/T_0$  needed to reach the maximum, and the normalized mean-square responses

$$r_{11}(\tau) = \frac{4\alpha\omega_0^2}{f_m^2} q_{11}(t_m\tau) \quad (4.45)$$

$$r_{22}(\tau) = \frac{4\alpha}{f_m^2} q_{22}(t_m \tau) \quad (4.46)$$

$$r_{12}(\tau) = \frac{4\alpha\omega_0}{f_m^2} q_{12}(t_m \tau) \quad (4.47)$$

which compare the responses to the equivalent stationary responses obtained for a constant modulation with power  $f_m^2$ . Then, the equations (8a-c) for the exact mean-square response take the form:

$$\begin{aligned} r'_{11}(\tau) &= 4\pi\eta r_{12}(\tau) \\ r'_{12}(\tau) &= 2\pi\eta (r_{22}(\tau) - r_{11}(\tau) - 2\zeta r_{12}(\tau)) \\ r'_{22}(\tau) &= 2\pi\eta \left( -2r_{12}(\tau) - 4\zeta r_{22}(\tau) + 4\zeta\tau^{2\beta} e^{2\beta(1-\tau)} \right) \end{aligned} \quad (4.48)$$

The first-order equation for the approximate mean-square response takes the form

$$r'_{11}(\tau) + 4\pi(\zeta\eta)r_{11}(\tau) = 4\pi(\zeta\eta)\tau^{2\beta} e^{2\beta(1-\tau)} \quad (4.49)$$

and it depends only on the product  $\eta\zeta$  and not on  $\zeta$  and  $\eta$  alone. Both exact and approximate solutions are obtained by numerically integrating equations (4.48) and (4.49), respectively. The results are presented and compared in Figures 4.2(a-d) for two values of  $\beta$  corresponding to different forms of the modulation envelope, and for four values of  $\eta$  ranging from  $\eta = 0.5$ , the short duration excitation, to  $\eta = 5$ , the long duration excitation.

The longer the duration of the excitation and the smaller the value of the critical damping, the better the approximation. In fact, for  $\eta = 2$  and  $\eta = 5$  (long duration excitation) the approximate mean-square response is almost identical to the exact one for values of the critical damping ranging from 1 to 25%. These results are consistent with the mathematical analysis since for long duration input the slowly-varying conditions (4.41) are satisfied. Also, the next highest-order term containing the derivative of  $g(t)$  is proportional to the damping ratio  $\zeta$ . Therefore, its contribution is small for lightly-damped oscillators.

The “large” discrepancies between the exact and the approximate mean-square response which exist in the very beginning of the response for short duration excitation are due to the violation of conditions (4.41). The quantity  $g(t)$  is close to zero in the very beginning and thus higher-order terms have a significant contribution

to  $r(t)$ . As time advances,  $g(t)$  builds up to higher values and conditions (4.41) specifying the slow variation of  $g(t)$  hold. Therefore, the approximation for  $r(t)$  is expected to be unrealistic in the beginning of the response, resulting in large differences between the exact and the approximate response as illustrated in Figures 4.2(a-d). However, the differences are not of particular interest because the mean-square response is negligibly small at these times. For  $n = 0.5$  (the short duration excitation) the modulation passes its peak before one cycle of oscillation which indicates that conditions (4.41) for neglecting the higher-order terms in the approximation for  $r(t)$  are violated. Therefore, the case  $\eta = 0.5$  shown in Figure 4.2(d) is an extreme test of the proposed approximation. Although significant discrepancies exists, the essential features of the response are still preserved.

Next, we numerically study the effect of the quantities  $\epsilon_{12}(t)$ ,  $\epsilon_{22}(t)$ , and  $\epsilon_a(t)$  in the expressions (4.20) and (4.23) relating the mean-square velocity and absolute acceleration with the mean-square displacement of the response. The exact values of  $\epsilon_{12}(t)$ ,  $\epsilon_{22}(t)$ , and  $\epsilon_a(t)$  are computed using (4.48) for different damping ratios. The results for  $\beta = 0.5$  shown in Figures 4.3(a) and 4.3(b) correspond to values of  $\eta = 5$  and  $\eta = 1$ , respectively. The results for  $\beta = 4$  and for the same values of  $\eta$  are shown in Figures 4.3(c) and 4.3(d). For illustration purposes, the normalized displacement response  $r_{12}(\tau)$  is included in these figures. After the response has built up to a few percent of its maximum value, the contribution of  $\epsilon_{12}(t)$ ,  $\epsilon_{22}(t)$ , and  $\epsilon_a(t)$  in equation (4.20) and (4.23) can be neglected, especially at the times near the maximum of the response. At all other times, the higher the damping ratio is, the higher the contribution of  $\epsilon_{12}(t)$ ,  $\epsilon_{22}(t)$ , and  $\epsilon_a(t)$  in the response. For excitations with longer durations, i.e., higher  $\eta$ , these quantities can be neglected without significant loss of accuracy.

Summarizing, the simplified formulas for approximating the mean-square response were found to be very accurate and extremely accurate for medium to long duration excitations, respectively. Also, no large discrepancies were found between the exact and the approximate response for excitation with very short duration. Although the Gamma modulation was used to illustrate the conditions under which the proposed approximate formulas work well, the results can be easily carried

through for other modulations as long as they satisfy the slowly-varying conditions. In the case of non-white excitation with slowly-varying correlation structure, which will be studied in Section 4.7,  $g(t)$  also turns out to be a slowly-varying function of time. Therefore, the results concerning the discrepancies between the exact and the approximate mean-square response corresponding to the modulated white-noise excitation can be carried through for non-white excitation with slowly-varying correlation structure.

The approximate first-order differential equation is used to derive additional response characteristics. The normalized mean-square response depends only on the product  $\eta\zeta$  and the modulation parameter  $\beta$ . Plots for different values of  $\beta$  and for values of  $\eta\zeta$  ranging from 0.01 to 0.5 are shown in Figures 4.4. The maximum normalized response can be computed by setting  $r' = 0$  in the equation (4.49). The maximum response  $r_m(\tau_m)$  attained at the time  $\tau_m$  is therefore given by

$$r_m(\tau_m) = f_N(\tau_m) \quad (4.50)$$

where the normalized modulation  $f_N(\tau_M) = f(t)/f_m$ . Thus, the maximum normalized response  $r_m$  is equal to the value of the normalized modulation computed at the time that the maximum mean-square response is attained. In other words, at the maximum, the normalized response crosses the normalized excitation. This is also depicted in Figures 4.4, where each individual figure corresponds to a fixed modulation parameter  $\beta$ . These figures give complete qualitative information about the nonstationary mean-square response for oscillators characterized by angular frequency  $\omega_0$  and damping ratio  $\zeta$  and for modulations characterized by the maximum intensity  $f_m$ , the time  $t_m$  that the maximum intensity occurs and the variable  $\beta$ .

#### 4.5 Formulation for the Mean-Square Response of Nonlinear SDOF Oscillators

The analysis developed to approximate the mean-square response of a linear SDOF oscillator provides background for analyzing and extending the approximations to the more complicated case of nonlinear SDOF oscillators. In the nonlinear case, there are certain difficulties because of the time variation of  $\alpha(t)$  and  $\omega(t)$  for the equivalent linear system which will be addressed in what follows.

### 4.5.1 Mean-Square Displacement

Eliminating  $q_{12}(t)$  and  $q_{22}(t)$  from the set of equations (4.8), the following third-order differential equation in terms of  $q_{11}(t)$  is obtained

$$\begin{aligned} q_{11}^{(3)}(t) + 6\alpha(t)q_{11}^{(2)}(t) + [4\omega^2(t) + 8\alpha^2(t) + 2\dot{\alpha}(t)]q_{11}^{(1)}(t) + \\ [8\alpha(t)\omega^2(t) + 4\omega(t)\dot{\omega}(t)]q_{11}(t) = 4L_{22}(t) + 8\alpha(t)L_{12}(t) + 2\dot{L}_{12}(t) \end{aligned} \quad (4.51)$$

Guided by the formulation developed for the linear oscillator, the third-order differential equation can be split into a first-order and a second-order differential equation. The complete set of equations is given in Appendix F. Utilizing the slowly-varying conditions (A.14a) for  $\alpha(t)$  and  $\omega(t)$  to neglect the small-order terms (Appendix F), it can be shown that the mean-square displacement response satisfies the first-order differential equation

$$\begin{aligned} \dot{q}_{11}(t) + 2[\alpha(t) + \delta(t)]q_{11}(t) &= 2r(t) \\ q_{11}(0) &= 0 \end{aligned} \quad (4.52)$$

with the excitation  $r(t)$  satisfying the second-order differential equation

$$\begin{aligned} \ddot{r}(t) + 4\left[\alpha(t) - \frac{1}{2}\delta(t)\right]\dot{r}(t) + 4\omega^2(t)r(t) &= g(t) \\ r(0) = 0, \quad \dot{r}(0) &= 0 \end{aligned} \quad (4.53)$$

where

$$\delta(t) = \frac{\dot{\omega}_d(t)}{2\omega_d(t)} \quad (4.54)$$

and the forcing term

$$g(t) = 2L_{22}(t) + 4\alpha(t)L_{12}(t) + \dot{L}_{12}(t) \quad (4.55)$$

In the case where

$$\alpha(t) \equiv \alpha(Q(t)) \quad \text{and} \quad \omega(t) \equiv \omega(Q(t)) \quad (4.56)$$

equations (4.52) and (4.53) are nonlinear. The mean-square displacement  $q_{11}(t)$  can be computed by solving (4.52) and (4.53) simultaneously or equivalently by solving the original Liapunov nonlinear matrix equation (4.7). The advantage of the above

formulation is that the transient mean-square displacement of the response satisfies a first-order, in general, nonlinear differential equation of the form (4.52). It will be shown that under certain conditions, the dynamics of the first-order differential equation provide all the essential characteristics of the response, while the dynamics of the second-order differential equation has only a secondary effect on the response. Also, the forcing term  $r(Q(t), t)$  will be approximated by a simple algebraic expression involving  $Q(t)$ . In the case where  $r$  is only a function of  $q_{11}(t)$ , the mean-square displacement can be obtained by solving only the first-order differential equation (4.52).

### 4.5.2 Mean-Square Velocity

Substituting  $q_{12}$  from (4.8a) into (4.8b) and using the first-order differential equation (4.52) for the mean-square displacement  $q_{11}(t)$ , it can be shown that the mean-square velocity  $q_{22}(t)$  is related to  $q_{11}(t)$  by the simple algebraic expression

$$q_{22}(t) = \omega^2(t)q_{11}(t) \{1 + \epsilon_{22}(t)\} - L_{12}(t) \quad (4.57)$$

where

$$\epsilon_{22}(t) = \frac{\dot{r}(t)}{\omega^2(t)q_{11}(t)} - \frac{\delta(t)}{\omega(t)} \frac{\dot{q}_{11}(t)}{\omega(t)q_{11}(t)} \quad (4.58)$$

### 4.5.3 Mean-Square Absolute Acceleration

If  $-G(t)$  represents the base acceleration of the oscillator, then the absolute acceleration  $a(t)$  of the response is given by

$$a(t) = \ddot{x}(t) - G(t) = -2\alpha(t)\dot{x}(t) - \omega^2(t)x(t) \quad (4.59)$$

Using (4.8), (4.52), and (4.57), the mean-square absolute acceleration  $q_a(t) = E[a^2(t)]$  takes the form

$$q_a(t) = \omega^4(t) (1 + 4\zeta^2(t)) q_{11}(t) \{1 + \epsilon_a(t)\} - 4\zeta^2(t)\omega^2(t)L_{12}(t) \quad (4.60)$$

where

$$\epsilon_a(t) = \frac{4\zeta^2(t)}{1 + 4\zeta^2(t)} \epsilon_{22}(t) + \frac{4\zeta(t)}{1 + 4\zeta^2(t)} \epsilon_{12}(t)$$

and

$$\epsilon_{12}(t) = \frac{\dot{q}_{11}(t)}{2\omega(t)q_{11}(t)} \quad (4.61)$$

#### 4.5.4 Displacement-Velocity Correlation

Using (4.52) and (4.8d),  $q_{12}(t)$  is related to the mean-square displacement  $q_{11}(t)$  by the simple algebraic expression

$$q_{12}(t) = -[\alpha(t) + \delta(t)]q_{11}(t) + r(t) \quad (4.62)$$

#### 4.5.5 Similarities Between Transient and Stationary Mean-Square Response

Consider an oscillator with natural frequency and ratio of critical damping which depend on the mean-square response, then its response under stationary excitation approaches stationarity after a sufficient amount of time. Therefore, treating all the quantities that appear in (4.7) as time invariant and setting  $\dot{Q} = 0$ , the stationary mean-square response is obtained in the form:

$$q_{11}(Q) = \frac{2L_{22}(Q) + 4\alpha(Q)L_{12}(Q)}{4\alpha(Q)\omega^2(Q)} \quad (4.63)$$

$$q_{22}(Q) = \omega^2(Q)q_{11}(Q) - L_{12}(Q) \quad (4.64)$$

$$q_a(Q) = \omega^4(Q)[1 + 4\zeta^2(Q)]q_{11}(Q) - 4\zeta^2(Q)\omega^2(Q)L_{12}(Q) \quad (4.65)$$

$$q_{12}(Q) = 0 \quad (4.66)$$

where  $\alpha(Q)$ ,  $\omega(Q)$  and  $L_{i2}(Q)$  depend on the stationary mean-square response. In general, expressions (4.63) to (4.66) are nonlinear and it is only in the linear case that they provide an explicit solution for the mean-square response.

The mean-square velocity and the mean-square absolute acceleration of the nonstationary response are related to the nonstationary mean-square displacement by simple algebraic expressions which could be viewed as a generalization of the stationary relations (4.64) and (4.65), respectively. The additional terms  $\epsilon_{22}(t)$ ,  $\epsilon_{12}(t)$  and  $\epsilon_a(t)$  appearing in the expressions (4.57) and (4.60) account for the nonstationarity of the response. As it will be seen in the numerical results,  $\epsilon_{22}(t)$ ,  $\epsilon_{12}(t)$

and  $\epsilon_a(t)$  are in general small compared to unity and they can be neglected. Therefore the mean-square velocity and absolute acceleration can be obtained in terms of the mean-square displacement by using the stationary relations, after replacing the time-invariant quantities with the time-varying ones corresponding at time  $t$ .

#### 4.6 Approximation of the Liapunov Matrix Equation for a Nonlinear SDOF Oscillator

For nonlinear oscillators represented by equivalent linear systems, that is, for linear second-order differential equations with time-varying coefficients, an exact series expansion for  $r(t)$  is not possible to deduce as was done in the time-invariant case. However, the formulation developed for the time-invariant case can be used as a guide to develop an approximate analysis for the time-varying one. In the time-invariant case, a) the effects of the initial conditions were neglected by eliminating the oscillatory terms in the series expansion for  $r(t)$ , and b) the slowly-varying conditions for  $g(t)$  were used to approximate the solution of the second-order differential equation by the dominant term  $r_0(t)$  of the particular solution. The same idea is applied to the time-varying case.

We seek a particular solution  $r_p(t)$  of the second-order differential equation

$$\ddot{r}_p(t) + 4 \left[ \alpha(t) - \frac{1}{2} \delta(t) \right] \dot{r}_p(t) + 4\omega^2(t)r_p(t) = g(t), \quad (4.67)$$

neglecting the effects of the initial conditions. If we write the solution  $r_p(t)$  as a series expansion in successively smaller terms

$$r_p(t) = r_0(t) + r_1(t) + r_2(t) + \dots \quad (4.68)$$

then equation (4.67) is satisfied by choosing

$$r_0(t) = \frac{g(t)}{4\omega^2(t)} \quad (4.69)$$

$$r_{i+1}(t) = \frac{\ddot{r}_i(t) + 4 \left[ \alpha(t) - \frac{1}{2} \delta(t) \right] \dot{r}_i(t)}{4\omega^2(t)}, \quad i = 0, 1, 2, \dots \quad (4.70)$$

The conditions for approximating  $r_p(t)$  by the dominant term  $r_0(t)$  in the series expansion are

$$\left| \frac{\dot{r}_i(t)}{2\omega(t)r_0(t)} \right| \ll 1 \quad \text{and} \quad \left| \frac{\ddot{r}_i(t)}{4\omega^2(t)r_0(t)} \right| \ll 1, \quad i = 0, 1, 2, \dots \quad (4.71)$$

The slowly-varying conditions can be rewritten in terms of the forcing term  $g(t)$  as

$$\left| \frac{g^{(i)}(t)}{(2\omega(t))^i g(t)} \right| \ll 1, \quad i = 1, 2, \dots \quad (4.72)$$

which are a generalization of the conditions obtained in the time-invariant case. These conditions have to be supplemented by the slowly-varying conditions for the time-varying coefficients  $\omega(t)$  and  $\alpha(t)$  which in terms of the first derivatives are given by (A.14a). The conditions (4.72) and (A.14a) quantify how slow  $g(t)$ ,  $\omega(t)$  and  $\alpha(t)$  should vary with time for the dominant solution to be an adequate approximation. Using (4.69) and (4.70), the contribution of the next higher derivative of  $g(t)$  in the expansion for  $r_p(t)$  can be found to be

$$\frac{r_1(t)}{r_0(t)} = 2 \left[ \zeta(t) - \frac{1}{2} \frac{\delta(t)}{\omega(t)} \right] \frac{\dot{g}(t)}{2\omega(t)g(t)} \quad (4.73)$$

Substituting the dominant solution  $r_0(t)$  into (4.52), the mean-square displacement of the response can be obtained by solving the simpler first-order differential equation

$$\dot{q}_{11}(t) + 2[\alpha(t) + \delta(t)]q_{11}(t) = \frac{g(t)}{2\omega^2(t)} \quad (4.74)$$

The solution of equation (4.74) may be expressed in terms of the convolution integral

$$q_{11}(t) = \int_0^t \exp \left[ \int_\tau^t -2[\alpha(s) + \delta(s)] ds \right] \frac{g(\tau)}{2\omega^2(\tau)} d\tau \quad (4.75)$$

The computational savings achieved by solving equation (4.74) instead of the original equation (4.6) will be discussed in a later section.

#### 4.6.1 Covariance of the Response: Modulated White-Noise Excitation

For *slowly-varying*  $\alpha(t)$  and  $\omega(t)$  and for modulated white-noise excitation, the expressions for the response covariances can be approximated by closed-form expressions. Substituting the approximations for  $\eta(t, s)$  and  $h(t, s)$  given by (A.15) into (4.15) and after algebraic manipulations, it can be shown that

$$S_{11}(t, s) = q_{11}(s) \sqrt{\frac{\omega'(t)}{\omega'(s)}} \exp \left\{ - \int_s^t \alpha_g(\xi) d\xi \right\} \frac{\cos \left\{ \int_s^t \omega'_g(\xi) d\xi - \phi_g(t, s) \right\}}{\cos \{ \phi_g(t, s) \}} \quad (4.76a)$$

where

$$\tan [\phi_g(t, s)] = \frac{r(s)}{q_{11}(s)\omega'(t)} \left\{ 1 + \frac{q_{11}(s)}{r(s)} [s^*(t) - s^*(s)] \right\} \quad (4.76b)$$

which is a generalization of the formula (4.33) derived for the special case of time-invariant  $\alpha(t)$  and  $\omega(t)$ . Similar expressions can be obtained for  $S_{22}(t, s)$  and  $S_a(t, s)$ .

#### 4.7 Approximation of the Forcing Integral Term of the Liapunov Matrix Equation

The integrals  $L_{12}(t)$  and  $L_{22}(t)$  in the Liapunov matrix equation can be rewritten as

$$L_{i2}(t) = \int_0^t \Phi_{i2}(t, t - \tau) E[G(t)G(t - \tau)] d\tau, \quad i = 1, 2 \quad (4.77)$$

In general, they cannot be evaluated analytically except in a few cases. Specifically, when  $G(t)$  is a modulated white-noise process or a stationary process with rational power spectral density (for example, a process modeled by a  $(2n)$ -th-order differential equation with white-noise input) and, in addition, the coefficients of the equivalent system are time invariant (for example, equation of motion of a linear oscillator), the integrals admit simple closed-form representations. It is the purpose of this section to study the general conditions for analytically approximating the integrals by simpler algebraic expressions. At the same time, specific applications will be given which cover more complicated cases than before which are of practical interest. These cases include excitation processes possessing certain evolutionary power spectral density and equivalent linear structural models with time-varying frequency and damping ratio.

##### 4.7.1 Broadband Excitation and Slowly-Varying Structural Parameters

Let  $T_c(t)$  be the length of the time interval of non-zero correlation of the stochastic process  $G(t)$  at time  $t$ , that is, the autocovariance  $r_g(t, t - \tau) E[(G(t)G(t - \tau)]$  satisfies

$$\begin{aligned} r_g(t, t - \tau) &\neq 0 && \text{for } \tau \in [0, T_c(t)] \\ r_g(t, t - \tau) &\approx 0 && \text{for } \tau > T_c(t) \end{aligned} \quad (4.78)$$

The more broadband the process is, the less the correlation length  $T_c(t)$ . The integrals  $L_{i2}(t)$  can be approximated by

$$L_{i2}(t) = \int_0^{T_c(t)} \Phi_{i2}(t, t - \tau) r_g(t, t - \tau) d\tau, \quad i = 1, 2 \quad (4.79)$$

where the integration in the interval  $[T_c(t), t]$  has been neglected because of the condition in (4.78). These integrals can be completely determined, at least numerically, by knowing the principal matrix solution  $\Phi(t, t - \tau)$  for  $\tau \in [0, T_c(t)]$  and the autocorrelation  $r_g(t, t - \tau)$  of the excitation. For constant matrix  $A(t) = A$ , a simple closed-form solution for the principal matrix exists in terms of exponential and trigonometric functions (Appendix A.2). For time-variant  $A(t)$ , a closed-form solution for the principal matrix cannot be obtained in general. In particular, when the matrix  $A(t) = A(Q(t))$ , i.e., it depends on the mean-square matrix of the response, equations (4.5) and (4.8) are no longer independent and they have to be solved simultaneously.

A formulation is next introduced to approximate the integrals  $L_{i2}(t)$  without solving (4.8). The idea is to assume that  $A(t)$  is slowly varying so that it can be considered to remain constant in the interval  $[t - T_c(t), t]$ . Therefore, the principal matrix  $\Phi(t, t - \tau)$  can be approximately obtained for  $\tau \in [t - T_c(t), t]$  by solving the time-invariant differential equation  $\dot{\Phi} = A\Phi$  with the fixed value of  $A = A(t)$ . A rigorous mathematical solution for  $\Phi(t, t - \tau)$  which takes into account the slow variation of  $A(t)$  and also provides the slowly-varying conditions for the solution to be sufficiently accurate is given in the Appendix A.2. The integral forcing terms can be approximated by

$$L_{i2}(t) = \int_0^{T_c(t)} \Phi_{i2}^*(t, t - \tau) r_g(t, t - \tau) d\tau, \quad i = 1, 2 \quad (4.80)$$

where the superscript  $\langle * \rangle$  denotes the approximation of  $h(t, \tau)$  and  $\eta(t, \tau)$  in the formulas for  $\Phi_{i2}(t, \tau)$  in the broadband case by  $h^*(t, t - \tau)$  and  $\eta^*(t, t - \tau)$ , respectively. The expressions for  $h^*(t, t - \tau)$  and  $\eta^*(t, t - \tau)$  which are given in Appendix A.2 simplify the integrals  $L_{12}(t)$  and  $L_{22}(t)$  to

$$L_{12}(t) = \frac{1}{\omega'(t)} \int_0^{T_c(t)} \exp[-\alpha(t)\tau] r_g(t, t - \tau) \sin[\omega'(t)\tau] d\tau \quad (4.81a)$$

and

$$L_{22}(t) = \frac{1}{\omega'(t)} \int_0^{T_c(t)} \exp[-\alpha(t)\tau] r_g(t, t - \tau) \cos[\omega'(t)\tau] d\tau - \left( \alpha(t) + \frac{\dot{\omega}'(t)}{2\omega'(t)} \right) L_{12}(t) \quad (4.81b)$$

The main result here is that the integrands involve exponential and trigonometric functions with the coefficients  $\alpha(t)$  and  $\omega(t)$  being independent of the variable of integration  $\tau$ .

#### 4.7.2 Lightly-Damped Oscillators

For the following application, an oscillator is considered to be lightly-damped if the damping ratio  $\zeta(t)$  is small enough so that the term  $\exp[-\zeta(t)\omega(t)\tau] \approx 1$  over the interval  $[0, T_c(t)]$ , i.e.,  $\zeta(t)\omega(t)T_c(t) \ll 1$ . Therefore, the integrals in (4.81) can be approximated by

$$L_{12}(t) = \frac{C(\omega(t), t)}{\omega(t)} \quad (4.82a)$$

and

$$L_{22}(t) = \frac{1}{2} S(\omega(t), t) - \left( \zeta(t) + \frac{\dot{\omega}(t)}{2\omega^2(t)} \right) C(\omega(t), t) \quad (4.82b)$$

where  $S(\omega, t)$  is the EPSD function of the excitation process given by

$$S(\omega, t) = 2 \int_0^\infty r_g(t, t - \tau) \cos(\omega\tau) d\tau \quad (4.83)$$

and  $C(\omega, t)$  is given by

$$C(\omega, t) = \int_0^\infty r_g(t, t - \tau) \sin(\omega\tau) d\tau \quad (4.84)$$

Neglecting the  $O(\zeta)$  terms and using the slowly-varying assumption to neglect terms involving time derivatives, the forcing term  $g(t)$  in (4.56) takes the simple form:

$$g(t) = S(\omega(t), t) \quad (4.85)$$

This forcing term includes the case of oscillators with slowly-varying angular frequency and damping ratio, and therefore it is a generalization of the result obtained by Spanos (1983) for time-invariant oscillators.

## 4.8 Application to Some Special Cases of Nonstationary Excitation

Consider stochastic loads with autocorrelation function of the form

$$r_g(t, t - \tau) = F(\underline{\lambda}(t), \tau) \quad (4.86)$$

where  $\underline{\lambda}(t)$  is the vector of the excitation model parameters accounting for the time variation of the correlation structure of the excitation process, and  $F(\bullet, \bullet)$  is a general functional operator of  $\underline{\lambda}(t)$  and  $\tau$ . For specific functions  $F(\underline{\lambda}(t), \bullet)$  of  $\tau$ , such as polynomials, exponentials, trigonometric functions or a combination of these, the integration in (4.81) can be carried out analytically without requiring the exact time variation of the equivalent structural parameters  $\alpha(t)$  and  $\omega(t)$  or the excitation model parameters  $\underline{\lambda}(t)$ . In this case, the forcing term  $g(t)$  takes the form

$$g(t) = g(\omega(t), \alpha(t), \underline{\lambda}(t)) \quad (4.87)$$

where  $g(\bullet, \bullet, \bullet)$  is a functional which depends only on the form of the functional operator  $F(\bullet, \tau)$ , that is, the general structure of the excitation model. The proposed formulation is next applied to simplify  $L_{i2}(t)$  and simplify the forcing term  $g(t)$  for three cases of excitation. Two of them are modulated filtered white-noise and filtered modulated white-noise excitations which have been widely used in the past to model nonstationary environmental loads, such as earthquake loads. The third case deals with nonstationarities in both the amplitude and the frequency content of the excitation and includes the particular case of the stochastic earthquake loading proposed in Chapters 2 and 3 of this thesis. The ground motion model in Chapter 3 is used as an example to verify the accuracy of the approximations.

### 4.8.1 Modulated Filtered White-Noise Excitation

The envelope modulated, filtered stationary white-noise process has an autocovariance function of the form

$$r(t, t - \tau) = f^2(t)R(\tau) \quad (4.88)$$

where the modulation  $f(t)$  is usually assumed to be slowly varying and  $R(\tau)$  is the autocovariance function of a stationary, usually broadband process. Using Priestley's definition, the evolutionary power spectral density of the broadband process

defined by (4.88) can be approximated by

$$S(\omega, t) = f^2(t)S_F(\omega) \quad (4.89)$$

where  $S_F(\omega)$  is the power spectral density of the stationary filtered white-noise process.

For time-invariant oscillators and for sufficiently large time  $t$ , the integrals in (4.81) take the form

$$\begin{aligned} L_{12}(t) &= f^2(t)I_c(\omega_0) \\ L_{22}(t) &= f^2(t)(I_s(\omega_0) + \alpha I_c(\omega_0)) \end{aligned} \quad (4.90)$$

where the integrals

$$I_c(\omega_0) = \frac{1}{\omega'} \int_0^\infty \exp(-\alpha\tau) \sin(\omega' \tau) R(\tau) d\tau \quad (4.91)$$

and

$$I_s(\omega_0) = \int_0^\infty \exp(-\alpha\tau) \cos(\omega' \tau) R(\tau) d\tau \quad (4.92)$$

are independent of  $t$ . In the case where analytical integration to obtain  $I_c(\omega)$  and  $I_s(\omega)$  is not possible, numerical integration is required only once. The expression for the forcing term  $g(t)$  becomes

$$g(t) = f^2(t) [2I_s(\omega_0) + 2\alpha I_c(\omega_0)] \left\{ 1 + \lambda(\omega_0) \frac{\dot{f}(t)}{2\omega_0 f(t)} \right\} \quad (4.93)$$

where

$$\lambda(\omega_0) = \frac{2\omega_0 I_c(\omega_0)}{I_s(\omega_0) + \alpha I_c(\omega_0)} \quad (4.94)$$

If we neglect the contribution of the term  $\lambda(\omega_0)\dot{f}(t)/(2\omega_0 f(t))$  then the mean-square response of an oscillator subjected to filtered modulated white-noise excitation can be approximately obtained by the mean-square response of the same oscillator subjected to a modulated white-noise excitation where the modulation is the same as before and the power spectral density of the white noise is  $2I_s(\omega_0) + 2\alpha I_c(\omega_0)$ . This argument has been used in the past (Caughey and Stumpf, 1961) to approximate the response of lightly-damped oscillators, with the quantity  $2I_s(\omega_0) + 2\alpha I_c(\omega_0)$

being replaced by its limit  $S_F(\omega_0)$  as  $\zeta \rightarrow 0$ . The expression (4.93) is general and independent of the damping ratio  $\zeta$  of the oscillator.

### 4.8.2 Filtered Modulated White-Noise Excitation

The filtered modulated white-noise process is generated by first multiplying the white-noise process by the envelope and then passing the output through the filter. The evolutionary power spectral density function of such a process is given exactly by (4.89), while the autocovariance function has the approximate form (4.88). The modulated filtered white-noise process and the filtered modulated white-noise process are approximately the same for slowly-varying modulation and for filters with a broadband transfer function. Therefore, the approximations developed in section 4.8.1 also apply for this case.

### 4.8.3 Stochastic Ground Motion Models

A general class of stochastic processes which is usually proposed to model the ground motion satisfies either of the following equations

$$\text{EQUATION I:} \quad P(t)x_g(t) = f(t)e(t), \quad G(t) = R(t)x_g(t) \quad (4.95)$$

$$\text{EQUATION II:} \quad P(t)x_g(t) = e(t), \quad G(t) = f(t)R(t)x_g(t) \quad (4.96)$$

where  $e(t)$  is a zero-mean Gaussian white-noise process,  $f(t)$  is a deterministic envelope function modeling the amplitude nonstationarity of the ground motion and  $P(t)$  and  $R(t)$  are linear time-varying differential operators modeling the frequency content of the ground motion which is assumed to vary with time. In the special case of time-invariant operators  $P(t)$  and  $R(t)$ , equation I and II correspond to filtered modulated white-noise and modulated filtered white-noise excitations, respectively.

Subclasses of the stochastic processes generated by (4.95) or (4.96), such as white noise, modulated white noise, filtered white noise and filtered modulated white noise with rational (usually second-order) time-invariant transfer function for the filter, have been extensively used in the past to model ground motion. In this section, we extend the previous approaches to include the time variation of the operators  $P(t)$  and  $R(t)$  and we demonstrate how these processes can be incorporated

in existing random vibration analyses in order to simplify the expressions for the mean-square transient response.

In particular, let the ground motion  $G(t)$  be described by one of the following models

$$\text{MODEL 1: } G_1(t) = x_g(t) \quad (4.97)$$

$$\text{MODEL 2: } G_2(t) = \dot{x}_g(t) \quad (4.98)$$

$$\text{MODEL 3: } G_3(t) = -2\alpha_g(t)\dot{x}_g(t) - \omega_g^2(t)x_g(t) \quad (4.99)$$

where  $x_g(t)$  is the output of the second-order differential equation

$$\ddot{x}_g(t) + 2\alpha_g(t)\dot{x}_g(t) + \omega_g^2(t)x_g(t) = f(t)e(t) \quad (4.100)$$

with  $\alpha_g(t)$ ,  $\omega_g(t)$  and  $f(t)$  being slowly-varying functions of time. Model 1 has been proposed in Chapter 3 to model the ground motion, while model 3 is the extended version of the well-known Kanai-Tajimi model with variable coefficients. Equation (4.100) is a special case of equation (4.1) with modulated white-noise input. Let the stochastic process  $G(t)$  be broadband, that is, its correlation time  $T_c(t)$  be sufficiently small so that the time variation of  $\alpha_g(t)$ ,  $\omega_g(t)$  and  $f(t)$  over the time interval  $[t - T_c(t), t]$  can be ignored without significant loss of accuracy. In this case, the statistical properties of  $G(t)$  in the neighborhood of  $t$  can be obtained by an equivalent stationary process generated by equation (4.1) with the values of the corresponding constant coefficients being the instantaneous values  $\alpha_g(t)$ ,  $\omega_g(t)$  and  $f(t)$ . Therefore, the autocovariance function of the ground motion  $G(t)$  can be approximately obtained from (4.33) by letting  $\dot{r} = q_{12} = 0$ . This results in the autocovariance function

$$E[G(t)G(s)] = q_g(t) \exp\{-\alpha_g(t)(t-s)\} \frac{\cos\{\omega_g'(t)(t-s) - \phi_g(t)\}}{\cos\{\phi_g(t)\}} \quad (4.101)$$

and the EPSD function

$$S(\omega, t) = \frac{\kappa_1 + \kappa_2\omega^4(t) + \kappa_3\omega_g^4(t) + 4\kappa_4\alpha_g^2(t)\omega^2(t)}{(\omega^2(t) - \omega_g^2(t))^2 + 4\alpha_g^2(t)\omega^2(t)} f^2(t) \quad (4.102)$$

where the form of  $q_g(t)$  and  $\phi_g(t)$  and the values of  $\kappa_1, \kappa_2, \kappa_3$  and  $\kappa_4$  depend on the particular model used for  $G(t)$ . If  $G(t) = G_1(t)$ , then

$$q_g(t) = q_{11}(t), \quad \tan [\phi_g(t)] = \frac{\alpha_g(t)}{\omega'_g(t)}, \quad \kappa_1 = 1, \quad \kappa_2 = \kappa_3 = \kappa_4 = 0 \quad (4.103)$$

If  $G(t) = G_2(t)$ , then

$$q_g(t) = q_{22}(t), \quad \tan [\phi_g(t)] = -\frac{\alpha_g(t)}{\omega'_g(t)}, \quad \kappa_2 = 1, \quad \kappa_1 = \kappa_3 = \kappa_4 = 0 \quad (4.104)$$

If  $G(t) = G_3(t)$ , then

$$q_g(t) = q_a(t), \quad \tan [\phi_g(t)] = \frac{\alpha_g(t) \omega_g^2(t) - 4\alpha_g^2(t)}{\omega'_g(t) \omega_g^2(t) + 4\alpha_g^2(t)}, \quad \kappa_3 = \kappa_4 = 1, \quad \kappa_1 = \kappa_2 = 0 \quad (4.105)$$

The autocovariance function has the general form (4.86) with

$$\underline{\lambda}(t) = ( \alpha_g(t), \omega_g(t), q_g(t) ).$$

The integration for evaluating  $L_{12}(t)$  and  $L_{22}(t)$  can be carried out analytically, resulting in two types of terms for each of the integrals. One type contains the factor  $\exp\{-[\alpha_g(t) + \alpha(t)]T_c(t)\}$  which is neglected in this approximation because it is zero for sufficiently large time  $t$ . Therefore, the value of each integral is approximated by the remaining term resulting in

$$L_{12}(t) = q_g(t)I_c(t) \quad (4.106a)$$

$$L_{22}(t) = q_g(t)I_s(t) - \left( \alpha(t) + \frac{\dot{\omega}_d(t)}{2\omega_d(t)} \right) q_g(t)I_c(t) \quad (4.106b)$$

where

$$I_c(t) = \frac{A(t)}{C(t)} \quad (4.107a)$$

$$I_s(t) = \frac{B(t)}{C(t)} \quad (4.107b)$$

$$A(t) = [\alpha(t) + \alpha_g(t)]^2 + [\omega'(t)]^2 - [\omega'_g(t)]^2 + 2[\alpha(t) + \alpha_g(t)]\omega'_g(t) \tan [\phi_g(t)] \quad (4.107c)$$

$$B(t) = [\alpha(t) + \alpha_g(t)] \left\{ [\alpha(t) + \alpha_g(t)]^2 + [\omega'(t)]^2 + [\omega'_g(t)]^2 \right\} + \omega'_g(t) \tan [\phi_g(t)] \left\{ [\alpha(t) + \alpha_g(t)]^2 - [\omega'(t)]^2 + [\omega'_g(t)]^2 \right\} \quad (4.107d)$$

$$C(t) = [\omega^2(t) - \omega_g^2(t)]^2 + 4\omega(t)\omega_g(t) [\alpha(t) + \alpha_g(t)] [\omega(t)\zeta_g(t) + \omega_g(t)\zeta(t)] \quad (4.107e)$$

The forcing term  $g(t)$  takes the form

$$g(t) = q_g(t) R_g(\omega(t), \alpha(t), \omega_g(t), \alpha_g(t)) \{1 + \epsilon_R(t)\} \quad (4.108)$$

where

$$R_g(\omega(t), \alpha(t), \omega_g(t), \alpha_g(t)) = 2I_s(t) + 2 \left( \alpha(t) - \frac{\dot{\omega}_d(t)}{2\omega_d(t)} \right) I_c(t) \quad (4.109)$$

and

$$\epsilon_R(t) = \frac{\dot{L}_{12}(t)}{R_g(t)} \quad (4.110)$$

For slowly-varying structural parameters and excitation parameters, the forcing term  $g(t)$  is a slowly-varying function of time as well. In most earthquake engineering applications, these approximations considerably reduce the computational effort for evaluating the integrals without sacrificing much in their accuracy. As it will be seen in Chapter 5, these expressions also provide direct insight into the response characteristics.

For lightly-damped oscillators, the following limit is true

$$\lim_{\zeta \rightarrow 0} q_g(t) R_g(\omega(t), \alpha(t), \omega_g(t), \alpha_g(t)) = S(\omega(t), \omega_g(t), \alpha_g(t)) \quad (4.111)$$

where  $S(\omega, \omega_g(t), \alpha_g(t)) \equiv S(\omega, t)$  as given by (4.102). Several studies (Spanos, 1983) restricted to the response of lightly-damped oscillators have used the EPSD function to approximate the forcing term  $g(t)$ . Contour plots of the fractional error

$$\epsilon_L(t) = \frac{S(\omega(t), \omega_g(t), \alpha_g(t)) - q_g(t) R_g(\omega(t), \alpha(t), \omega_g(t), \alpha_g(t))}{q_g(t) R_g(\omega(t), \alpha(t), \omega_g(t), \alpha_g(t))} \quad (4.112)$$

introduced by the lightly-damped approximation are shown in Figure 4.5 for the ground motion model 1. These plots, which cover different ranges of oscillator and ground motion parameters of practical interest, show the ranges where the error is significant. For accurate estimation in these ranges, the original approximate expression (4.108) for evaluating  $g(t)$  has to be used. Since it is usually not known apriori where the error  $\epsilon_L(t)$  is large, it is best to always use (4.108).

Next, to get an estimate of  $\epsilon_R(t)$ , we consider the case of linear oscillators and ground models with time-invariant coefficients  $\omega_0$  and  $\zeta$ . This is a special case of the filtered modulated white-noise model discussed in section 4.8.2 with

$$\epsilon_R(t) = \lambda(\omega_0) \frac{\dot{f}(t)}{2\omega_0 f(t)} \quad (4.113)$$

where  $\lambda(\omega_0)$  is defined in (4.94).

Using the slowly-varying condition  $|\dot{f}(t)/(2\omega_0 f(t))| \ll 1$ , the contribution of  $\epsilon_R(t)$  would be significant only if  $\lambda(\omega_0) \gg 1$  or more. Contour curves for  $\lambda(\omega_0)$  are shown in Figure 4.6 for the model 1. These curves cover a wide range of oscillator and ground motion parameters and provide an insight into those values of the parameters for which the quantity  $\epsilon_R(t)$  can be neglected.

#### 4.8.4 Accuracy of the Approximations Using the Proposed Stochastic Ground Motion Model

The excitation model proposed in Chapter 3 to model the ground motion is used to check the accuracy of the approximations and numerically illustrate the discrepancies between the approximate and the exact mean-square response. An efficient but still time-consuming method for evaluating the exact mean-square response is to rewrite the structural model equation (4.1) and the ground model equation (4.100) as a four-dimensional first-order vector equation and numerically integrate the corresponding Liapunov matrix equation for the mean-square response. This is done here to provide a basis for assessing the approximate results presented above.

It is not possible to perform a complete numerical study and illustrate the order of the accuracy of the approximations for a wide range of oscillator and excitation parameters. Of the infinite number of possible time variations for the excitation parameters, only two are examined. The first case corresponds to the Orion Blvd. recording where the standard deviation and damped-frequency of the excitation process are shown in Figure 4.7. The Orion Blvd. recording shows a significant time variation of the model parameters and therefore it is supposed to be a representative case expected in modeling strong ground motion. The exact and the approximate mean-square response of a linear oscillator are compared in Figure 4.8 for 5% damping and for  $\omega_0 = 7, 5, 3$  and 1Hz. The approximations are quite accurate with a maximum percentage error of the order of 1%. The second case is an extreme case artificially designed to violate the slowly-varying conditions. The corresponding standard deviation and damped-frequency of the excitation process

are shown in Figure 4.9. This case is unrealistic for processes modeling strong ground motion. The exact and the approximate mean-square response of a linear oscillator are compared in Figure 4.10 for 5% damping and for  $\omega_0 = 7, 5, 3$  and 1Hz. The discrepancies are of the order of a few percent, preserving the essential characteristics of the response.

For a nonlinear structure, the time variation of the equivalent linear parameters  $\omega(t)$  and  $\alpha(t)$  depends on the nonlinearity of the restoring force. The dependence will be addressed in more detail in Chapter 5. However, to complete this analysis we use the dependence as given by equations (5.5) and (5.6) to check the accuracy of the approximations for the nonlinear case. Comparison between the exact (solid curves) and the approximate (dashed curves) STD response are shown in Figures 4.11(a) and 4.12(a) for two different nonlinear oscillators. The excitation parameters are shown in Figure 4.7 for the Orion Blvd. recording. The initial damping ratio for both oscillators is  $\zeta_0 = 0.05$ . The time-varying frequency  $\omega(t)$  is computed by the expression (5.5) and it is shown in Figures 4.11(b) and 4.12(b) for the two oscillators. The parameter  $\alpha(t) = \zeta_0\omega_0$  is constant for both cases. The differences between the exact and the approximate solution observed in Figures 4.11(a) and 4.11(b) for the oscillator with initial frequency  $\omega(0) = 5\text{Hz}$  are of the order of a few percent. Discrepancies of similar order were also observed for other variations of  $\omega(t)$  and  $\alpha(t)$  provided that the conditions validating the approximations were satisfied. For example, for the oscillator with initial frequency  $\omega(0) = 1\text{Hz}$ , shown in Figure 4.12(a) and (b), the discrepancies between the exact and the approximate mean-square displacement are of the order of 20% or higher. In this case, the excitation parameters  $\omega_g(t)$  and  $q_g(t)$  shown in Figure 4.7 vary significantly over the equivalent period of the oscillator which is approximately 10 seconds (see Figure 4.12(b)). Therefore, the large discrepancies between the exact and the approximate solutions are due to the violation of the slowly-varying conditions.

#### 4.8.5 Computational Aspects

By approximating the original expressions (4.8) for the transient mean-square displacement, velocity and absolute acceleration of the response by the

simplified expressions, we reduce considerably the computational effort involved in a digital computer for evaluating the response quantities. Compared with the time-consuming operations in the numerical integration of (4.8), the computational savings achieved by these approximations are as follows:

- a. For stable and accurate numerical scheme for integrating (4.8), the time step depends on the shortest period  $2\pi/\omega_d(t)$  of the oscillator. However, the time step for integrating the corresponding first-order scalar equation is independent of the equivalent period of the oscillator since the oscillations have been eliminated. Therefore, much longer time steps can be used which reduce considerably the number of numerical operations required for computing the mean-square response.
- b. In general, numerical integration is required for each time step to evaluate the integrals  $L_{12}(t)$  and  $L_{22}(t)$ . However, the simple and quite accurate algebraic approximations in (4.87) are another source of considerable reduction of the computational effort.
- c. An additional source of reduction is that a one-dimensional scalar equation requires less numerical operations than a three-dimensional vector equation.

The computational savings are noticeable, for example, when linear or nonlinear probabilistic response spectra are to be computed using the existing approximate formulas in random vibration theory (Mason and Iwan, 1983) for solving the first-passage problem. In such a case, the number of times that the solution is required is very large since it depends on the range of initial stiffnesses, damping ratios and ductilities of the nonlinear structural model used to compute the response spectra, as well as on the number of iterations required for each of the above structural parameters to obtain results of acceptable accuracy.

#### **4.9 Extension of the Approximations to Classically-Damped MDOF Linear Systems**

Consider an  $n$ -degree-of-freedom, viscous damped, linear system having classical modes, then the response at some point of the system can be expressed in terms

of modal contributions as

$$x(t) = \sum_{i=1}^N p_i x_i(t) \quad (4.114)$$

where  $p_i$  is the effective participation factor for mode  $i$  at the point of interest, and  $x_i(t)$  is the response of the  $i$ -th normal mode satisfying the modal equation

$$\ddot{x}_i(t) + 2\zeta_i \omega_i \dot{x}_i(t) + \omega_i^2 x_i(t) = G(t) \quad (4.115)$$

In this equation the forcing functions  $G(t)$  could be the base excitation and  $\omega_i$  and  $\zeta_i$  are the  $i$ -th modal frequency and damping coefficient, respectively. The mean-square response  $R(t) = E[x^2(t)]$  can be written as:

$$R(t) = \sum_{i=1}^n \sum_{j=1}^n p_i p_j R_{ij}(t) \quad (4.116)$$

where

$$R_{ij}(t) = E[x_i(t)x_j(t)] \quad (4.117)$$

Therefore, the mean-square response can be obtained by the weighted summation of the mean-square response  $R_{ii}(t)$  of each mode, plus the covariance response  $R_{ij}(t)$  of two modes  $i$  and  $j$ , with the weighting coefficients being the product of the corresponding effective modal participation factors.

The equation for  $R_{ij}(t)$  is next formulated and approximations are introduced to simplify the original exact equations. The state-space representation of, say, the  $i$ -th modal equation is given by (4.2) with  $\omega_0$  and  $\zeta$  replaced by  $\omega_i$  and  $\zeta_i$ . Let

$$Q^{(ij)}(t) = E[\underline{x}_i(t)\underline{x}_j^T(t)] \quad (4.118)$$

be the covariance of the  $i$  and  $j$  state vectors, then it satisfies the matrix differential equation (assume zero initial conditions)

$$\begin{aligned} \dot{Q}^{(ij)}(t) &= A_i Q^{(ij)}(t) + Q^{(ij)}(t) A_j^T + L^{(i)}(t) + L^{(j)T}(t) \\ Q^{(ij)}(0) &= 0 \end{aligned} \quad (4.119)$$

where

$$A_i = \begin{pmatrix} 0 & 1 \\ -\omega_i^2 & -2\zeta_i \omega_i \end{pmatrix}, \quad (4.120)$$

$$L^{(i)} = \int_0^t \Phi^{(i)}(t-\tau) [g(\tau)g^T(t)] d\tau, \quad (4.121)$$

and  $\Phi^{(i)}(t - \tau)$  is the principal solution matrix for the  $i$ -th modal equation. If  $i = j$ , then the equation for the symmetric matrix  $Q^{(ii)}$  is exactly the same as the matrix equation (4.6). Therefore, the approximation developed previously also holds for the components of  $Q^{(ii)}$ . In particular,  $R_{ii}(t) \equiv Q_{11}^{(ii)}(t)$  can be obtained either exactly by a third-order equation or approximately by a first-order equation. For  $i \neq j$ , the components of  $Q^{(ij)}$  satisfy

$$\dot{Q}_{11} = Q_{21} + Q_{12} \quad (4.122a)$$

$$\dot{Q}_{12} = Q_{22} - \omega_j^2 Q_{11} - 2\zeta_j \omega_j Q_{12} + L_{12}^{(i)} \quad (4.122b)$$

$$\dot{Q}_{21} = Q_{22} - \omega_i^2 Q_{11} - 2\zeta_i \omega_i Q_{21} + L_{12}^{(j)} \quad (4.122c)$$

$$\dot{Q}_{22} = -\omega_i^2 Q_{12} - 2\zeta_i \omega_i Q_{22} - \omega_j^2 Q_{21} - 2\zeta_j \omega_j Q_{22} + L_{22}^{(i)} + L_{22}^{(j)} \quad (4.122d)$$

where the superscript  $[(ij)]$  has been dropped in the above equations, for clarity. Eliminating  $Q_{12}$ ,  $Q_{21}$ , and  $Q_{22}$  from the above equations, a fourth-order equation for  $Q_{11}^{(ij)}(t) \equiv R_{ij}(t)$  is obtained. Treating for simplicity the case  $\zeta_i = \zeta_j = \zeta$ , the characteristic polynomial of the fourth-order equation has the roots

$$\begin{aligned} \rho_{1,2} &= -2\zeta\omega \pm 2i\omega\sqrt{1 - \zeta^2} \\ \rho_{3,4} &= -2\zeta\omega \pm 2i\omega\lambda\sqrt{1 - \zeta^2} \end{aligned} \quad (4.123)$$

where

$$\omega = \frac{\omega_i + \omega_j}{2} \quad (4.124)$$

$$\lambda = \frac{\omega_i - \omega_j}{\omega_i + \omega_j} \quad (4.125)$$

Following ideas similar to those in Section 4.3.1, the fourth-order differential equation for  $R_{ij}(t)$  can be split into two second-order differential equations as follows

$$\ddot{R}_{ij} + 4\zeta\omega\dot{R}_{ij} + 4\omega^2[\zeta^2 + \lambda^2(1 - \zeta^2)]R_{ij} = 2r_{ij}(t) \quad (4.126)$$

$$\ddot{r}_{ij}(t) + 4\zeta\omega\dot{r}_{ij}(t) + 4\omega^2 r_{ij}(t) = g_{ij}(t) \quad (4.127)$$

where

$$g_{ij}(t) = \dot{F}_{ij}(t) + 2\zeta\omega F_{ij}(t) \quad (4.128)$$

with

$$\begin{aligned} F_{ij}(t) &= (L_{22}^{(i)}(t) + L_{22}^{(j)}(t)) + 2\zeta\omega(L_{12}^{(i)}(t) + L_{12}^{(j)}(t)) \\ &\quad + \frac{1}{2}(\dot{L}_{12}^{(i)}(t) + \dot{L}_{12}^{(j)}(t)) + \zeta\omega(\lambda + 2)(L_{12}^{(i)}(t) - L_{12}^{(j)}(t)) \end{aligned} \quad (4.129)$$

For modulated white-noise input,  $g(t) = f^2(t)$  where  $f(t)$  is the input modulation. Although for demonstration purposes it is assumed that  $\zeta_i = \zeta_j$ , similar analyses can be performed for  $\zeta_i \neq \zeta_j$ .

Based on the approximate analysis in Section 4.4, the solution of the second-order differential equation (4.127) can be approximated by

$$r_{ij}(t) = \frac{g_{ij}(t)}{4\omega^2} \quad (4.130)$$

provided that  $g_{ij}(t)$  is slowly-varying. Conditions (4.41) with  $\omega_0$  and  $g(t)$  replaced by  $\omega$  and  $g_{ij}(t)$  determine the conditions for the approximation to be valid. Substituting (4.130) in (4.126), the covariance of the  $i$  and  $j$  mode can be obtained approximately by solving the second-order differential equation

$$\ddot{R}_{ij} + 4\zeta\omega\dot{R}_{ij} + 4\omega^2[\zeta^2 + \lambda^2(1 - \zeta^2)]R_{ij} = \frac{\dot{F}_{ij}(t) + 2\zeta\omega F_{ij}(t)}{2\omega^2} \quad (4.131)$$

The terms in expression  $F_{ij}(t)$  can be approximated according to the analysis in Section 4.7. In Section 4.8.4, the approximation was found to be very accurate for “earthquake-like” excitations.

Next, numerical results are presented to check the accuracy of the approximate second-order differential equation and compare it with existing approximations (Bucher, 1988). A first-order differential equation was proposed by Bucher to approximate  $R_{ij}(t)$ . In his analysis, he first treated the case of modulated white-noise excitation and then he generalized his approximations for colored white-noise by defining, without mathematical justification, the form of the input in his first-order differential equation. The approximation proposed here, which is based on a more rigorous mathematical analysis, predicts different response characteristics from the ones proposed by Bucher. Also, the proposed approximation treats general excitations with nonstationarities in both amplitude and frequency content. Comparisons between the different approximations and the exact one for modulated white-noise input and for various values of  $\omega$ , and  $\lambda$  are shown in Figures 4.13 and 4.14 for  $\zeta = 0.02$  and  $\zeta = 0.05$ , respectively. The modulation is of the form (4.44) with  $f_m = 1$ ,  $t_m = 1$ , and  $\beta = 0.5$ . Bucher’s approximation fails to predict the qualitative features of the response in some cases. In other cases, it is less accurate

than the proposed approximation which seems to be extremely accurate for all cases examined.

#### 4.10 Conclusions

The transient equivalent linearization method was used to replace the equation of motion of a nonlinear oscillator by an equivalent second-order linear differential equation with time-varying coefficients. The special case of time-invariant coefficients corresponds to the equation of motion of a linear oscillator. An approximate formulation was developed to replace the original, computationally lengthy expressions for the second-moment statistics of the transient response by much simpler expressions. The conditions for the approximations are: a) the excitation process is broadband and b) the coefficients of the second-order linear differential equation are slowly-varying functions of time. The analysis treats general excitations with nonstationarities in both the amplitude and the frequency content. The approximations provide meaningful insight into the characteristics of the nonstationary response. Similarities with the stationary response exist and were identified by the analysis. The formulation was extended to approximate the covariance response of MDOF systems.

The proposed approximations preserve the essential characteristics of the response without significant loss of accuracy. They are also computationally efficient with typical reduction in computing time of one to two orders of magnitude. The stochastic process proposed to model earthquake loads in Chapter 3 was used as an example to numerically validate the approximations. Earthquake loads, in general, fulfill the conditions developed for the approximations. Therefore, the approximate equations are suitable to apply for the seismic analysis of linear and nonlinear structures.

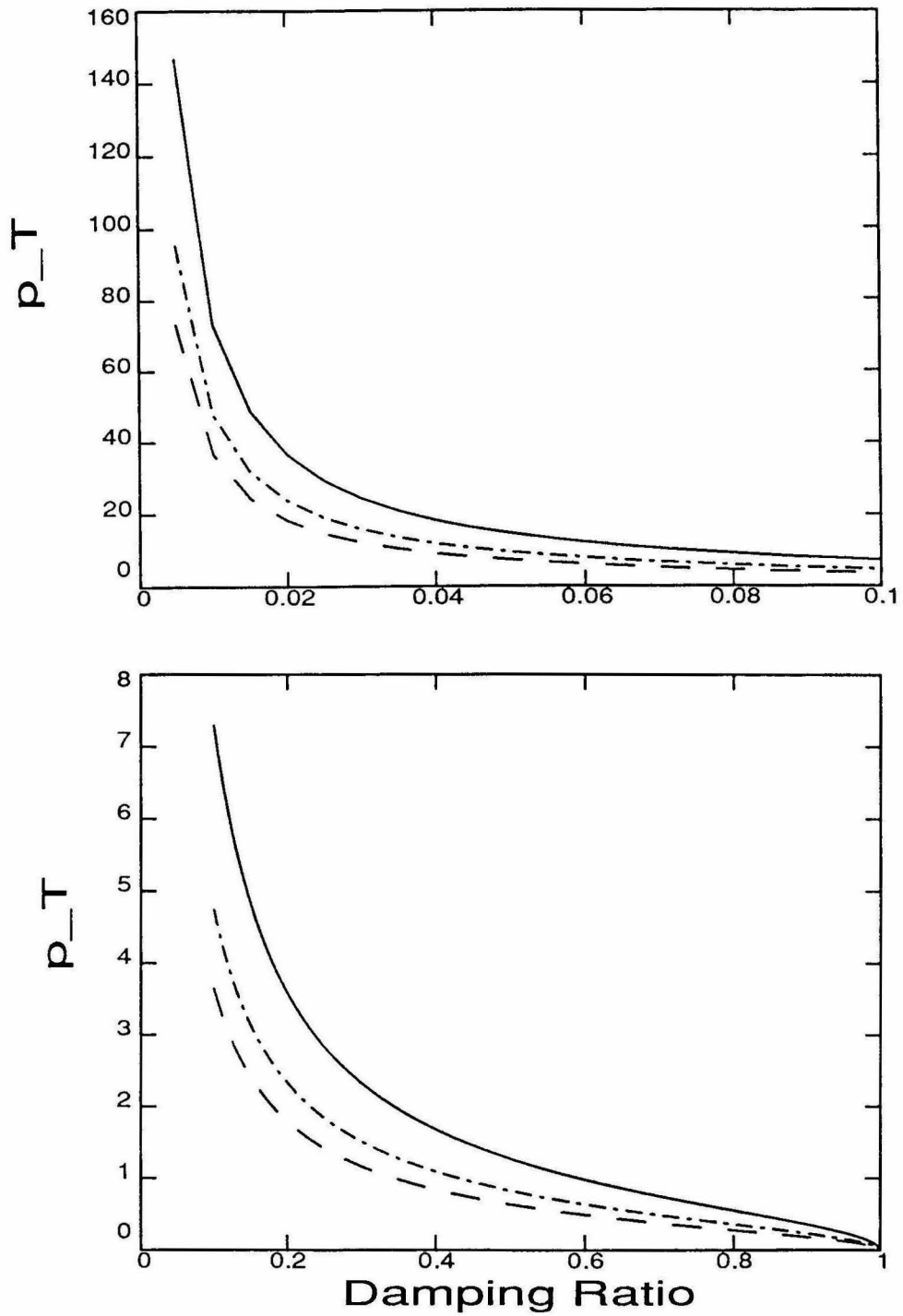


Figure 4.1. Number of cycles of oscillations needed for the oscillatory term to decay to  $n\%$  of its maximum value.  $n=1$  (solid curve),  $n=5$  (dashed-dotted curve),  $n=10$  (dotted curve).

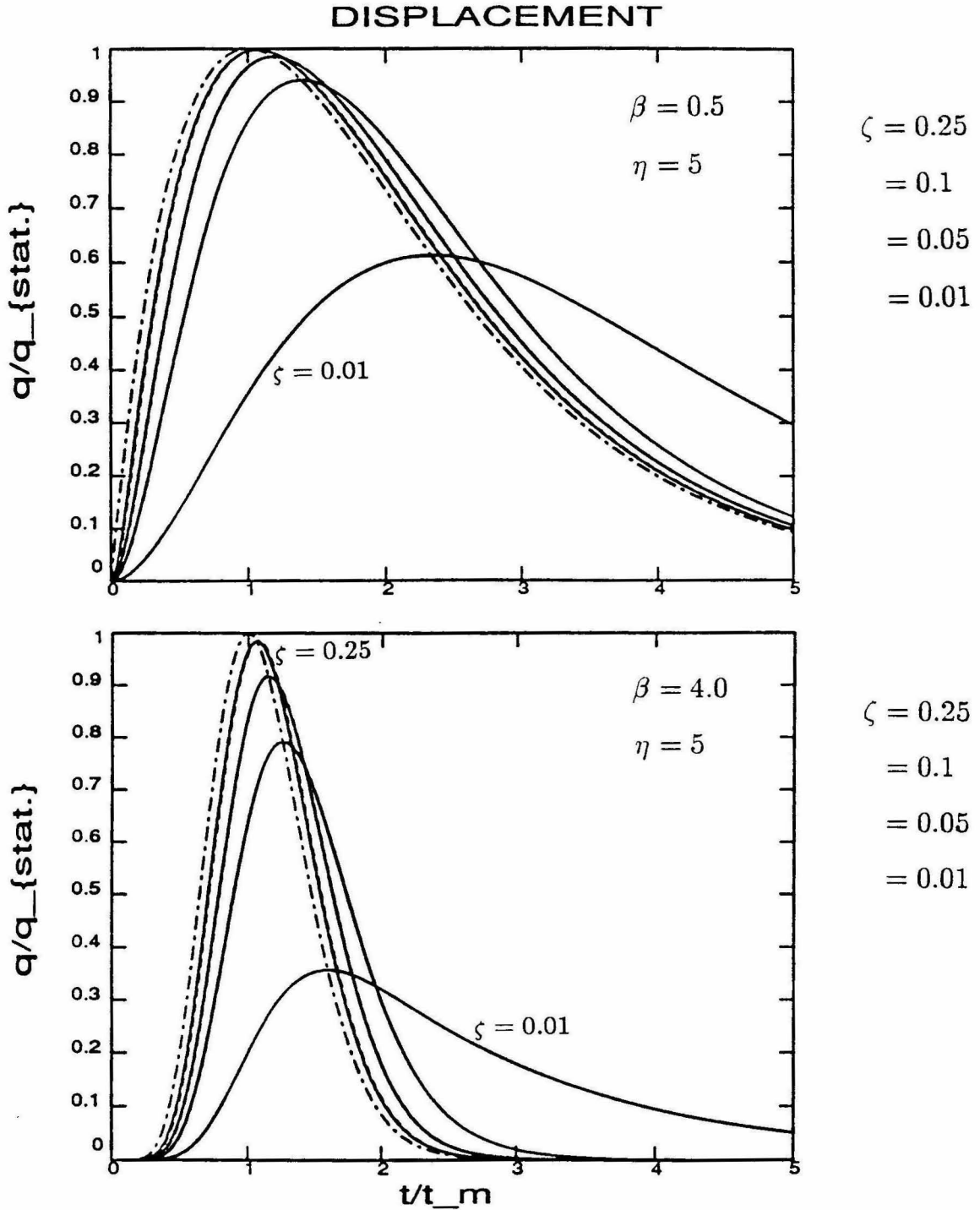


Figure 4.2. (a) Comparison between the nondimensional exact (dashed curve) and approximate (solid curve) mean-square displacement response of a linear SDOF oscillator subjected to a modulated (dashed-dotted curve) white-noise excitation.  $\eta = \frac{t_m}{T_0} = 5.0$ .

### DISPLACEMENT

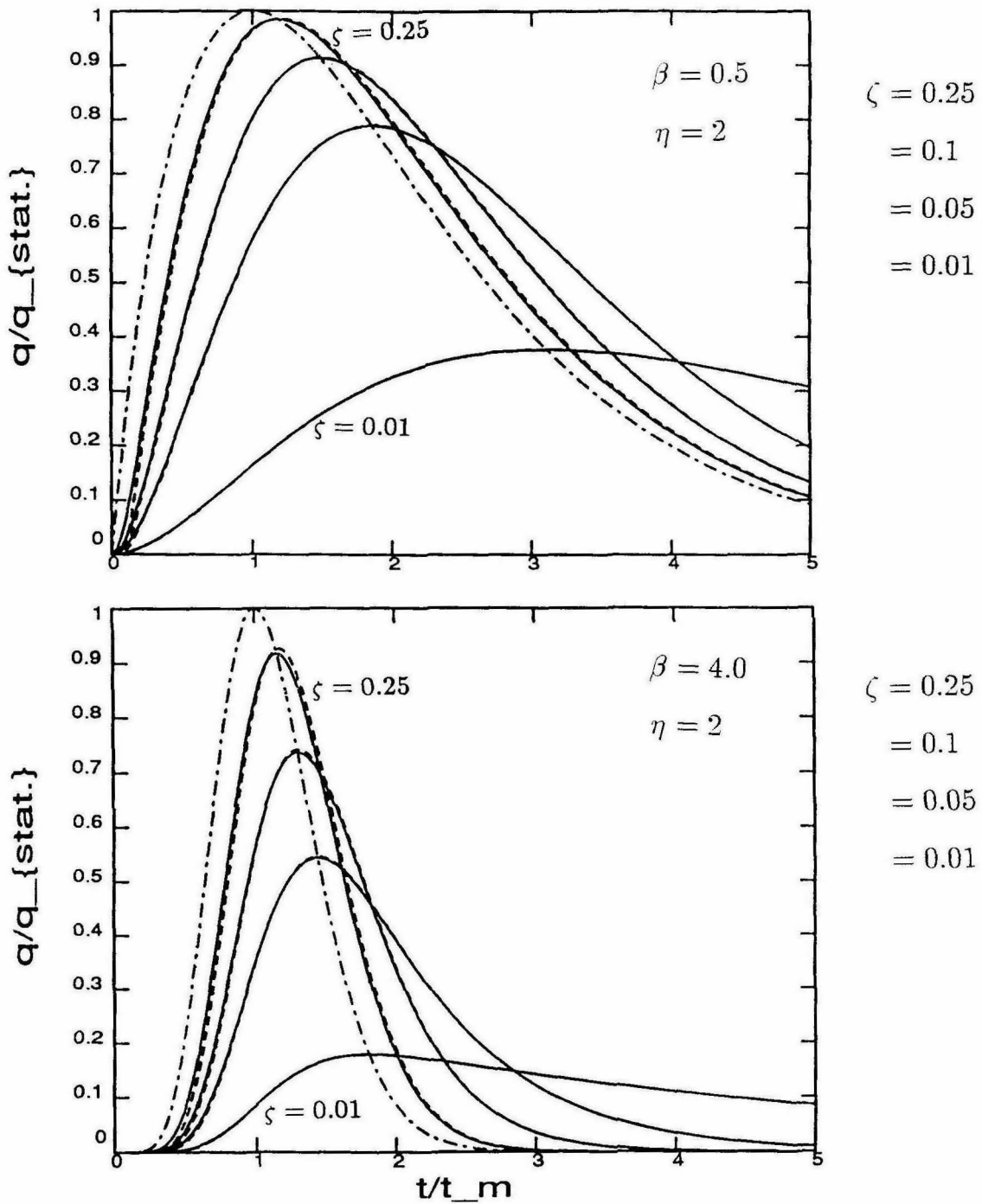


Figure 4.2. (b) Comparison between the nondimensional exact (dashed curve) and approximate (solid curve) mean-square displacement response of a linear SDOF oscillator subjected to a modulated (dashed-dotted curve) white-noise excitation.  $\eta = \frac{t_m}{T_0} = 2.0$ .

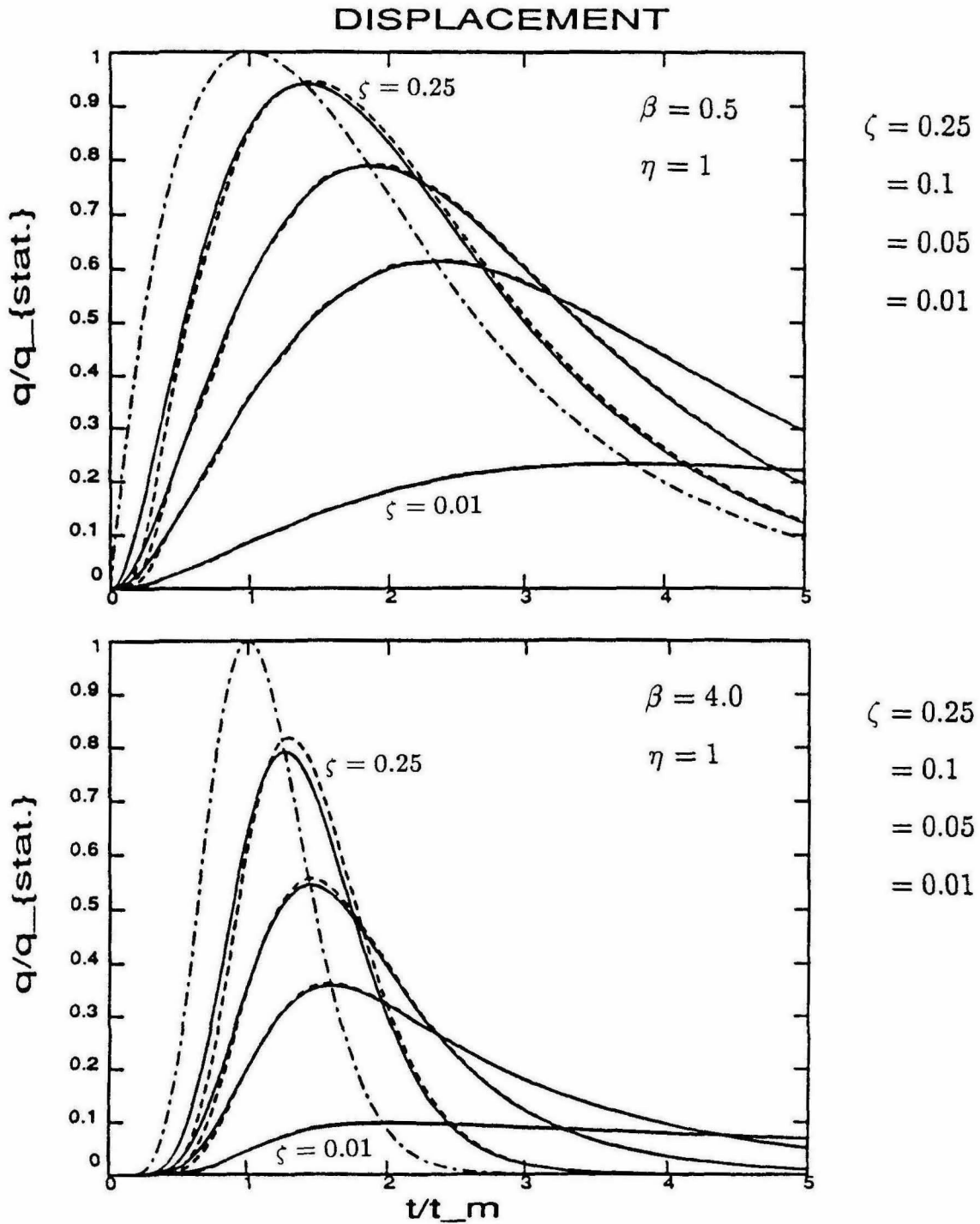


Figure 4.2. (c) Comparison between the nondimensional exact (dashed curve) and approximate (solid curve) mean-square displacement response of a linear SDOF oscillator subjected to a modulated (dashed-dotted curve) white-noise excitation.  $\eta = \frac{t_m}{T_0} = 1.0$ .

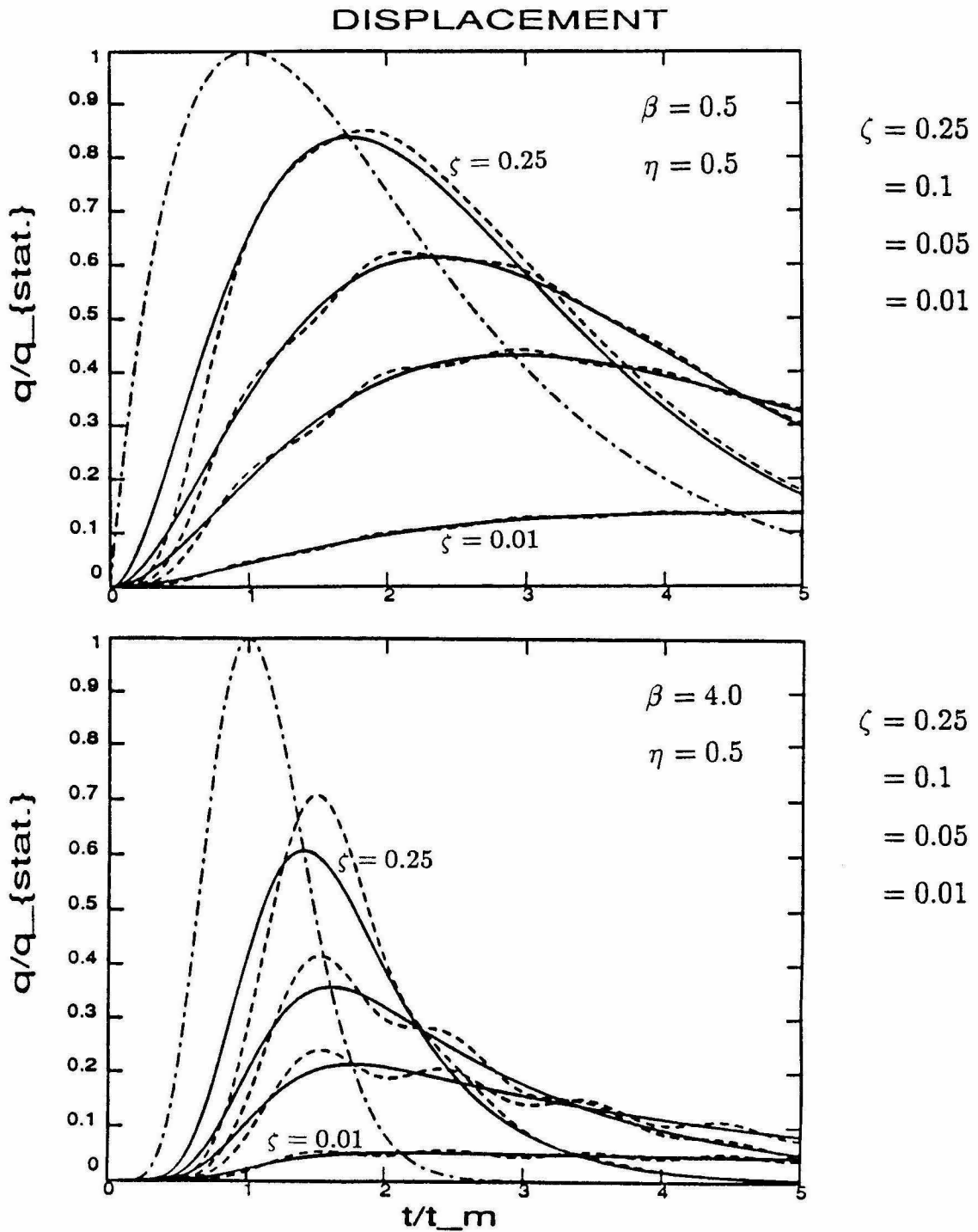


Figure 4.2. (d) Comparison between the nondimensional exact (dashed curve) and approximate (solid curve) mean-square displacement response of a linear SDOF oscillator subjected to a modulated (dashed-dotted curve) white-noise excitation.  $\eta = \frac{t_m}{T_0} = 0.5$ .

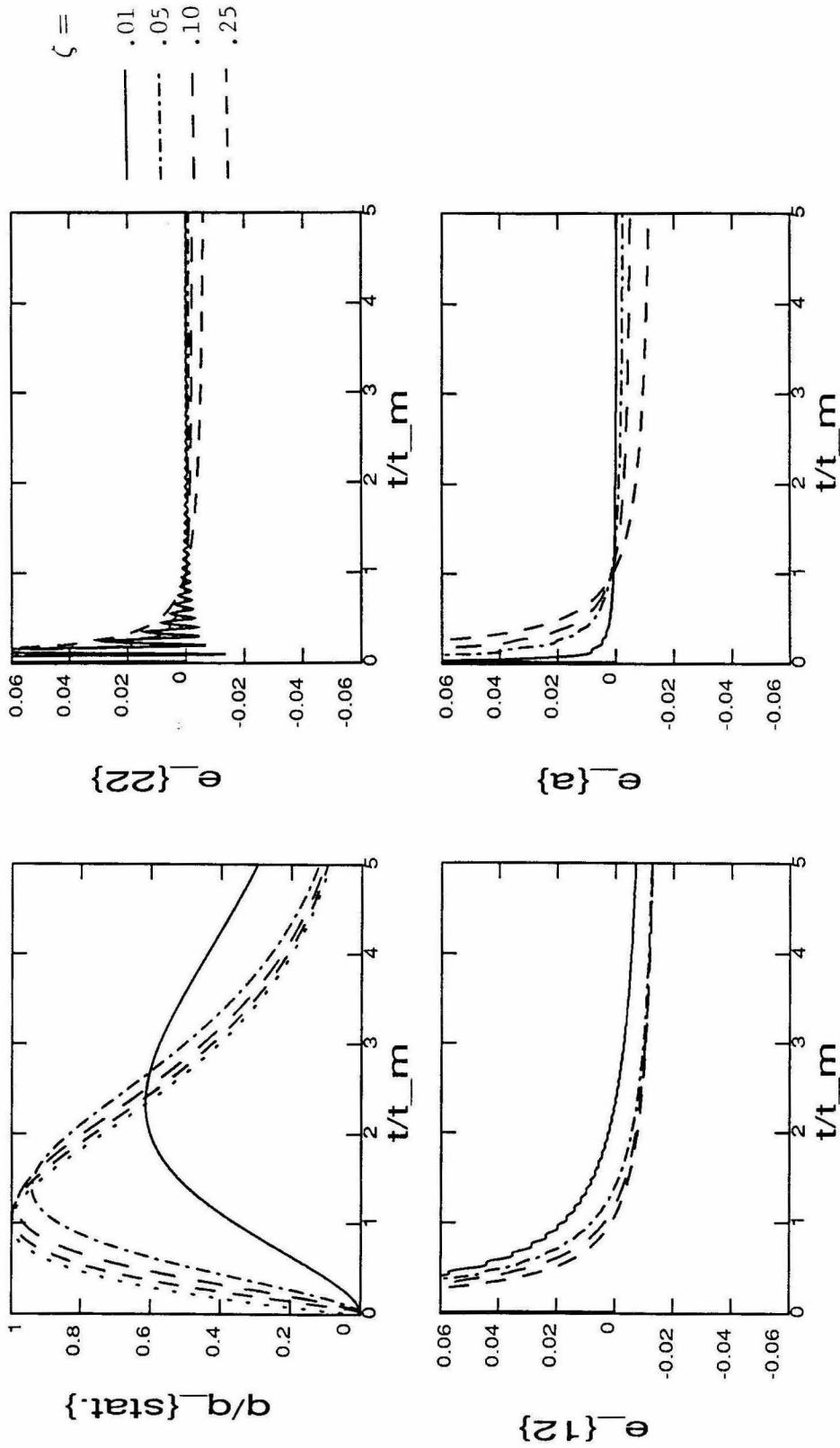


Figure 4.3. (a) Time variation of normalized mean-square displacement,  $\epsilon_{12}$ ,  $\epsilon_{22}$ , and  $\epsilon_a$ , for different damping ratios.  $\beta = 0.5$ ,  $\eta = 5$ . Dotted curve corresponds to the time variation of the input modulation.

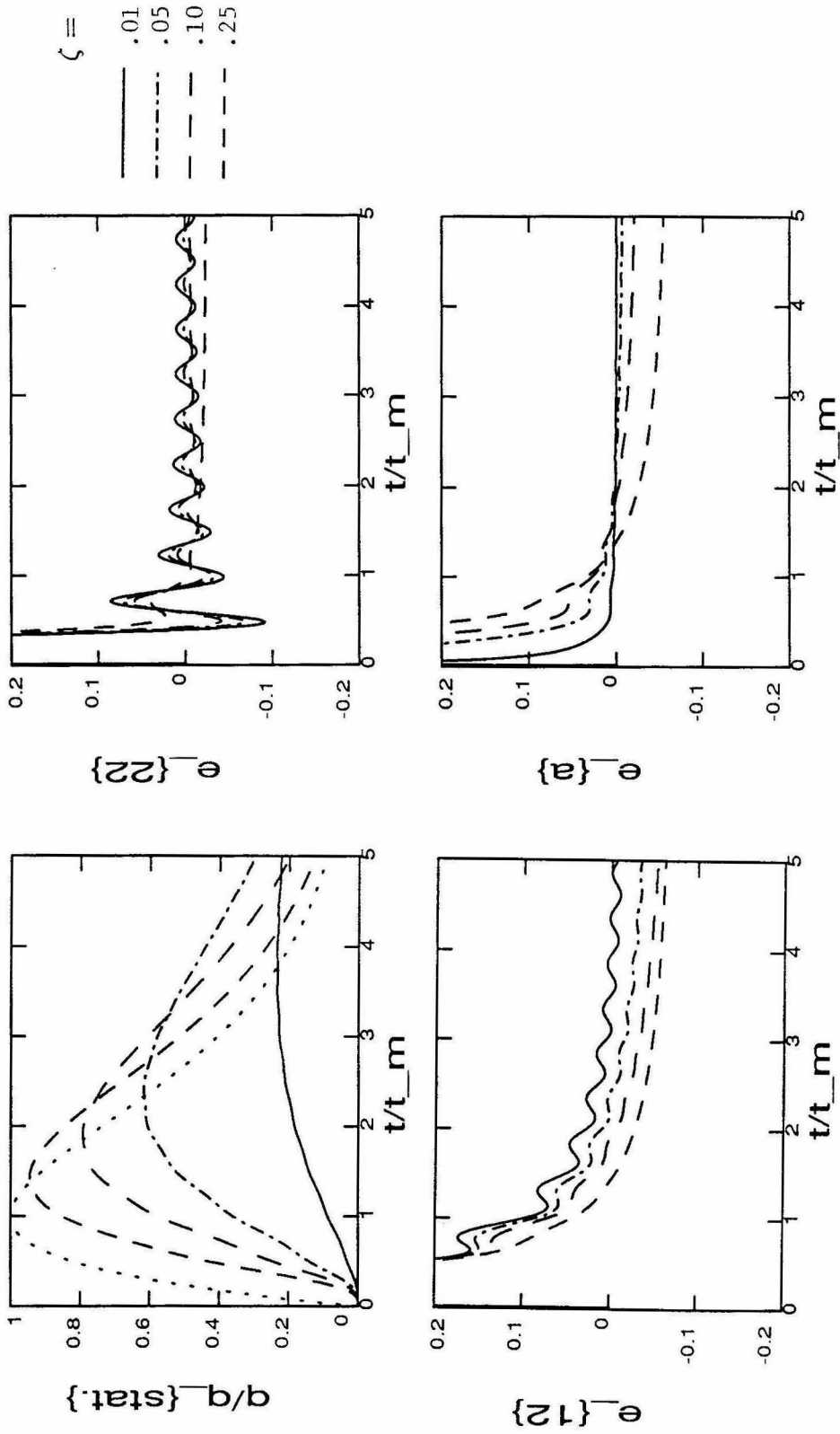


Figure 4.3. (b) Time variation of normalized mean-square displacement,  $\epsilon_{12}$ ,  $\epsilon_{22}$ , and  $\epsilon_a$  for different damping ratios.  $\beta = 0.5$ ,  $\eta = 1$ . Dotted curve corresponds to the time variation of the input modulation.

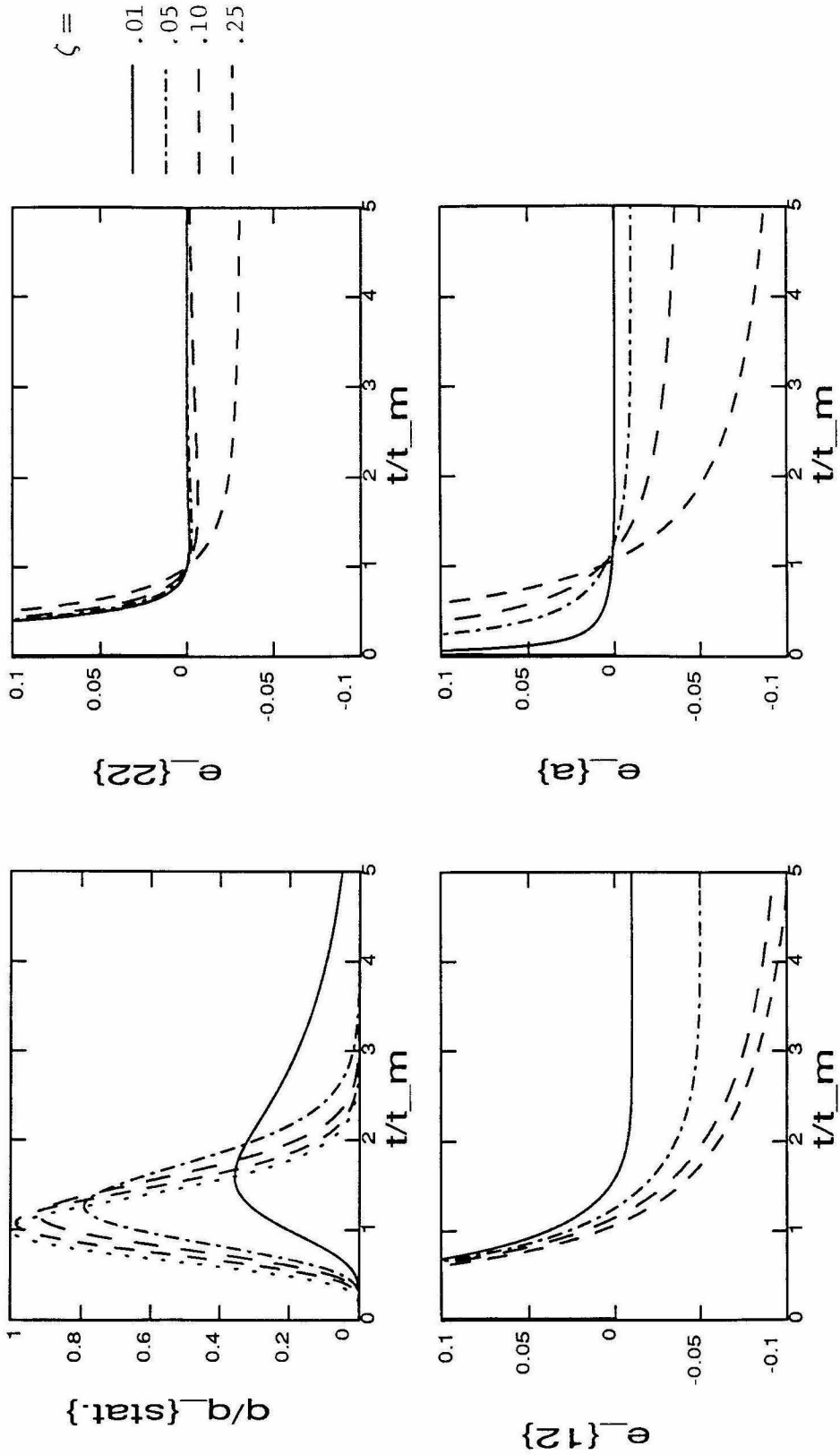


Figure 4.3. (c) Time variation of normalized mean-square displacement,  $\epsilon_{12}$ ,  $\epsilon_{22}$ , and  $\epsilon_a$  for different damping ratios.  $\beta = 4$ ,  $\eta = 5$ . Dotted curve corresponds to the time variation of the input modulation.

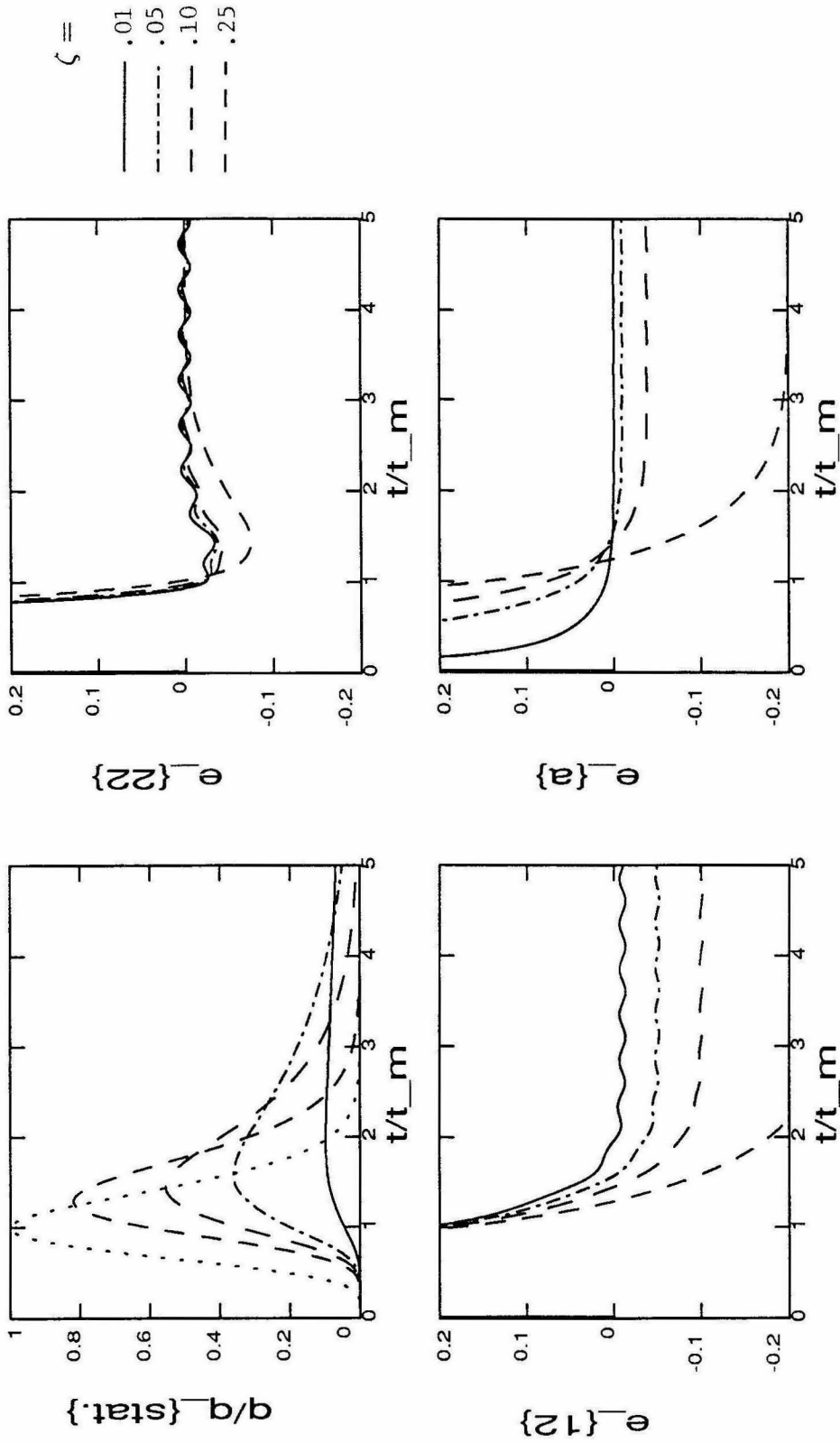


Figure 4.3. (d) Time variation of normalized mean-square displacement,  $\epsilon_{12}$ ,  $\epsilon_{22}$ , and  $\epsilon_a$  for different damping ratios.  $\beta = 4$ ,  $\eta = 1$ . Dotted curve corresponds to the time variation of the input modulation.

### DISPLACEMENT

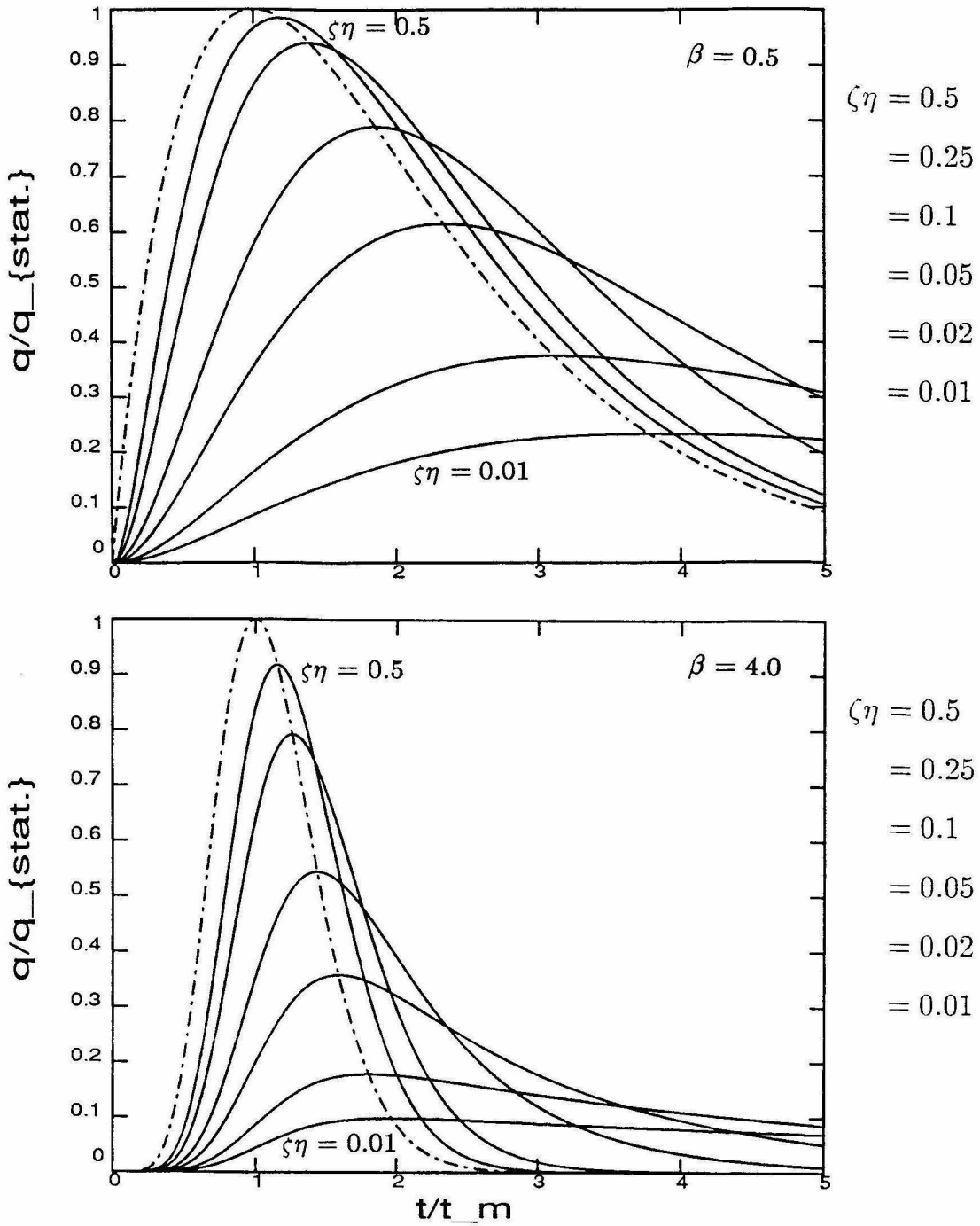


Figure 4.4. Approximate nondimensional mean-square displacement (solid curves) of the response of a linear SDOF oscillator subjected to a modulated (dashed-dotted curve) white-noise excitation.

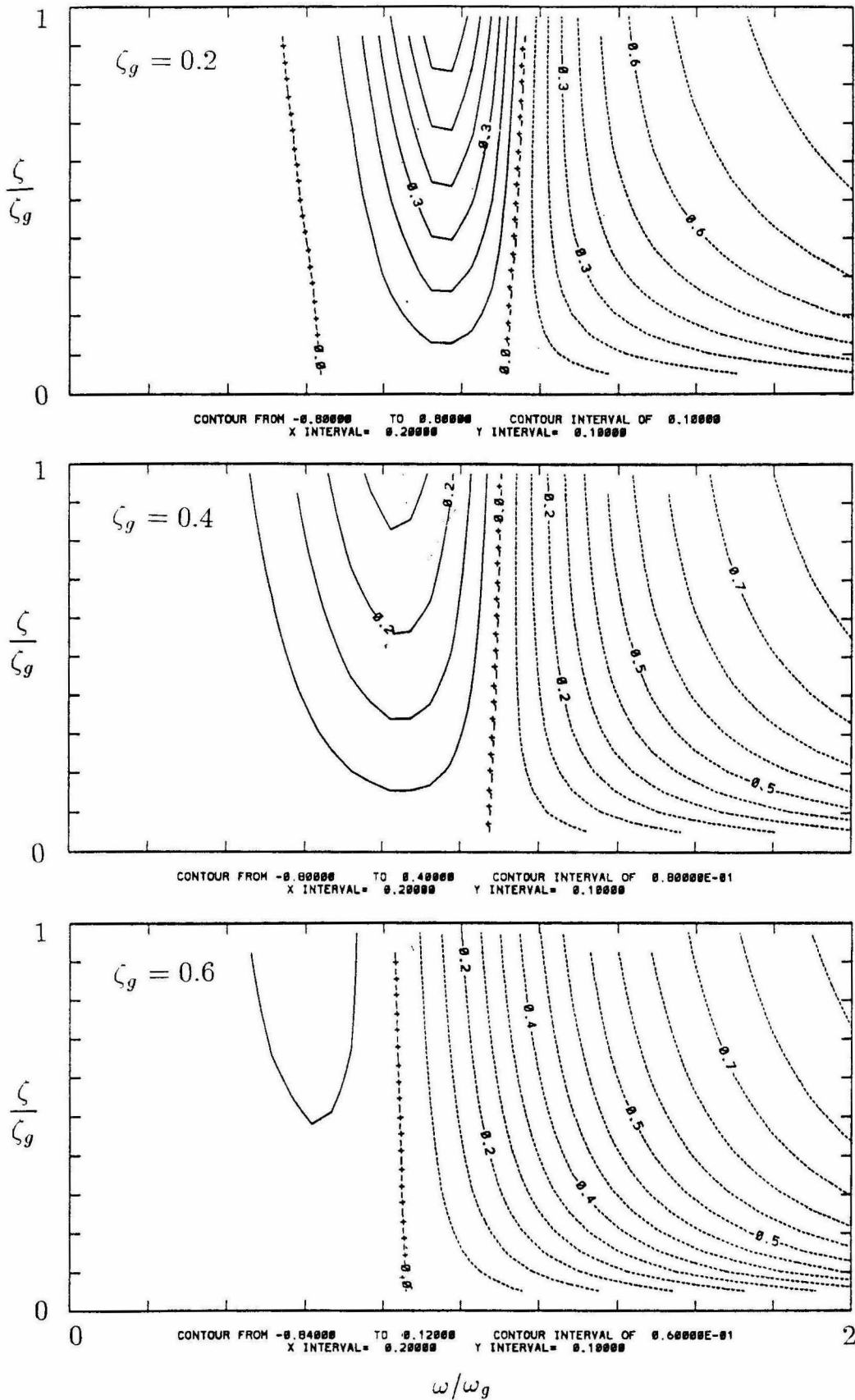


Figure 4.5. Contour plots of the fractional error  $\epsilon_L$  as defined in (4.112). The excitation is modeled by MODEL 1.

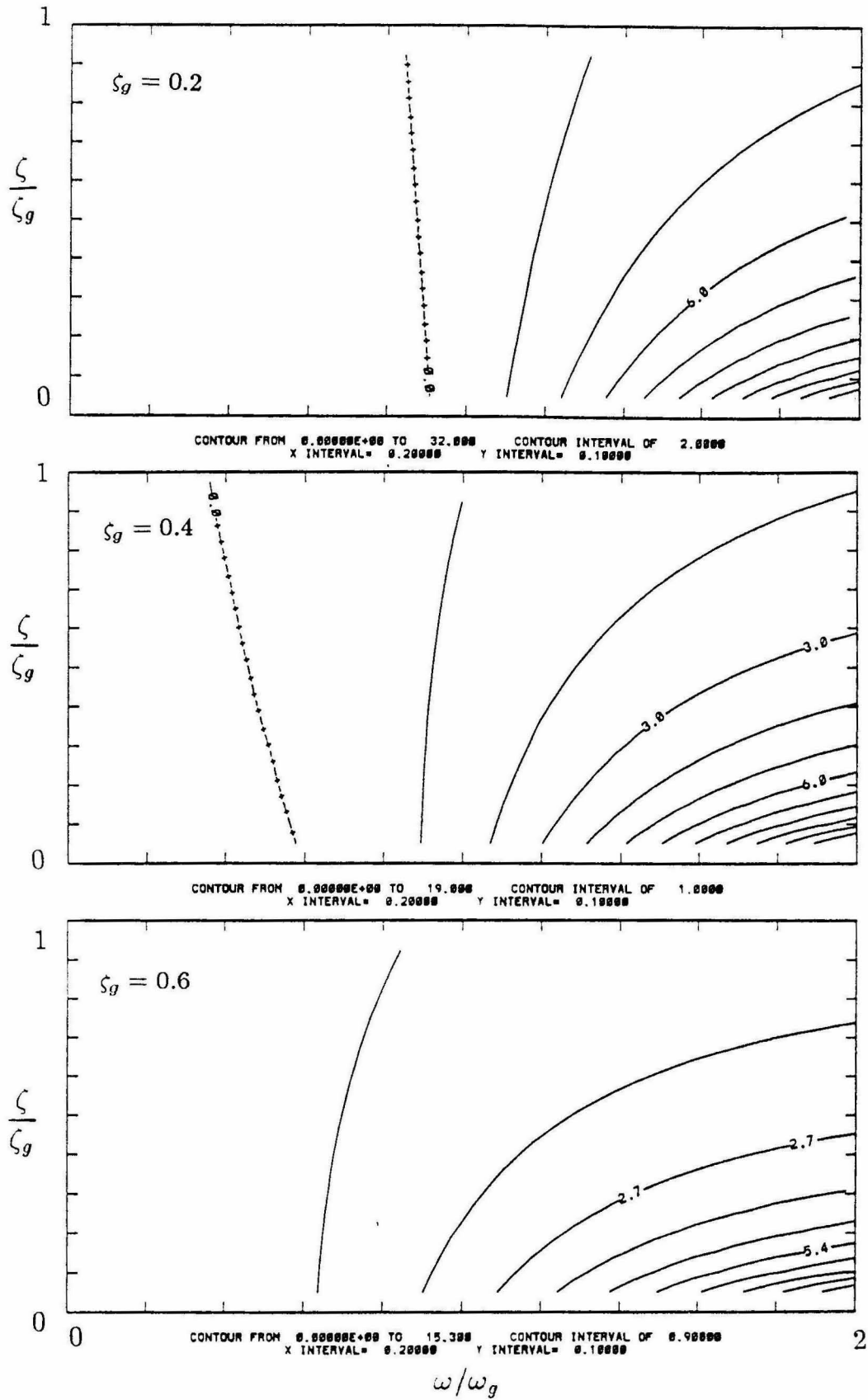


Figure 4.6. Contour plots of  $\lambda(\omega_0)$  as defined in (4.94). The excitation is modeled by MODEL 1.

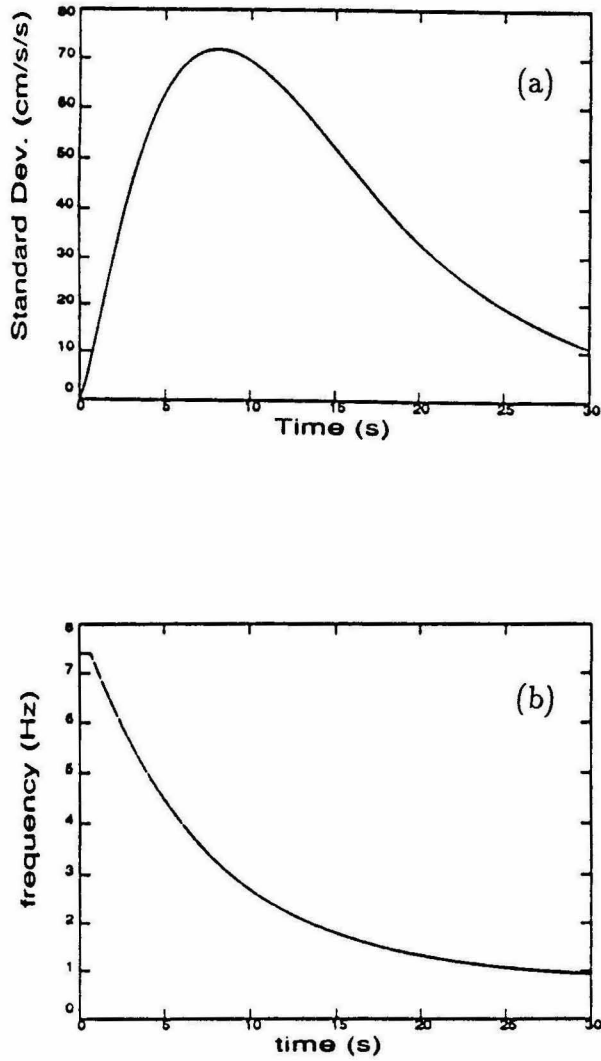


Figure 4.7. Time variation of (a) the standard deviation and (b) the damped-frequency of the nine-parameter earthquake model fitted to the Orion Blvd. recording.

### LINEAR RESPONSE

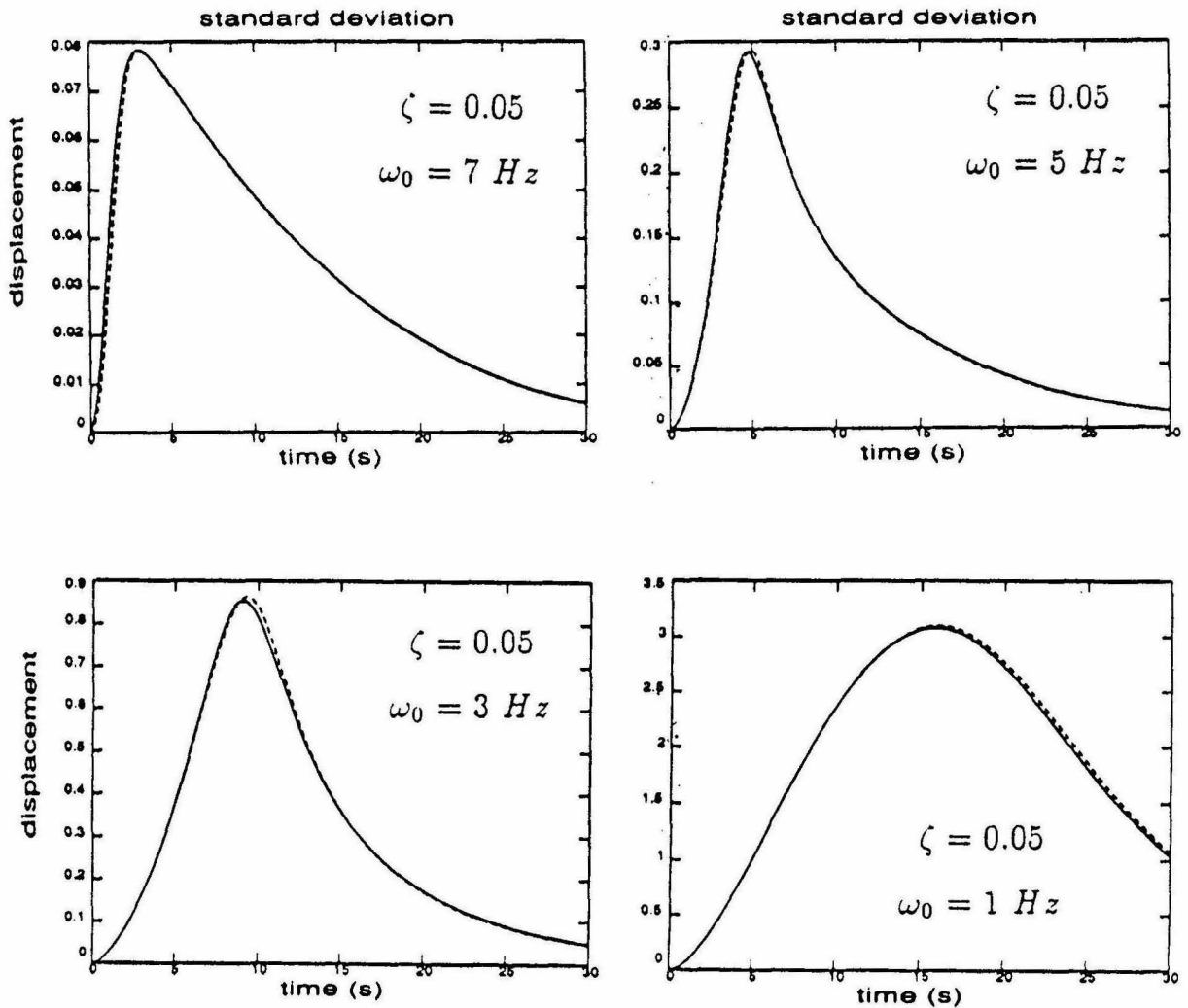


Figure 4.8. Comparison between the exact (solid curve) and approximate (dashed curve) mean-square displacement response of a linear SDOF oscillator with 5% damping and  $\omega_0 = 7, 5, 3, 1 \text{ Hz}$ . The excitation is the nine-parameter model shown in Figure 4.7.

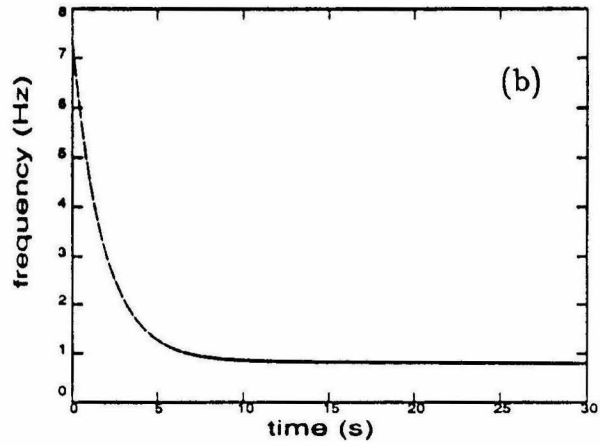
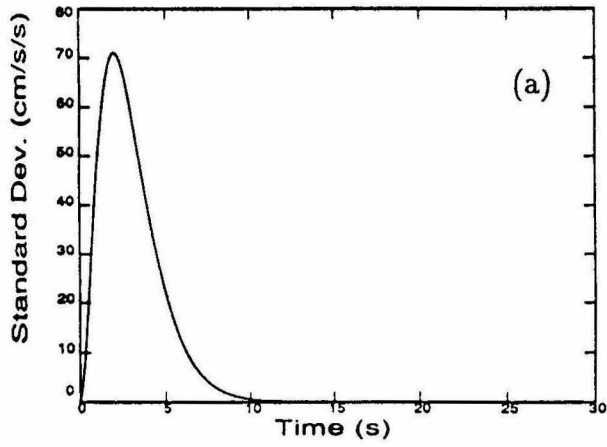


Figure 4.9. Artificially designed time variation of the standard deviation and the damped-frequency of the nine-parameter excitation model.

### LINEAR RESPONSE

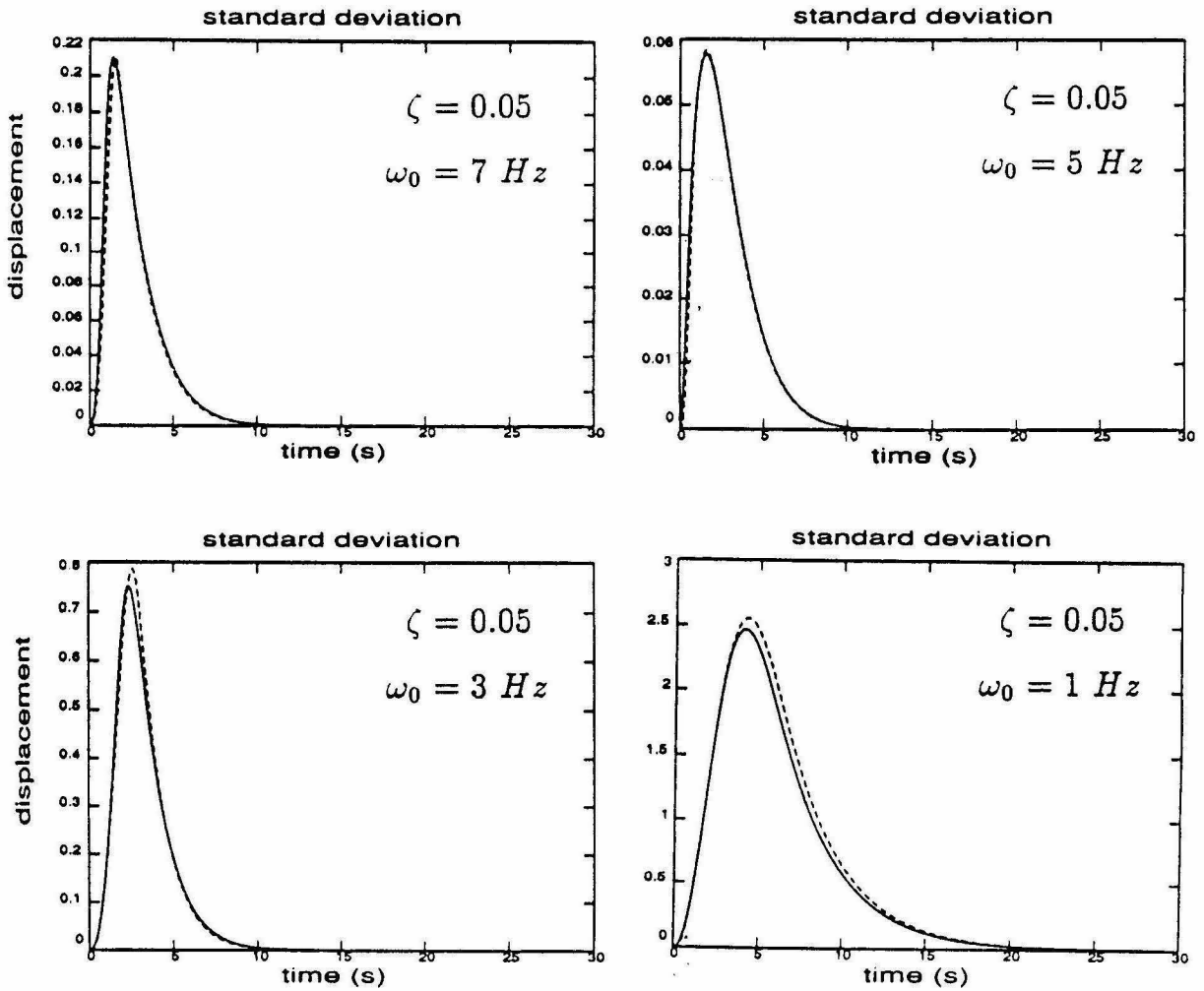


Figure 4.10. Comparison between the exact (solid curve) and approximate (dashed curve) mean-square displacement response of a linear SDOF oscillator with 5% damping and  $\omega_0 = 7, 5, 3, 1$  Hz. The excitation is the nine-parameter model shown in Figure 4.9.

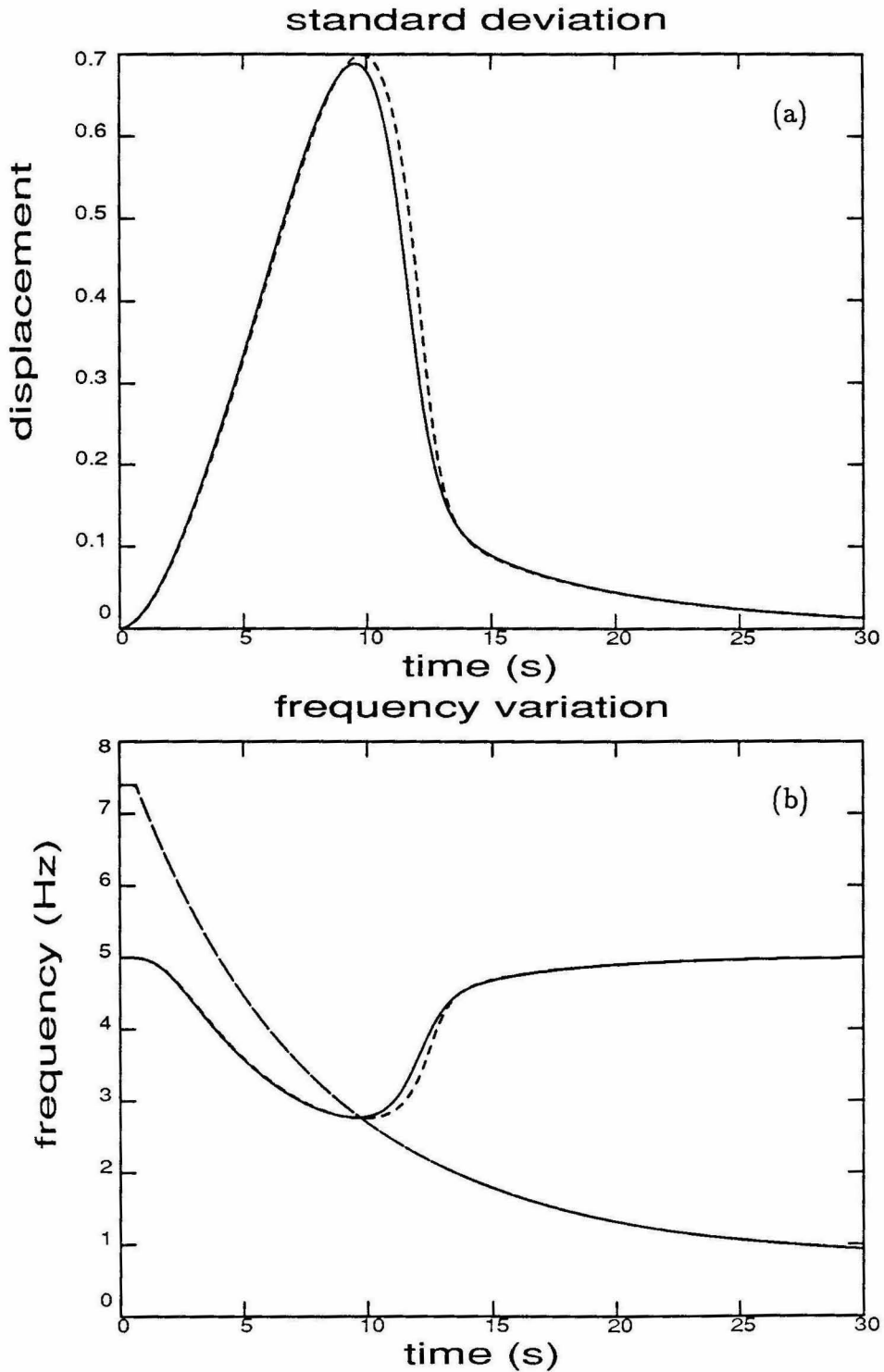


Figure 4.11. Comparison between the exact (solid curve) and approximate (dashed-curve) response of an equivalent linear SDOF oscillator. (a) STD of the response (b) structural frequency  $\omega(t)$ .  $\omega_0 = 5\text{Hz}$ ,  $\zeta_0 = 0.05$ . The excitation is the nine-parameter model shown in Figure 4.7 whose damped frequency variation is repeated again in (b).

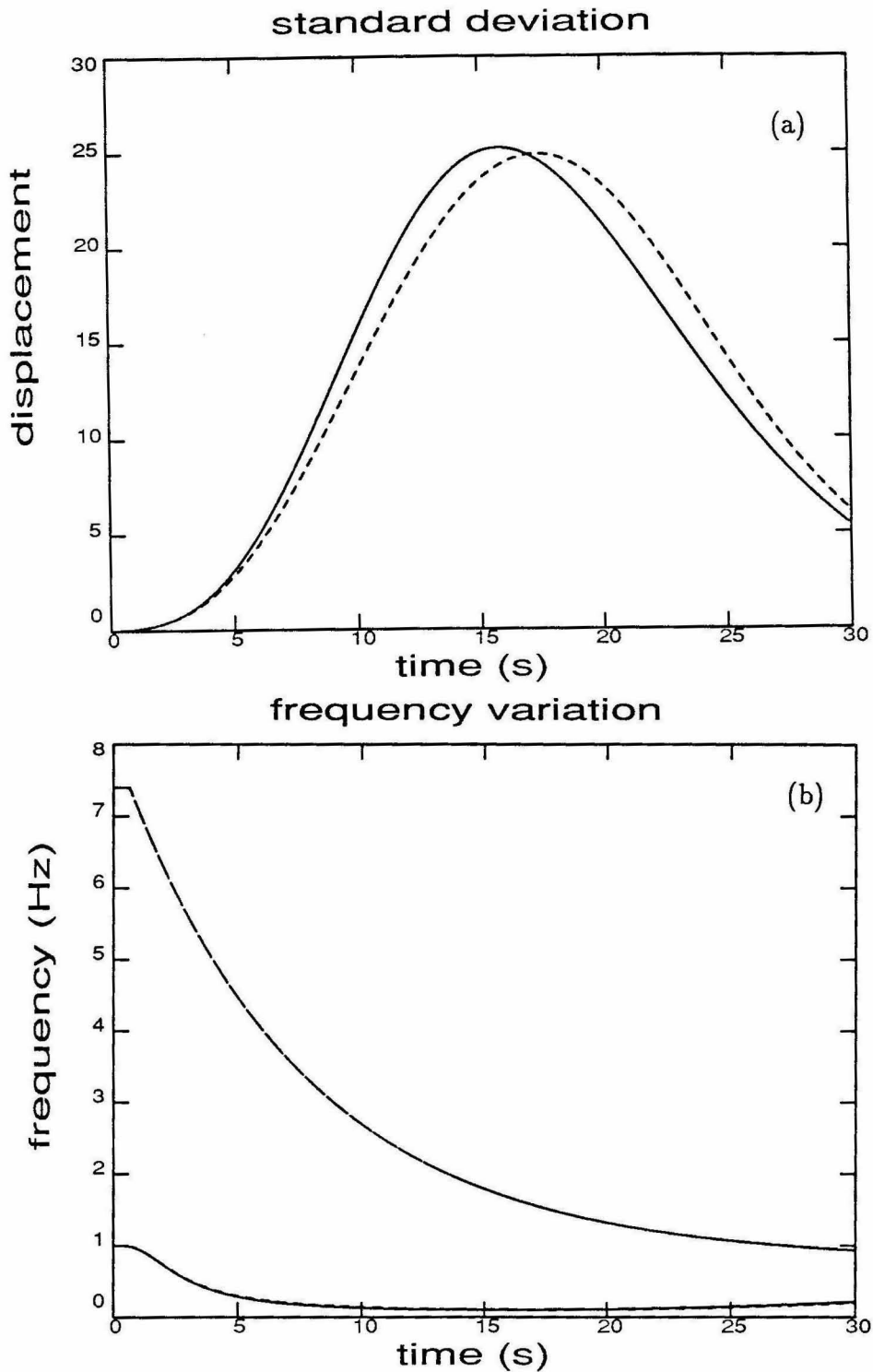


Figure 4.12. Comparison between the exact (solid curve) and approximate (dashed-curve) response of an equivalent linear SDOF oscillator. (a) STD of the response (b) structural frequency  $\omega(t)$ .  $\omega_0 = 1\text{Hz}$ ,  $\zeta_0 = 0.05$ . The excitation is the nine-parameter model shown in Figure 4.7 whose damped frequency variation is repeated again in (b).

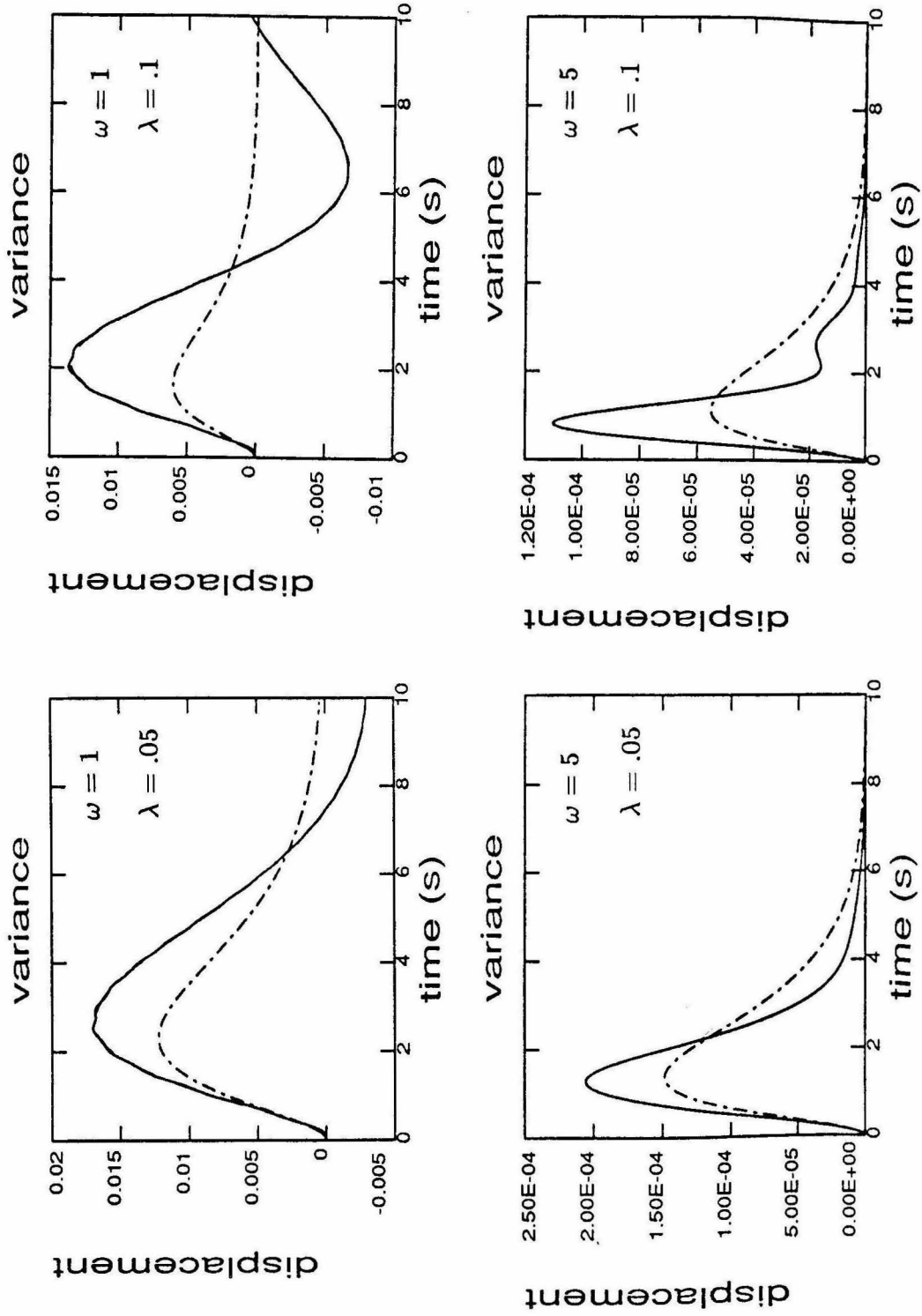


Figure 4.13. Comparisons between the exact (solid curve), the proposed approximate (dashed curve), and Bucher's approximate (dashed-dotted curve) solution for the covariance response of two modes  $i$  and  $j$ .  $\beta = 0.5, \zeta = 0.02$ .

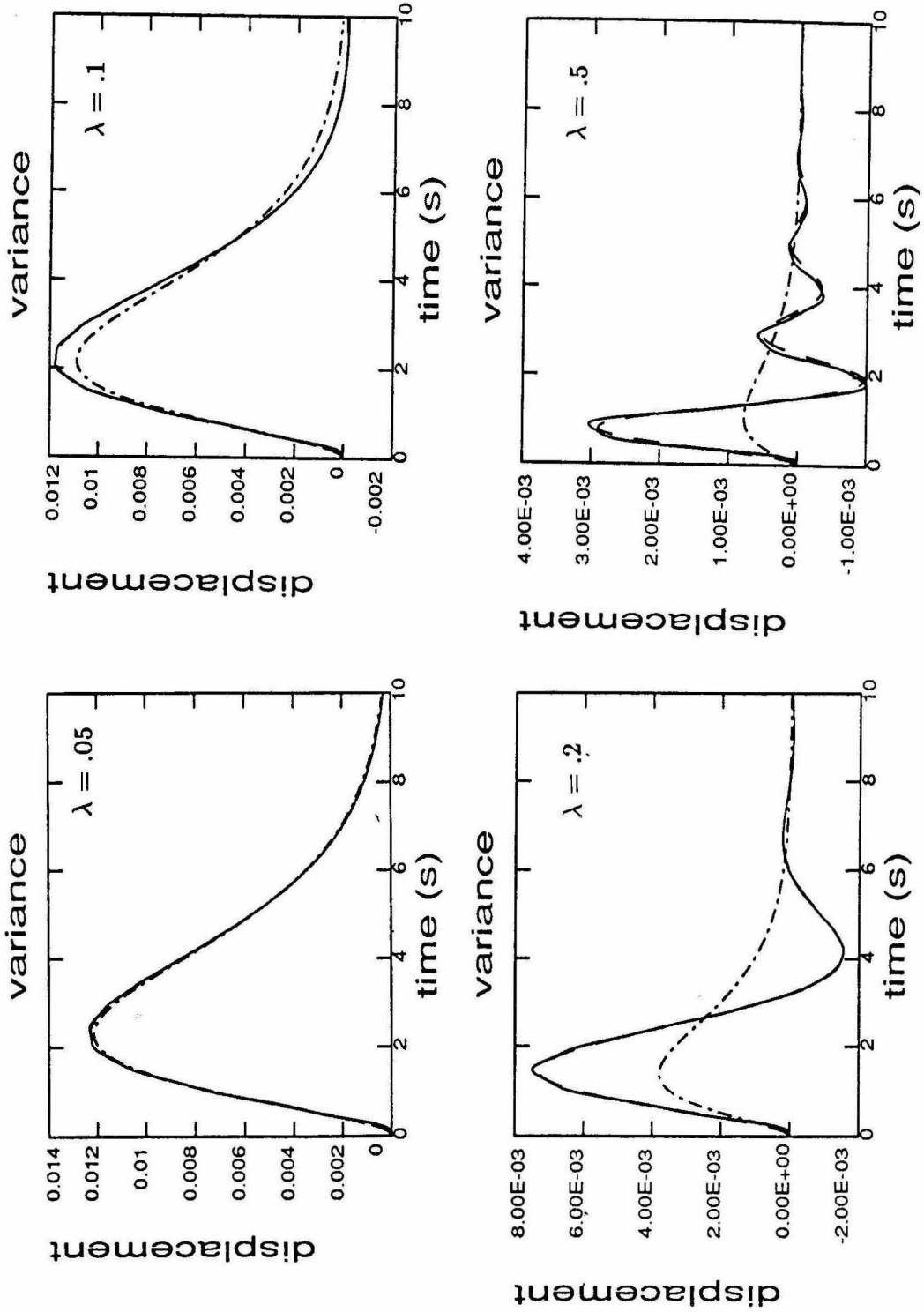


Figure 4.14. Comparisons between the exact (solid curve), the proposed approximate (dashed curve), and Bucher's approximate (dashed-dotted curve) solution for the covariance response of two modes  $i$  and  $j$ .  $\beta = 0.5$ ,  $\zeta = 0.05$ ,  $\omega = 1\text{Hz}$ .

## Chapter 5

### Importance of Temporal Nonstationarity In the Frequency Content of Ground Motion for Linear and Nonlinear Structural Models

#### 5.1 Introduction

The two features which are clearly observed in real accelerograms are the changes of intensity and frequency content with time. Past models dealing with ground motion modeling, in order to simplify the random vibration analysis, have often neglected the change of the frequency content with time. This is also partly because it was difficult to incorporate this change in simple continuous ground motion models and identify it from earthquake records, and also partly because it was believed that it had no significant effect on linear structural response. Recently, several models have been developed to include the time variation of the frequency content since it is believed to be very important for inelastic response of structures.

Conte *et al.* (1989) used time-varying ARMA models to represent the change in the frequency content with time, and then they used simulations to study the variability of various inelastic structural response parameters. However, the sensitivity of the structural response parameters to the time-varying frequency content was not addressed in their study. Yeh and Wen (1989) proposed a continuous model to represent the time variation in the frequency content of the ground motion which is efficient to use in random vibration analysis. Using statistical linearization and Wen's hysteretic model, they studied the sensitivity of the response to the nonstationarity in the frequency content of the ground motion. In their work, various response parameters were compared for two types of nonstationary excitation. The first type is the uniformly modulated random process with time-variant intensity but time-invariant frequency content, while the second type is the amplitude and

frequency modulated random process with time-variant amplitude and frequency content. The frequency content of the uniformly modulated random process was chosen to approximately match the frequency content of the amplitude and frequency modulated random process during the high intensity excitation period.

Comparisons presented by Yeh and Wen (1989) show that the maximum of the standard deviation of the displacement, the energy dissipation and the ductility differ for the two types of excitations by a factor of two or more for low structural frequencies. No differences were found for high structural frequencies. The differences were attributed to the fact that the lengthening of the structural periods coincide with the change in the frequency content of the ground motion resulting to strong amplification of the response. However, it is not clear whether the differences in the various response parameters computed by Yeh and Wen are due to their explanation or due to the significant differences of the excitation processes in the lower intensity excitation periods.

Further analyses are needed to study in detail the importance of the temporal nonstationarity in the frequency content of the ground motion and to demonstrate convincingly that the lengthening of the structural period may sometimes track the time variation of the dominant frequency of the ground motion. In Chapter 3, a simple and yet general model was used to incorporate a realistic time variation of the amplitude and frequency content of the ground motion. In Chapter 4, the ground motion model was used in conjunction with a simplified approximate method to calculate efficiently the mean-square response of linear and equivalent linear SDOF oscillators. It is the purpose of this chapter to use the simple formulation developed previously for the mean-square response to provide insight into the effect of the time-varying frequency content on the response of both linear and nonlinear structures.

## 5.2 Description of Earthquake Ground Motions

For the purpose of this study, two types of excitation are used to model the same ground acceleration time history. Both excitations model the amplitude nonstationarity of the ground motion and they differ only in the way they model the frequency content of the ground motion. The first excitation, denoted by (TV), has

time-varying frequency content, while the second excitation, denoted by (TI), has time-invariant frequency content throughout the duration of the excitation. The (TV) excitation is generated by the nine-parameter ground motion model proposed in Chapter 3. The (TI) excitation is generated by the time-invariant frequency content model proposed in Chapter 2.

The parameter of the (TV) and (TI) model are estimated as described in Chapters 2 and 3 using the Orion Blvd. accelerogram in Figure 2.1(a). The frequency content of the (TI) model is chosen to fit the frequency content of the segment of the accelerogram with the stronger intensity, that is, from 2 to 12 seconds. Therefore, the frequency content of the (TI) model is about the same as the frequency content of the (TV) model during the high intensity of the S-wave groups of the ground motion. The time variation of the standard deviation is the same for both models and it is plotted in Figure 5.1(a). The time variation of the damped frequency  $\omega'_g$  of both ground motion models is plotted in Figure 5.1(b). The damped frequency  $\omega'_g$  is an approximate measure of the predominant frequency present in the ground motion at time  $t$ .

### 5.3 Linear SDOF Structural Model

From the results in Chapter 4, the characteristics of the mean-square displacement of the response of a linear structure can be obtained approximately by examining the first-order differential equation

$$\dot{q}_{11}(t) + 2\zeta\omega_0 q_{11}(t) = \frac{q_g(t)}{2\omega_0^2} R_g(\omega_0, \zeta\omega_0, \omega_g(t), \alpha_g(t)) \quad (5.1)$$

where  $\omega_0$  is the structural frequency,  $\zeta$  is the damping ratio, and  $q_g(t)$  is the mean-square acceleration of the excitation measuring the time variation of the intensity of the ground motion. The form of  $R_g(\omega_0, \zeta\omega_0, \omega_g(t), \alpha_g(t))$  depends on the structure of the normalized evolutionary power spectral density (EPSD) of the ground acceleration defined by

$$S_N(\omega, \omega_g(t), \alpha_g(t)) = \frac{S(\omega, \omega_g(t), \alpha_g(t))}{q_g(t)}$$

where  $S(\omega, \omega_g(t), \alpha_g(t))$  is the EPSD of the ground motion model. As  $\zeta \rightarrow 0$ ,

$$R_g(\omega_0, \zeta\omega_0, \omega_g(t), \alpha_g(t)) \rightarrow S_N(\omega_0, \omega_g(t), \alpha_g(t)).$$

The characteristics of the mean-square displacement of the response depend on the characteristics of the forcing term in the right hand side of (5.1). The contribution of the time variation of the intensity of the ground motion to the response is directly controlled by  $q_g(t)$ . The contribution of the time variation of the frequency content of the ground motion is controlled by the form of  $R_g(\omega_0, \zeta\omega_0, \omega_g(t), \alpha_g(t))$  independently from the amplitude. It is evident that both the amplitude and the frequency content nonstationarity control the shape and the intensity of the forcing term in (5.1). Consider the case of lightly-damped oscillators and for ground motion with constant frequency content, that is, constant normalized PSD function, then the shape of the forcing term is controlled only by the amplitude nonstationarity  $q_g(t)$  of the ground motion while the normalized PSD computed at the oscillator frequency  $\omega_0$  remains constant throughout the shaking. However, when the time-varying frequency content is included, the spectral component of the ground motion computed at the oscillator frequency  $\omega_0$  varies with time, altering the shape of the forcing term in (5.1). Therefore, the characteristics of the response in the time-varying case are expected to be different from those in the time-invariant one.

To demonstrate the importance of the time variation of the frequency content of the ground motion, we compute and compare the mean-square displacement of the response for the two types of excitations shown in Figure 5.1. The maximum of the standard deviation (STD) of the response, the corresponding time that the maximum occurs and the duration of the STD of the response are computed for oscillator frequencies ranging from 1 to 8Hz. Comparisons are shown in Figure 5.2 for the two types of excitation. The response quantities considered in these figures are both the displacement and the absolute acceleration. The duration is defined herein as the difference between the two times that the STD of the response upcrosses and downcrosses 50% of its maximum value. The maximum response, the time of the maximum response, and the duration of the response approximately describe the shape of the nonstationary response. The complete time histories of the STD of the displacement response are plotted in Figures 5.3(a), 5.4(a), and 5.5(a) for three representative cases corresponding to  $\omega_0 = 1.5\text{Hz}$ ,  $3.2\text{Hz}$ , and  $6\text{Hz}$ , respectively. The structural frequency  $\omega_0 = 3.2\text{Hz}$  was chosen to be very close to the predominant frequency  $\omega'_g$  of the (TI) ground motion model. Figures 5.3(b), 5.4(b), 5.5(b), show

the time variation of the corresponding structural frequency  $\omega_0$ . For comparison purposes, each figure includes the time variation of the dominant frequencies  $\omega'_g(t)$  (dashed curves) of each ground motion model. The solid curves in these figures correspond to the (TV) model while the dashed-dotted curves correspond to the (TI) model. All numerical results correspond to 5% damping ratio.

For the (TI) excitation, the time variation of the forcing term in (5.1) remains the same regardless of the values of the oscillator parameters  $\omega_0$  and  $\zeta$  which control only the intensity of the forcing term. Therefore, the resulting shape for the r.m.s. of the response is controlled mainly by the product  $\zeta\omega_0$ . The time of the maximum and the duration of the STD of the response shown by the dashed-dotted lines in Figure 5.2 demonstrate numerically that the shape of the nonstationary STD of the response does not vary significantly over the oscillator frequencies examined. For the (TV) excitation, however, the shape of the forcing term in (5.1) is significantly altered depending on the values of the oscillator parameters  $\omega_0$  and  $\zeta_0$ . The resulting shape of the STD of the response in Figure 5.2 is therefore expected to be different for different values of  $\omega_0$ . The solid lines in Figure 5.2 corresponding to the time of the maximum and the duration of the STD of the response demonstrate the dependence of the response characteristics on the oscillator frequency  $\omega_0$ . From Figure 5.2, and from Figures 5.3(a), 5.4(a) and 5.5(a), it is concluded that the maximum responses as well as the duration of the responses corresponding to the (TI) and the (TV) excitations may differ by a factor of 2 or higher.

From Figures 5.3, 5.4 and 5.5, it is evident that the time that the STD response achieves its maximum is controlled approximately by the time the predominant frequency curve  $\omega_g(t)$  of the ground motion crosses the oscillator frequency curve. This phenomenon, which will be referred to as the resonance effect, considerably amplifies the response only when the dominant frequency of the ground motion approximately coincides with the oscillator frequency. Because of the time variation in the frequency content of the ground motion, the duration of the resonance effect is small compared to the duration of the excitation. For the (TI) excitation, however, once the oscillator and the excitation are in resonance, they continue to be throughout the duration of the excitation. Despite this, the (TV) excitation still

gives a slightly larger maximum STD even when the oscillator frequency and the (TI) excitation frequency coincide, as shown in Figure 5.4.

Concluding, the time variation in the frequency content of the ground motion significantly affects the characteristics of the linear response. Ground motion models should therefore take into account the temporal nonstationarity in the frequency content of the ground motion whenever the response of linear structures is to be studied.

## 5.4 Nonlinear SDOF Structural Model

A simple nonlinear structural model of softening type is used to obtain an insight into the effect of the temporal nonstationarity in the frequency content of the ground motion on nonlinear response. The simplified equation obtained in Chapter 4 for the mean-square response of the equivalent linear systems is used to mathematically analyze this effect. In addition, the amplification of the response due to the “moving resonance” effect is mathematically modeled and is numerically demonstrated using realistic ground motion models.

### 5.4.1 Force-Deflection Relation

The nonlinearity of the oscillator is modeled by a nonlinear elastic softening restoring force. The force-deflection relation is shown in Figure 5.6 and it is similar to the backbone curve of a yielding system in that the stiffness decreases as the displacement increases. The mathematical relation is

$$\begin{aligned} R(t) &= \frac{2}{\pi} R_u \tan^{-1} \left( \frac{\pi K_0 x}{2 R_u} \right) \\ &= \frac{2}{\pi} K_0 x_y \tan^{-1} \left( \frac{\pi x}{2 x_y} \right) \end{aligned} \tag{5.2}$$

where  $R_u$  and  $K_0$  is the ultimate strength and the initial stiffness of the system, respectively. The quantity  $x_y = R_u/K_0$  is similar to the elastic limit displacement of a yielding system and is called the nominal yield displacement. The quantity  $\mu = x/x_y$  is similar to the ductility ratio of a yielding system. The ductility ratio  $\mu$  measures the nonlinearity of the system and it varies from 0 (linear oscillator) to

$\infty$ .

Inelastic behavior is not modeled by the nonlinear relation since for an inelastic system which is loaded beyond some point, the unloading path differs from the loading path. However, the nonlinear elastic model (5.2) is useful to assess and demonstrate the effect of the temporal nonstationarity in the frequency content of the ground motion on the response of nonlinear structures of softening type.

#### 5.4.2 Equation of Motion Using the Equivalent Linearization Method

The response of the SDOF nonlinear oscillator to a ground excitation is governed by the equation of motion

$$\ddot{x}(t) + 2\zeta_0\omega_0\dot{x}(t) + \omega_0^2(t)\frac{R(t)}{K_0} = G(t) \quad (5.3)$$

where  $R(t)/K_0$  is given in (5.2),  $\omega_0$  is the initial (small-amplitude) structural frequency,  $\zeta_0$  is the viscous damping ratio, and  $G(t)$  is taken to be a zero-mean Gaussian stochastic process. For the complicated restoring force (5.2) and for the ground excitation considered in this study, an exact solution for the response statistics is not available. The equivalent linearization method is used to obtain approximate response statistics. The method of equivalent linearization was first introduced independently by Booton (1954) and Caughey (1963), and later it was generalized by Iwan and Yang (1971), and Atalik and Utku (1976). Iwan and Mason (1980) extended the method to general nonstationary response.

According to the equivalent linearization method, the nonlinear equation (5.3) is replaced by the equivalent linear one

$$\ddot{x}(t) + 2\zeta(t)\omega(t)\dot{x}(t) + \omega^2(t)x(t) = G(t) \quad (5.4)$$

The equivalent linear parameters  $\omega(t)$  and  $\zeta(t)$  are obtained by minimizing the mean-square of the error that arises in estimating the nonlinear system by a linear one. This error is defined by the difference between the nonlinear and the linear equation. Comparisons with numerical simulations suggest that the method approximates the nonlinear response well.

It turns out that for the restoring force (5.2), the equivalent linear parameters are given by (Jeong, 1985)

$$\omega(t) = \omega(q_{11}(t)) = \omega_0 [\sqrt{\pi} \gamma \exp(\gamma^2) \operatorname{erfc}(\gamma)]^{\frac{1}{2}} \quad (5.5)$$

$$\alpha(t) = \alpha(q_{11}(t)) = \zeta(t)\omega(t) = \zeta_0\omega_0 \quad (5.6)$$

where

$$\gamma = \frac{\sqrt{2}}{\pi} \frac{x_y}{\sqrt{q_{11}(t)}} \quad (5.7)$$

Therefore, the equivalent linear parameters depend only on the mean-square displacement of the response. Similarly, the standard deviation of the ductility ratio is

$$STD(\mu(t)) = \frac{\sqrt{q_{11}(t)}}{x_y} \quad (5.8)$$

and depends only on  $q_{11}(t)$ . The response of the equivalent linear system (5.4) depends on the viscous damping  $\zeta_0$ , initial structural frequency  $\omega_0$ , and the nominal yield displacement  $x_y$ .

### 5.4.3 Characteristics of the Mean-Square Response; Moving Resonance Effect

Substituting the expression (4.108) into the equation (4.75) and using expressions (5.5) and (5.6), the characteristics of the mean-square displacement of the response of the equivalent linear oscillator (5.4) are obtained approximately by examining the simple first-order differential equation

$$\dot{q}_{11}(t) + 2[\zeta_0\omega_0 + \delta(q_{11}(t))]q_{11}(t) = \frac{q_g(t)}{2\omega^2(q_{11}(t))} R_g(\omega(q_{11}(t)), \zeta_0\omega_0, \omega_g(t), \alpha_g(t)) \quad (5.9)$$

where  $\omega_0$  is the initial structural frequency,  $\zeta_0$  is the initial damping ratio, and  $q_g(t)$  is the mean-square acceleration of the excitation measuring the time variation of the intensity of the ground motion. The form of  $R_g(\omega(q_{11}(t)), \zeta_0\omega_0, \omega_g(t), \alpha_g(t))$  depends on the structure of the normalized power spectral density of the ground acceleration.

Several factors affect the mean-square displacement of the response of simple nonlinear oscillators. The time variation of the intensity  $q_g(t)$  of the ground variation is one factor that controls the forcing term in equation (5.9). The degree of

nonlinearity of the oscillator described by the ductility ratio  $\mu$  is another factor to affect the response. For the softening force-deflection relation (5.2) and for a fixed ductility ratio  $\mu$ , the instantaneous equivalent frequency  $\omega(q_{11}(t))$  decreases with increasing  $q_{11}(t)$ . The forcing term in (5.9) is amplified for softening systems due to the presence of  $\omega(q_{11}(t))$  in the denominator.

Next, consider for simplicity lightly damped oscillators. As  $\zeta(t) \rightarrow 0$ ,

$$R_g(\omega(q_{11}(t)), \zeta_0 \omega_0, \omega_g(t), \alpha_g(t)) \rightarrow S_N(\omega(q_{11}(t)), \omega_g(t), \alpha_g(t)), \quad (5.10)$$

the normalized evolutionary power spectral density of the ground motion model. The time variation of the value of the EPSD computed at the instantaneous equivalent frequency of the oscillator also affects the response by increasing it or decreasing it, depending on the shape and the time variation of the normalized EPSD. As an example, the normalized EPSD corresponding to the Orion Blvd. recording is shown in Figure 5.7. It is clear that the predominant frequencies of the ground motion shifts to the lower frequencies with increasing time. This is often the case expected in earthquake ground motions. It may happen that the decrease of the structural frequency of the softening structure tracks the decrease of the predominant frequency of the ground motion resulting in significant amplification of the response. This “locking” of the structural frequency with the predominant frequency of the ground motion will be referred to as the “moving resonance” effect. If the condition that the oscillator is lightly damped is removed, then similar arguments hold by considering the function  $R_g(\omega(q_{11}(t)), \zeta_0 \omega_0, \omega_g(t), \alpha_g(t))$  instead of the normalized EPSD function  $S_N(\omega(q_{11}(t)), \omega_g(t), \alpha_g(t))$ .

The moving resonance effect for the (TI) excitation is less likely to occur. The reason is that as soon as the structural frequency coincides with the dominant frequency of the ground motion, the response is considerably amplified and the structure softens. The softening, which is reflected as a decrease of the structural frequency, moves the structure out of resonance with the ground motion.

Numerical results are next presented to illustrate the effects of the temporal nonstationarity in the frequency content on the response of the simple nonlinear structure. The responses corresponding to the (TI) and the (TV) excitations de-

scribed in Section 5.2 are compared. The normalized EPSD function for both excitations are plotted and compared in Figure 5.7. All numerical results correspond to 5% initial damping ratio. The maximum of the STD response, the corresponding time that the maximum occurs and the duration of the STD response are computed for oscillator initial frequencies ranging from 1 to 8Hz. The responses are compared in Figure 5.8 for the two types of excitation. The response quantities considered are both the displacement and the absolute acceleration. The solid curves correspond to the (TV) model while the dashed-dotted curves correspond to the (TI) model. It is evident from these plots that although both excitations model the same earthquake record, the characteristics of the response differ considerably. This is an indication that the change in the frequency content with time observed in ground motion is important to incorporate in the ground motion models.

In order to reveal in detail the characteristics of the response and their dependence on the ground motion model, representative nonlinear oscillators are used to compare the full time history of the response. The STD of the displacement responses corresponding to (TI) and (TV) excitations are compared in Figures 5.9(a), 5.10(a), 5.11(a) and 5.12(a). Each figure corresponds to different parameters of the nonlinear oscillator. The time variation of the corresponding equivalent structural frequencies  $\omega(q_{11}(t))$  computed by (5.5) are plotted in Figures 5.9(b), 5.10(b), 5.11(b) and 5.12(b). For comparison purposes, each figure also includes the time variation of the dominant frequency  $\omega'_g(t)$  of each ground motion model (dashed curves).

In Figure 5.9, the maximum STD response corresponding to the (TV) excitation differs from the maximum response corresponding to the (TI) excitation by a factor as high as three. For the (TI) excitation, the oscillator is behaving almost linearly since the equivalent frequency does not vary significantly. Recalling the case of linear oscillators in Figure 5.3(a), the responses were different only by a factor of two. The additional difference computed for the nonlinear oscillator is attributed to the moving resonance effect occurring for the (TV) excitation from approximately the first to the seventh second of the excitation, as seen in Figure 5.9(b) where the structural frequency tracks the changing predominant ground motion frequency

over this time period.

In Figure 5.10 the initial structural frequency is the same as that in 5.9 but the strength  $R_u$  of the structural model is lower. Both responses are nonlinear as indicated by the large changes in equivalent structural frequencies in the plots in Figure 5.10(b). The responses have approximately the same maximum value, but they differ in duration. The moving resonance effect is also demonstrated in Figure 5.10(b) for the (TV) excitation.

In Figures 5.11 and 5.12 the initial structural frequencies were chosen to be close to the dominant frequencies of the strong S-waves of the ground motion. In Figure 5.12(b) and for the (TI) excitation, the equivalent linear oscillator is never in resonance with the ground motion. Similarly, for the (TV) excitation, over the first 10 to 15 seconds of the highest ground intensity, the equivalent linear oscillator is not in resonance with the ground motion. However, at later times when the weaker surface waves of the ground motion are arriving, the equivalent linear oscillator resonates with the ground motion from approximately 15 to 22 seconds, causing an amplification of the response. Therefore, in this case, the maximum STD response is controlled primarily by surface waves rather than the S-waves. Modeling the ground motion by the (TI) excitation where the S-waves control the response results in an underestimation of the importance of the weaker intensity surface waves. Comparing the solid curves in Figures 5.11(a) and 5.12(a), it is clear that the resonance effect occurring at later times in Figure 5.12(b) causes a significant increase in the duration of the response. This large change in duration between structures with initial structural frequencies  $\omega_0 = 3$  and  $\omega_0 = 4Hz$  also shows up in Figure 5.8.

Concluding, the temporal nonstationarity in the frequency content of the ground motion has a significant effect on the response of nonlinear structures of softening type, especially when lengthening of the structural periods tracks the shifting of the dominant frequencies of the ground motion.

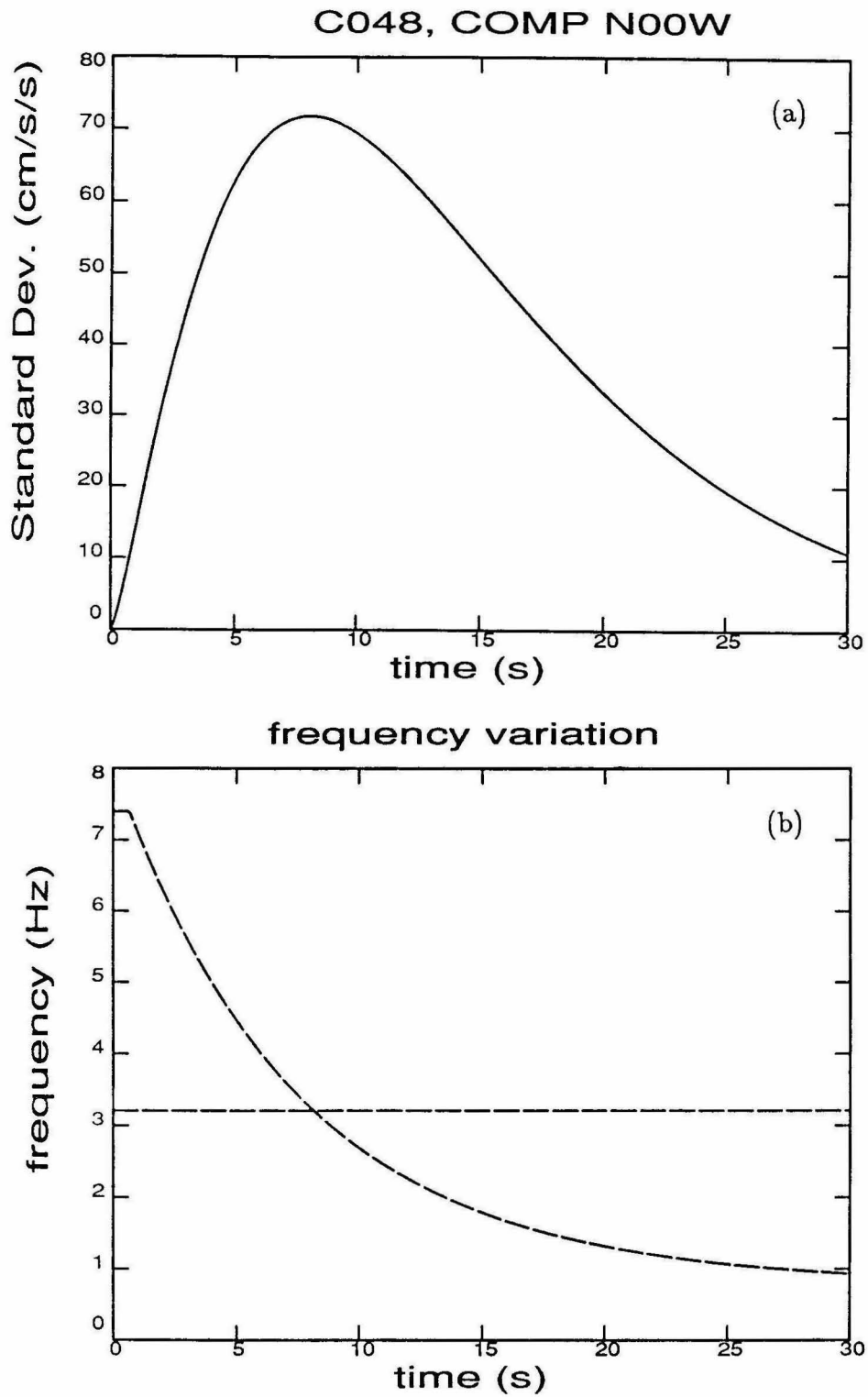


Figure 5.1. Time variation of (a) the standard deviation  $\sqrt{q_g(t)}$  and (b) the dominant frequency  $\omega'_g(t)$  for the (TV) and the (TI) excitation models fitted to the Orion Blvd. record shown in Figure 2.1(a).

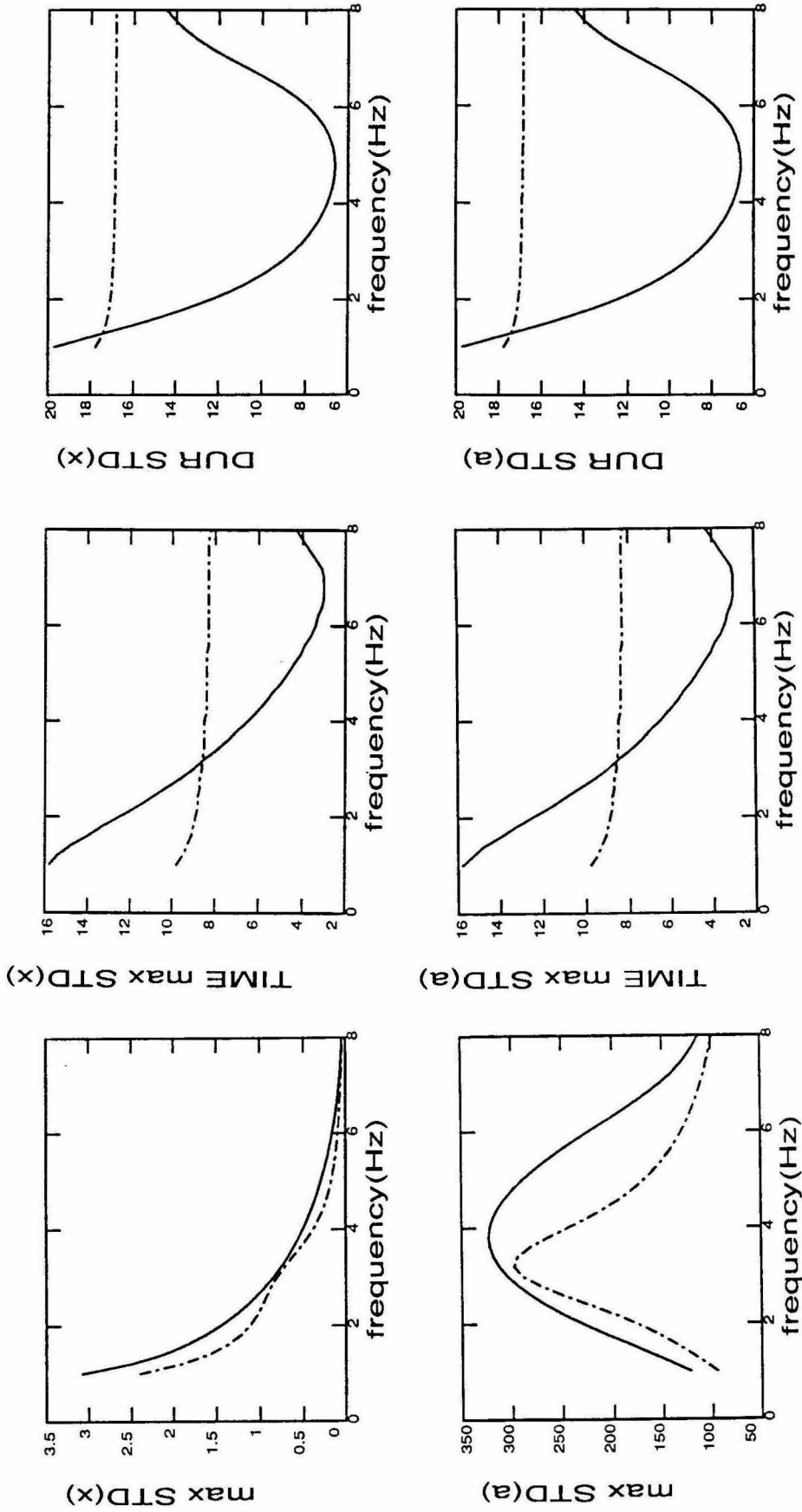


Figure 5.2. Nonstationary linear response characteristics computed for the (TV) (solid curves) and for the (TI) excitation (dashed-dotted curves) for varying structural frequencies  $\omega_0$ . Damping  $\zeta = 0.05$ .

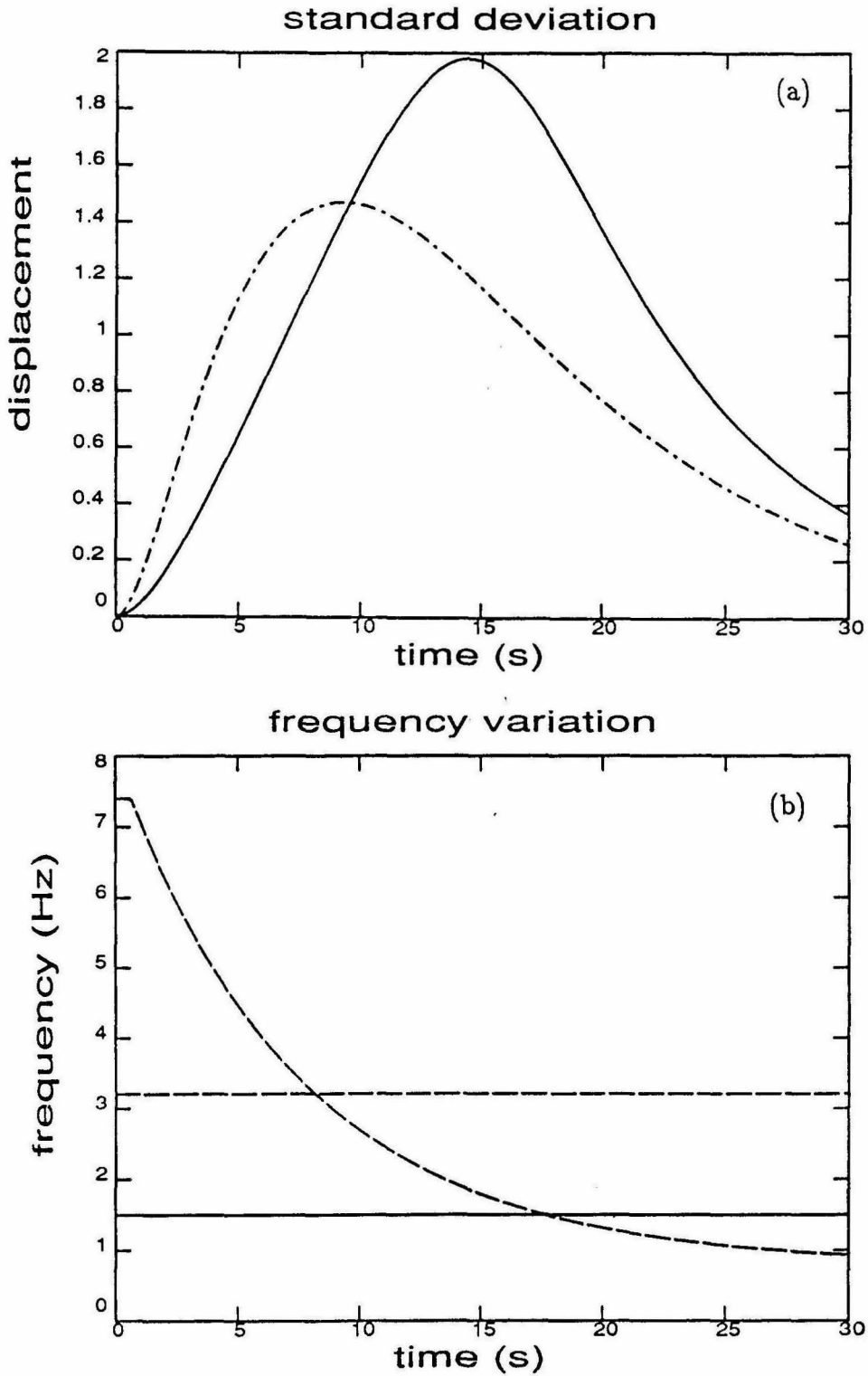


Figure 5.3. Comparison of (a) the r.m.s. displacement responses and (b) the equivalent linear structural frequencies, for the (TV) (solid curve) and (TI) (dashed-dotted curve) excitation.  $\omega_0 = 1.5\text{Hz}$ ,  $\zeta = 0.05$ . Dashed curves correspond to the damped frequencies  $\omega'_g$  of (TV) and (TI) excitations.

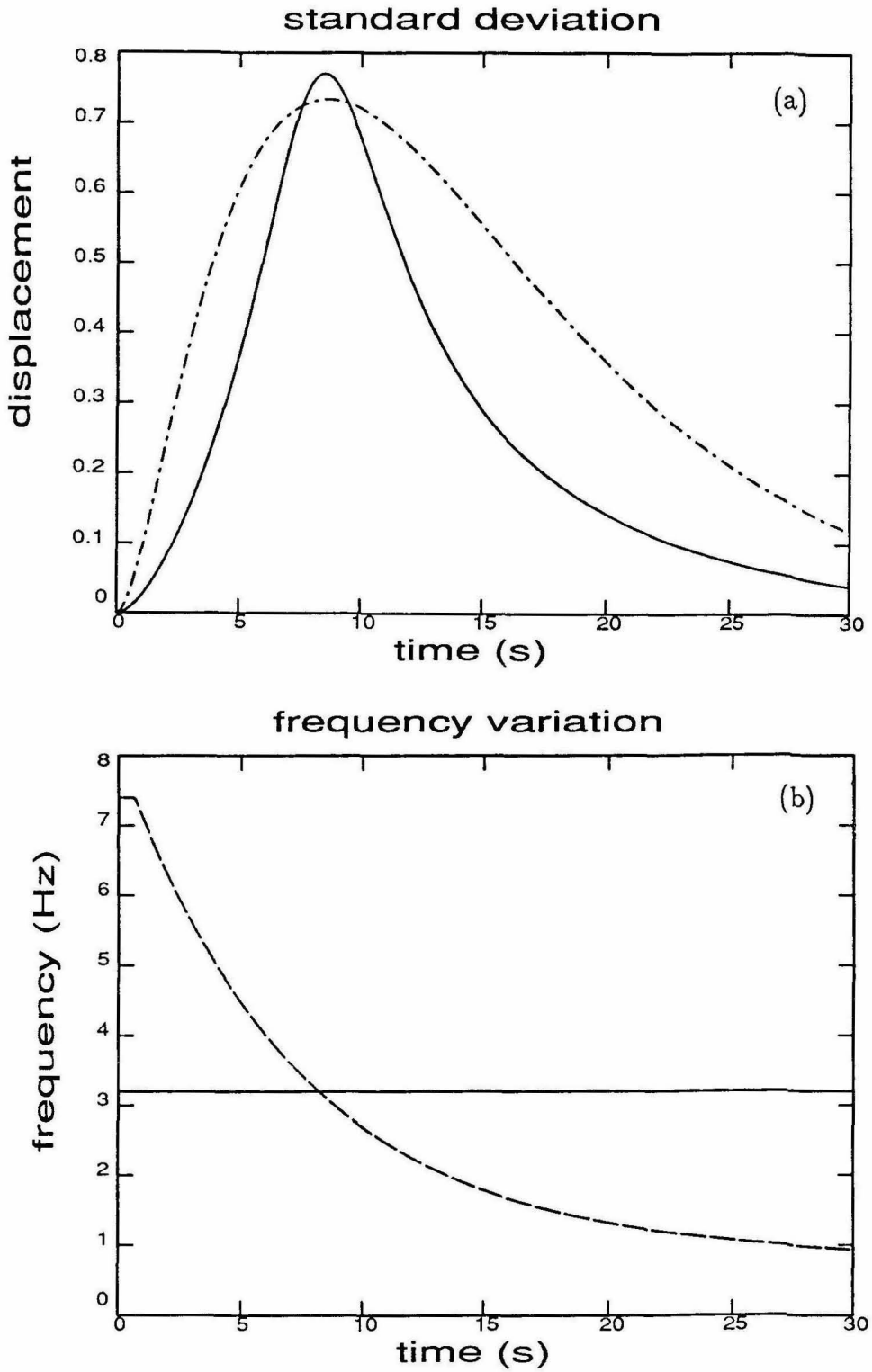


Figure 5.4. Comparison of (a) the r.m.s. displacement responses and (b) the equivalent linear structural frequencies, for the (TV) (solid curve) and (TI) (dashed-dotted curve) excitation.  $\omega_0 = 3.2$  Hz,  $\zeta = 0.05$ . Dashed curves correspond to the damped frequencies  $\omega'_g$  of (TV) and (TI) excitations.

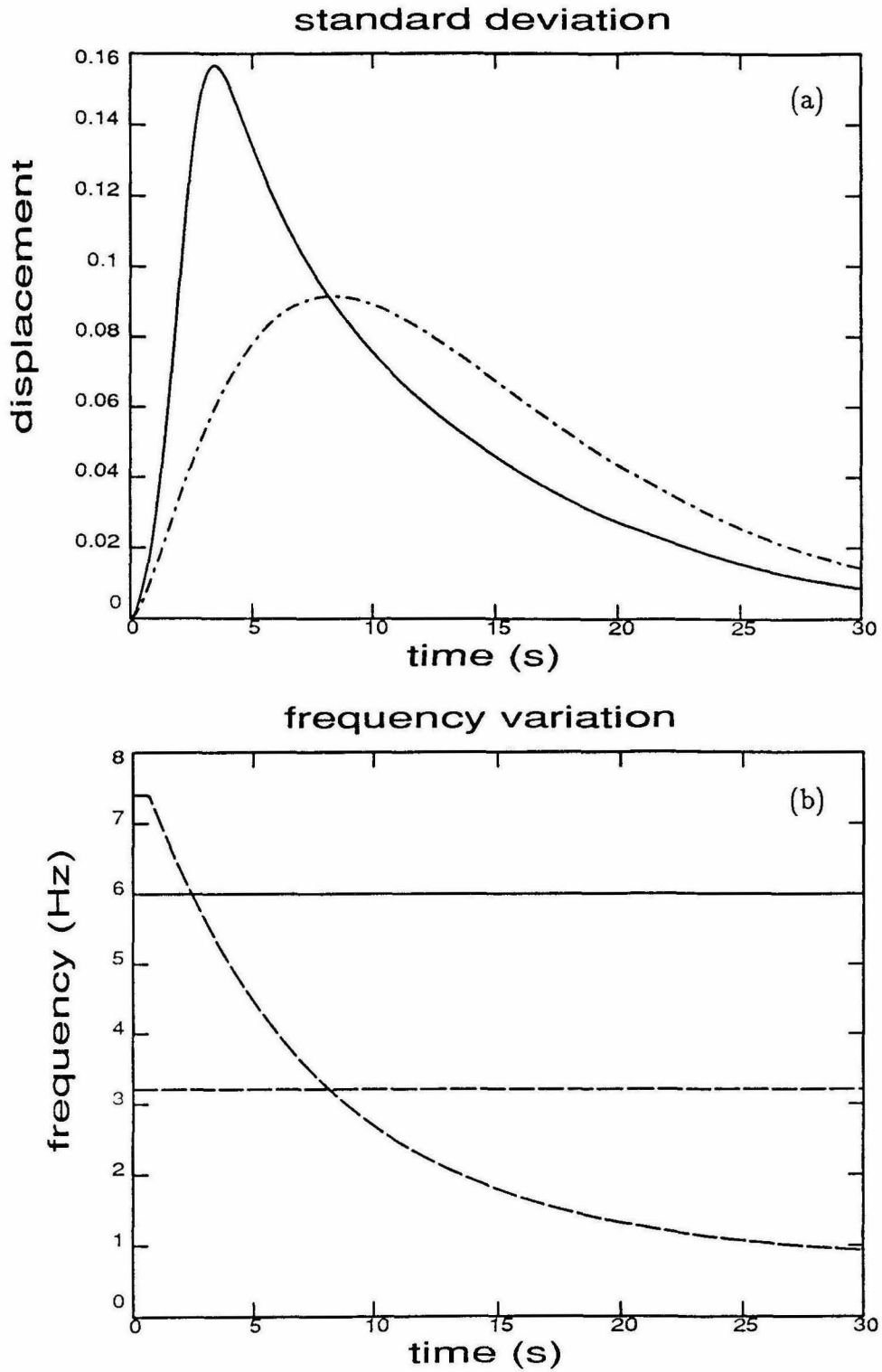


Figure 5.5. Comparison of (a) the r.m.s. displacement responses and (b) the equivalent linear structural frequencies, for the (TV) (solid curve) and (TI) (dashed-dotted curve) excitation.  $\omega_0 = 6\text{Hz}$ ,  $\zeta = 0.05$ . Dashed curves correspond to the damped frequencies  $\omega'_j$  of (TV) and (TI) excitations.

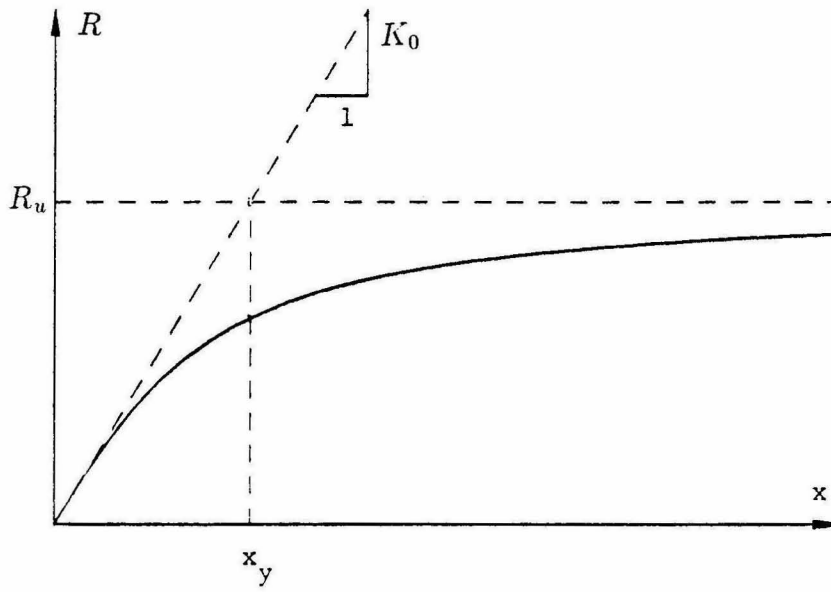


Figure 5.6. Softening elastic restoring force.

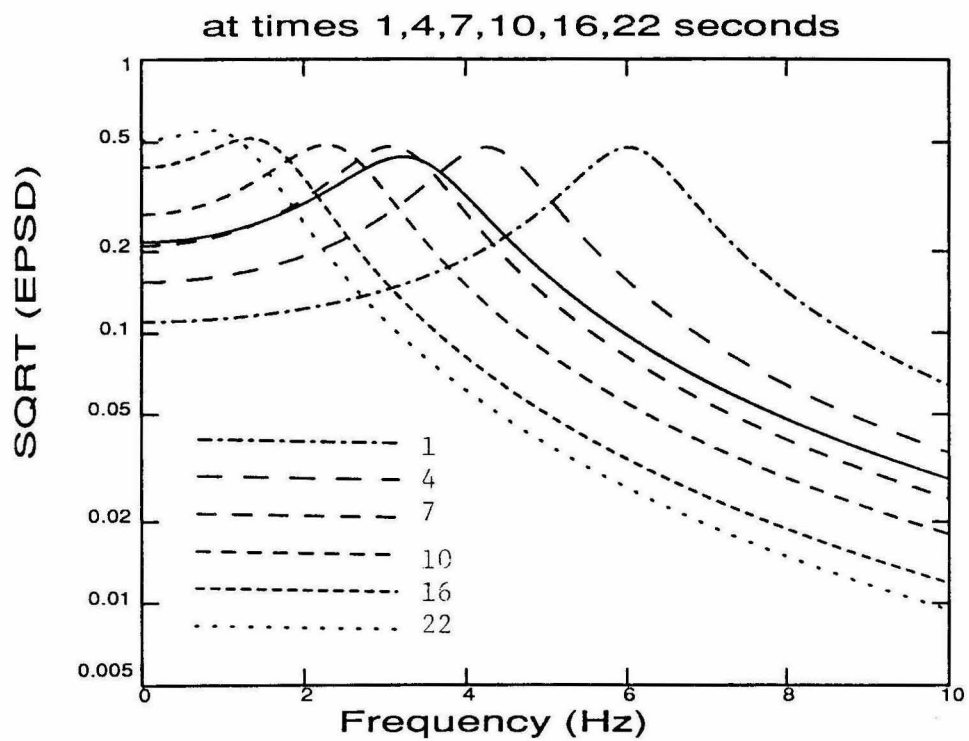


Figure 5.7. Comparison between the normalized EPSD functions computed by the (TV) (dashed curves) model at times 1, 4, 7, 10, 16, 22 seconds and the (TI) (solid curve) model for the Orion Blvd. recording.

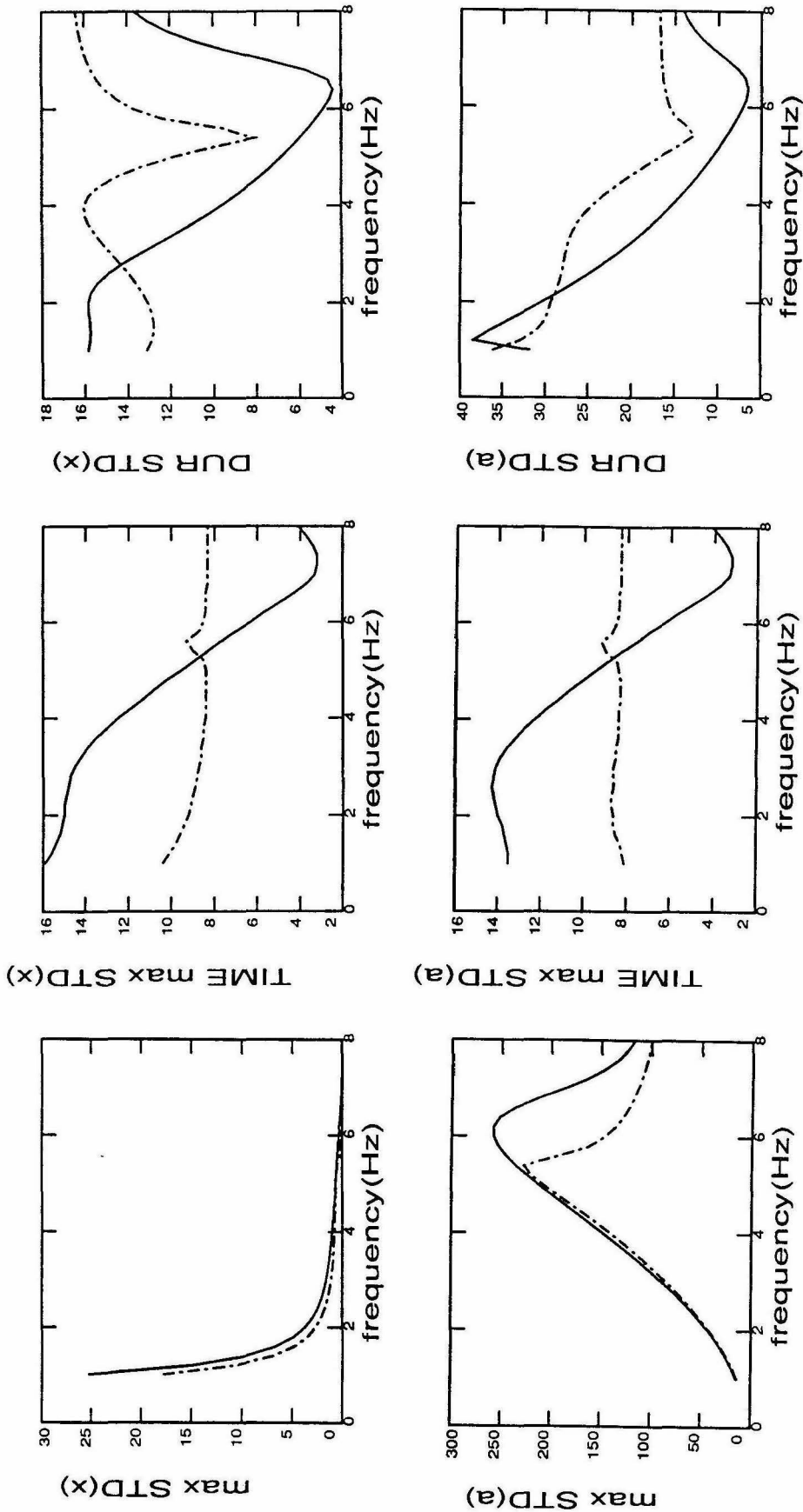


Figure 5.8. Nonstationary nonlinear response characteristics computed for the (TV) excitation (solid curves) and the (TI) (dashed-dotted curves) excitations for varying initial structural frequencies.  $\xi_0 = 0.05$ ,  $x_y = 1/3$ .

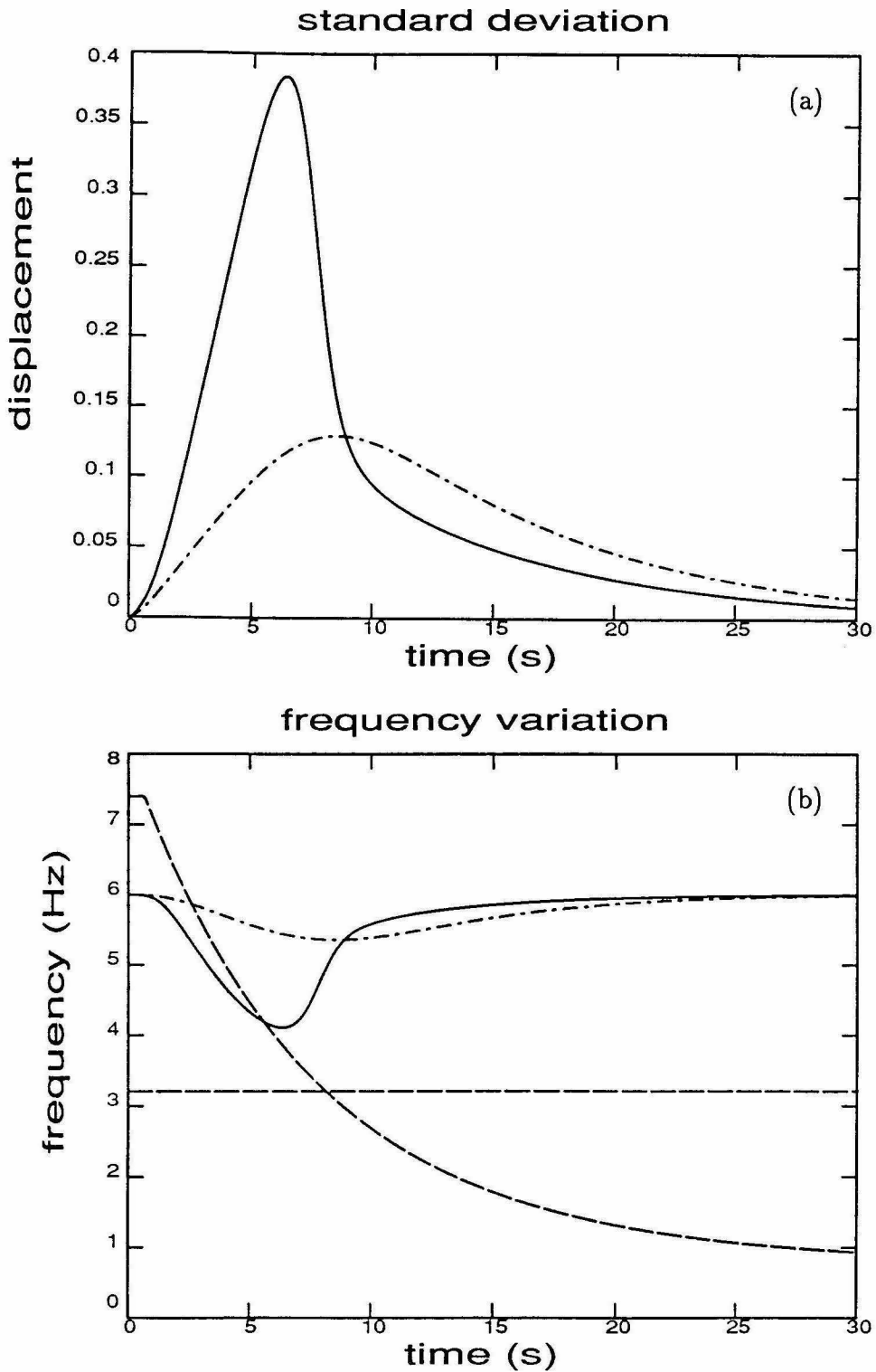


Figure 5.9. Comparison between the response characteristics computed for the (TV) (solid curves) and the (TI) (dashed-dotted curves) excitation. (a) r.m.s. displacement of the response (b) equivalent linear structural frequency.  $\omega_0 = 6\text{Hz}$ ,  $\zeta_0 = 0.05$ ,  $x_y = 1/3$ . Dashed curves correspond to the damped frequencies  $\omega'_g$  of (TV) and (TI) excitations.

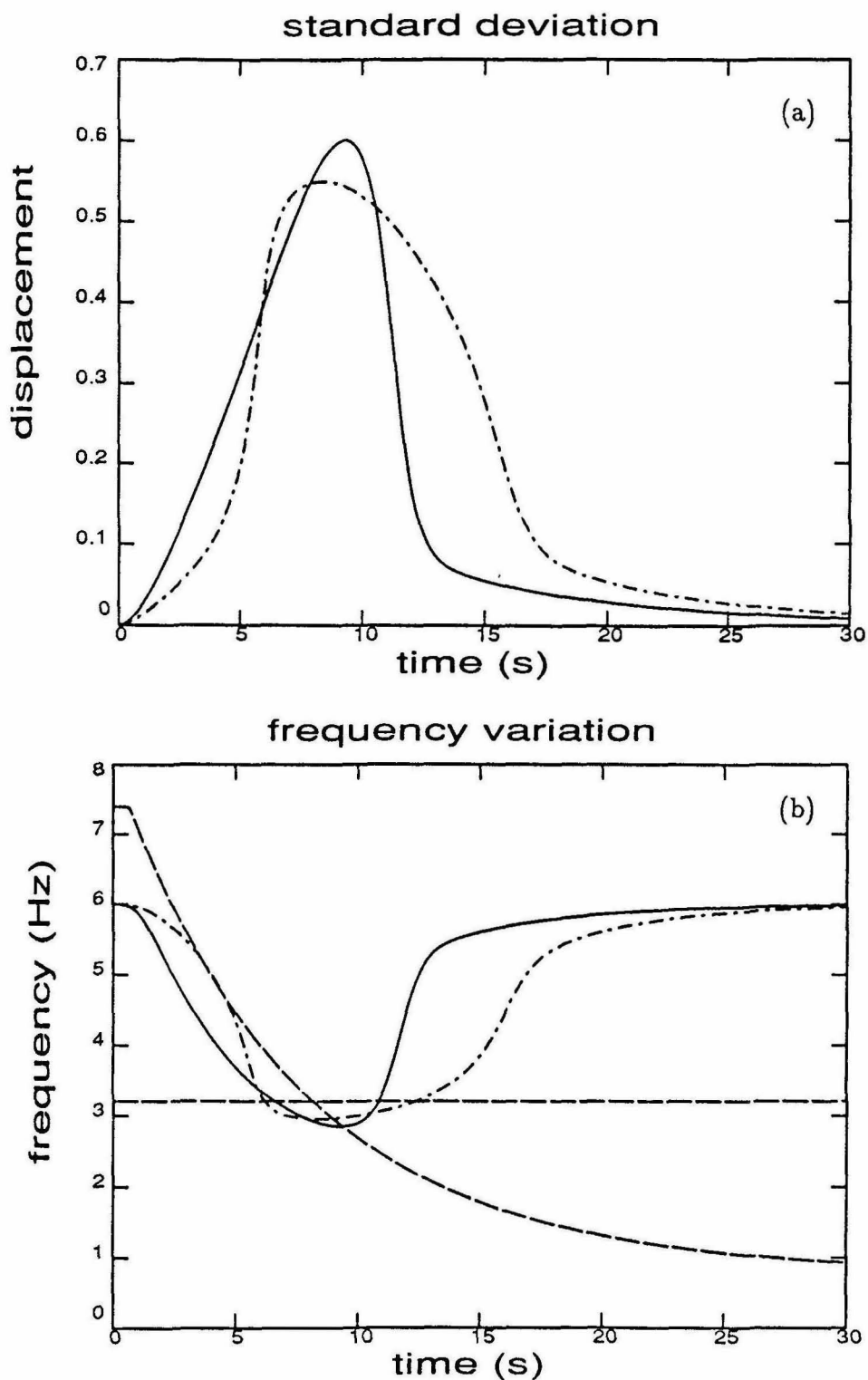


Figure 5.10. Comparison between the response characteristics computed for the (TV) (solid curves) and the (TI) (dashed-dotted curves) excitation. (a) r.m.s. displacement of the response (b) equivalent linear structural frequency.  $\omega_0 = 6\text{Hz}$ ,  $\zeta_0 = 0.05$ ,  $\alpha_y = 1/5$ . Dashed curves correspond to the damped frequencies  $\omega'_g$  of (TV) and (TI) excitations.

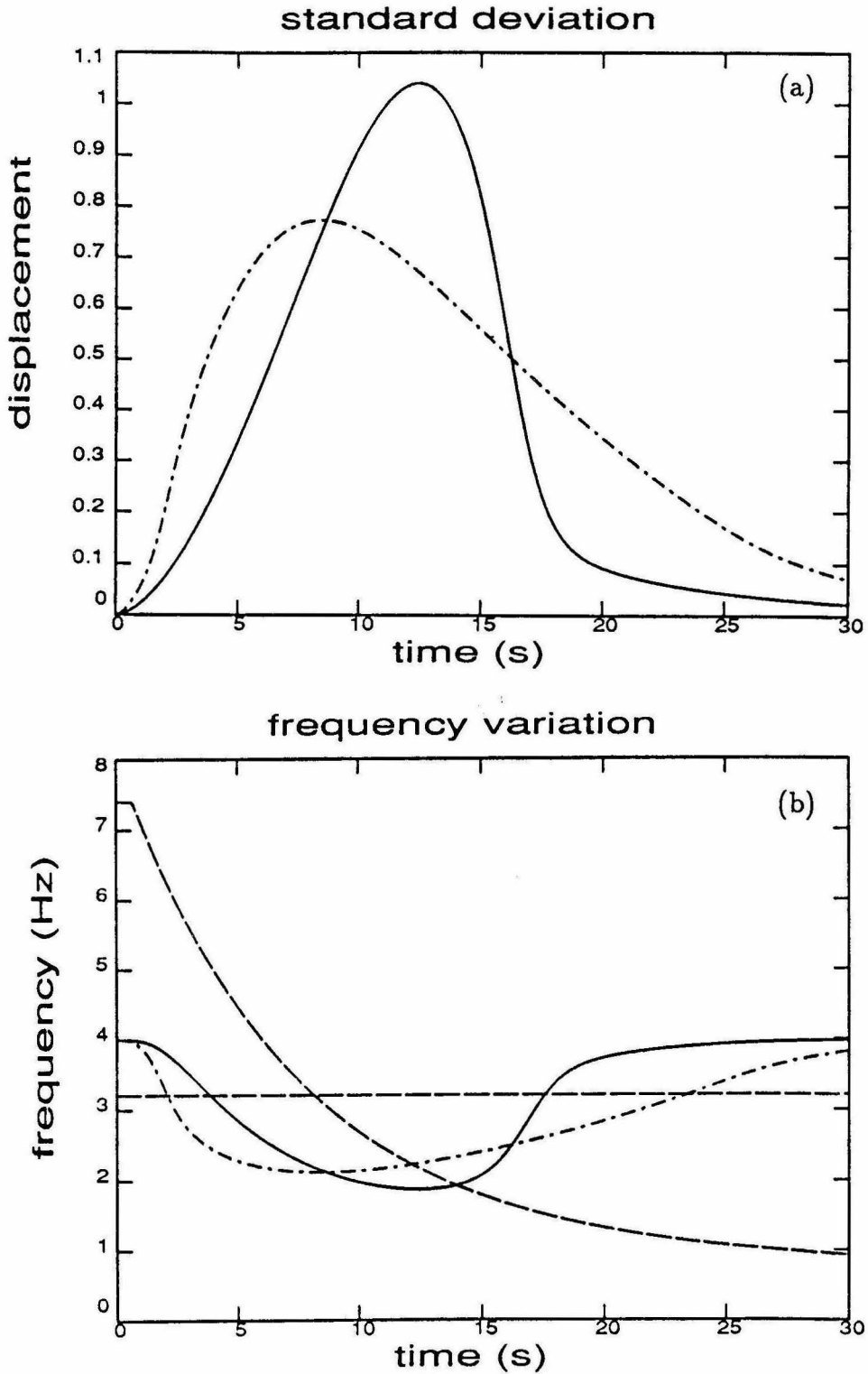


Figure 5.11. Comparison between the response characteristics computed for the (TV) (solid curves) and the (TI) (dashed-dotted curves) excitation. (a) r.m.s. displacement of the response (b) equivalent linear structural frequency.  $\omega_0 = 4\text{Hz}$ ,  $\zeta_0 = 0.05$ ,  $x_y = 1/3$ . Dashed curves correspond to the damped frequencies  $\omega'_g$  of (TV) and (TI) excitations.

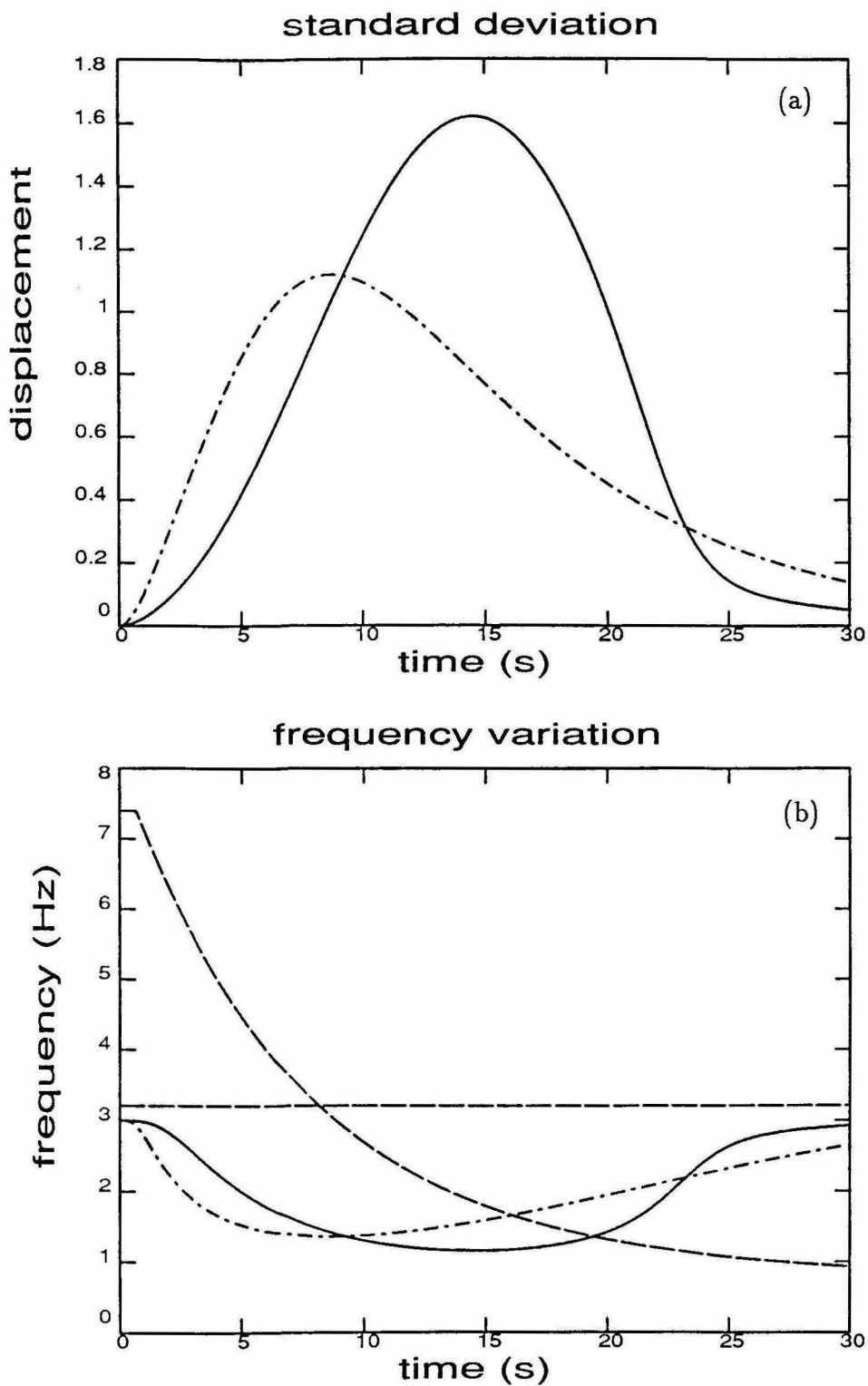


Figure 5.12. Comparison between the response characteristics computed for the (TV) (solid curves) and the (TI) (dashed-dotted curves) excitation. (a) r.m.s. displacement of the response (b) equivalent linear structural frequency.  $\omega_0 = 3\text{Hz}$ ,  $\zeta_0 = 0.05$ ,  $x_y = 1/3$ . Dashed curves correspond to the damped frequencies  $\omega'_g$  of (TV) and (TI) excitations.

## Chapter 6

### Conclusions

In this study, a new nonstationary ground motion model was proposed which is complete enough for structural response studies and yet is simple enough for ground motion predictions. The model captures with at most nine parameters all the features of the ground motion which are important for computing dynamic response, and it probabilistically treats the uncertainty in the remaining details associated with the ground acceleration time history. The model is formulated in both continuous and discrete time by stochastic differential and difference equations respectively, and conversion relationships are developed to link the two formulations. The modeling of the time-varying characteristics which are observed in real accelerograms is accomplished by varying the coefficients of these equations in a continuous manner. The maximum intensity of shaking, the time that the maximum occurs, the duration of shaking, the corner frequency, and the average dominant frequencies of the different wave groups present in an accelerogram are the explicit parameters of the model. One can exploit the simple interpretation of the model parameters to construct full acceleration time histories with certain desired characteristics. Uncertainties associated with the general ground motion characteristics may be handled by treating probabilistically the model parameters.

Using a Bayesian probabilistic framework and the discrete formulation of the model, an effective method was developed for estimating the most probable model that best fits, in a statistical sense, the nonstationary characteristics of a given “target” accelerogram. Unlike other methodologies applied to estimation of model parameters from earthquake data, the proposed methodology is simple to implement and it simultaneously treats the amplitude and the frequency content nonstationarities. Applications to a large database of accelerograms can provide the means of

associating each accelerogram with a nine-parameter description which covers both amplitude and frequency nonstationarities.

The proposed ground motion model can be efficiently applied in simulations as well as analytical response and reliability studies of linear and nonlinear structures. Extracting a stochastic model from an accelerogram allows the sensitivity of the structural response to variation in the details of the ground motion to be examined, while the overall features of the excitation are fixed. The discrete model provides a simple and computationally efficient algorithm for the generation of an ensemble of artificial digitized accelerograms with similar characteristics to a given earthquake accelerogram. Such simulated accelerograms were used in response studies of linear elastic and inelastic structures. The results of such studies indicate that the lower the structural frequency of linear structures, the more the displacement, velocity and acceleration are sensitive to the details of the ground motion. Also, the more inelastic the response of a structure is, the less sensitive the maximum velocity and absolute acceleration is to the ground motion details. However, the maximum ductility and especially the residual ductility of the inelastic response are very sensitive to the details of an acceleration time history which has its overall features fixed.

The simplified statistical structure of the continuous model can be efficiently used in analytical random vibration studies and for mathematically studying the importance of the temporal nonstationarity in both the amplitude and frequency content of ground motion on the response of both linear and nonlinear structures. Such analytical random vibration studies were considered in this work. Using the equivalent linearization method, an equivalent second-order linear differential equation with time-varying coefficients replaced the equation of motion of a nonlinear oscillator. The special case of time-invariant coefficients corresponds to the equation of motion of a linear oscillator. An approximate formulation was developed to replace the original, computationally lengthy expressions for the covariance of the transient response by much simpler expressions. The approximations provide meaningful insight into the characteristics of the nonstationary response. Similarities with the stationary response exist and were identified by the analysis. The formulation was extended to approximate the covariance response of multi-degree-

of-freedom systems. The proposed approximations preserve the essential characteristics of the response without significant loss of accuracy. They are also computationally efficient with typical reduction in computing time of one to two orders of magnitude.

The approximate random vibration analysis treats “earthquake like” excitations with nonstationarities in both amplitude and frequency content, and therefore the approximate equations are suitable to apply in the seismic analysis of linear and nonlinear structures. The simplified approximate formulation was used to mathematically analyze and demonstrate the effect of the temporal nonstationarity in the frequency content of the ground motion on the response of linear and nonlinear single-degree-of-freedom oscillators. From the analysis, it was concluded that the characteristics of both linear and nonlinear response strongly depend on the time variation of the frequency content of the excitation. Time-invariant frequency content models are inappropriate to model ground motions with time-varying frequency content. In particular, the temporal nonstationarity in the frequency content of the ground motion can have a substantial effect on the response of nonlinear structures of softening type, especially when the lengthening of the structural periods due to the softening of the structure tracks the shift of the dominant frequencies of the ground motion.

The proposed ground motion model is also promising for use in seismic risk analyses in which uncertainties in the variables accounting for the seismic environment at a site would be reflected in uncertainties in the model parameters. Employing such studies, it would be possible to probabilistically specify future ground motions at a site in terms of the full acceleration time history rather than the simplified peak ground quantities commonly used in present practice.

In future work, it is proposed to use probability as a mathematical tool to simultaneously treat ground motion uncertainties, structural model uncertainties as well as damage model uncertainties, and to study the sensitivity of various response parameters indicative of damage to these uncertainties, and finally to probabilistically assess reaching various limit states such as structural damage. This will allow more comprehensive seismic risk studies to be done for major structures which can

deal directly with inelastic response, avoiding the difficulties that arise in current practice when peak ground motion quantities or elastic response spectra are used to describe potential ground motions at a site.

## References

1. Anderson and Hough, “A Model for the Shape of Fourier Amplitude Spectrum of Acceleration at High Frequencies,” *Bulletin of Seismological Society of America*, Vol. 74, No. 5, pp. 1969-1993, (1984).
2. Atalik, T.S. and Utku, S., “Stochastic Linearization of Multi-Degree-of-Freedom Non-Linear Systems,” *Earthquake Engineering and Structural Dynamics*, Vol. 4, (1976).
3. Beck, J.L., “Statistical System Identification of Structures,” *Structural Safety and Reliability*, ASCE, New York, (1990).
4. Beck, J.L. and Park, H., “Optimal Algorithms for Calculating the Response of Linear Oscillator to Digitized Ground Accelerograms,” *Proc. Eight World Conference in Earthquake Engineering*, IV, 347-354, (1984).
5. Boore, D.M., “Stochastic Simulation of High-Frequency Ground Motions Based On Seismological Models of the Radiated Spectra,” *Bulletin of Seismological Society of America*, Vol. 73, No. 6, pp. 1865-1894, (1983).
6. Booton, R.C., “The Analysis of Nonlinear Control Systems with Random Inputs,” *IRE Trans. Circuit Theory*, Vol. 1, (1954).
7. Box, G.E.P. and Jenkins, G.M., “Time Series Analysis: Forecasting and Control,” rev. ed., Holden-Day, San Francisco, (1976).
8. Box, G.E.P. and Tiao, T.C., “Bayesian Inference,” Addison-Wesley, Reading, (1973).
9. Brune, J.N., “Tectonic Stress and the Spectra of Seismic Shear Waves from Earthquakes,” *J. Geophys. Res.*, 75, 4997-5009, (1970).
10. Brune, J.N., “Corrections,” *J. Geophys. Res.*, 76, 5002, (1971).

11. Bucher, C.G., “Approximate Nonstationary Random Vibration Analysis for MDOF Systems,” *Journal of Applied Mechanics*, ASME, 1988, Vol. 55, pp. 197-200.
12. Caughey, T.K., “Equivalent Linearization Techniques,” *The Journal of the Acoustical Society of America*, Vol. 35, No. 11, (1963).
13. Caughey, T.K. and Stumpf, H.J., “Transient Response of a Dynamic System under Random Excitation,” *Journal of Applied Mechanics*, Vol. 28, 1961, pp. 563-566.
14. Chang, M.K, Kwiatkowski, G.M., Nau, R.F., Oliver, R.M., and Pister, K.S., “ARMA Models for Earthquake Ground Motions,” *Earthquake Engineering and Structural Dynamics*, Vol. 10, 651-662, (1982).
15. Chang, M.K, Kwiatkowski, J.W., Nau, R.F., R.M., and Pister, K.S., “ARMA Models for Earthquake Ground Motions,” ORC 79-1, Operation Research Center, University of California, Berkeley, (1979).
16. Clough, R.W. and Penzien, J., “Dynamics of Structures,” McGraw-Hill, New York, 1975.
17. Conte, J.P., Pister, K.S., and Mohin, S.A., “Variability of Structural Response Parameters Within an Earthquake,” *Proceeding of Fourth National Conference on Earthquake Engineering*, Vol. I, 1990.
18. Crandall, A.H. and Zhu, W.Q., “Random Vibration: a Survey of Recent Developments,” *Journal of Applied Mechanics*, ASME, 1983, Vol. 50, pp. 953-962.
19. Gersch, W., and Kitagawa, G., “Time Varying AR Coefficient Model for Modeling and Simulating Earthquake Ground Motion,” *Earthquake Engineering and Structural Dynamics*, Vol. 13, 243-254, (1985).

20. Hou, Z., "Nonstationary Response of Structures and Its Application to Earthquake Engineering," Ph.D. Thesis, California Institute of Technology, Report No. EERL 90-01, 1990.
21. Housner, G.W. and Jennings, P.C., "Generation of Artificial Earthquakes," Journal of Engineering Mechanics Division, Proceedings of the American Society of Civil Engineers, EM1, pp. 113-150, (1964).
22. Igusa, T., "Characteristics of Response to Nonstationary White Noise: Theory," J. of Engrg. Mech. Div., ASCE, Vol. 115(9), 1989, pp. 1904-1934.
23. Igusa, T., "Characteristics of Response to Nonstationary White Noise: Applications," J. of Engrg. Mech. Div., ASCE, Vol. 115(9), 1989, pp. 1920-1935.
24. Iwan, W.D. and Hou, Z.K., "Explicit Solutions for the Response of Simple Systems Subjected to Nonstationary Excitations," Structural Safety, 6(1989), pp. 77-86.
25. Iwan, W.D. and Mason, A.B. "Equivalent Linearization for Systems Subjected to Non-stationary Random Excitation," Int. J. Non-Linear Mechanics, Vol. 15, (1980).
26. Iwan, W.D. and Papanizos, L.G., "The Stochastic Response of Strongly Yielding Systems," Probabilistic Engineering Mechanics, Vol. 3, No. 2, 1988.
27. Iwan, W.D. and Yang, I.M., "Statistical Linearization for Nonlinear Structures," ASCE J. Eng. Mech. Div., Vol. 97, (1971).
28. Jayakumar, P., "Modeling and Identification in Structural Dynamics," Ph.D. Thesis, California Institute of Technology, Report No. EERL 87-01, 1987.
29. Jeong, G.D., "Cumulative Damage of Structures Subjected to Response Spectrum Consistent Random Processes." Ph.D. Thesis, California Institute of Technology, Report No. EERL 85-03, 1985.

30. Jurkevics, A. and Ulrych, T.J., "Representing and Simulating Strong Ground Motion," *Bulletin of Seismological Society of America*, Vol. 68, No. 3, pp. 781-801, (1978).
31. Jurkevics, A. and Ulrych, T.J., "Autoregressive Parameters for A Suite of Strong-Motion Accelerograms," *Bulletin of Seismological Society of America*, Vol. 69, No. 6, pp. 2025-2036, (1979).
32. Kanai, K., "Semi-Empirical Formula for the Seismic Characteristics of the Ground Motion," *Bulletin of the Earthquake Research Institute, University of Tokyo*, Vol. 35, (1957), 309-325.
33. Kubo, T. and Penzien, J., "Simulation of Three-Dimensional Strong Ground Motions Along Principal Axes, San Fernando Earthquake," *Earthquake Engineering and Structural Dynamics*, Vol. 7, pp. 279-294, (1979).
34. Mason, A.B. Jr. and Iwan, W.D., "An Approach to the First Passage Problem in Random Vibrations," *J. of Applied Mechanics, ASME*, 1983, Vol. 50, pp. 641-646.
35. McGuire, R.K. and Hanks, T.C. "RMS Accelerations and Spectral Amplitudes of Strong Ground Motion During the San Fernando Earthquake," *Bulletin of Seismological Society of America*, Vol. 70, No. 5, pp. 1907-1919, (1980).
36. Nau, R.F., Oliver, R.M. and Pister, K.S., "Simulating and Analysing Artificial Nonstationary Earthquake Ground Motions," ORC 80-16, Operation Research Center, University of California, Berkeley, (1980).
37. Nau, R.F., Oliver, R.M. and Pister, K.S., "Simulating and Analysing Artificial Nonstationary Earthquake Ground Motions," *Bulletin of Seismological Society of America*, Vol. 72, No. 2, pp. 615-636, April 1982, (1980).

38. Ozdemir, H., "Nonlinear Transient Dynamic Analysis of Yielding Structures," Ph.D. Dissertation, Division of Structural Engineering and Structural Mechanics, Department of Civil Engineering, University of California, Berkeley, California, June, 1976.
39. Pandit, S.M. and Wu, S.M., "Time Series and System Analysis with Applications," John Wiley and Sons, Inc., (1983).
40. Polhemus, N.W. and Cakmak, A.S., "Simulation of Earthquake Ground Motions Using Autoregressive Moving Average (ARMA) Models," Earthquake Engineering and Structural Dynamics, Vol. 9, 343-354, (1981).
41. Priestley, M.B., "Evolutionary Spectra and Nonstationary Process," J. Roy. Statist. Soc., 1965, Vol. 27, pp. 204-228.
42. Priestley, M.B., "Power Spectral Analysis of Nonstationary Random Processes," J. Sound and Vibration, 1967, Vol. 6, pp. 86-97.
43. Safak, E., "Analytical Approach to Calculation of Response Spectra from Seismological Models of Ground Motion," Earthquake Engineering and Structural Dynamics, Vol. 16, 121-134, (1988).
44. Saragoni, G.R. and Hart, G.C., "Simulation of Artificial Earthquakes," Earthquake Engineering and Structural Dynamics, Vol. 2, 249-267, (1974).
45. Shinozuka, M. and Sato, Y., "Simulation of Nonstationary Random Process," Journal of Engineering Mechanics Division, ASCE, Vol. 93, No. EM1, pp. 11-40, (1967).
46. Spanos, P.T.D., "Probability of Response to Evolutionary Process," J. of Engrg. Mech. Div., ASCE, Vol. 106, No. EM2, 1980, pp. 213-224.

47. Spanos, P.T.D., and Solomos, G.P., “Markov Approximation to Transient Vibration,” *J. of Engrg. Mech. Div., ASCE*, Vol. 109(4), 1983, pp. 1134-1148.
48. Spanos, P.T.D., and Lutes, L.D., “A Primer of Random Vibration Techniques in Structural Engineering,” *The Shock and Vibration Digest*, 18(4), 1986, pp. 3-5.
49. Tajimi, H., “A Statistical Method of Determining the Maximum Response of a Building During an Earthquake,” *Proc. of 2nd WCEE*, Vol. II, Science Council of Japan, Tokyo, Japan, 1960, pp. 781-798.
50. Thyagarajan, R.S., “Modeling and Analysis of Hysteretic Structural Behavior,” Ph.D. Thesis, California Institute of Technology, Report No. EERL 89-03, 1989.
51. Wen, Y.K., “Equivalent Linearization for Hysteretic Systems Under Random Excitation,” *Journal of Applied Mechanics*, ASME, Vol. 47(1), 150-154, March, 1980.
52. Wen, Y.K., “Method for Random Vibration of Hysteretic Systems,” *Journal of the Engineering Mechanics Division*, ASCE, Vol. 102(2), 249-263, April, 1976.
53. Yeh, C.H. and Wen, Y.K., “Modeling of Nonstationary Earthquake Ground Motion and Biaxial and Torsional Response of Inelastic Structures,” University of Illinois, Urbana, Report UILU-ENG-89-2005, (1989).

## APPENDIX A

### 1. Solutions of Homogenous Second-Order Differential Equation with Slowly-Varying Coefficients

In general, there is no closed-form solution of the second-order differential equation

$$\ddot{x} + 2\zeta_g(t)\omega_g(t)\dot{x} + \omega_g^2(t)x = 0 \quad (\text{A.1})$$

where a dot denotes derivative with respect to the independent variable  $t$  and  $\zeta_g$  and  $\omega_g$  are time varying. However, in the case of slowly-varying coefficients, approximate closed-form solutions can be derived. A perturbation technique is used here to approximately solve the equation (A.1).

Introducing a new variable  $\tau$  by:

$$\tau = \frac{t}{\lambda} \quad , \quad \lambda \text{ large} \quad (\text{A.2})$$

then,

$$\frac{d}{dt} = \frac{1}{\lambda} \frac{d}{d\tau} \quad \text{and} \quad \frac{d^2}{dt^2} = \frac{1}{\lambda^2} \frac{d^2}{d\tau^2} \quad (\text{A.3})$$

Setting

$$\tilde{x}(\tau) = x(\lambda\tau), \quad \tilde{\zeta}_g(\tau) = \zeta_g(\lambda\tau), \quad \tilde{\omega}_g(\tau) = \omega_g(\lambda\tau) \quad (\text{A.4})$$

equation (A.1) may be rewritten in the form:

$$\tilde{x}'' + 2\lambda\tilde{\zeta}_g(\tau)\tilde{\omega}_g(\tau)\tilde{x}' + \lambda^2\tilde{\omega}_g^2(\tau)\tilde{x} = 0 \quad (\text{A.5})$$

where now a prime denotes derivative with respect to the independent variable  $\tau$ . Define a new dependent function  $\phi(\tau)$  by:

$$\phi(\tau) = \frac{\tilde{x}'}{\tilde{x}} \quad (\text{A.6a})$$

then,

$$\phi'(\tau) = \frac{\tilde{x}''}{\tilde{x}} - \left( \frac{\tilde{x}'}{\tilde{x}} \right)^2 \quad (\text{A.6b})$$

Solving (A.6a) and (A.6b) for  $\tilde{x}'$  and  $\tilde{x}''$  and substituting into equation (A.5), we find that  $\phi(\tau)$  satisfies the first-order nonlinear differential equation:

$$\phi' + \phi^2 + 2\lambda\tilde{\zeta}_g(\tau)\tilde{\omega}_g(\tau)\phi + \lambda^2\tilde{\omega}_g^2(\tau) = 0 \quad (\text{A.7})$$

Expanding  $\phi(\tau)$  in powers of  $\lambda$ :

$$\phi(\tau) = \lambda\phi_0(\tau) + \phi_1(\tau) + \frac{1}{\lambda}\phi_2(\tau) + \dots, \quad (\text{A.8})$$

substituting (A.8) into (A.7) and equating terms of the same order, we finally obtain the equations for the first two terms in the form

$$\phi_0^2 + 2\tilde{\zeta}_g(\tau)\tilde{\omega}_g(\tau)\phi_0 + \tilde{\omega}_g^2(\tau) = 0 \quad (\text{A.9a})$$

$$\phi_0' + 2\phi_0\phi_1 + 2\tilde{\zeta}_g(\tau)\tilde{\omega}_g(\tau)\phi_1 = 0 \quad (\text{A.9b})$$

The condition between the first two terms under which the expansion (A.8) is valid is:

$$\left| \frac{\phi_1(\tau)}{\phi_0(\tau)} \right| \ll \lambda \quad (\text{A.10})$$

Solving (A.9a) and (A.9b) for  $\phi_0$  and  $\phi_1$  respectively, we get:

$$\phi_0(\tau) = -\tilde{\zeta}_g\tilde{\omega}_g \pm i\tilde{\omega}_g\sqrt{1 - \tilde{\zeta}_g^2} \quad (\text{A.11a})$$

$$\phi_1(\tau) = -\frac{\phi_0'}{2(\phi_0 + \tilde{\zeta}_g\tilde{\omega}_g)} \quad (\text{A.11b})$$

Noting from (A.6a) that:

$$\tilde{x}(\tau) = \exp \left[ \int^\tau \phi(\theta) d\theta \right] \quad (\text{A.12a})$$

and using the expansion (A.8) we get:

$$\tilde{x}(\tau) = \exp \left[ \int^\tau \phi_0(\theta) d(\lambda\theta) \right] \exp \left[ - \int^\tau \frac{\phi_0'(\theta) d\theta}{2(\phi_0 + \tilde{\zeta}_g\tilde{\omega}_g)} \right] \quad (\text{A.12b})$$

Changing the variable of integration in (A.12b) according to (A.2), the two linearly independent solutions of (A.1) are finally obtained as

$$x_h^{(l)}(t) = \frac{\exp \left[ - \int^t \zeta_g(s)\omega_g(s) ds \right]}{\sqrt{\omega_d(t)}} \exp \left[ \pm i \int^t \omega_d(s)(1 + \rho_g(s)) ds \right], \quad l = 1, 2 \quad (\text{A.13a})$$

where

$$\rho_g(s) = -\frac{d}{ds} [\zeta_g(s)\omega_g(s)] / 2\omega_d^2(s) \quad (\text{A.13b})$$

and

$$\omega_d(s) = \omega_g(s) \sqrt{1 - \zeta_g^2(s)}. \quad (\text{A.13c})$$

Using the values of  $\phi_0$  and  $\phi_1$ , the condition under which the expansion (A.8) is valid becomes:

$$\frac{|\dot{\phi}_0|}{2\omega_d\omega_g} \ll 1 \quad (\text{A.14})$$

or equivalently,

$$\frac{|\dot{\alpha}_g|}{2\omega_d\omega_g} \ll 1 \quad \text{and} \quad \frac{|\dot{\omega}_d|}{2\omega_d\omega_g} \ll 1, \quad (\text{A.14a})$$

where  $\alpha_g(t) = \zeta_g(t)\omega_g(t)$ . Introducing the period  $T_d$  of the system as  $T_d = 2\pi/\omega_d$  we can rewrite (A.14a) in the form:

$$\frac{|\dot{\alpha}_g|}{2\omega_d\omega_g} \ll 1 \quad \text{and} \quad \frac{|T_d|}{4\pi} \sqrt{1 - \zeta^2} \ll 1 \quad (\text{A.14c})$$

The responses  $\eta(t, \tau)$  to a unit initial displacement and  $h(t, \tau)$  to a unit initial velocity applied at time  $\tau$  are

$$\eta(t, \tau) = \omega_d(\tau)g(t, \tau) + \left\{ \alpha_g(\tau) + \frac{\dot{\omega}_d(\tau)}{2\omega_d(\tau)} \right\} h(t, \tau) \quad (\text{A.15a})$$

$$h(t, \tau) = \frac{\exp\left[-\int_{\tau}^t \zeta_g(s)\omega_g(s) ds\right]}{\sqrt{\omega_d(t)\omega_d(\tau)}} \sin\left[\int_{\tau}^t \omega_d(s) ds\right] \quad (\text{A.15b})$$

respectively, where

$$g(t, \tau) = \frac{\exp\left[-\int_{\tau}^t \zeta_g(s)\omega_g(s) ds\right]}{\sqrt{\omega_d(t)\omega_d(\tau)}} \cos\left[\int_{\tau}^t \omega_d(s) ds\right] \quad (\text{A.15c})$$

## 2. Principal Matrix Solution

The principal matrix solution  $\Phi(t, \tau)$  satisfies

$$\begin{aligned} \dot{\Phi}(t, \tau) &= A(t)\Phi(t, \tau) \\ \Phi(\tau, \tau) &= I \end{aligned} \quad (\text{A.16})$$

where  $A(t)$  is given by (4.3). It is straightforward to show that

$$\Phi_{11}(t, \tau) = \eta(t, \tau) \quad (\text{A.17})$$

$$\Phi_{21}(t, \tau) = \dot{\eta}(t, \tau) \quad (\text{A.18})$$

$$\Phi_{12}(t, \tau) = h(t, \tau) \quad (\text{A.19})$$

$$\Phi_{22}(t, \tau) = \dot{h}(t, \tau) = \omega_d(t)g(t, \tau) - \left\{ \alpha_g(t) + \frac{\dot{\omega}_d(t)}{2\omega_d(t)} \right\} h(t, \tau) \quad (\text{A.20})$$

where the slowly-varying formulas were used in (A.20).

For large enough  $\zeta_g(t)$ , both  $\eta(t, \tau)$  and  $h(t, \tau)$  decay quickly to zero after a few cycles of oscillations. For slowly-varying  $\alpha_g(t)$  and  $\omega_g(t)$ , we can ignore their time variation over the first few cycles and approximate the expressions (A.15a) and (A.15b) by the simpler ones

$$\eta^*(t, \tau) = \omega_d(t)g^*(t, \tau) + \left\{ \alpha_g(t) + \frac{\dot{\omega}_d(t)}{2\omega_d(t)} \right\} h^*(t, \tau) \quad (\text{A.21a})$$

$$h^*(t, \tau) = \frac{\exp[\zeta_g(t)\omega_g(t)(t-\tau)]}{\omega_d(t)} \sin[-\omega_d(t)(t-\tau)] \quad (\text{A.21b})$$

where

$$g^*(t, \tau) = \frac{\exp[-\zeta_g(t)\omega_g(t)(t-\tau)]}{\omega_d(t)} \cos[\omega_d(t)(t-\tau)] \quad (\text{A.21c})$$

These expressions are exact for time-invariant  $\zeta_g$  and  $\omega_g$ .

### 3. Evolutionary Spectral Representation of A Stochastic Process

For a stationary process  $x(t)$ , the covariance function  $R_x(t, s)$  depends only on the time difference  $\tau = t - s$ . A useful quantity referred to as the power spectral density (PSD) can be introduced in this case as the Fourier transform of the covariance function. The PSD, which describes the frequency decomposition of the total energy of the process, is also a complete description of the zero-mean Gaussian stationary process because the covariance function can be determined from the inverse Fourier transform.

For the case of a nonstationary process, Priestley (1965, 1967) extended the definition of the PSD. If a zero-mean Gaussian stochastic process admits the spectral

representation

$$x(t) = \int_{-\infty}^{\infty} H(\omega) e^{i\omega t} dZ(\omega) \quad (\text{A.22})$$

where  $H(\omega)$  is deterministic and  $dZ(\omega)$  is an orthogonal stochastic process such that

$$E[dZ(\omega)] = 0 \quad (\text{A.23a})$$

$$E[dZ(\omega_1) dZ^*(\omega_2)] = \delta(\omega_1 - \omega_2) d\omega, \quad (\text{A.23b})$$

then the PSD of  $x(t)$  is given by:

$$S_{xx}(\omega) = |H(\omega)|^2 \quad (\text{A.24})$$

Similarly, a nonstationary stochastic process can be generated from the spectral representation

$$x(t) = \int_{-\infty}^{\infty} G(\omega, t) e^{i\omega t} dZ(\omega) \quad (\text{A.25})$$

where in this case  $G(\omega, t)$  varies with time. According to Priestley, the evolutionary power spectral density (EPSD) for such a process is defined as

$$S_{xx}(\omega, t) = |G(\omega, t)|^2 \quad (\text{A.26})$$

In this case, the EPSD is not a complete description of the nonstationary process because the crucial quantity  $R_{xx}(t, s)$ , which turns out to be given by

$$R_{xx}(t, s) = E[x(t)x(s)] = \int_{-\infty}^{\infty} G^*(\omega, t) G(\omega, s) e^{i\omega(t-s)} d\omega, \quad (\text{A.27})$$

depends also on the phase of  $G(\omega, t)$ . For  $t = s$  the variance of the process is obtained in the form

$$R(t) = R_{xx}(t, t) = E[x^2(t)] = \int_{-\infty}^{\infty} S(\omega, t) d\omega \quad (\text{A.28})$$

The variance  $R(t)$  may be interpreted as a measure of the total power of the process at time  $t$  and (A.28) gives a frequency decomposition of the total power in which the contribution from frequency  $\omega$  is  $S(\omega, t)d\omega$ . Therefore, the EPSD retains its interpretation as a frequency decomposition of the total energy.

Next, we derive an approximate closed-form expression for the EPSD of the process defined by (3.1). Substituting the spectral representation of white noise

$$e(t) = \int_{-\infty}^{\infty} e^{i\omega t} dZ(\omega) \quad (\text{A.29})$$

into (3.2) and interchanging the order of integration, we get that

$$y(t) = \int_{-\infty}^{\infty} \left[ \int_0^t h(t,s) f(s) e^{-i\omega(t-s)} ds \right] e^{i\omega t} dZ(\omega) \quad (\text{A.30})$$

According to the definition, the EPSD is

$$S_{yy}(\omega, t) = \left| \int_0^t h(t,s) f(s) e^{-i\omega(t-s)} ds \right|^2 \quad (\text{A.31})$$

where in the case of slowly-varying coefficients,  $h(t,s)$  is approximated by (3.6).

## APPENDIX B

### Relationships Between the Coefficients of Second-Order Discrete and Continuous Equations

Solving the algebraic system (3.26) for the two unknowns  $a_1(k)$  and  $a_2(k)$  at each  $k$  and using expressions (A.13) for  $x_h^{(1)}(t_k)$  and  $x_h^{(2)}(t_k)$ , we finally obtain that

$$a_1(k) = \sqrt{\frac{\omega_d(t_{k-1})}{\omega_d(t_k)}} \exp \left[ - \int_{t_{k-1}}^{t_k} \alpha_g(s) ds \right] \frac{\sin(\Theta_k - \Theta_{k-2})}{\sin(\Theta_{k-1} - \Theta_{k-2})} \quad (B.1a)$$

$$a_2(k) = - \sqrt{\frac{\omega_d(t_{k-2})}{\omega_d(t_k)}} \exp \left[ - \int_{t_{k-2}}^{t_k} \alpha_g(s) ds \right] \frac{\sin(\Theta_k - \Theta_{k-1})}{\sin(\Theta_{k-1} - \Theta_{k-2})} \quad (B.1b)$$

where

$$\Theta_k - \Theta_l = \int_{t_l}^{t_k} \omega_d(s) ds \quad k, l \text{ integers} \quad (B.1c)$$

In practice,  $\Delta t$  is very small and  $\alpha_g(t)$  and  $\omega_d(t)$  can be assumed to remain essentially constant over the period  $\Delta t$ . Therefore, without losing accuracy, expressions (B.1) can be approximated by:

$$a_1(k) = 2 \exp[-\zeta_g(t_k) \omega_g(t_k) \Delta t] \cos[\omega_d(t_k) \Delta t] \quad (B.2a)$$

$$a_2(k) = - \exp[-2\zeta_g(t_k) \omega_g(t_k) \Delta t] \quad (B.2b)$$

## APPENDIX C

### Second-Order Discrete Equation

The general solution of the discrete equation (3.25) and the autocovariance of its output is derived herein. The discrete impulse response  $u_{k,m}$  is first derived by solving the auxiliary problem

$$u_{k,m} - a_1(k) u_{k-1,m} - a_2(k) u_{k-2,m} = \delta_{k,m} \quad ; \quad k \geq m \quad (C.1a)$$

$$u_{k,m} = 0 \quad ; \quad k < m, \quad (C.1b)$$

where  $\delta_{k,m}$  is the Kronecker-delta given by:

$$\delta_{k,m} = \begin{cases} 1, & \text{if } k = m; \\ 0, & \text{if } k \neq m. \end{cases} \quad (C.2)$$

Since the coefficients of  $a_1(k)$  and  $a_2(k)$  have been chosen so that the free vibration solutions of (C.1) are  $x_h^{(l)}(k\Delta t)$ ,  $l = 1, 2$ , we can express the solution to this problem in the form:

$$u_{k,m} = \begin{cases} Ax_h^{(1)}(k\Delta t) + Bx_h^{(2)}(k\Delta t), & \text{if } k \geq m; \\ 0, & \text{if } k < m, \end{cases} \quad (C.3)$$

then (C.1) is satisfied for every  $k$  different from  $m$ ,  $m + 1$ . The constants A and B are determined by enforcing  $u_{k,m}$  to satisfy equation (C.1) at  $k = m$  and  $k = m + 1$ . Finally, using the expressions (A.13) and (B.2b) for  $x_h^{(i)}(k\Delta t)$ ,  $i = 1, 2$  and  $a_2(m)$  respectively, the exact relation for  $u_{k,m}$  becomes:

$$\begin{aligned} u_{k,m+1} &= \frac{h(t_k, t_m)}{h(t_{m+1}, t_m)} \\ &= 0 \quad ; \quad k < m \end{aligned} \quad (C.4)$$

Using the principle of superposition,  $y_k$  may be written in the form:

$$y_k = \sum_{m=1}^k u_{k,m} \sigma(m) e_m = \sum_{m=0}^k u_{k,m+1} \sigma(m+1) e_{m+1}, \quad k = 1, \dots, N \quad (C.5)$$

Using (C.4), and the property of the discrete white-noise process

$$E[e_m e_l] = \delta_{ml}, \quad (C.6)$$

the discrete autocovariance function of the process  $y_k$ ,  $k = 1, \dots, N$  becomes

$$E[y_k y_s] = \sum_{m=0}^k u_{k,m+1} u_{s,m+1} \sigma^2(m+1) \quad ; \quad s \geq k \quad (C.7a)$$

$$= \sum_{m=0}^k h(t_k, t_m) h(t_s, t_m) \frac{\sigma^2(m+1)}{h^2(t_{m+1}, t_m)}; \quad s \geq k \quad (C.7b)$$

On the other hand, the ACF of the continuous process  $y(t)$  can be approximated by numerically integrating expression (3.3). Using the trapezoidal rule, the integral in (3.3) is replaced by the summation:

$$R_y(t, s) = \sum_{m=0}^k h(t, t_m) h(s, t_m) f^2(t_m) \Delta t - \frac{1}{2} h(t, t_0) h(s, t_0) f^2(t_0) \Delta t \quad (C.8)$$

where  $t_m = m\Delta t$  and  $k\Delta t = \min\{t, s\}$ . From (C.7b) and (C.8) and assuming that  $f(t_0) = 0$ , it is found that relation (3.28) holds if

$$\sigma(k+1) = f(t_k) h(t_{k+1}, t_k) \sqrt{\Delta t} \quad (C.9)$$

The accuracy of the approximation deteriorates as the oscillator frequency  $\omega_g(t)$  approaches the Nyquist frequency, that is, as the number of time-steps  $\Delta t$  per period decreases. That is so, because the trapezoidal rule approximation applied for the integral in (3.3) becomes less accurate for large time steps. For ten time-steps per period, an accurate numerical integration algorithm is obtained. Assuming that the variation of  $\omega_g(t)$  and  $\alpha_g(t)$  is not significant over the interval  $\Delta t$ , expression (C.9) is further approximated by (3.29).

## APPENDIX D

### Solution of the Second-Order Differential Equation Using the Two-Timing Method

Consider the second-order differential equation

$$\ddot{r}(t) + 2\zeta\omega_0\dot{r}(t) + \omega_0^2r(t) = g(t) \quad (D.1)$$

with initial conditions

$$r(0) = 0 \quad \text{and} \quad \dot{r}(0) = 0 \quad (D.2)$$

We seek a solution in the form of a series such that when  $g(t)$  varies slowly with time and the angular frequency  $\omega_0$  is high, the first few terms in the series expansion would provide a reasonable approximation to the solution  $r(t)$ . For this, the two-timing method is used with the slow time to be governed by  $t$  and the fast time to be governed by the reciprocal of the angular frequency  $\omega_0$ .

Introducing the fast time  $\tau$  by

$$\tau = \omega_0 t \quad (D.3)$$

then

$$r(t) = r\left(\frac{\tau}{\omega_0}\right) \equiv x(\tau) \quad (D.4)$$

where  $x(\tau)$  is a function of the independent variable  $\tau$  with

$$x'(\tau) = \frac{1}{\omega_0}\dot{r}(t) \quad \text{and} \quad x''(\tau) = \frac{1}{\omega_0^2}\ddot{r}(t). \quad (D.5)$$

The differential equation for  $x(\tau)$  becomes

$$Lx(\tau) \equiv x''(\tau) + 2\zeta x'(\tau) + x(\tau) = \epsilon^2 g(\epsilon\tau) \quad (D.6)$$

with initial conditions

$$x(0) = 0 \quad \text{and} \quad x'(0) = 0 \quad (D.7)$$

where

$$t = t(\tau) = \frac{1}{\omega_0}\tau = \epsilon\tau \quad (D.8)$$

We seek a solution of the form  $x(\tau) = X(\tau, t(\tau))$  where  $X(\tau, t)$  is a function of two variables  $\tau$  and  $t$ . Then

$$x'(\tau) = \frac{dX(\tau, t(\tau))}{d\tau} = \frac{\partial X(\tau, t)}{\partial \tau} + \epsilon \frac{\partial X(\tau, t)}{\partial t} \quad (D.9)$$

$$x''(\tau) = \frac{d^2 X(\tau, t(\tau))}{d\tau^2} = \frac{\partial^2 X(\tau, t)}{\partial \tau^2} + 2\epsilon \frac{\partial^2 X(\tau, t)}{\partial t \partial \tau} + \epsilon^2 \frac{\partial^2 X(\tau, t)}{\partial t^2} \quad (D.10)$$

We expand  $X(\tau, t)$  into powers of  $\epsilon$

$$X(\tau, t) = X_0(\tau, t) + \epsilon X_1(\tau, t) + \epsilon^2 X_2(\tau, t) + \epsilon^3 X_3(\tau, t) + \epsilon^4 X_4(\tau, t) + \dots, \quad (D.11)$$

and we substitute it into the equation (D-6) and (D-7). Collecting terms of the same order in  $\epsilon$  we have the system

$$\epsilon^0 : \left\{ \begin{array}{l} L X_0(\tau, t) = 0 \\ X_0(0, 0) = 0, \quad \frac{\partial X_0(0, 0)}{\partial \tau} = 0 \end{array} \right\} \quad (D.12)$$

$$\epsilon^1 : \left\{ \begin{array}{l} L X_1(\tau, t) = 0 \\ X_1(0, 0) = 0, \quad \frac{\partial X_1(0, 0)}{\partial \tau} = 0 \end{array} \right\} \quad (D.13)$$

$$\epsilon^2 : \left\{ \begin{array}{l} L X_2(\tau, t) = g(t) \\ X_2(0, 0) = 0, \quad \frac{\partial X_2(0, 0)}{\partial \tau} = 0 \end{array} \right\} \quad (D.14)$$

$$\epsilon^i : \left\{ \begin{array}{l} L X_i(\tau, t) = -2 \frac{\partial^2 X_{i-1}(\tau, t)}{\partial t \partial \tau} - \frac{\partial^2 X_{i-2}(\tau, t)}{\partial t^2} - 2\zeta \frac{\partial X_{i-1}(\tau, t)}{\partial t} \\ X_i(0, 0) = 0, \quad \frac{\partial X_i(0, 0)}{\partial \tau} + \frac{\partial X_{i-1}(0, 0)}{\partial t} = 0 \end{array} \right\} \quad (D.15)$$

which can be solved successively. Integrating the equations and eliminating the secular terms produces

$$X_0(\tau, t) = X_1(\tau, t) = 0 \quad (D.16)$$

$$X_2(\tau, t) = g(t) - g(0) \varphi\left(\frac{1}{\sqrt{1-\zeta^2}}, \zeta\right) \quad (D.17)$$

$$X_3(\tau, t) = -2\zeta \frac{\partial g(t)}{\partial t} + \frac{\partial g(0)}{\partial t} \varphi\left(\frac{1}{\sqrt{1-\zeta^2}}, -(1-2\zeta^2)\right) \quad (D.18)$$

$$X_4(\tau, t) = -(1-4\zeta^2) \frac{\partial^2 g(t)}{\partial t^2} + \frac{\partial^2 g(0)}{\partial t^2} \varphi\left(\frac{1}{\sqrt{1-\zeta^2}}, -\zeta(3-4\zeta^2)\right) \quad (D.19)$$

$$X_i(\tau, t) = \mathcal{O}\left(g^{(i)}(t)\right) + \mathcal{O}\left(g^{(i)}(0) \varphi(\rho, \sin \phi)\right) \quad (D.20)$$

where  $\varphi(\rho, \sin \phi)$  denotes the exponentially decaying oscillatory function

$$\varphi(\rho, \sin \phi) = \rho \exp(-\zeta \tau) \cos\left(\sqrt{1-\zeta^2} \tau + \phi\right) \quad (D.21)$$

Substituting  $\tau = \omega_0 t$  and using the expansion (D-11), the final expression for  $r(t)$  becomes

$$\begin{aligned} r(t) = \frac{1}{(2\omega_0)^2} & \left\{ g(t) - g(0)\varphi\left(\frac{1}{\sqrt{1-\zeta^2}}, \zeta\right) \right. \\ & - 2\zeta \frac{\dot{g}(t)}{2\omega_0} + \frac{\dot{g}(0)}{2\omega_0} \varphi\left(\frac{1}{\sqrt{1-\zeta^2}}, -(1-2\zeta^2)\right) \\ & - (1-4\zeta^2) \frac{\ddot{g}(t)}{(2\omega_0)^2} + \frac{\ddot{g}(0)}{(2\omega_0)^2} \varphi\left(\frac{1}{\sqrt{1-\zeta^2}}, -\zeta(3-4\zeta^2)\right) \\ & \left. + \sum_{i=3}^{\infty} \circ \left(\frac{g^{(i)}(t)}{(2\omega_0)^i}\right) + \sum_{i=3}^{\infty} \circ \left(\frac{g^{(i)}(0)}{(2\omega_0)^i} \varphi(\rho, \sin \phi)\right) \right\} \quad (D.22) \end{aligned}$$

where  $\varphi(\rho, \sin \phi)$  is the exponentially decaying oscillatory function

$$\varphi(\rho, \sin \phi) = \rho \exp(-\zeta \omega_0 t) \cos(\omega_d t + \phi) \quad (D.23)$$

## APPENDIX E

### Covariance Response of A Linear Oscillator Subjected to Modulated White-Noise Excitation

Substituting the time-invariant version of expressions (A.17) to (A.20) into equation (4.15) and after algebraic manipulations, it can be shown that the covariance  $S(t, s)$  of a response quantity takes the simple form

$$S(t, s) = q(s) \exp(-\zeta \omega_0(t - s)) \frac{\cos[\omega_d(t - s) + \phi(s)]}{\cos[\phi(s)]} \quad (E.1)$$

where  $q(s)$  and  $\phi(s)$  are given as follows.

For the covariance of the displacement response

$$q(s) = q_{11}(s), \quad \tan[\phi(s)] = \frac{\zeta}{\sqrt{1 - \zeta^2}} + \epsilon_{12}(s) \quad (E.2)$$

For the covariance of the velocity response

$$q(s) = q_{22}(s), \quad \tan[\phi(s)] = -\frac{\zeta}{\sqrt{1 - \zeta^2}} - \frac{\epsilon_{12}(s)}{1 + \epsilon_{22}(s)} \quad (E.3)$$

For the covariance of the absolute acceleration of the response

$$q(s) = q_a(s), \quad \tan[\phi(s)] = \frac{\zeta \{ [1 + 2\epsilon_{22}(s)] - 4\zeta^2 [1 + \epsilon_{22}(s)] \} + (1 + 4\zeta^2) \epsilon_{12}(s)}{1 + 4\zeta^2 [1 + 2\epsilon_{22}(s)] + 4\zeta \epsilon_{12}(s)} \quad (E.4)$$

For stationary response,  $\epsilon_{22}(s) = \epsilon_{12}(s) = \epsilon_a(s) = 0$ .

## APPENDIX F

### Complete Set of Equations for the Mean-Square Displacement of the Nonlinear Response

The differential equation (4.51) can be split into the first-order differential equation

$$\begin{aligned} \dot{q}_{11}(t) + 2s^*(t)q_{11}(t) &= 2r(t) \\ q_{11}(0) &= 0 \end{aligned} \tag{F.1}$$

with the excitation  $r(t)$  satisfying the second-order differential equation

$$\begin{aligned} \ddot{r}(t) + 4\alpha^*(t)\dot{r}(t) + [2\omega^*(t)]^2 r(t) &= g(t) \\ r(0) = 0, \quad \dot{r}(0) &= 0 \end{aligned} \tag{F.2}$$

where

$$\alpha^*(t) = \alpha(t) - 0.5\delta(t) \tag{F.3}$$

$$s^*(t) = \alpha(t) + \delta(t) \tag{F.4}$$

$$[2\omega^*(t)]^2 = [2\omega(t)]^2 - 2\dot{\alpha}(t) - 4\alpha(t)\delta(t) - \dot{\delta}(t) + 4\delta^2(t) \tag{F.5}$$

$$g(t) = 2L_{22}(t) + 4\alpha(t)L_{12}(t) + \dot{L}_{12}(t) \tag{F.6}$$

and  $\delta(t)$  satisfies the nonlinear differential equation

$$\ddot{\delta} - 6\delta\dot{\delta} + 4(\omega^2 - \alpha^2 - \dot{\alpha})\delta + 4\delta^3 = 2\omega\dot{\omega} - 2\alpha\dot{\alpha} - \ddot{\alpha} \tag{F.7}$$

Assuming that  $\alpha(t)$  and  $\omega(t)$  are slowly-varying, the dominant solution for  $\delta(t)$  becomes

$$\delta(t) = \frac{\omega\dot{\omega} - \alpha\dot{\alpha}}{2(\omega^2 - \alpha^2)} = \frac{\dot{\omega}_d}{2\omega_d} \tag{F.8}$$

and it can be used to simplify the expressions (F-1) to (F-6) in the form shown in section 4.5.1.